Investigation into the effects of the tobacco smoke procarcinogen benzo[*a*]pyrene on gene expression profiles in oesophageal cancer

Alexis J. Bick

Supervisor: Prof. M. Iqbal Parker

International Centre for Genetic Engineering and Biotechnology
and
Division of Medical Biochemistry, University of Cape Town

Presented for MSc (Med) degree
Faculty of Health Sciences
University of Cape Town
August 2011

Acknowledgements

I would like to thank my supervisor Prof. M. Iqbal Parker and the researchers involved in this project for their assistance and support: Prof. Chris Mathew and Dr Peter Green from the Department of Medical and Molecular Genetics at King's College London, Dr Hasan Otu from the Istanbul Bilgi University and Department of Medicine at the BIDMC Genomics Centre, Harvard Medical School, Dr Luiz Zerbini, Dr Nicki Tiffin at SANBI at the University of the Western Cape and Dr Dong-Ping Li.

I would like to thank all the members of the ICGEB laboratory for their assistance and friendship, especially Marike Janse van Rensburg, Beverley van Rooyen, Dr Catherine Kaschula and Dr Juliano Paccez, as well as Luke Esau from the Division of Medical Biochemistry and Dr Collet Dandara from the Division of Human Genetics for assistance with techniques.

I would like to acknowledge the financial assistance of the National Research Foundation (NRF) towards this research. The opinions expressed and conclusions arrived at, are mine and are not necessarily to be attributed to the NRF.

I would also like to acknowledge the financial assistance of the Deutscher Akademischer Austausch Dienst (DAAD), University of Cape Town and scholarships from the Marion Beatrice Waddel and KW Johnstone Bequests.

Finally, a huge thank you to my supportive family and friends, especially Daniel Sheward.

Plagiarism Declaration

1. I know that plagiarism is wrong. Plagiarism is to use another's work and pretend that it is one's own.

2. I have used the Mendeley Reference Manager for citation and referencing and the citation style used in the Journal Molecular Carcinogenesis. Each significant contribution to and quotation in, this thesis from the work(s) of other people has been attributed, and has been cited and referenced.

3. This thesis is my own work.

4. I have not allowed, and will not allow, anyone to copy my work with the intention of passing it off as his/her own work.

Signature: _____
A. J. Bick

Student number: _____

Date: _____

Table of Contents

List of Abbreviations

AhR	aryl hydrocarbon receptor
AhRE	AhR responsive element
AHRR	AhR repressor
AIP	AhR interacting protein (also XAP2 or ARA9)
AKR	aldo-keto reductase
ALD	alcohol dehydrogenase
ALDH	aldehyde dehydrogenase
αNF	α-naphthoflavone
ARNT	aryl hydrocarbon receptor nuclear translocator
ASIR	age-standardized incidence rate
BaP	benzo[a]pyrene
bHLH	basic helix-loop-helix
bp	base pairs
BPDE	anti-benzo[a]pyrene-7,8-diol-9,10-epoxide
BPDE-N^6-dA	BPDE-N^6-deoxyadenosine
BPDE-N^2-dG	BPDE-N^2-deoxyguanosine
BPE	bovine pituitary extract
BPQ	BaP quinone
BrdU	bromodeoxyuridine
COX2	cyclooxygenase 2
CYP	cytochrome P450
DMBA	7,12-dimethylbenz[a]anthracene
DME	drug metabolizing enzyme
DMEM	Dulbecco's modified Eagle medium
DMSO	dimethyl sulfoxide
DNA	deoxyribose nucleic acid
ECM	extracellular matrix
EGF	epidermal growth factor
EROD	7-ethoxyresorufin O-deethylase
ELISA	enzyme-linked immunosorbent assay
EPC-2	epithelial cells
EPXH/EH	epoxide hydrolase
ER	estrogen receptor
FCS	foetal calm serum
GAPDH	glyceraldehyde phosphate dehydrogenase
GO	gene ontology
GOstat	gene ontology statistics
GOrilla	gene ontology enrichment and visualization tool
GST	glutathione S-transferase
GR	glucocorticoid receptor
H_2O_2	hydrogen peroxide
HPV	human papilloma virus
HSP90	heat shock protein 90
IARC	International Agency for Research in Cancer

ICGEB	International Centre for Genetic Engineering & Biotechnology
IPA	Ingenuity Pathway Analysis
kDa	kilo Daltons
KSFM	keratinocyte serum-free medium
KYSE	Japanese cell line
MAPK	mitogen activated protein kinase
3-MC	3-methylcholanthrene
MTT	3-(4,5-dimethylthiazol-2-yl)-2,5-diphenyl tetrazolium bromide
mRNA	messenger RNA
NADPH	reduced nicotinamide adenine dinucleotide phosphate
NAT	N-acetyltransferase
NES	nuclear export signal
NFκB	nuclear factor kappa B
NLS	nuclear localization signal
NQO	NADPH quinone oxidoreductase
O_2^-	superoxide radical
OC	oesophageal cancer
$^{\cdot}OH$	hydroxyl radical
OSCC	oesophageal squamous cell carcinoma
PAH	polycyclic aromatic hydrocarbon
PAS	Per-ARNT-Sim domain
PCR	polymerase chain reaction
PKC	protein kinase C
POD/HRP	horseradish peroxidase
Pol	DNA polymerase
qRT-PCR	quantitative real-time reverse transcription PCR
RARβ2	retinoic acid receptor beta 2
Rb	retinoblastoma protein
RFLP	restriction fragment length polymorphism
RNA	ribose nucleic acid
ROS	reactive oxygen species
SANBI	South African National Bioinformatics Institute
SNP	single nucleotide polymorphism
SULT	sulfotransferase
TCDD	2,3,7,8-tetrachlorodibenzo-p-dioxin
TMB	tetramethyl-benzidine
UGT	uridine diphosphate (UDP)-glucuronosyltransferase
WHCO	South African cell line
XME	xenobiotic metabolizing enzyme
XRE	xenobiotic response element

Abstract

Tobacco smoking is a major risk factor in the development of oesophageal squamous cell carcinoma (OSCC). Benzo[a]pyrene (BaP) is a tobacco smoke procarcinogen that is metabolically activated into the carcinogenic benzo[a]pyrene diol-epoxide (BPDE) by the CYP1 family of cytochrome P450 enzymes. BaP is a ligand for the aryl hydrocarbon receptor (AhR) which activates CYP1 gene transcription. Polymorphisms in these genes affect enzyme activity and therefore BaP bioactivation.

The effects of BaP on expression of CYP1A1, CYP1B1 and the AhR and cell proliferation were compared between a normal oesophageal epithelial cell line (EPC-2) and an OSCC cell line (WHCO1). Transcriptional profiling of the effects of BaP treatment on global gene expression in WHCO1 and EPC-2 cells was carried out using an Illumina microarray system and the data analyzed using Ingenuity Pathways Analysis (IPA) software. Treatment with BaP induced CYP1A1 and CYP1B1 mRNA and protein to a greater extent in WHCO1 compared to EPC-2 cells, and their levels remained elevated when BaP was removed. Nuclear translocation and exit of AhR and ARNT was more rapid in EPC-2 cells during BaP treatment and withdrawal than in WHCO1 cells. Genes involved in inflammation and xenobiotic metabolism were differentially expressed in WHCO1 cells, while genes involved in cell cycle regulation and the DNA damage response were differentially expressed in EPC-2 cells.

These results suggest that WHCO1 cells are more efficient at CYP1 induction and therefore BaP bioactivation than normal cells. Prolonged CYP1 induction and nuclear AhR-ARNT signaling events in WHCO1 cells may contribute to cancer maintenance or promotion, while reduced CYP1 induction in EPC-2 cells may result in less efficient BaP detoxification and subsequent accumulation of DNA-damaging metabolites which cause reduced cell proliferation to allow for DNA repair.

Chapter 1
Introduction

1.1 Incidence of Oesophageal Cancer (OC) and Oesophageal Squamous Cell Carcinoma (OSCC)

OC is the eighth most common cancer worldwide and the sixth most common cause of cancer-related deaths worldwide (Ferlay *et al*., 2010). In 2008, there were an estimated 482 000 new OC cases and 407 000 deaths worldwide, with more than 80% of cases and deaths occurring in developing countries (Ferlay *et al.,* 2010). The global incidence and mortality of OC are highest along the "oesophageal cancer belt" from Southern and Eastern Africa to the Middle East and Eastern Asia (Fig. 1.1-1.2).

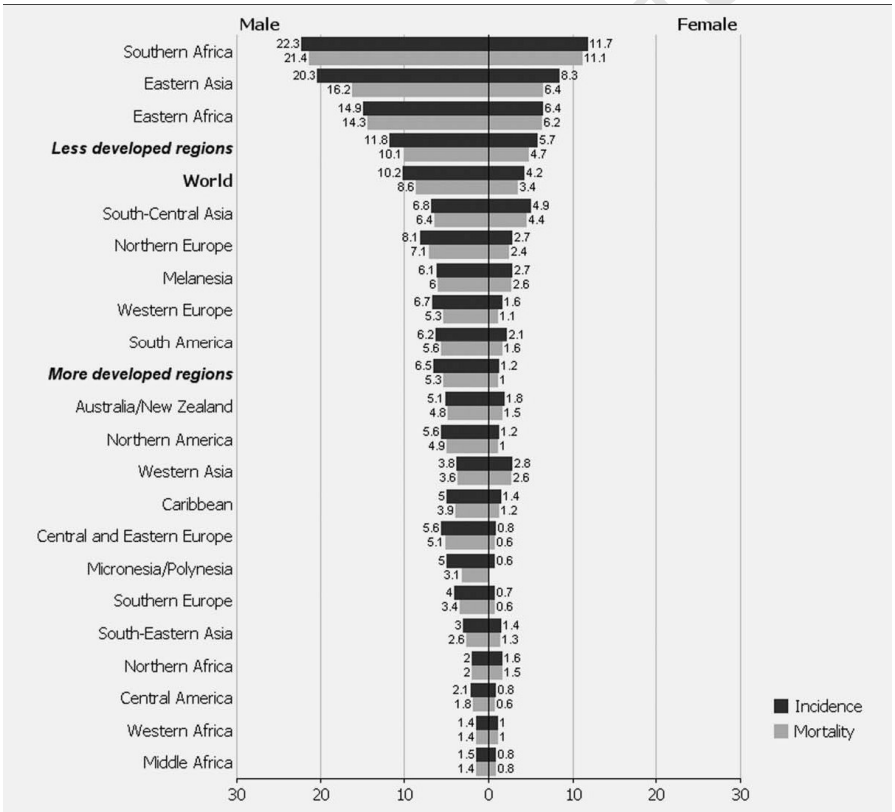

Figure 1.1 Global incidence and mortality of OC. The estimated age-standardized incidence and mortality rates of oesophageal cancer in males and females according to global region. Incidence and mortality rates are higher in Southern and Eastern Africa and Asia, and less developed areas of the world (Taken from Ferlay *et al.,* 2010)

The incidence of OC is two to four times higher in males than females, with age-standardized incidence rates (ASIR) in males varying from 1.4 to 22.3 per 100 000, depending on the region (Ferlay *et al.,* 2010). The global ASIR distribution for OC in males per 100 000 is shown in Figure 1.2.

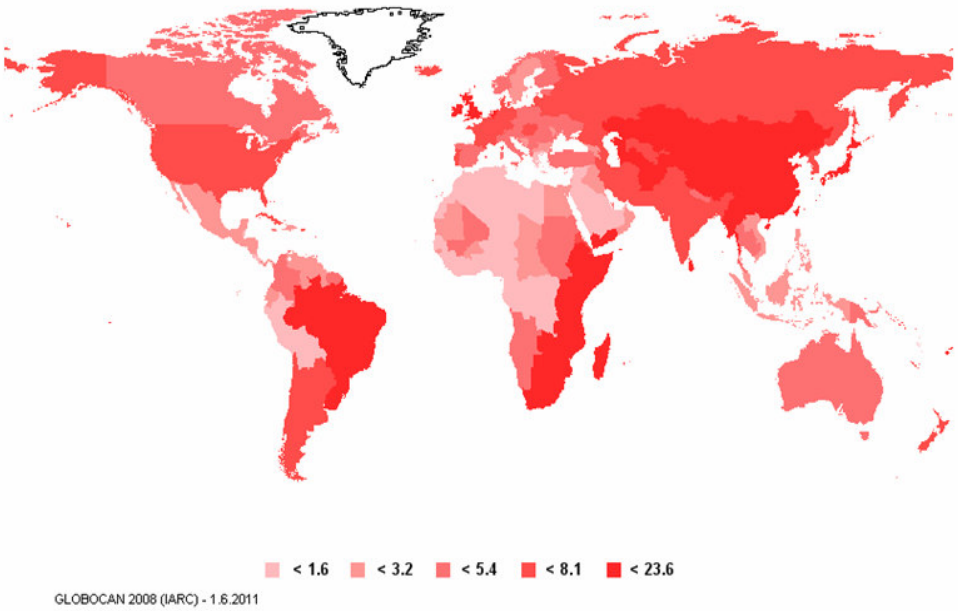

Figure 1.2 Global distribution of OC ASIR per 100 000 males. Global regions with highest incidence rates of OC include Southern and Eastern Africa and Asia, with ASIR exceeding 20 per 100 000 (dark red areas). OC incidence is two to four times higher in males than females. (Taken from IARC Globocan 2008: http://globocan.iarc.fr/)

There are two histological types of OC: adenocarcinoma, which is more prevalent in developed countries; and squamous cell carcinoma (OSCC), which comprises 90% of OC cases in developing countries (Pisani *et al*., 1999). Adenocarcinoma and Barret's oesophagus occur in the lower third of the oesophagus mainly at the gastroesophageal junction, whereas OSCC occurs in the upper two thirds of the oesophagus (Fig. 1.3).

In South Africa, OSCC is the third leading cancer in Black males, who have a lifetime risk of 1 in 59 for developing the disease (Hendricks and Parker, 2002, Mqoqi *et al*., 2004, Pickens and Orringer, 2003). The ASIR is 32.7/100 000 for males and 20.2/100 000 for females (Somdyala *et al.,* 2010). The mortality rate is very high: 75% of patients die within the first year after diagnosis and the 5-year survival rate is less than 10% (Hendricks and Parker, 2002, Hiyama *et al*., 2007). This is due to the fact that patients are asymptomatic until the disease has progressed to an advanced stage.

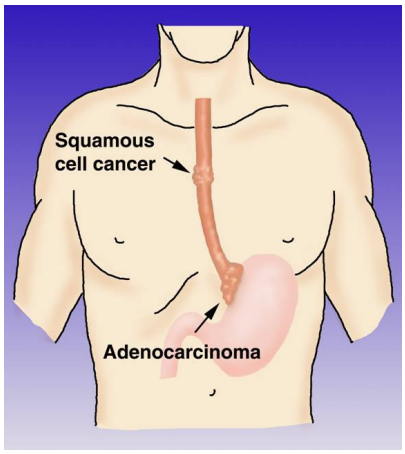

Figure 1.3 Positions of the histological types of OC. Oesophageal adenocarcinoma occurs in the lower third of the oesophagus, mainly at the gastroesophageal junction, whereas OSCC develops in epithelial cells from the upper two thirds of the oesophagus (Taken from http://www.sts.org/patient-information/esophageal-surgery/esophageal-cancer)).

1.2 Risk Factors for the Development of OSCC

Epidemiological evidence has suggested that the major risk factors for the development of OSCC include tobacco smoking, alcohol consumption and defects in the genes encoding enzymes involved in their metabolism. Gene-environment interactions therefore play an important role in oesophageal carcinogenesis. Several minor risk factors have also been identified; however they will not be the focus of this study. Minor risk factors include infection with the human papilloma virus (HPV) (Matsha *et al.,* 2002), a diet lacking in fruit and vegetables (Franceschi *et al*., 2000), reduced dietary vitamin D intake (Lipworth *et al.,* 2009), contamination of food with aflatoxins and fumonisin (Marasas, 2001, Wild and Gong, 2010), exposure to smoke while cooking on open fires (Pacella-Norman *et al*., 2002) and physical injury due to consumption of hot beverages (Islami *et al*., 2009) or forced vomiting, which is a form of ritual cleansing in some cultures (Matsha *et al*., 2006).

1.2.1 Genetic Polymorphisms

Inter-individual genetic differences can explain why susceptibility to cancer varies despite similar exposures to environmental carcinogens. These genetic differences occur as a result of polymorphic genes within the genome. Polymorphisms are variations in a gene that occur with a frequency of at least 1% within a population. The gene's two copies, or alleles, could therefore contain either the common base or the variant. Specific sites within a gene can have either a

common allele (which has the highest frequency within a population) or a polymorphic variant. For example, this can be represented by the notation CYP1A1 4889A>G, which indicates that at base pair 4889 in the CYP1A1 gene, the common A allele can be replaced by the polymorphic variant, the G allele.

Polymorphic variants in detoxification genes or xenobiotic metabolism give rise to enzymes with altered specificity, increased, reduced or abolished catalytic activity, or altered regulation and expression (Ingelman-Sundberg, 2001). In the case where polymorphic variants result in increased enzyme activity, the common allele can be referred to as the "slow" or "low activity" allele, and the polymorphic allele is referred to as the "fast" or "high activity" allele. These alterations can influence the enzyme's detoxification efficiency and therefore also susceptibility to cancer.

The frequency of polymorphic alleles may also vary between ethnic groups, thereby contributing to inter-ethnic variation. Several case-control studies have shown that genetic polymorphisms in various genes are associated with increased or decreased risk of developing OSCC. Polymorphisms in several xenobiotic metabolism genes are associated with increased risk for the development of OSCC (Li *et al*., 2005, Dandara *et al*., 2005, Dandara *et al*., 2006, Li *et al*., 2008, Li *et al*., 2010). Furthermore, this effect on OSCC risk is often enhanced by smoking or alcohol consumption, which highlights their roles as major risk factors for OSCC (Table 1.1).

Mutations in important cell cycle regulatory genes, such as p53, can also play a role in the development of OSCC. p53, a known tumour suppressor gene, is a transcription factor that regulates the transcription of genes involved in cell cycle progression, DNA repair and apoptosis (Levine, 1997). p53 is mutated in more than 50% of human tumours, including lung cancers (Hahn and Weinberg, 2002, Hainaut and Pfeifer, 2001). Mutations in p53 have been identified in OSCC (Vos *et al*., 2003, Shibagaki *et al*., 1995) and may occur at early stages (Gao *et al*., 1994).

Table 1.1 Polymorphisms in xenobiotic metabolism genes and their association with OSCC development in South African populations. CYP: cytochrome P450, SULT: sulfotransferase, GST: glutathione S-transferase, ADH: alcohol dehydrogenase, ALDH: aldehyde dehydrogenase

Gene	Polymorphism	Association with OSCC	Smoking/ alcohol consumption and risk	Reference
CYP2E1*6	7632T>A	Higher risk in Black males	Smoking/alcohol consumption have synergistic effect	Li *et al*., 2005
CYP3A5*3	6986A>G	Higher frequency in Mixed Ancestry controls; GG homozygotes have reduced OSCC risk	AA or AG genotype associated with increased risk in tobacco smokers and alcohol consumers	Dandara *et al.,* 2005
SULT1A1*2	638G>A	Associated with OSCC	Higher risk in tobacco smokers	Dandara *et al.,* 2006
GSTP1	341 C>T	T allele associated with increased risk	Higher risk in tobacco smokers and alcohol consumers	Li *et al.,* 2010
GSTT1*0	Deletion	Increased risk	-	Li *et al.,* 2010
GSTM1*0	Deletion	Decreased risk in Mixed Ancestry subjects	-	Li *et al.,* 2010
ADH3*2	1119A>G	Increased risk in Black subjects	Higher frequency in non-alcohol consumers	Li *et al.,* 2008
ALDH2*2	1543G>A	Increased risk in Black subjects	-	Li *et al*., 2008

1.2.2 Alcohol Consumption

Alcohol consumption is a major risk factor for the development of OSCC. In South Africa, consumption of traditional home-brewed beer in rural high-incidence areas may be a major contributory factor to the risk of alcohol consumption-associated OSCC (Matsha *et al*., 2006).

Alcohol dehydrogenases (ADH) in the liver metabolize ethanol to acetaldehyde and aldehyde dehydrogenases (ALDH) then metabolize acetaldehyde to acetate. Acetaldehyde is carcinogenic and forms mutagenic adducts with DNA (Seitz and Stickel, 2007). Genetic polymorphisms that result in acetaldehyde accumulation, such as reduced or abolished ALDH activity, are associated with increased OSCC risk (Yokoyama *et al*., 2003, Li *et al*., 2008). Alcohol metabolism also increases levels of reactive oxygen species (ROS) through the action of cytochrome P450 (CYP) 2E1, which can lead to DNA damage and lipid peroxidation. The role of ethanol metabolism in carcinogenesis is shown in Figure 1.4.

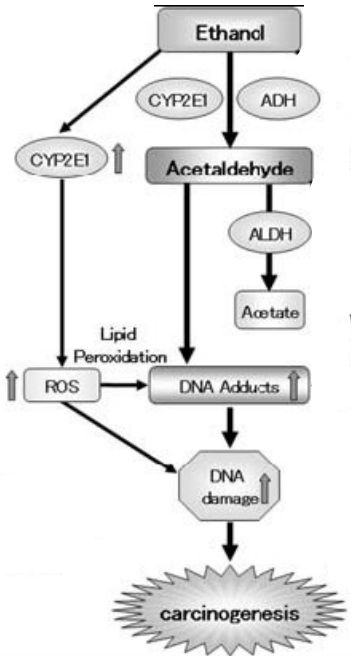

Figure 1.4 Schematic representation of ethanol metabolism and its role in carcinogenesis. Ethanol is metabolized by ADH and CYP2E1 in the liver to the carcinogenic acetaldehyde, which is metabolized to acetate by ALDH, thereby completing the ethanol detoxification pathway. Acetaldehyde, however, also binds DNA and forms DNA adducts. Increased CYP2E1 activity results in increased ROS, which together with DNA adduct formation, increase the DNA damage that leads to carcinogenesis. ADH: alcohol dehydrogenase, ALDH: aldehyde dehydrogenase, CYP2E1: cytochrome P450 2E1, ROS: reactive oxygen species. (Adapted from Toh *et al*., 2010.)

1.2.3 Tobacco Smoking

Tobacco smoking is the major risk factor for the development of OSCC, lung, kidney, bladder, pharyngeal, laryngeal, pancreatic, breast and oral cancers (Hecht, 2006). About 4800 compounds have been identified in tobacco smoke (Green & Rodgman, 1996) including more than 60 known carcinogens (IARC, 2004). The most important groups of carcinogens in cigarette smoke are the polycyclic aromatic hydrocarbons (PAHs) and N-nitrosamines, although aromatic amines, formaldehyde, organic compounds, metals and other chemicals are also listed as carcinogens (Hecht, 2006). Some of the toxic and carcinogenic compounds in cigarette smoke are indicated in Figure 1.5.

Many intermediates generated during the metabolism of compounds in tobacco smoke are highly reactive with DNA. Their molecular mechanism of action is via their ability to bind covalently to DNA and form mutagenic adducts (Toh *et al*., 2010). The role of cigarette smoke compounds in carcinogenesis is summarized in Figure 1.6.

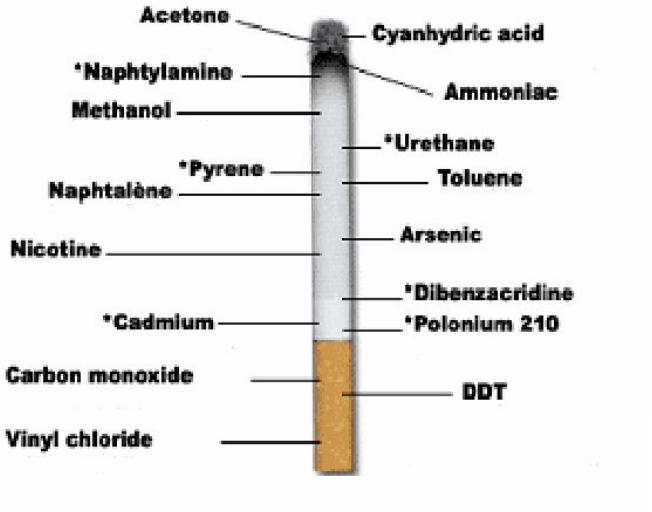

Figure 1.5 Compounds present in cigarettes. Known carcinogenic chemicals are indicated by *. PAHs are products of combustion formed during tobacco and cigarette smoking. DDT: dichloro-diphenyltrichloroethane. (Adapted from http://flatobaccolitigation.com/nsmoke.htm)

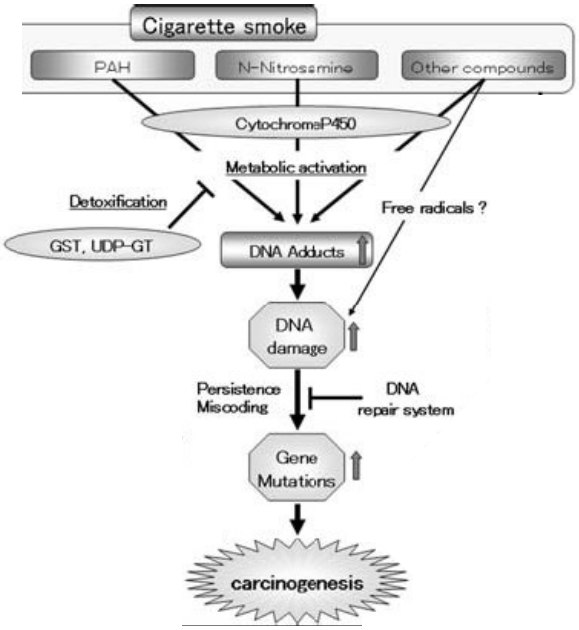

Figure 1.6 Schematic representation of the role of cigarette smoke compounds in carcinogenesis. Compounds in cigarette smoke, e.g. PAHs or N-nitrosamines, are metabolically activated by cytochrome P450s into metabolites that bind DNA. Increased DNA adducts enhance DNA damage and the genetic mutations that precede carcinogenesis. PAH: polycyclic aromatic hydrocarbon, GST: glutathione S-transferase, UDP-GT: uridine diphosphate glucuronosyltransferase. (Adapted from Toh *et al*., 2010).

PAHs are combustion products in tobacco smoke and require metabolic activation by xenobiotic metabolizing enzymes to generate their carcinogenic intermediates. Exposure to PAHs has been associated with lung, bladder and breast cancer (Bostrom *et al*., 2002). The hydrophobic ring structure common to all PAHs allows their passive entry through cell membranes and into cells, where they can accumulate and exert their carcinogenic effects. One of the 10 PAHs identified in tobacco smoke is benzo[a]pyrene (IARC, 2004, Ding *et al*., 2007), which is the focus of this study.

1.3 Benzo[a]pyrene (BaP)

1.3.1 BaP Sources and History

BaP is a five-ring hydrophobic PAH (Fig. 1.7) found in tobacco smoke, burning wood, fuel exhaust emissions, environmental pollution and charred meat (Bostrom *et al*., 2002, Phillips, 1999). It has been estimated that there is 25ng of BaP per one cigarette (Schmeltz *et al*., 1974) and that the average daily environmental BaP intake is 600ng/day (Scherer *et al*., 2000). It is the prototypic and most commonly studied PAH, probably because it is a good indicator for levels of exposure to all PAHs (Fertmann *et al*., 2002). BaP was first isolated from coal tar in the 1930s (Cook *et al.,* 1933) and shown to form papillomas and tumours when repeatedly applied to mouse skin and rabbit ears (Yamagiwa and Ichikawa, 1977, Rubin, 2001, Baird *et al*., 2005). BaP can act as both an initiator and promoter of tumorigenesis (Rubin, 2001) and is a procarcinogen that requires metabolic activation to form its carcinogenic metabolites.

1.3.2 BaP Metabolism: Detoxification and Metabolic Activation

BaP is metabolized in a two-phase reaction by several xenobiotic metabolizing enzymes (XMEs), generating more than a dozen metabolites (Fig. 1.7). Phase I metabolism is carried out by cytochrome P450 (CYP) enzymes and epoxide hydrolase, generating intermediate metabolites such as diols, oxides and phenols. These intermediates are then conjugated to endogenous compounds by the phase II enzymes UDP-glucuronosyltransferases (UGTs), sulfotransferases (SULTs), glutathione S-transferases (GSTs), aldo-keto reductases (AKRs) and NADPH quinone oxidoreductases (NQO1s). The products formed by these conjugation reactions are sufficiently water-soluble to allow easy excretion from the body (Guengerich and Shimada, 1998, Nebert and Dalton, 2006).

While this system usually results in efficient BaP detoxification, highly reactive intermediates are formed during phase I metabolism (which in this case is called metabolic activation). CYP1A1, CYP1B1 and epoxide hydrolase enzymes metabolically activate BaP to form anti-benzo[a]pyrene-7,8-diol-9,10-epoxide (BPDE), the ultimate carcinogen generated by BaP metabolism. BPDE has four isomers, ± anti and ± syn, of which the + isomer of anti-BPDE is the most active (Fig. 1.8, Miller and Ramos, 2001). In cases where phase II metabolism is absent or reduced, exposure to BaP results in accumulation of BPDE.

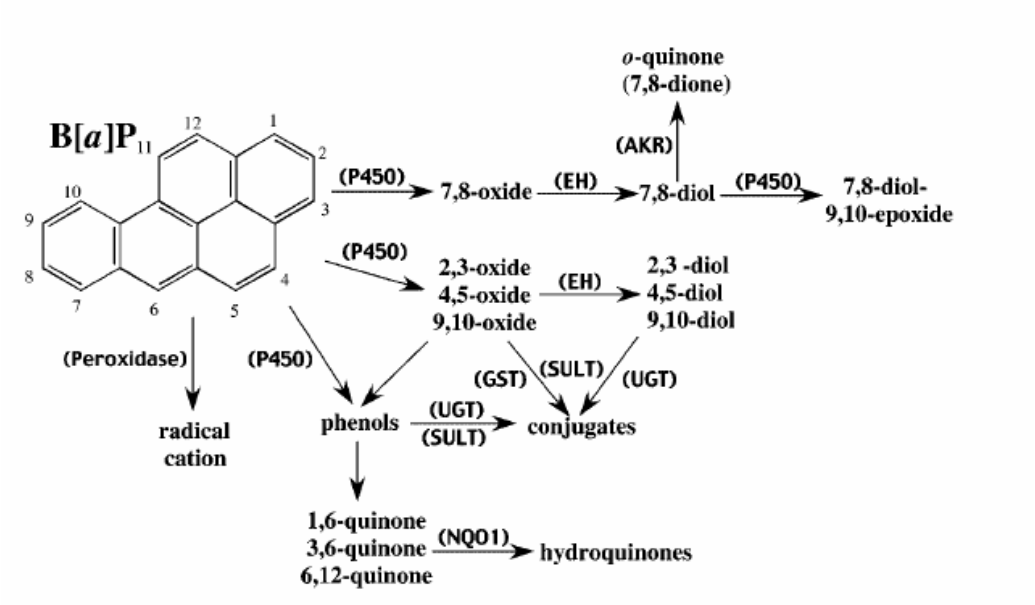

Figure 1.7 Metabolism of BaP by phase I and II enzymes and the metabolites generated. See text for discussion. Phase I enzymes: P450, EH; Phase II enzymes: UGT, SULT, GST, NQO1, AKR. P450: cytochrome P450 (CYP), EH: epoxide hydrolase, SULT: sulfotransferase, UGT: UDP-glucuronosyltransferase, GST: glutathione S-transferase, AKR: aldo-keto reductase, NQO1: NADPH quinone oxidoreductase (Taken from Shimada, 2006)

1.3.3 BaP Mechanism of Carcinogenicity

BaP exposure is believed to contribute to carcinogenesis in two ways: by enhancing oxidative stress during its metabolism and by forming adducts with cellular components. Carcinogen-DNA adducts have been identified in human oesophagus (Harris *et al*., 1979).

The generation of oxidized BaP metabolites during phase I metabolism increases cellular ROS levels, which promote oxidative and genotoxic stress, including lipid peroxidation and DNA damage. Increased ROS, oxidative stress and inflammation have been linked to cancer (Coussens and Werb, 2002, Valko *et al*., 2006). ROS like the BaP-quinones (BPQ) 1,6-BPQ and 3,6-BPQ generated during BaP metabolism form the superoxide anion (O_2^-) and hydrogen peroxide (H_2O_2) in breast epithelium (Burdick *et al*., 2005). BaP metabolism also forms $^{\cdot}OH$ (hydroxyl radical, Miller and Ramos, 2001).

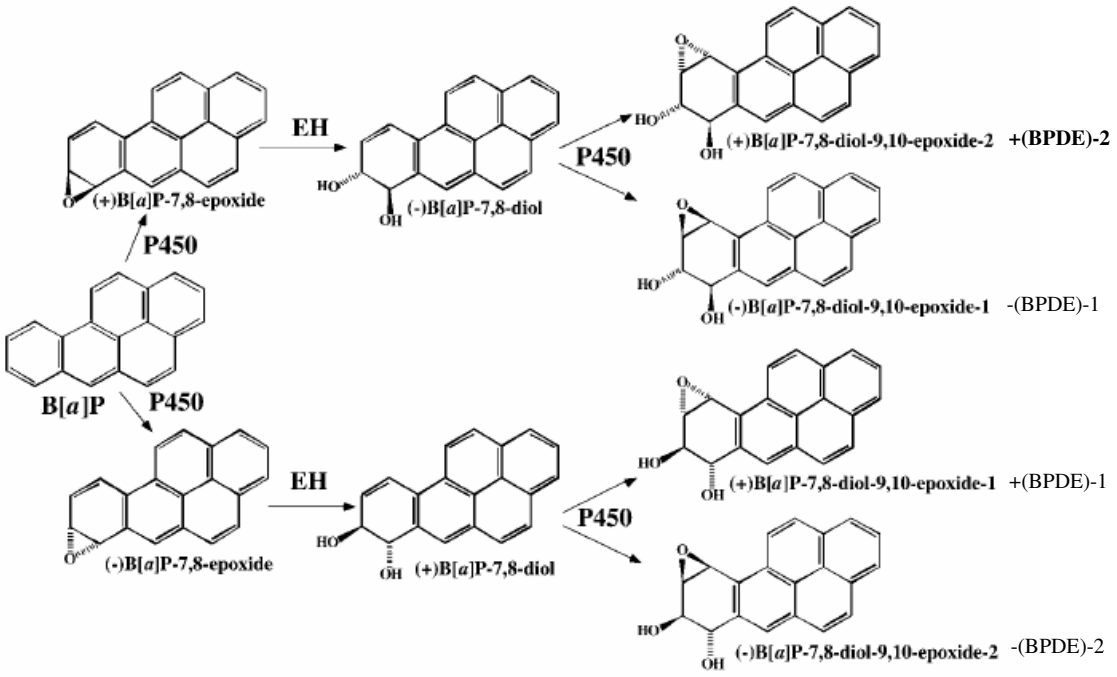

Figure 1.8 Mechanism of metabolic activation of BaP. During phase I metabolism, CYP1A1, CYP1B1 and epoxide hydrolase metabolically activate BaP and form anti BPDE-1 and -2. The + isomer of anti-BPDE is the most active BPDE isomer (+(BPDE)-2). EH: epoxide hydrolase, P450: cytochrome P450 (CYP). (Taken from Shimada, 2006).

Most studies have focused on the formation of DNA adducts by the carcinogenic BaP metabolite, BPDE. Covalent binding of BPDE to DNA residues results in the formation of bulky BPDE-N^2-deoxyguanosine (BPDE-N^2-dG, Fig. 1.9) and BPDE-N^6-deoxyadenosine (BPDE-N^6-dA) adducts (Cheng *et al.*, 1989). The BPDE-N^2-dG adduct occurs more frequently and results in G>T transversion mutations (Glick *et al.,* 2009, Chiapperino *et al*., 2002), especially in mutational hotspots of the p53 tumour suppressor gene (Denissenko *et al.*, 1996, Chen *et al*., 1998, Hainaut and Pfeifer, 2001) and in other genes, such as the *c-Ha-ras*1 proto-oncogene (Yang *et al*., 1999). The BPDE-N^2-dG adduct occurs in the minor groove of B-DNA and is 5′-oriented along the modified strand, resulting in a bulky change in DNA conformation (Fig. 1.10, Kropachev *et al*., 2009). The formation of mutations is influenced by the DNA sequence context around the adduct (Miller and Ramos, 2001, Kropachev *et al.*, 2009), the conformational change caused by the adduct (Kozack *et al*., 2000) and the state of methylation of CpG sites (Glick *et al*., 2009, Chen *et al*., 1998). The removal of BPDE-DNA adducts occurs through the nucleotide excision repair (NER) mechanism, however, mutations can be introduced during DNA replication if low fidelity polymerases bypass the adduct without repairing the mutation (Jia *et al*., 2008). For example, while pol κ accurately repairs BPDE-DNA lesions, pol η is error-prone (Chiapperino *et al.,* 2002, Rechkoblit *et al*., 2002). These mutations can result in the development of cancer (Luch, 2005).

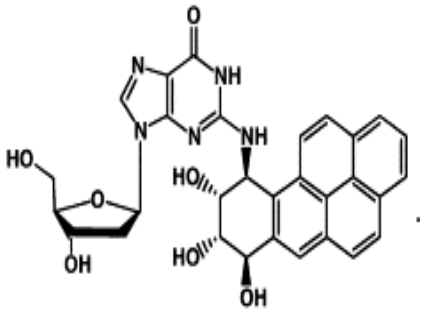

Figure 1.9 Chemical structure of the BPDE-N^2-dG adduct. BPDE binds to either deoxyadenosine or deoxyguanosine residues in DNA. BPDE-N^2-dG is the major BPDE-DNA adduct which, if not correctly repaired, results in G>T transversion mutations, especially in the p53 gene. Mutations caused by BPDE-DNA adducts also depend on the sequence context surrounding the adduct.

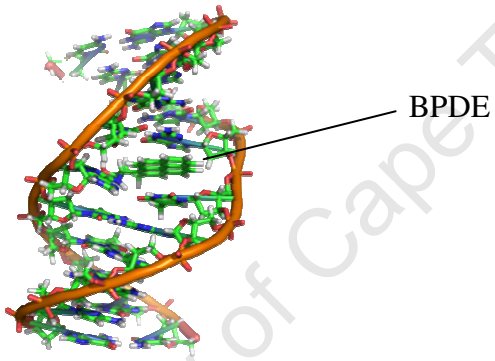

Figure 1.10 Conformation of the BPDE-N^2-dG adduct in the minor groove of DNA. The bulky structure of BPDE causes a conformational change in the double helix. Error-prone DNA polymerases bypass the bulky adduct without repairing it and G>T transversion mutations occur as a result. (Taken from http://www.rcsb.org)

1.3.4 Effect of BaP and BPDE on the Cell and Signal Transduction Pathways

BaP has been shown to be carcinogenic, cytotoxic, mutagenic and teratogenic (Uno *et al*., 2004). Both BaP and BPDE induce apoptosis (Solhaug *et al*., 2004b). BaP affects DNA methylation in breast cancer cells (Sadikovic and Rodenhiser, 2006) which is interesting in light of the evidence that BPDE preferentially targets methylated CpG sites for G>T mutations (Yoon *et al*., 2001). BaP has been shown to affect the normal function of signal transduction cascades, including Ca^{2+} signaling, epidermal growth factor (EGF) signaling, protein kinase C (PKC) signaling and phosphorylation (Miller and Ramos, 2001) and insulin-like growth factor signaling (Tannheimer *et al*., 1998). BaP has also been shown to affect the expression of various genes, for example, inducing expression of cyclooxygenase 2 (COX-2, Yan *et al*., 2000), an enzyme which is

involved in inflammation and frequently upregulated in OSCC (Shamma *et al*., 2000). BaP exposure has been shown to cause altered expression of nuclear proteins and alternative mRNA splicing in response to DNA damage (Yana *et al*., 2010).

BPDE has been shown to induce aberrations in chromosome 9p21 in bladder cancer (Hazra *et al*., 2004, Gu *et al*., 2008), chromosome 3p21.3 in lung cancer (Wu *et al*., 1998) and chromosome instability and the amplification of centromeres in lung cancer (Shinmura *et al*., 2008). BPDE affects the expression of various genes, including repression of the retinoic acid receptor beta 2 gene (Song *et al*., 2005).

BaP is able to regulate the expression of some genes by activating the aryl hydrocarbon receptor (AhR). BaP, along with other PAHs and the environmental pollutant 2,3,7,8-tetrachlorodibenzo-p-dioxin (TCDD), is a ligand for the AhR. Ligand-activated AhR is a transcription factor that regulates the transcription of several genes, including some phase I xenobiotic metabolism genes. The influence of xenobiotics such as BaP on abnormal cell growth and cancer through the AhR and increased ROS is summarized in Figure 1.11. PAHs can also induce gene expression in an AhR-independent manner (Nebert *et al*., 2000).

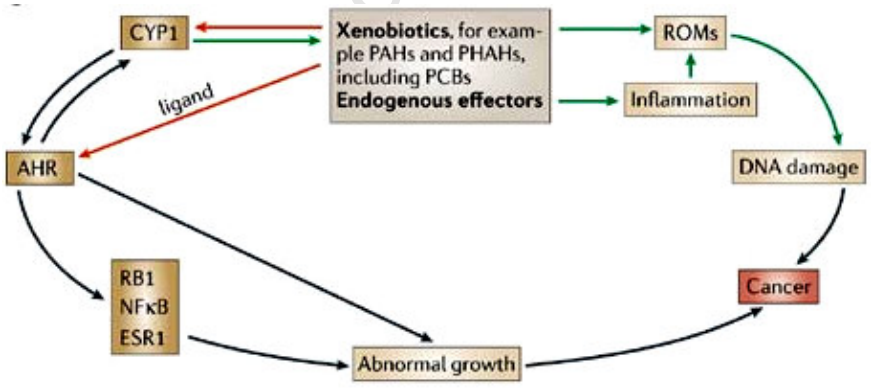

Figure 1.11 Xenobiotic exposure as a risk factor for cancer development. Xenobiotics such as BaP contribute to abnormal cell growth and cancer by affecting the expression and regulation of cancer-related genes, including RB1 and NFκB, and increasing DNA damage through ROS and inflammation. CYP1: cytochrome P450 1 family, AHR: aryl hydrocarbon receptor, RB1: retinoblastoma protein, NFκB: nuclear factor kappa B, ESR1: estrogen receptor 1, PAHs: polycyclic aromatic hydrocarbons, PHAHs: polycyclic halogenated aromatic hydrocarbons, PCBs: polychlorinated biphenyls, ROMs: reactive oxygenated metabolites, referred to as ROS. (Taken from Nebert and Dalton, 2006).

1.4 Xenobiotic Metabolizing Enzymes (XMEs)

1.4.1 Xenobiotic Exposure as a Risk for Cancer

Humans are exposed to xenobiotics or foreign compounds through many sources including environmental pollution, pharmaceutical drugs, tobacco smoke, alcohol, preservatives and insecticides in food and petrol exhaust emissions. The oesophagus is a target organ for most of these xenobiotics. Many of these chemicals are harmful to the body if they accumulate during prolonged exposure, which may result in toxicity and eventually, cancer. XMEs evolved in order to detoxify and eliminate these foreign chemicals from the body and thereby protect against carcinogenesis.

1.4.2 Mechanism of Xenobiotic Metabolism

Metabolism of xenobiotics such as BaP occurs in a two-phase reaction catalyzed by phase I and II XMEs (Fig. 1.12). Phase III XMEs are responsible for the transport and removal of the detoxified product.

1.4.2.1 Phase I XMEs

Phase I metabolism is carried out primarily by cytochrome P450 (CYP) enzymes that catalyze the oxidation, reduction or hydrolysis of the xenobiotic substrate, to form an electrophilic intermediate (Nebert and Dalton, 2006). Metabolic activation of procarcinogens such as BaP occurs during Phase I metabolism (Fig. 1.8). Other phase I XMEs include epoxide hydrolase (EPHX). Polymorphisms in EPHX1 have been associated with increased risk of lung and oesophageal cancers (Gsur *et al*., 2003, Jain *et al*., 2008, Ihsan *et al*., 2010).

1.4.2.2 Phase II XMEs

Phase II metabolism is carried out by conjugation enzymes that catalyze the conjugation of the intermediate from Phase I metabolism to an endogenous compound, such as glutathione, uridine diphosphate (UDP)-glucuronic acid or sulfate groups. These XMEs include glutathione S-transferase (GST), UDP-glucuronosyltransferase (UGT), sulfotransferase (SULT), N-acetyltransferase (NAT), aldo-keto reductase (AKR) and NADPH quinone oxidoreductase (NQO1) (Nebert and Dalton, 2006). Conjugated products are more water-soluble and are easily excreted from the body. Conjugation of BaP intermediates is catalyzed by all of the abovementioned phase II XMEs (Fig. 1.7).

1.4.2.3 Phase III XMEs

Phase III XMEs are transporter proteins expressed in the liver and intestine that play a role in absorption, distribution and excretion of the detoxified xenobiotic (Bozina *et al*., 2009). Transporters include P-glycoprotein, organic anion transporting polypeptide 2 and multi-drug resistance associated proteins (Bozina *et al*., 2009).

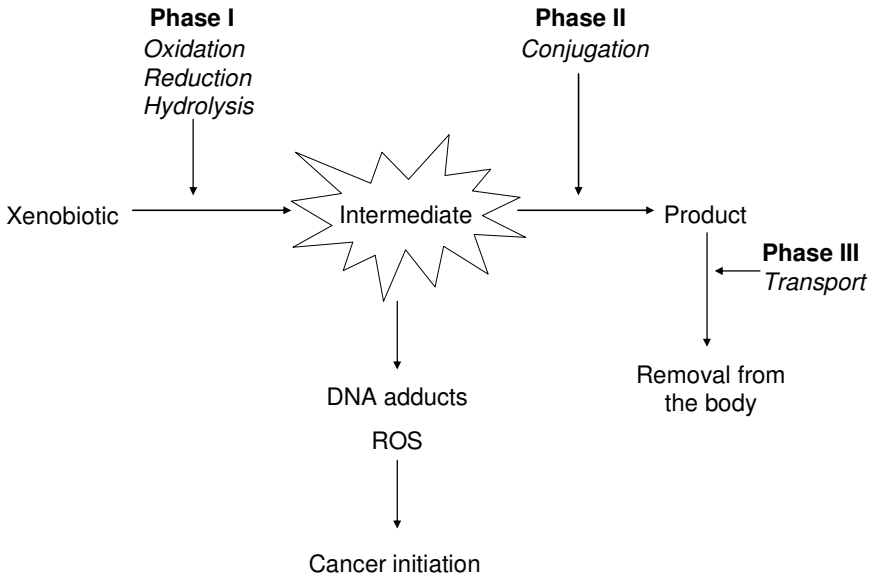

Figure 1.12 Mechanism of xenobiotic metabolism. Phase I XMEs oxidize the xenobiotic to form a reactive electrophilic intermediate. Phase II XMEs then conjugate the intermediate to an endogenous compound such as glutathione, rendering the product more water-soluble to facilitate elimination from the body. Increased activity of Phase I XMEs and decreased activity of phase II XMEs results in deregulated xenobiotic metabolism and an accumulation of carcinogenic intermediates that contribute to the development of cancer.

1.4.3 Deregulated Xenobiotic Metabolism as a Risk for Cancer Development

While the two-phase system normally functions efficiently to detoxify and remove xenobiotics, deregulated xenobiotic metabolism can lead to an imbalance of the intermediates and products formed and may contribute to the development of cancer when the xenobiotic is a procarcinogen. Increased activity of Phase I XMEs and decreased or abolished activity of phase II XMEs can result in an accumulation of carcinogenic intermediates such as BPDE because the rate of phase I metabolism exceeds that of phase II metabolism (Fig. 1.12). Polymorphisms in phase I and II XMEs may contribute to deregulated xenobiotic metabolism as they result in enzymes with

increased, decreased or abolished enzyme activity or different substrate specificity (Ingelman-Sundberg, 2001).

1.5 Cytochrome P450 enzymes (CYPs)

CYPs are haem-thiolate monooxygenases that form 70-80% of all phase I XMEs (Ingelman-Sundberg, 2004). They are membrane-bound microsomal enzymes that function, with an NADPH cytochrome P450 reductase as a two-step electron donor, to catalyze reactions involving the incorporation of one atom of molecular oxygen into its substrate (Bernhardt, 2006). These reactions include hydroxylation, epoxidation, N, S and O-dealkylation and oxygenation. All CYPs have a conserved peptide motif – Phe-$X_{(6-9)}$-Cys-X-Gly, where X is any amino acid – in the iron-binding thiol group (Nebert and Dalton, 2006). The nomenclature of all human CYPs is maintained by the Human CYP Allele Nomenclature Committee, which is accessible at http://www.cypalleles.ki.se/ (Ingelman-Sundberg *et al*.).

1.5.1 Role of CYPs in Xenobiotic Metabolism

CYPs are classified according to amino acid sequence similarity, with families and subfamilies sharing 40% and 55% sequence identity, respectively (Nebert and Russell, 2002). While 57 CYP genes have been identified and classified into 18 families and 42 subfamilies, only the CYP1, CYP2, CYP3 and CYP4 families are involved in xenobiotic metabolism (Kawajiri and Fuji-Kuriyama, 2007). Of these, important xenobiotic metabolizing CYPs include CYP1A1, CYP1B1, CYP1A2, CYP2E1, CYP3A4, CYP3A5 and CYP2D6. Since these CYP enzymes are responsible for most phase I xenobiotic metabolism, they also play a role in metabolic activation of procarcinogens. The CYP1 family is particularly interesting because of their role in metabolism of BaP. Tissue-specific expression of one or more of these CYPs may influence procarcinogen activation and therefore susceptibility to xenobiotic-associated cancer.

1.5.2 CYP1 Family

The CYP1 family plays an important role in xenobiotic metabolism and comprises three highly conserved isomers: CYP1A1, CYP1A2 and CYP1B1. The expression of the CYP1 genes is induced by PAHs such as BaP; the current understanding of PAH-inducible CYP1 gene expression is discussed in full below.

1.5.2.1 CYP1A1

CYP1A1 is located on chromosome 15q22-24 and consists of 6 introns and 7 exons, encoding a protein consisting of 512 amino acids (Jaiswal *et al*., 1985). CYP1A1 is primarily expressed in extrahepatic tissues including the oesophagus (Nakajima *et al*., 1996, Lechevral *et al*., 1999). CYP1A1 is responsible for the metabolism of many xenobiotics including theophylline, caffeine, 7-ethoxyresorufin and chlorzoxazone and various PAHs (Bozina *et al*., 2009, Shimada, 2006). CYP1A1 mRNA and protein are present at very low, almost undetectable basal levels, but are highly inducible by various compounds (Nebert *et al*., 2004, Ma and Lu, 2007). These include PAHs such as BaP and the classical inducer of CYP1A1, TCDD (Whitlock, 1999). CYP1A1 induction has been linked to the toxicity and resulting cell death from BaP treatment in cultured cells (Ma and Lu, 2007).

Several polymorphic variants of CYP1A1 have been identified, including CYP1A1*2B, *2C, *3, *4, *5, *6, *7, *8, *9, *11 that result in amino acid changes (Bozina *et al*., 2009). Several CYP1A1 polymorphisms have been associated with cancer susceptibility in smoking-associated cancers including lung, oral, oesophageal, breast and colon cancers (Taioli *et al*., 2003, Kao *et al*., 2002, Nimura *et al*., 1997, Miyoshi *et al*., 2002, Pande *et al*., 2010). While some studies have linked these polymorphic gene variants to enzymes with different catalytic activities, it remains unclear whether polymorphisms can be linked to increased enzyme activity in all cases. For example, there is contradictory data implicating the CYP1A1*2C allele (4889A>G in exon 7 or Ile462Val) with increased risk of lung cancer (Landi *et al*., 2005, Houlston, 2000, Le Marchand *et al*., 2003). CYP1A1*2C is also associated with increased enzyme activity and mRNA induction (London *et al*., 2000, Agudo *et al*., 2009). Differences in polymorphism frequencies between populations may influence inter-population differences in cancer susceptibility, especially in cancers where CYP1A1 plays a role in carcinogen metabolism. For example, the frequency of the CYP1A1 4889A/A genotype is highest in Africans (94.8%) and Caucasians (90.2%), while the A/G genotype occurs with the highest frequency in Asians (36%). The 4889G/G genotype occurs with highest frequency in Asians (4.9%) but is very rare in Caucasians (0.6%) and does not occur in Africans (0%) (http://www.ncbi.nlm.nih.gov/SNP/). Since CYP1A1 is involved in PAH metabolism and therefore metabolic activation, the high-inducibility of the CYP1A1*2C polymorphism may play a role in susceptibility to PAH-associated cancers.

1.5.2.2 CYP1B1

CYP1B1 is located on chromosome 2p21 and consists of 2 introns and 3 exons, of which exons 2 and 3 encode a protein of 543 amino acids (Sutter *et al*., 1994). CYP1B1 shares 40% amino acid homology with CYP1A1 (Shimada *et al*., 1996) and while they have overlapping substrate specificity, they differ in metabolic efficiency (Shimada and Fujii-Kuriyama, 2004). CYP1B1 has higher basal levels than CYP1A1 and is also inducible by PAHs, but to a lesser extent (Nebert *et al*., 2004).

CYP1B1 is expressed in extrahepatic tissues including the oesophagus (Nakajima *et al*., 1996, Lechevral *et al*., 1999), lung, kidney, heart and brain (Bozina *et al*., 2009). CYP1B1 is responsible for the metabolism of xenobiotics such as 7,12-dimethylbenz[a]anthracene (DMBA), PAHs and other diverse procarcinogens as well as endogenous compounds (Shimada *et al*., 1996). The 4-hydroxylation of estradiol by CYP1B1 variants has been associated with breast cancer (Li *et al*., 2000).

At least 26 polymorphisms have been identified in the human CYP1B1 gene and 19 of these variants confer amino acid changes (Ingelman-Sundberg *et al*, http://www.cypalleles.ki.se/). The A4390G polymorphism (Asn453Ser) has been associated with increased degradation of CYP1B1 protein (Bandiera *et al*., 2005). The variants in codons 119 (Ala119Ser) and 432 (Leu432Val) are associated with different catalytic activities of the enzymes (Shimada *et al*., 1999, Li *et al*., 2000) and have been shown to have higher 4-hydroxylation activities than the wild type enzyme (Hanna *et al*., 2000). Inter-ethnic differences in polymorphism frequencies may affect susceptibility to cancer. For example, Asians have the highest frequency of the CYP1B1 4326 C/C genotype (73.3-84.1%), while Caucasians have the highest frequency of the C/G genotype (41.7-45%) and Africans have the highest frequency of the G/G genotype (73.3%) (http://www.ncbi.nlm.nih.gov/SNP).

CYP1B1 has been suggested to play a role in carcinogenesis. In addition to its role in carcinogen activation (Shimada *et al*., 1996), CYP1B1 is frequently overexpressed in human cancers (Port *et al*., 2004), and CYP1B1 variants have been associated with cancers such as breast (Paracchini *et al*., 2006), lung (Watanabe *et al*., 2000), endometrial (Sasaki *et al*., 2003), prostate (Tanaka *et al*., 2002), ovarian (Goodman *et al*., 2001), head and neck (Ko *et al*., 2001) and colorectal cancer (Fritsche *et al*., 1999, Gibson *et al*., 2003). Accordingly, CYP1B1 has been suggested as a possible therapeutic drug target in hormonal cancers (Guengerich *et al*., 2003) and oesophageal

cancer (Wen and Walle, 2007) and CYP1B1 inhibitors have been suggested as potential anti-cancer agents (Chun and Kim, 2003).

1.5.2.3 CYP1A2

CYP1A2 is located on chromosome 15 and consists of 6 introns and 7 exons, while the 515 amino acid protein is translated from exon 2 (Ikeya *et al*., 1989). CYP1A2 shares 72% amino acid sequence similarity with CYP1A1 (Bartsch *et al*., 2000). CYP1A2 is a hepatic enzyme that is responsible for the metabolism of aryl, heterocyclic aromatic and nitroaromatic amines and pharmaceutical drugs such as 2-aminoanthracene and 2-acetylaminofluorene, acetaminophen, antipyrine, caffeine, 7-ethoxyresorufin, lidocaine, phenacetin, aflatoxin B1, theophylline, and *R*-warfarin (Bozina *et al*., 2009). CYP1A2 metabolizes BaP only to a limited degree (Shimada *et al*., 1996) and while CYP1A2 is inducible in rodent lungs, it is not clear whether it is significantly expressed in human extrahepatic tissues (Uno *et al*., 2006).

At least 16 polymorphic variants have been identified in CYP1A2, both in coding and untranslated regions (Ingelman Sundberg *et al*., http://www.cypalleles.ki.se/). The CYP1A2*1F allele (-163C>A) is associated with higher inducibility of CYP1A2 in smokers than non-smokers (Bozina *et al*., 2009). In addition, CYP1A2*1F (-163C>A) is associated with increased enzyme activity, while CYP1A2*1C (-3860G>A) is associated with decreased enzyme activity (MacLeod *et al*., 1998, Nakajima *et al*., 1999). Differences in CYP1A2 enzyme activities may contribute to inter-individual and inter-ethnic variations in xenobiotic metabolism and cancer susceptibility. For example, the frequency of the CYP1A2 -163C>A polymorphism is 18.3% in Africans, 6.5% in Caucasians (6.5%) and 4.2-15.9% among Asians (http://www.ncbi.nlm.nih.gov/SNP). The frequencies of the CYP1A2 -163C>A and 63C>G SNPs have been determined in Zimbabwean and Tanzanian populations but not yet in South African populations (Dandara *et al*., 2004).

Less is known about the role of CYP1A2 in cancer risk, although some studies have shown CYP1A2 variants to be associated with colorectal, pancreatic and lung cancer (Bozina *et al*., 2009). Since the effects of CYP1A2 variants on cancer susceptibility are modified by smoking, CYP1A2 may play a role in metabolic activation of tobacco smoke components.

1.5.2.4 CYP1 Knockout Mouse Models

Since the establishment of the Cyp1a1(-/-) knockout mouse model (Dalton *et al*., 2000), studies using either intraperitoneal (i.p.) or oral doses of BaP have shown that the Cyp1a1(-/-) mouse has lower survival, lower blood BaP clearance rates and higher levels of BaP-DNA adducts than the Cyp1a1(+/+) wild type mouse (Uno *et al*., 2001, Uno *et al*., 2004). These findings suggest that CYP1A1 plays more of a protective role in the intact mouse (Uno *et al*., 2004). Since CYP1B1 levels increase when CYP1A1 is absent, there may be a compensatory role by CYP1B1 in BaP metabolism (Uno *et al*., 2006).

Studies on the cyp1b1(-/-) knockout mouse line (Buters *et al*., 1999) showed that tissue damage and DNA adduct formation were similar between cyp1b1(-/-) and wild type mice, and the authors concluded that CYP1B1 is more responsible for the metabolic activation of BaP than its detoxification (Uno *et al*., 2006). The effects of oral BaP on the cyp1a1/1b1(-/-) double knockout mouse were similar to the cyp1a1(-/-) mouse, further highlighting the importance of CYP1A1 in detoxification and CYP1B1 in metabolic activation (Uno *et al*., 2006).

The establishment of a cyp1a2(-/-) knockout mouse line (Liang *et al*., 1996) allowed the effects of i.p. TCDD or oral BaP administration on CYP1A1 induction to be investigated (Liang *et al*., 1997, Uno *et al*., 2006). While hepatic CYP1A1 levels decreased after oral BaP administration (Uno *et al*., 2006), there was no difference in CYP1A1 inducibility after i.p TCDD treatment (Liang *et al*., 1997), which suggests different effects between BaP and TCDD metabolism or route of administration (Uno *et al*., 2006).

The effects of oral BaP administration in the cyp1a2/1b1(-/-) double knockout mouse showed DNA adduct levels similar to wild type mice, suggesting a rescued phenotype due to the presence of CYP1A1. The authors concluded that basal and inducible CYP1A2 plays a negligible role in the tissue damage induced by BaP (Uno *et al*., 2006). The cyp1a1/1a2(-/-) double knockout mouse exhibited the same severity of immunosuppression after oral BaP administration as the cyp1a1(-/-) mouse, which is explained by the lack of BaP detoxification by CYP1A1 (Dragin *et al*., 2008).

The effects of oral BaP treatment on the cyp1a1/1a2/1b1(-/-) triple knockout mouse were recently determined (Dragin *et al*., 2008). These mice show a rescued phenotype similar to the cyp1a2/1b1(-/-) mice, which occurs because the absence of CYP1B1 prevents damage in immune

tissues. These mice also exhibit reduced viability and altered metabolic pathways, especially in eicosanoid metabolism (Dragin *et al*., 2008). Collectively, the CYP1 knockout mouse models allow vast insight into the effects of BaP in the intact mouse.

1.6 The Aryl Hydrocarbon Receptor (AHR)

1.6.1 The AhR and AhR-Mediated Transcriptional Regulation Pathway

The AhR is a receptor for PAH ligands such as BaP and is part of a transcription factor that regulates the transcription of several XMEs. The AhR protein consists of 805 amino acids (Burbach *et al*., 1992). It is a member of the basic helix-loop-helix-Per-ARNT-Sim (bHLH-PAS) family of transcription factors owing to its bHLH and PAS domains. The bHLH region is involved in DNA binding, while the PAS region is involved in ligand binding and dimerization (Ma and Lu, 2007). The AhR contains both nuclear localization (NLS) and nuclear exit signals (NES) in its bHLH region (Kawajiri and Fujii-Kuriyama, 2007).

The schematic representation of ligand-activated AhR-mediated transcription is shown in Figure 1.13. In its unliganded state, the AhR resides in the cytoplasm in a chaperone complex consisting of two units of heat shock protein 90 (HSP90, Perdew, 1988), the immunophilin XAP2 (also known as AhR interacting protein or AIP, Meyer *et al*., 1988) and the co-chaperone p23 (Kaslauskas *et al*., 1999, Cox and Miller, 2004). Upon ligand binding, the AhR dissociates from its cytoplasmic complex and translocates into the nucleus (Pollenz and Barbour, 2000) where it binds to the AhR nuclear translocator (ARNT) to form a heterodimeric transcription factor (Whitelaw *et al*., 1993, Probst *et al*., 1993). The AhR-ARNT dimer binds to the xenobiotic response elements (XREs, also known as AhR responsive elements, AhREs, Whitelaw *et al*., 1993, Probst *et al*., 1993) in the enhancer regions upstream of its target genes. The AhR binds to the 5'TNGC-3' half site of the highly conserved XRE motif: 5'- TNGCGTG-3' (where N is any nucleotide) (Ramos *et al*., 2007).

Genes transcribed by ligand-activated AhR include CYP1A1, CYP1B1 and NQO1 (Androutsopoulos *et al*., 2009). In this way, ligands of the AhR induce their own metabolism by activating AhR-mediated transcription of Phase I and II XMEs. The AhR also plays a role in the cellular response to oxidative stress and in determining the balance between cell cycle progression and apoptosis (Nebert *et al*., 2000).

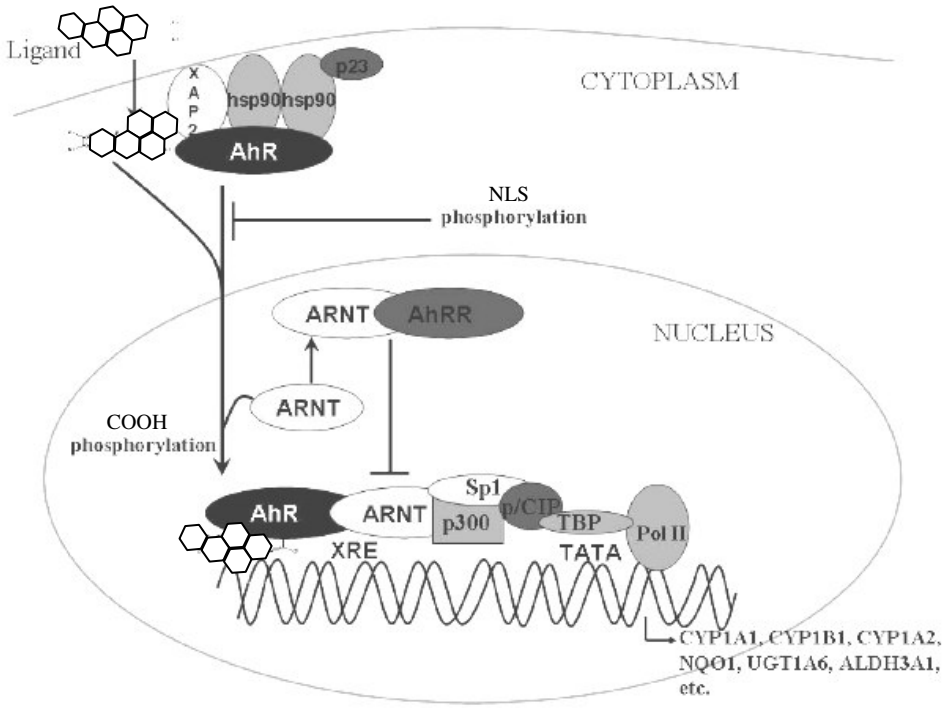

Figure 1.13 Regulation of phase I and II XME gene transcription by ligand-activated AhR. BaP passively enters the cell through the hydrophobic cell membrane. Upon binding to BaP, AhR dissociates from XAP2, HSP90 and p23 (its chaperone complex) and translocates to the nucleus. Phosphorylation of residues within its NLS inhibits AhR nuclear import, but phosphorylation of the AhR carboxy terminal is required for heterodimer formation with the ARNT. The AhR-ARNT dimer complex binds to XRE sequences upstream of target genes such as CYP1A1, and activates their transcription by recruitment of transcription initiation factors such as Sp1, p300, p/CIP, TBP and Pol II. AhR-ARNT binding to XREs is inhibited by AHRR-ARNT complexes which compete for XRE binding.
XAP2: AhR interacting protein; p23: co-chaperone; HSP90: heat-shock protein 90; AhR: aryl hydrocarbon receptor; ARNT: AhR nuclear translocator; AHRR: AhR repressor; NLS: nuclear localization signal; XRE: xenobiotic response element; CYP1A1: cytochrome P450 1A1; CYP1B1: cytochrome P450 1B1; CYP1A2: cytochrome P450 1A2; NQO1: NADPH quinone oxidoreductase; UGT1A6: uridine diphosphate glucuronosyltransferase 1A6; ALDH3A1: aldehyde dehydrogenase 3A1; Sp1: transcription factor; p300 and p/CIP: co-activators; TBP: TATA binding protein; Pol II: RNA polymerase II. (Adapted from Androutsopoulos *et al*., 2009).

1.6.2 Role of the AhR in Cancer

Substantial evidence has shown that deregulated expression and function of the AhR may play a role in carcinogenesis. AhR is overexpressed in human breast, lung and pancreatic cancers (Schlezinger *et al*., 2006, Lin *et al*., 2003, Koliopanos *et al*., 2002). In mice, a constitutively active AhR induces tumorigenesis in the stomach and promotes hepatocarcinogenesis (Andersson *et al*., 2002, Moennikes *et al*., 2004), while overexpression stimulates proliferation of A549 lung adenocarcinoma cells in culture (Shimba *et al*., 2002). At least 10 AhR polymorphic variants have

been identified; some of these are associated with increased risk of lung and breast cancer and modulate CYP activity (Chen *et al*., 2009, Bozina *et al*., 2009, Kim *et al*., 2007, Long *et al*., 2006).

The role of the AhR in BaP-initiated cancer was further substantiated when it was observed that AhR(-/-) knockout mice are protected against BaP-induced skin tumours (Shimizu *et al*., 2000). These mice are unable to induce CYP expression through the AhR and therefore BaP cannot be metabolically activated to BPDE. There is evidence of cross-talk between the AhR and other survival pathways (Puga *et al*., 2009) through direct interactions between the AhR and NFKB (Kim *et al*., 2000, Tian, 2009), estrogen receptor α (Ohtake *et al*., 2003, Matthews and Gustafsson, 2006, Wormke *et al*., 2000), glucocorticoid receptor (Dvorak *et al*., 2008), retinoblastoma protein (Puga *et al*., 2000), MAPK pathways (Tan *et al*., 2002) and the E2F1 transcription factor (Watabe *et al*., 2010). The AhR has been shown to act as both a positive and negative regulator of cell cycle progression, depending on cell type (Kawajiri and Fujii-Kuriyama, 2007, Abdelrahim *et al*., 2003). Collectively, this evidence suggests an important role for the AhR in the development of cancer.

1.6.3 The AhR Nuclear Translocator (ARNT)

The AhR heterodimerization partner, the ARNT, is a ~90 kDa protein that is also a member of the bHLH-PAS family of transcription factors. The bHLH and PAS domains are necessary for DNA binding and protein interactions, respectively (Beischlag *et al*., 2008, Reisz-Porszasz *et al*., 1994). The interaction between AhR and ARNT occurs in the nucleus and requires ligand binding to the AhR (Whitelaw *et al*., 1993, Probst *et al*., 1993, Beischlag *et al*., 2008). The ARNT binds to the 5'-GTG-3' half site of the target gene's XRE sequence prior to transcriptional activation (Ramos *et al*., 2007).

ARNT(-/-) knockout mice are not viable, but mice in which ARNT has been deleted only in adult skin epidermis are protected against BaP-initiated skin tumours (Shi *et al*., 2009). These results suggest that the ARNT is essential for BaP-associated tumour initiation (Shi *et al*., 2009). Recent evidence suggests that ARNT activity is required more during early than late stages of tumour growth (Shi *et al*., 2010). ARNT, also known as hypoxia inducible factor (HIF) 1β, also plays a role in the hypoxic response by interacting with HIF1α and HIF2α, which are known to promote

tumour growth (Shi *et al*., 2010). The ARNT therefore plays a role, together with the AhR, in mediating the effects of BaP.

1.6.4 The AhR Repressor (AHRR)

The AHRR gene has been identified in humans (Watanabe *et al*., 2001) and its transcriptional activation is regulated by the ligand-activated AhR-ARNT complex. AHRR mRNA is expressed in adult liver, breast, lung, uterus, colon, kidney, testis, ovary, adrenal gland and bladder (Tsuchiya *et al*., 2003). The AHRR is also inducible by the PAHs TCDD and 3-methylcholanthrene (3-MC) in cancer cell lines (Tsuchiya *et al*., 2003). High levels of AHRR mRNA are thought to be responsible for low PAH-inducibility of the CYP1 isoforms in HeLa cells (Tsuchiya *et al*., 2003). AHRR mRNA levels are down-regulated in various human cancer tissues, including colon, lung and breast (Zudaire *et al*., 2008).

The AHRR has been shown to repress the ability of the AhR to activate transcription of its target genes by competing with the AhR for binding to the ARNT (Mimura *et al*., 1998, Fig. 1.13). Since the AHRR has no transactivation domain, the AHRR-ARNT complex blocks transcription, thereby forming a negative feedback loop by which the AhR is regulated (Mimura *et al*., 1999). Owing to the role of the AhR in cancer, the AHRR has been suggested as a putative tumour suppressor in multiple tumour types (Zudaire *et al*., 2008). Recent evidence suggests that the AHRR may repress AhR function not by competition but by protein-protein interactions (Evans *et al*., 2008). This evidence collectively suggests that the AHRR may be important in regulation of the AhR in cancer.

1.7 Transcriptional Profiling of the Effects of BaP on Global Gene Expression

1.7.1 Microarrays as Tools for the Analysis of Whole Genome Expression

Microarray technology is a fast and easy way to examine the effects of various compounds on the expression of the approximately 37000 genes in the human genome. Microarray platforms are synthesized by different methods, such as printing or photolithography, depending on the manufacturing company. Spotted chips, often produced in-house for a laboratory's own experiment, contain DNA probes that are printed onto the array surface, whereas oligonucleotide arrays are made by attaching oligonucleotide probes to a surface such as glass or silica. Affymetrix arrays use shorter 25-mer probes (www.affymetrix.com), while Agilent arrays use longer 60-mer probes (www.agilent.com). Illumina chips are manufactured using microscopic

beads in place of a solid surface (www.illumina.com). Despite different manufacturing procedures, all microarray platforms share a common principle and can be used in different applications such as gene expression profiling, comparative genomic hybridization, or detection of single nucleotide polymorphisms (SNPs).

Through analysis of global gene expression profiling, expressed genes can be grouped according to their biological function and the cellular pathway to which they belong, which allows researchers to understand the biological context behind their expression pattern. The types of genes that are differentially expressed allow for compounds to be classified according to their therapeutic, toxicological or carcinogenic effects. Transcriptional responses to carcinogens such as BaP may give insights into their molecular mechanisms of carcinogenesis. BaP has been recognized for its carcinogenic potential for many years (IARC, 2004) but scientists are still uncovering the detailed molecular mechanisms behind how BaP exposure initiates cancer.

1.7.2 Transcriptional Profiling of the Effects of BaP and BPDE in Human Cell Lines

Since BaP may play an important role in tobacco smoking-associated cancers, scientists have used microarrays to carry out transcriptional profiling of the effects of BaP on global gene expression in various human cell lines. Microarray data has been published for the effects of BaP or BPDE on HepG2 (van Delft *et al*., 2004, Staal *et al*., 2006, Lee *et al*., 2006, Hockley *et al*., 2006, 2007, 2009, Iwano *et al*., 2010), MCF-7 (Mahadevan *et al*., 2005, Hockley *et al*., 2006, 2007, Kemp *et al*., 2006), A549 (Yoshino *et al*., 2007, Kometani *et al*., 2009), Caco-2 (de Waard *et al*., 2008), HCT116 (Hockley *et al*., 2008), TK6 (Akerman *et al*., 2004, Luo *et al*., 2005), HeLa (Yu *et al*., 2000), NHMEC (Gwinn *et al*., 2005, Keshava *et al*., 2005, John *et al*., 2008), HIOEC (Li *et al*., 2008), WI38 (Sohn *et al*., 2008), HME87 (Wang *et al*., 2003), FL (Lu *et al*., 2009), NHBE (Belitskaya-Levy *et al*., 2007), and NHEK (Perez *et al*., 2008) cell lines. The tissue origins of each cell line and the BaP or BPDE treatment conditions for each microarray are summarized in Tables 1.2 and 1.3, respectively. The differential expression of hundreds of genes in these microarrays suggests that BaP exposure has common and cell type-specific effects on gene expression patterns in human normal and cancer cell lines. To date, no microarray data is available on the effects of BaP on global gene expression in normal or cancer cell lines from the oesophagus. Microarray studies continue to uncover more about the transcriptional response to BaP exposure and contribute to our understanding of the role of BaP in carcinogenesis and cancer maintenance.

Table 1.2 List of published microarray data using normal and cancer cell lines treated with BaP

Cell line	Origin	[BaP]	Incubation	Reference
HepG2	Hepatocarcinoma	9mM	24h	Van Delft *et al*., 2004
NHMEC	Normal human mammary epithelial cells	4 μM	12h	Gwinn *et al*., 2005
NHMEC	Normal human mammary epithelial cells	4 μM	6h, 24h	Keshava *et al*., 2005
MCF-7	Breast carcinoma	0.404μg/μl	24h	Mahadevan *et al*., 2005
HepG2	Hepatocarcinoma	3, 10, 30 μM	6h	Staal *et al*., 2006
HepG2	Hepatocarcinoma	10 μM	12h	Lee *et al*., 2006
MCF-7 HepG2	Breast carcinoma Hepatocarcinoma	0.25, 1, 2.5, 5 μM	6h, 24h, 48h	Hockley *et al*., 2006
MCF-7	Breast carcinoma	5 μM	24h	Kemp *et al*., 2006
A549	Lung adenocarcinoma	1 μM	24 weeks	Yoshino *et al*., 2007
HIOEC	Human immortalized oral epithelial cells	0.1-1.2mg/l	6 months	Li *et al*., 2008
WI38	Foetal lung fibroblasts	10 μM	72h	Sohn *et al*., 2008
NHEK	Normal human epidermal keratinocytes	2 μM	24h	Perez *et al*., 2008
Caco-2	Human colorectal adenocarcinoma	1 μM	24h	De Waard *et al*., 2008
HCT116	Human colorectal carcinoma	2.5, 5 μM	6h, 24h, 48h	Hockley *et al*., 2008
NHMEC	Normal human mammary epithelial cells	4 μM	24h	John *et al*., 2008
A549	Lung adenocarcinoma	1 μM	24 weeks	Kometani *et al*., 2009
HepG2	Hepatocarcinoma	2.5, 3 μM	6h, 24h	Hockley *et al*., 2009
HepG2	Hepatocarcinoma	1, 3, 10 μM	24h	Iwano *et al*., 2010

Table 1.3 List of published microarray data using normal and cancer cell lines treated with BPDE

Cell line	Origin	[BPDE]	Incubation	Reference
HeLa	Cervical carcinoma	0.4 μM	53h	Yu *et al*., 2000
HME87	Human mammary epithelial cells	1μM	0.5h	Wang *et al*., 2003
TK6	Human lymphoblastoid cells	0.01, 0.1, 1μg/ml	4h, 24h	Akerman *et al*., 2004
TK6	Human lymphoblastoid cells	0.017, 0.034, 0.12 μM	1h	Luo *et al*., 2005
NHBE	Normal human bronchial epithelial cells	N/A	4h, 24h	Belitskaya-Levy *et al*., 2007
MCF-7 HepG2	Breast carcinoma Hepatocarcinoma	0.5, 1 μM	2h, 6h, 24h	Hockley *et al*., 2007
HCT116	Human colorectal carcinoma	0.5, 1 μM	2h, 6h, 24h	Hockley *et al*., 2008
FL	Human amnion epithelial cells	0, 0.005, 0.05, 0.5 μM	2h	Lu *et al*., 2009

1.8 Aim and Objectives of the Study

1.8.1 Aim

The aim of this project is to investigate the differential effects of BaP treatment on normal and cancer cell lines from the oesophagus, in order to further our understanding of the molecular mechanisms of BaP-associated development and maintenance of OSCC.

1.8.2 Objectives

There are 3 main objectives within the aim of comparing the effects of BaP treatment between a normal oesophageal cell line and an oesophageal cancer cell line:

(a) To investigate the effect of BaP treatment on induction of xenobiotic metabolizing genes and investigate the role of the AhR,

(b) To investigate the effect of BaP treatment on cellular proliferation and morphology, and

(c) To investigate the effect of BaP treatment on global gene transcription using microarray analysis. Within the third objective of transcriptional profiling, there are 5 sub-objectives:

(i) To determine what genes are affected by BaP treatment in normal and cancer cells,

(ii) To determine the fundamental difference in gene expression between normal and cancer cells,

(iii) To investigate whether normal cells treated with BaP become like cancer cells,

(iv) To investigate whether normal cells and cancer cells respond in the same way to BaP treatment, and

(v) To determine whether oesophageal normal and cancer cells respond to BaP treatment in the same way as other normal and cancer cell lines from published microarray data.

Chapter 2
Induction of CYP1A1 and CYP1B1 in normal and tumour oesophageal epithelial cells by benzo[a]pyrene

2.1 Introduction

In this chapter, a normal oesophageal epithelial cell line and an OSCC cell line were used as a model to further our understanding of the molecular mechanisms of tobacco smoke-associated cancer initiation and promotion in the oesophagus. The effects of the major PAH in tobacco smoke, BaP, on the expression of xenobiotic metabolism genes in oesophageal cancer cell lines were investigated. Since Phase I metabolism and therefore bioactivation of BaP to BPDE is catalyzed by CYP1A1 and CYP1B1, gene transcription, protein levels and enzyme activity of CYP1A1 and CYP1B1, and nuclear translocation of AhR and its dimerization partner ARNT in response to BaP, were investigated.

The polymorphic variants of CYP1 exhibit differential enzyme activity and may therefore influence the balance between metabolic activation and detoxification of BaP. The variants investigated in this study have been shown to be associated with increased enzyme activity (Hanna *et al*., 2000, London *et al*., 2000) as indicated in Table 2.1.

Table 2.1 Polymorphisms of the CYP1A1 and CYP1B1 genes

Gene	Position of polymorphism*	Common "low activity" allele	Polymorphic "high activity" allele	Amino acid substitution	Effect on enzyme function
CYP1A1	4889	A	G	I462V	Increased inducibility and enzyme activity
CYP1B1	4326	C	G	L432V	Increased catalytic activity

* relative to transcription start site

2.2 Results

2.2.1 CYP1 genotypes and enzyme activity of oesophageal cell lines

The genotypes for CYP1A1 (4889A>G) and CYP1B1 (4326C>G) were determined in the normal oesophageal epithelial cell line, EPC-2, in four OSCC cell lines derived from South African patients, WHCO1, WHCO3, WHCO5 and WHCO6, and in seven OSCC cell lines derived from

Japanese patients, KYSE 30, KYSE 70, KYSE 150, KYSE 180, KYSE 410, KYSE 450 and KYSE 520, using PCR-RFLP. The results are shown in Table 2.2 below.

Table 2.2 Genotypes of CYP1A1 and CYP1B1 in normal oesophageal epithelial cells and oesophageal cancer cell lines.

Cell Line	CYP1A1 (4889A>G)	CYP1B1 (4326C>G)
EPC-2	A/A	G/G
WHCO1	A/A	C/G
WHCO3	A/A	C/C
WHCO5	A/A	C/C
WHCO6	A/A	C/G
KYSE 30	A/A	C/C
KYSE 70	A/A	C/G
KYSE 150	A/G	C/C
KYSE 180	A/A	G/G
KYSE 410	A/A	C/C
KYSE 450	A/A	C/C
KYSE 520	A/A	C/G

Genotyping for the CYP1B1 4326C>G polymorphism showed that WHCO3, WHCO5, KYSE 30, KYSE 150, KYSE 410 and KYSE 450 were homozygous for the common allele (C/C), whereas WHCO1, WHCO6, KYSE 70 and KYSE 520 were heterozygous (C/G) and only EPC-2 and KYSE 180 were homozygous for the polymorphic allele (G/G). These results suggest that EPC-2 and KYSE 180 should have the highest CYP1B1 enzyme activity, the heterozygous cell lines have intermediate CYP1B1 enzyme activity and the C/C cell lines have normal or baseline CYP1B1 activity.

Genotyping for the CYP1A1 4889A>G polymorphism showed that all oesophageal cell lines are homozygous for the low activity allele (A/A), except for KYSE 150, which is heterozygous (A/G). These results suggest that most cell lines have low CYP1A1 activity, while KYSE 150 cells have intermediate CYP1A1 enzyme activity.

2.2.2 Induction of CYP1A1 and CYP1B1 mRNA by BaP in oesophageal cell lines

CYP1A1 and CYP1B1, and to a lesser extent, CYP1A2, are involved in BaP metabolism. The relative levels of these CYP1 mRNAs were therefore determined in WHCO1 (OSCC) and EPC-2 (normal) cells in response to treatment with 10μM BaP. A time course was carried out to determine (i) the time-dependent induction of the CYP1 genes by BaP and (ii) the effect of BaP withdrawal on CYP1 gene expression.

In WHCO1 cells, treatment with BaP resulted in a 10-fold and 44-fold induction of CYP1A1 mRNA at 24h and 48h, respectively, compared to the DMSO control, while subsequent removal of BaP resulted in almost no change after 1h and a 60% reduction in mRNA levels after 6h (Fig. 2.1). CYP1B1 mRNA induction was somewhat lower, with a significant 7-fold and 20-fold increase at 24h and 48h, respectively, while removal of BaP resulted in almost no change in mRNA levels after 1h and 75% reduction after 6h. CYP1A2 mRNA induction was even lower, with a 3-fold and 17-fold increase at 24h and 48h, respectively, while removal of BaP resulted in no change after 1h and an 80% decrease after 6h.

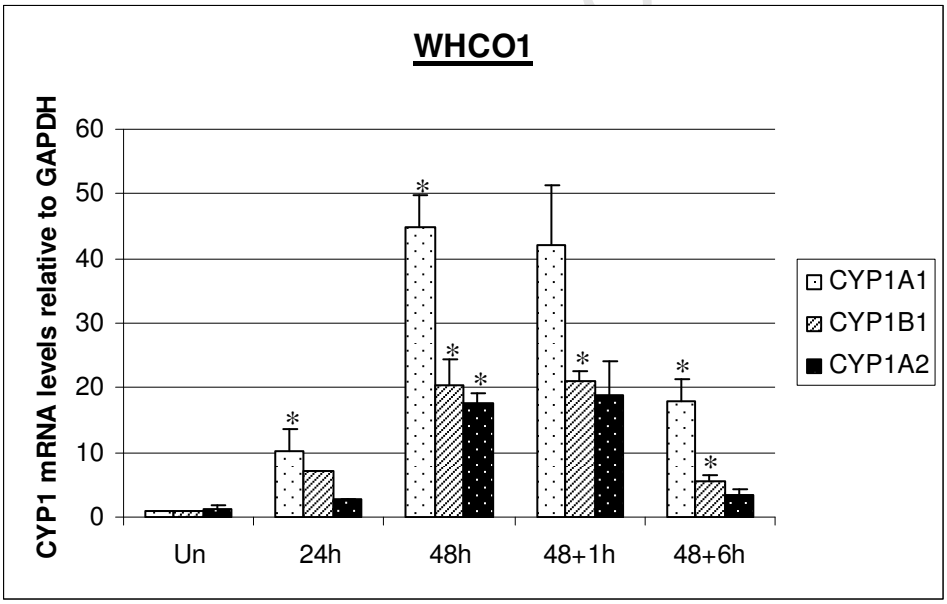

Figure 2.1 Induction of the CYP1 mRNAs in BaP-treated WHCO1 and EPC-2 cells. 7.5×10^5 of WHCO1 cells were plated in 100mm dishes and after 24 hours were treated with 10μM BaP for 24 or 48 hours as described in *Methods*. Cells treated with 0.1% DMSO for 24 hours were used as a control and are indicated as Un (untreated). To investigate reversal after withdrawal of BaP, cells were incubated in fresh medium without BaP for 1 hour or 6 hours after treatment with 10μM BaP for 48 hours. CYP1A1 and CYP1B1 mRNA levels were detected by qRT-PCR using GAPDH as a control. The data are shown as mean ± S.D. of three independent experiments. * indicates significant differences ($p \leq 0.05$) compared to untreated cells.

In EPC-2 cells, there was no induction of CYP1A1 or CYP1B1 mRNA at 48h BaP treatment; in fact mRNA levels were significantly down-regulated (Fig. 2.3). CYP1A1 and CYP1B1 mRNA were not detectable at the other time points, and CYP1A2 mRNA was not detectable at all time points in EPC-2 cells.

These results suggest that CYP1A1 and CYP1B1 mRNA are more readily inducible by BaP in oesophageal cancer cells compared to normal cells and return to basal levels occurs more rapidly in normal cells compared to cancer cells.

2.2.3 Induction of CYP1A1 and CYP1B1 protein by BaP in oesophageal cell lines

In order to confirm that the induction of CYP1 mRNA reflected an increase in CYP1 protein, the levels of cytoplasmic CYP1A1, CYP1A2 and CYP1B1 proteins in response to treatment with 10μM BaP were investigated in WHCO1 and EPC-2 cells by Western blotting.

BaP treatment of WHCO1 cells resulted in a 3.2-fold and 31.5-fold induction of CYP1A1 protein at 24h and 48h, respectively; whereas for CYP1A2 there was a much lower increase in protein levels at 1.6-fold and 18.7-fold for the same time points, while CYP1B1 protein was greatly elevated by 5.2-fold and 26.9-fold after 24h and 48h of BaP treatment, respectively (Fig. 2.2A/B). One hour after removal of BaP from the medium, CYP1A1, CYP1A2 and CYP1B1 protein levels reduced somewhat to 14.6-, 13.4- and 13.9-fold, respectively, whereas after 6h in fresh media, CYP1A1 levels declined sharply to 3.74-fold, similar to the 24h induction point, and CYP1A2 and CYP1B1 levels declined even further to 2.8- and 3.9-fold, respectively (Fig. 2.2A/B). Antibody cross-reactivity allowing detection of both CYP1A1 and CYP1A2 proteins shown in Figure 2.2A has been reported by other researchers (Lechreval *et al*., 1999, Galvan *et al*., 2005, Bao *et al*., 2002).

In EPC-2 cells, lower CYP1 protein inducibility was observed. CYP1A1 was induced 3.2-fold and 5.6-fold at 24h and 48h, respectively, while CYP1A2 levels increased by only 1.6-fold at 48h, and CYP1B1 levels increased slightly by 1.8-fold at 24h (Fig. 2.2C/D). After removal of BaP from the medium, CYP1A2 proteins returned to near basal levels, while CYP1A1 levels gradually declined to 4.2-fold at 1h and to near basal levels at 6h after BaP withdrawal (Fig. 2.2C/D). CYP1B1 levels decreased to around basal levels at 48h which was maintained at 1h after BaP withdrawal, but increased to 1.8-fold after 6h in fresh medium (Fig. 2.2C/D).

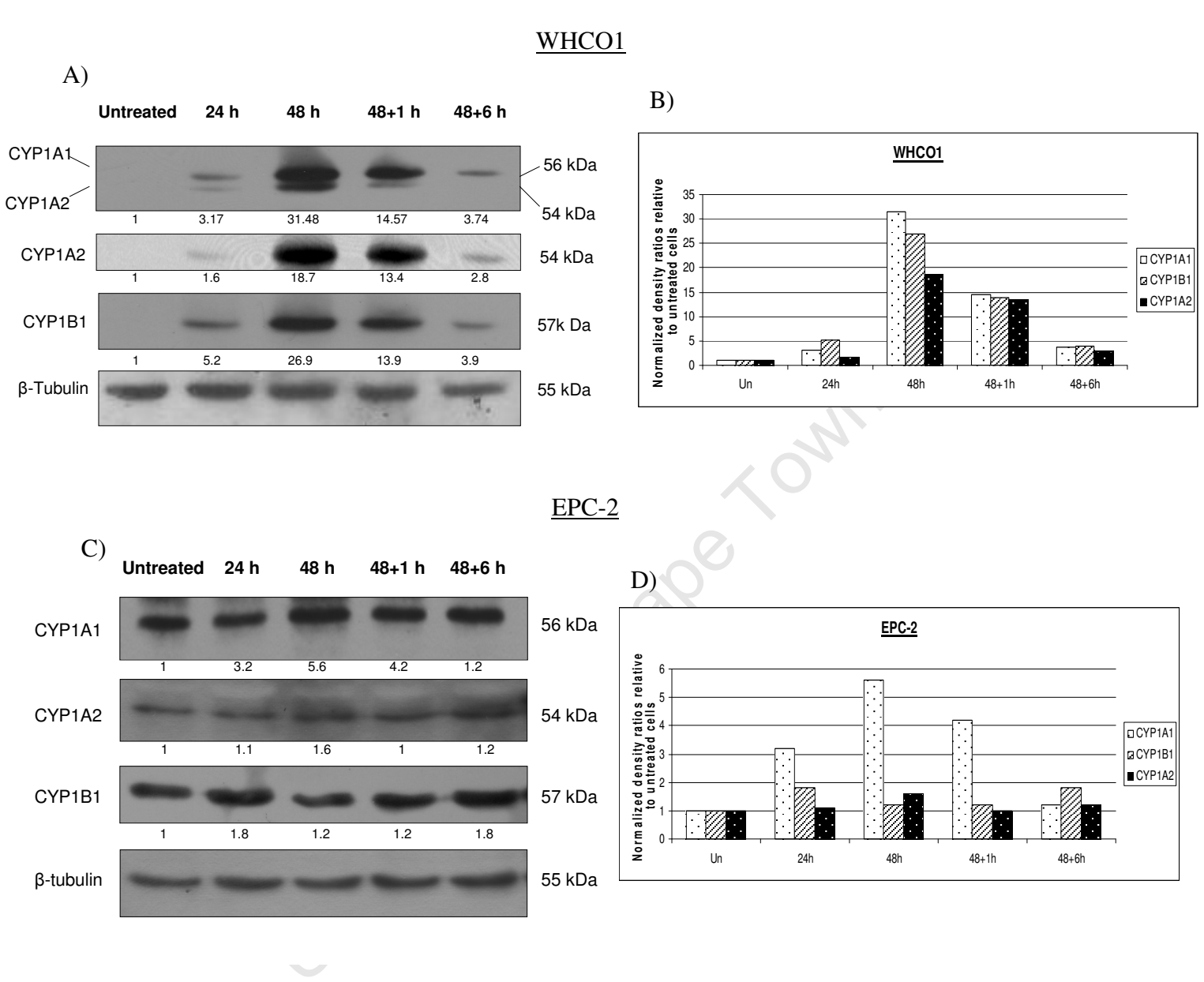

Figure 2.2 Induction of the CYP1 proteins by BaP in WHCO1 and EPC-2 cells. 1×10^6 of WHCO1 **(A)** or EPC-2 **(C)** cells were plated in 100mm dishes and after 24 hours were treated with 10μM BaP for 24 or 48 hours as described in *Methods*. Cytoplasmic extracts were separated on a 10% SDS-PAGE and probed for CYP1A1, CYP1A2 or CYP1B1. Cells treated with 0.1% DMSO for 24 hours were used as a control (Un). To investigate reversal after withdrawal of BaP, cells were incubated in fresh medium without BaP for 1 hour or 6 hours after treatment with 10μM BaP for 48 hours. β-tubulin was used as a loading control. The data represents three independent experiments. Densitometry ratios of CYP1A1, CYP1A2 and CYP1B1 protein levels normalized to β-tubulin and relative to untreated cytoplasmic extracts are indicated graphically for WHCO1 **(B)** and EPC-2 **(D)** cells and are indicated below western blots.

These results show that while basal levels of the CYP1 isoforms in WHCO1 cells were very low, they were highly inducible upon BaP treatment; whereas in EPC-2 cells these proteins were constitutively expressed at low levels but were not as inducible as in WHCO1. CYP1A2 did not appear to be playing a significant role in BaP metabolism in EPC-2 cells and therefore subsequent experiments focused on CYP1A1 and CYP1B1.

2.2.4 Analysis of CYP1 expression in WHCO and KYSE cell lines

From the results in Figure 2.1 and 2.2, it can be seen that CYP1 induction by BaP was highest at 48h BaP treatment. In order to compare CYP1A1 and CYP1B1 induction by BaP at 48h between South African patient-derived cell lines (WHCO series) and Japanese patient-derived cell lines (KYSE series), CYP1A1 and CYP1B1 mRNA and protein levels were investigated in all cell lines by qRT-PCR and Western blotting.

BaP induced CYP1A1 mRNA in all WHCO and KYSE cell lines with the exception of KYSE 520. CYP1A1 mRNA induction was highest in WHCO6 (949-fold) whereas no induction was observed in the control cells, EPC-2 (0.3-fold) and KYSE 520 (0.9-fold, Fig. 2.3A). KYSE 410 (439-fold) had the highest induction of CYP1A1 of the KYSE series, while WHCO1 CYP1A1 induction (29-fold) was comparable to the 44-fold induction at 48h in the time course (Fig. 2.1). On average, CYP1A1 mRNA levels were induced by approximately 226-fold by BaP.

CYP1B1 mRNA induction was much lower than that observed for CYP1A1, with the highest induction seen in WHCO3 (20-fold) followed by WHCO6 (14.8-fold), and again no induction was observed in EPC-2 (0.6-fold) and KYSE 520 (0.9-fold, Fig. 2.3B). KYSE 180 (11-fold) had the highest induction of the Japanese cell lines, followed by KYSE 30 (10.5-fold). On average, CYP1B1 mRNA levels underwent a 7-fold induction by BaP treatment.

The average fold change for CYP1A1 and CYP1B1 was 330- and 11-fold, respectively, in the WHCO series, and a much lower 198- and 5.5-fold induction, respectively, in the KYSE series. These results suggest that, on average, CYP1A1 and CYP1B1 mRNA were more inducible in the South African OSCC cell lines than the Japanese OSCC cell lines. A correlation between CYP1A1 or CYP1B1 genotype and mRNA induction was not evident.

A)

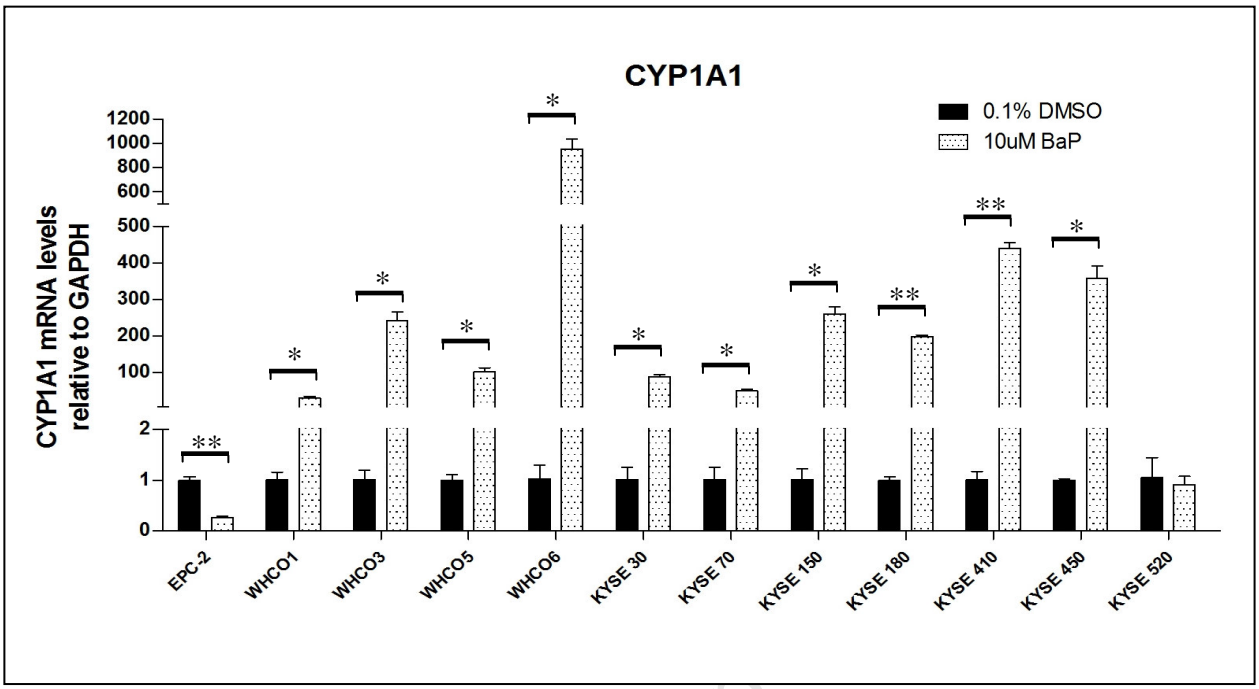

B)

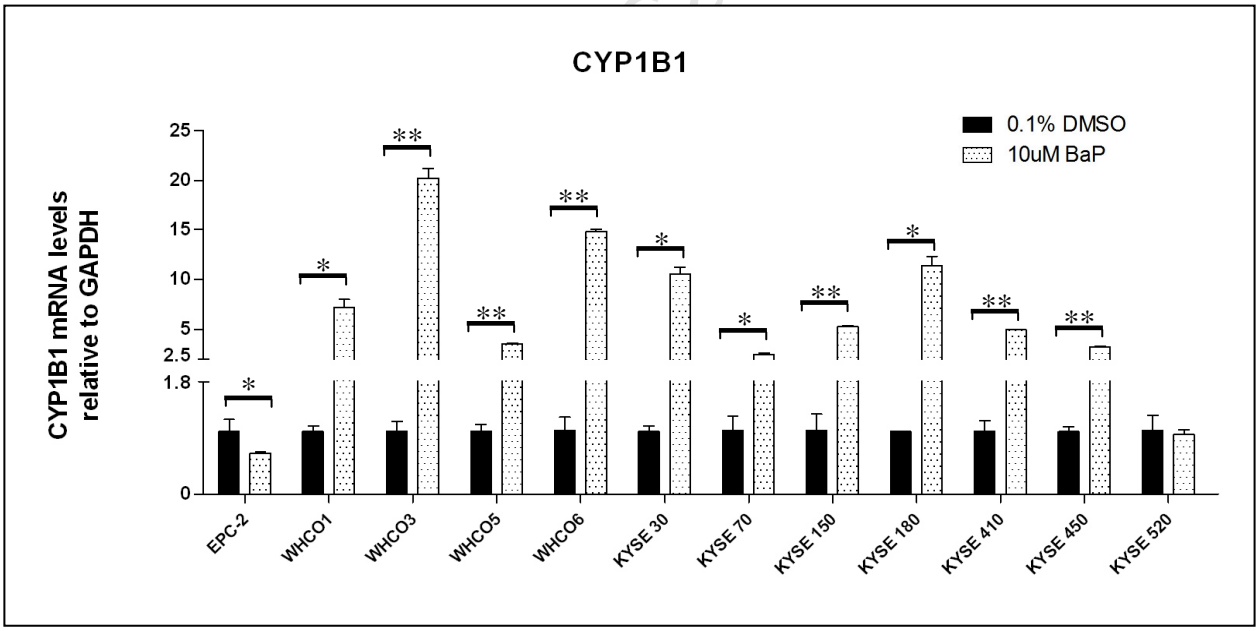

Figure 2.3 Induction of CYP1A1 and CYP1B1 mRNA in South African and Japanese oesophageal cell lines. 7.5×10^5 of EPC-2, WHCO1, WHCO3, WHCO5, WHCO6, KYSE 30, KYSE 70, KYSE 150, KYSE 180, KYSE 410, KYSE 450 and KYSE 520 cells were plated in 100mm dishes and after 24 hours were treated with 10μM BaP for 48 hours as described in *Methods*. Cells treated with 0.1% DMSO for 24 hours were used as a control (Un). CYP1A1 **(A)** and CYP1B1 **(B)** mRNA levels were detected by qRT-PCR using GAPDH as a control. The data are shown as mean ± S.D. of three independent experiments. Stars indicate significant differences (* $p \leq 0.05$; ** $p \leq 0.001$) compared to untreated cells.

The changes in CYP1A1 and CYP1B1 protein levels as investigated by Western blotting showed that protein levels also varied among the twelve cell lines (Fig. 2.4).

CYP1A1 protein induction was highest for KYSE 180 (36-fold, Fig. 2.4C) and KYSE 410 (7.5-fold, Fig. 2.4C) and lowest for KYSE 520 (0.4-fold, Fig. 2.4C). Within the WHCO series, WHCO6 had the highest induction (2-fold, Fig. 2.4B), while WHCO3 had no induction (Fig. 2.4A). CYP1A1 was induced by 2-fold in EPC-2 (Fig. 2.4A). On average, CYP1A1 protein levels were induced by 5-fold in response to BaP treatment.

As for the mRNA levels, CYP1B1 induction was lower than CYP1A1. CYP1B1 induction was highest in KYSE 30 (10.5-fold, Fig. 2.4B), KYSE 180 (7-fold, Fig. 2.4C) and KYSE 410 (6-fold, Fig. 2.4C) and lowest in EPC-2 (0.7-fold, Fig. 2.4A), KYSE 150 (0.8-fold, Fig. 2.4B) and KYSE 520 (0.7-fold, Fig. 2.4C). For the WHCO series, CYP1B1 induction was highest in WHCO1 (4-fold, Fig. 2.4A) and lowest in WHCO6 (1.7-fold, Fig. 2.4B). On average, CYP1B1 protein levels were induced 3-fold by BaP treatment.

The average induction for CYP1A1 and CYP1B1 was 1.4- and 2.6-fold, respectively, in the WHCO series, and 7.6- and 4-fold, respectively, in the KYSE series. These results suggest that there is not necessarily an association between mRNA and protein levels and that CYP1A1 and CYP1B1 protein levels were more inducible in Japanese OSCC cell lines than South African OSCC cell lines.

However, CYP1A1 mRNA and protein levels were clearly related for KYSE 410, WHCO6 and KYSE 520, while CYP1B1 mRNA and protein levels agreed for KYSE 30, KYSE 180, KYSE 520 and EPC-2. Similar to mRNA levels, an association between CYP1A1 or CYP1B1 protein levels and genotype was not evident.

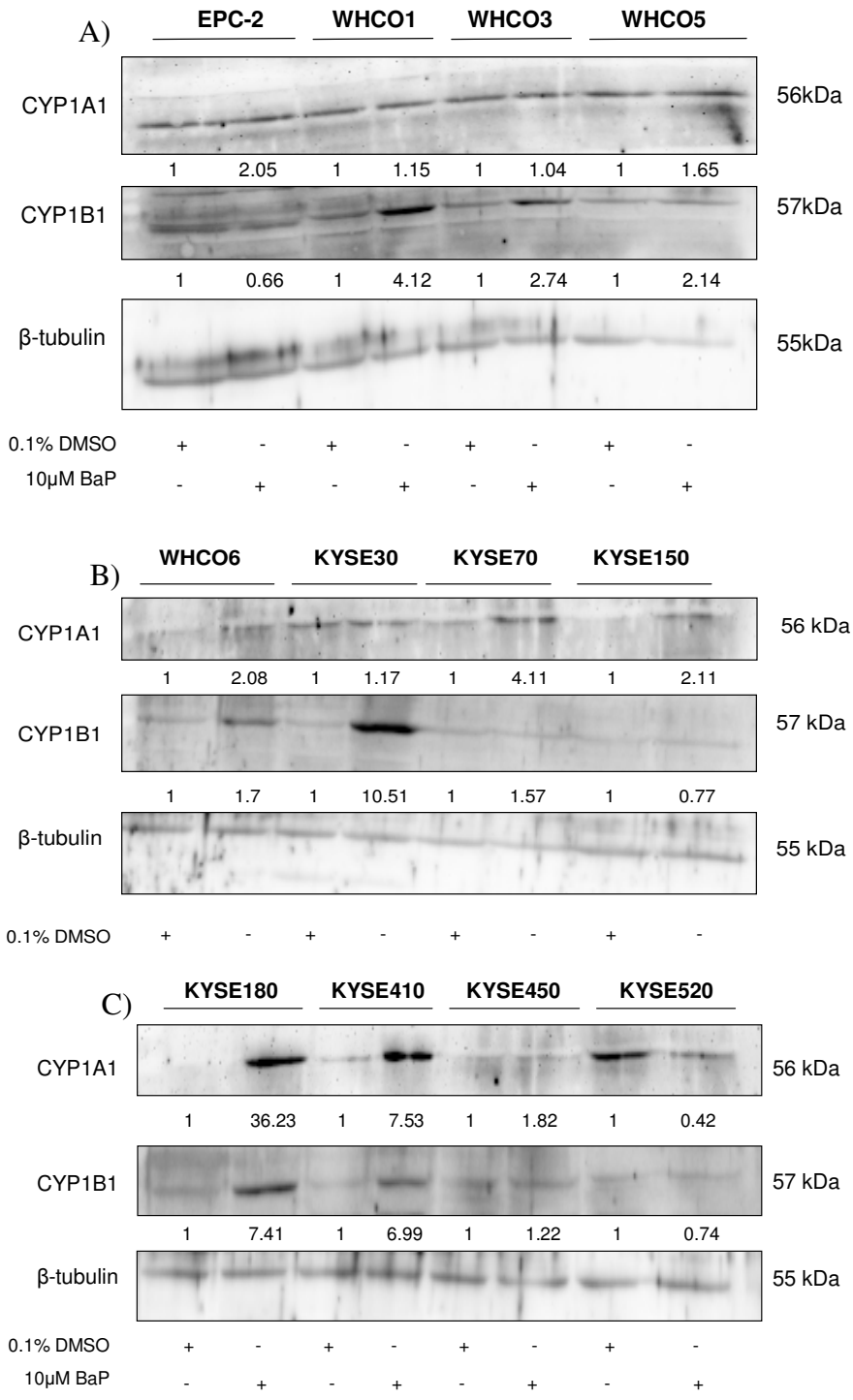

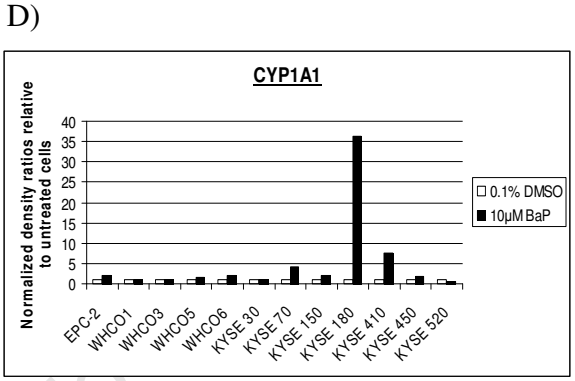

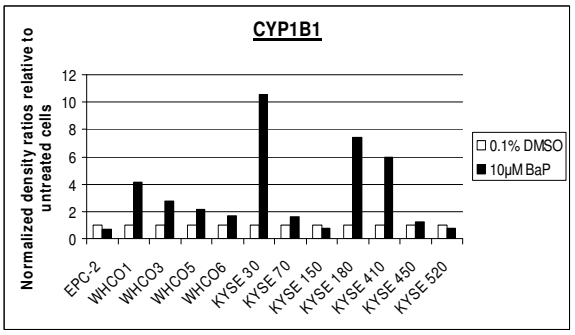

Figure 2.4 Induction of CYP1A1 and CYP1B1 protein in South African and Japanese oesophageal cell lines. 7.5×10^5 of EPC-2, WHCO1, WHCO3, WHCO5 **(A)**, WHCO6, KYSE 30, KYSE 70, KYSE 150 **(B)**, KYSE 180, KYSE 410, KYSE 450 and KYSE 520 **(C)** cells were plated in 100mm dishes and after 24 hours were treated with 10μM BaP for 48 hours as described in *Methods*. Cells treated with 0.1% DMSO for 24 hours were used as a control (Un). CYP1A1 and CYP1B1 protein levels were detected by western blotting using β-tubulin as a control. The data represents two independent experiments. Densitometry ratios of CYP1A1 and CYP1B1 protein levels relative to β-tubulin in total protein extracts from all cell lines are indicated below the western blots and graphically in **(D)** and **(E)**.

2.2.5 Induction of AhR and ARNT mRNA, protein and nuclear translocation

Since BaP is a ligand for the AhR, which together with its dimerization partner, ARNT, increases transcription of CYP1 genes in a feedback loop, the effect of BaP treatment and withdrawal on the mRNA and nuclear protein levels of the AhR and ARNT was investigated. AhR and ARNT mRNA levels were determined by qRT-PCR.

In WHCO1 cells, AhR mRNA levels increased 4-fold after 24h BaP treatment and 8.6-fold after 48h BaP treatment (Fig. 2.5A). After BaP withdrawal, AhR levels declined by 19% after 1h and by 77% after 6h. ARNT levels increased 1.5-fold and 3-fold after 24h and 48h BaP treatment, respectively (Fig. 2.5A) One hour after BaP withdrawal, ARNT mRNA levels further increased to 5-fold, but declined by 81% after 6h. Basal AhR and ARNT mRNA levels were higher than in EPC-2 cells.

In EPC-2 cells, AhR mRNA levels were significantly increased by 2.2-fold after 24h BaP treatment, which was maintained at 48h and after BaP withdrawal, AhR mRNA returned to basal levels (Fig. 2.5B). ARNT levels were significantly up-regulated by 2.4-fold after 24h BaP treatment, which was maintained at 48h BaP treatment and even 1h after BaP withdrawal (Fig. 2.5B). ARNT levels declined by 40% after 6h post BaP removal.

These results suggest that AhR and ARNT mRNA levels were higher in WHCO1 compared to EPC-2 cells. In WHCO1 cells, AhR levels follow a similar induction pattern to that of CYP1A1 and CYP1B1, while ARNT levels continued to rise even after 1h post BaP removal. In EPC-2 cells, AhR levels declined after 24h, reaching basal levels after BaP withdrawal, whereas ARNT levels reached maximum induction after 24h, which was maintained even 1h after BaP removal. The varied induction patterns may suggest differential roles for AhR and ARNT in normal and cancer cell lines.

A)

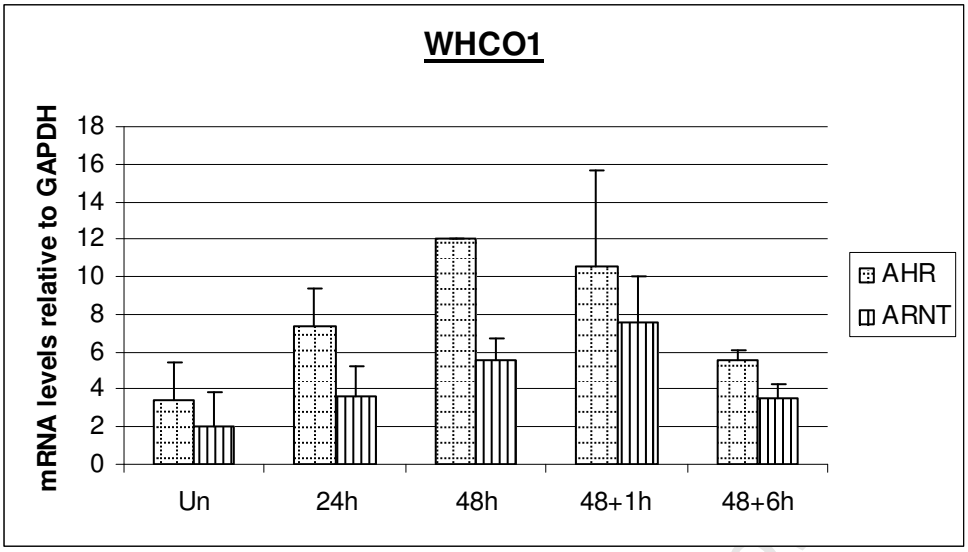

B)

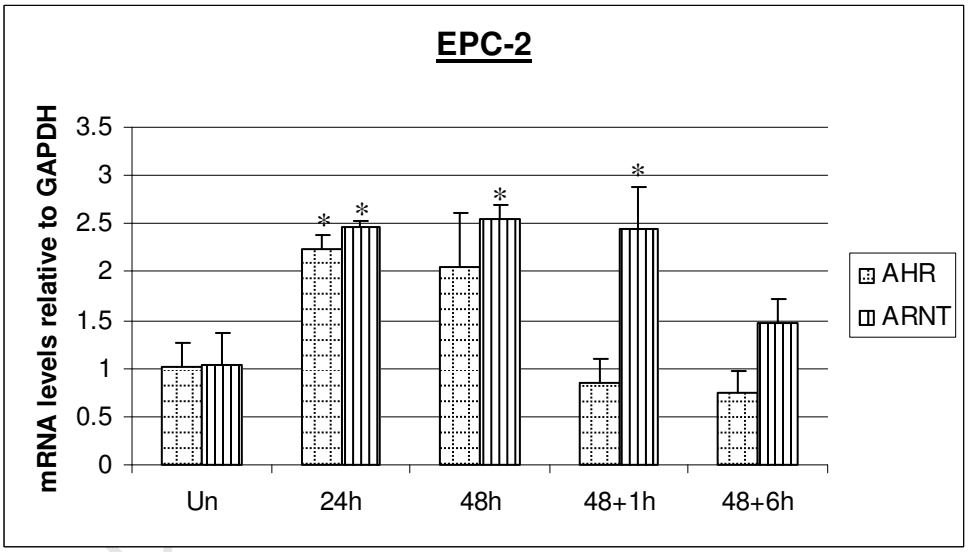

Figure 2.5 Induction of AhR and ARNT in BaP-treated WHCO1 and EPC-2 cells. 7.5×10^5 of WHCO1 **(A)** or EPC-2 **(B)** cells were plated in 100mm dishes and after 24 hours were treated with 10μM BaP for 24 or 48 hours as described in *Methods*. Cells treated with 0.1% DMSO for 24 hours were used as a control (Un). To investigate reversal after withdrawal of BaP, cells were incubated in fresh medium without BaP for 1 hour or 6 hours after treatment with 10μM BaP for 48 hours. AhR and ARNT mRNA levels were detected by qRT-PCR using GAPDH as a control, using the same samples as for Figure 2.1. The data are shown as mean ± S.D. of three independent experiments. * indicates significant differences ($p \leq 0.05$) compared to untreated cells.

In order to relate mRNA with protein levels, nuclear AhR and ARNT protein levels were determined by Western blotting.

In nuclear extracts from WHCO1 cells, there was a 1.9-fold increase in ARNT levels at 24h and a 1.4- and 3.3-fold increase in AhR and ARNT levels, respectively, at 48h (Fig. 2.6A). After removal of BaP from the medium, AhR protein levels declined to basal levels after 1h in fresh medium, whereas ARNT levels declined to 1.9-fold by 1h and remained unchanged after 6h in fresh medium (Fig. 2.6A). Cytoplasmic AhR and ARNT levels increased 1.8- and 1.7-fold, respectively, at 24h BaP treatment and then rapidly declined at 48h and after BaP withdrawal to below basal levels (Fig. 2.6B).

In EPC-2 extracts, AhR and ARNT levels were not significantly altered from basal levels at all time points (Fig. 2.6C). Lower levels of the loading control, Lamin B1, were observed in untreated cells compared to BaP-treated cells (Fig. 2.6C). Cytoplasmic AhR and ARNT levels did not change significantly (Fig. 2.6D). Although background was subtracted during densitometry analysis, it appears to be higher in blots from EPC-2 extracts. Taking this into consideration, the results should be cautiously interpreted as showing the trend that AhR and ARNT protein levels are higher in WHCO1 than EPC-2 cells.

These results suggest that Lamin B1 protein levels may be affected by BaP treatment in EPC-2 cells. In addition, nuclear AhR-ARNT levels were elevated in oesophageal cancer cells in response to BaP exposure but were not affected in normal oesophageal epithelial cells. Increased nuclear levels of AhR and ARNT in WHCO1 cells may result from increased nuclear translocation.

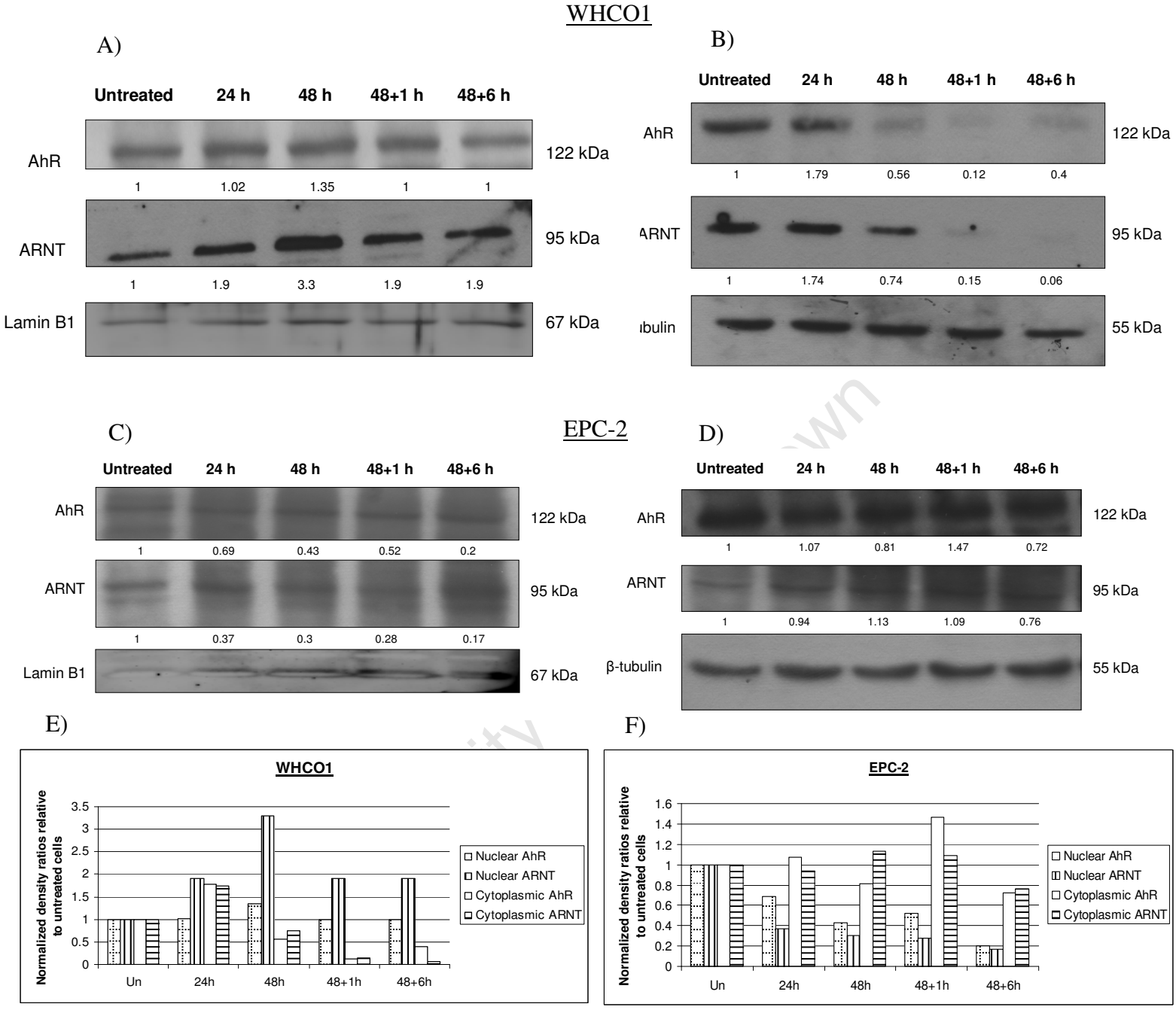

Figure 2.6 Induction of nuclear AhR and ARNT protein by BaP in WHCO1 and EPC-2 cells. 1×10^6 of WHCO1 **(A)** or EPC-2 **(C)** cells were plated in 100mm dishes and after 24 hours were treated with 10μM BaP for 24 or 48 hours as described in *Methods*. Nuclear extracts were separated on a 7% SDS-PAGE and probed for AhR and ARNT. Cells treated with 0.1% DMSO for 24 hours were used as a control (Un). To investigate reversal after BaP withdrawal, cells were incubated in fresh medium without BaP for 1 hour or 6 hours after treatment with 10μM BaP for 48 hours. Lamin B1 was used as a loading control. The data represent three independent experiments. Cytoplasmic AhR and ARNT levels at the same time points are shown in WHCO1 **(B)** and EPC-2 **(D)** cells. β-tubulin was used as a loading control. Normalized densitometry ratios of AhR and ARNT protein levels relative to untreated cells are indicated below the western blots and graphically for WHCO1 **(E)** and EPC-2 **(F)**.

In order to confirm that increased nuclear AhR and ARNT protein levels was due to increased nuclear translocation, the rate of nuclear entry and exit of AhR and ARNT in response to BaP treatment and removal was investigated in WHCO1 and EPC-2 cells using immunofluorescence.

In both WHCO1 and EPC-2 cells, both AhR and ARNT were visible at low levels in the cytoplasm in the absence of BaP (Fig. 2.7). In WHCO1 cells, AhR and ARNT showed a stronger signal in the nucleus after 24h BaP treatment, which was further increased after 48h treatment (Fig. 2.7A). In EPC-2 cells, however, AhR and ARNT accumulated in the nucleus after 24h BaP treatment and their levels were maintained at 48h (Fig. 2.7B). After BaP withdrawal and 6h growth in fresh medium, AhR and ARNT levels declined sharply in EPC-2 cells but only decreased slightly in WHCO1 cells (Fig. 2.7).

These results suggest that AhR-ARNT nuclear entry and exit occurred more rapidly in EPC-2 cells than in WHCO1 cells, and therefore that AhR-ARNT have prolonged duration in the nuclei of WHCO1 cells. These results imply that AhR-ARNT transcriptional events cease after BaP removal in EPC-2 cells but continue even after 6h in fresh medium in WHCO1 cells.

A)

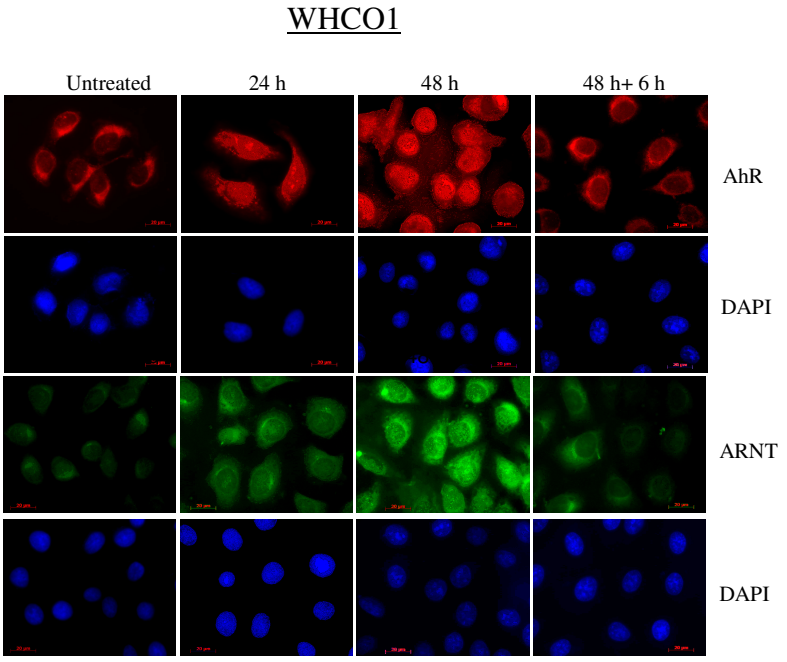

B)

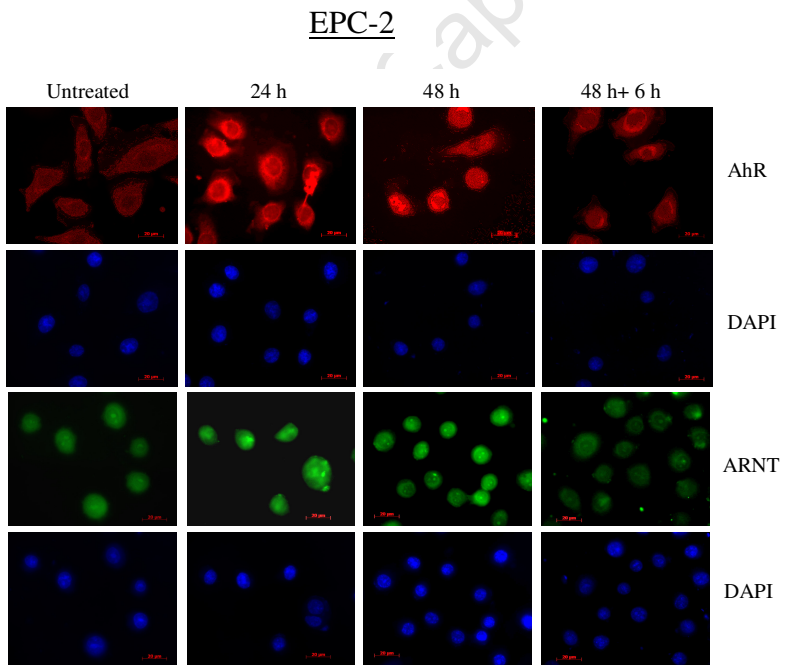

Figure 2.7 Nuclear translocation and exit of AhR and ARNT in response to BaP treatment in WHCO1 and EPC-2 cells. 0.5×10^5 of WHCO1 **(A)** or EPC-2 **(B)** cells were seeded and after 24 hours, cells were exposed to 10μM BaP for 24 hours, 48 hours, and 48 hours + 6 hours in fresh medium. Cells were incubated with anti-AhR or anti-ARNT and fluorescent-labeled secondary antibodies and visualized by fluorescent microscopy to determine cellular localization as described in *Methods*. DAPI was used to stain nuclei. The above experiment is one of three independent experiments.

2.2.6 BaP-induced changes in cellular proliferation

The above results have shown that treatment with BaP resulted in increased mRNA levels, protein levels and nuclear translocation of the AhR and ARNT in WHCO1 cells compared to EPC-2 cells. In order to determine whether the increased AhR levels and associated signaling events might enhance the proliferative potential of BaP-treated cells, cell proliferation was measured in EPC-2 and WHCO1 cells in response to 10μM BaP treatment.

Cell viability measured using the MTT assay showed significantly ($p<0.05$) increased viability in BaP-treated WHCO1 cells compared to untreated cells at 72h and 96h whereas BaP-treated EPC-2 cells showed significantly ($p<0.05$) reduced viability after 72h compared to untreated cells (Fig. 2.8A).

To confirm the MTT results and to show that the difference in cell viability was not solely due to mitochondrial reductase activity, a BrdU ELISA was carried out to measure DNA synthesis in treated and untreated cells. These results showed no significant difference between untreated and BaP-treated WHCO1 cells, but indicated significantly reduced cell division in BaP-treated compared to untreated EPC-2 cells at 72h, 96h ($p<0.001$) and 120h ($p<0.05$) of BaP exposure (Fig. 2.8B).

Cell proliferation was also measured over 5 days (Fig. 2.8C). BaP treatment resulted in reduced cell number for both WHCO1 and EPC-2 cells compared to untreated cells (Fig. 2.8C). Cell number was significantly reduced by BaP treatment at 96h for both WHCO1 ($p<0.05$) and EPC-2 ($p<0.001$) and at 120h for EPC-2 cells ($p<0.05$, Fig. 2.8C). The increased MTT activity is possibly accounted for by increased metabolism in BaP-treated WHCO1 cells, despite the lower cell number.

These results suggest that WHCO1 cells were resistant to BaP-induced reduction in cell growth and continued to grow almost normally in the presence of BaP, whereas EPC-2 cells were sensitive to BaP-associated cell growth reduction and showed lower cell viability, cell division and cell number in the presence of BaP.

A)

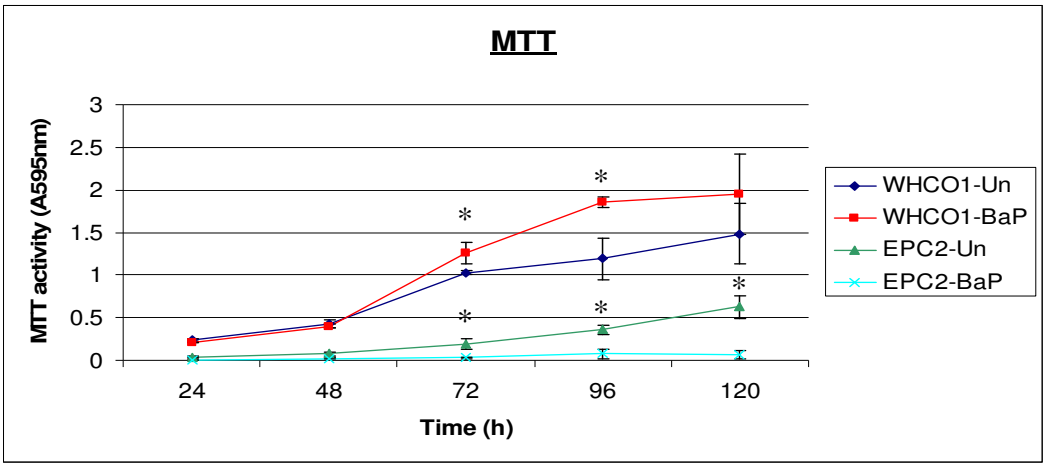

B)

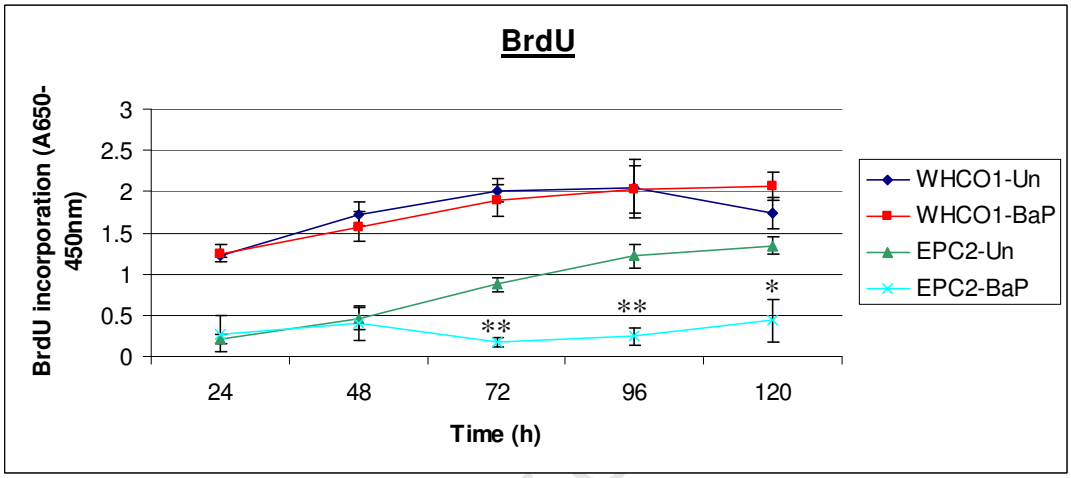

C)

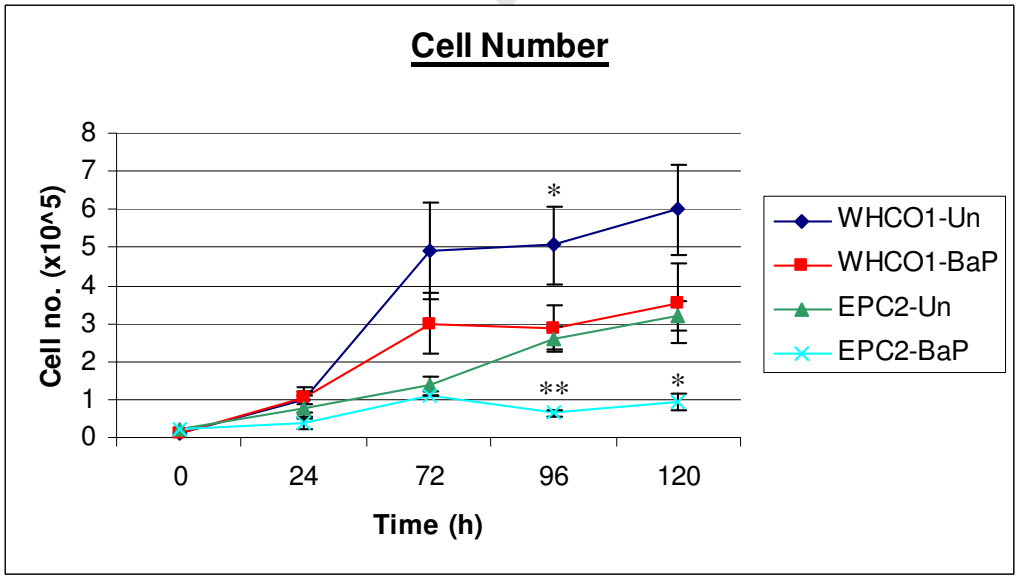

Figure 2.8 Changes in cellular proliferation of WHCO1 and EPC-2 cells induced by BaP treatment. 2 x 10^3 of WHCO1 and EPC-2 cells were seeded in 96-well plates and after 24 hours were treated with either 0.1% DMSO (Un) or 10µM BaP (BaP) for 1, 2, 3, 4 or 5 days as described in *Methods*. ♦ WHCO1 cells treated with 0.1% DMSO. ■ WHCO1 cells treated with 10µM BaP. ▲ EPC-2 cells treated with 0.1% DMSO. **x** EPC-2 cells treated with 10µM BaP. **(A)** Measurement of cellular proliferation using the MTT assay. **(B)** Measurement of cellular proliferation using the BrdU ELISA. **(C)** Growth curve of WHCO1 and EPC-2 cells. The data shows mean ± S.D. of three independent experiments. * indicates significant differences (* $p<0.05$, ** $p<0.001$) compared to untreated cells.

2.2.7 Effects of long-term BaP treatment on EPC-2 cell morphology

Previous studies have shown that prolonged BaP or BPDE treatment can lead to the transformation of normal cell lines (Du *et al*., 2006, Ouyang *et al*., 2007, Srivastava *et al*., 2007, Ding *et al*., 2009). Since transformed cells exhibit altered cell morphology, EPC-2 cells exposed to BaP for prolonged periods were monitored by phase contrast microscopy.

Compared to untreated cells (Fig. 2.9A), after the first 48h BaP treatment, some cells displayed an elongated shape (Fig. 2.9B, arrows) and while some cells appeared to have recovered to a normal shape after one week's growth in BaP-free media, all cells were smaller and some had started to lose adhesion to the plate, an indication of cell death (Fig. 2.9C, arrows). After a second BaP treatment, cells again exhibited an elongated shape (Fig. 2.9D, arrows) which was still apparent in cells after one week's growth in BaP-free media, despite recovery of most cells to their original round shape (Fig. 2.9E, arrows).

After a third round of BaP treatment, cells were either elongated or round with evidence of cell shrinkage and membrane blebbing, an indication of cells undergoing apoptosis (Fig 2.9F, arrows). After one week following the final BaP treatment, most cells had blebbing cell membranes and had rounded and lost adhesion (Fig. 2.9G, arrows).

These results suggest that EPC-2 cells exposed to prolonged treatment with BaP had altered morphology, which was represented by the loss of integrity of their cell membranes and change in shape from round to elongated. This implies that BaP is toxic to the cells and links with the cell proliferation experiments in Figure 2.8, where BaP-treated EPC-2 cells decreased their growth rate over 5 days compared to untreated cells. WHCO1 cells showed no change in morphology during BaP treatment.

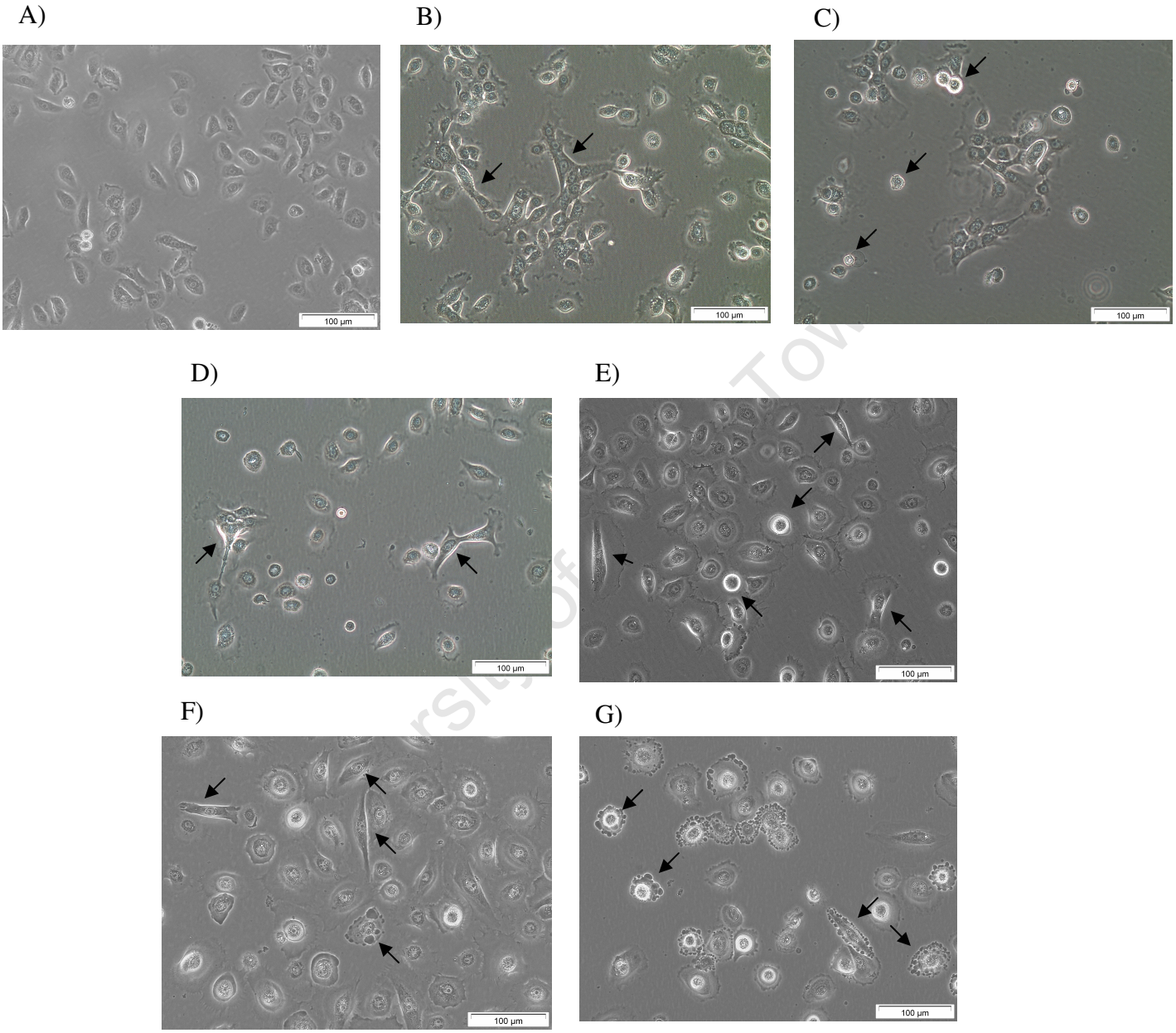

Figure 2.9 EPC-2 cell morphology changes during prolonged BaP treatment. EPC-2 cells were treated with 10µM BaP for 48 hours followed by incubation in media without BaP for one week. The same cells were then treated again with 10µM BaP for 48h followed by incubation in media without BaP for another week. The same cells were treated a third time and grown for a third week. Cells were split as necessary during the weeks of incubation in BaP-free media. Phase contrast photographs were taken at 20x magnification directly before BaP treatment **(A, C, E, G)** after 7 days growth and directly after 48h in BaP-containing media **(B, D, F)** before incubation in fresh media, as described in *Methods*. Photographs are representative of whole dishes. Scale bar indicates 100µm.

2.3 Discussion

This study compared the response of oesophageal cancer cell lines and a normal oesophageal epithelial cell line to treatment with the tobacco smoke procarcinogen BaP and explored differences in CYP1 genotype, CYP1 mRNA and protein induction, AhR-ARNT nuclear translocation and cellular proliferation between WHCO1 and EPC-2 cells. This work may contribute to our understanding of BaP-associated oesophageal cancer promotion and carcinogenesis.

It should be noted that a limitation of this study is the use of only one control cell line. While other normal human oesophageal epithelial cell lines exist, they were difficult to obtain for this study. The influence of telomerase immortalization on the observed results can be ruled out, since EPC-2 cells share the biochemical, morphological and cytogenetic properties of normal oesophageal epithelium (Lim *et al*., 2009) and have functional p53 and Rb pathways (Harada *et al*., 2003). EPC-2 cells therefore represent normal oesophageal cells and may give an indication as to how the normal epithelium might respond to BaP treatment.

2.3.1 CYP1 polymorphisms

CYP1A1 and CYP1B1 are the primary enzymes involved in the metabolic activation of BaP to its carcinogenic metabolite BPDE. The polymorphic variants in CYP1A1 (4889A>G) and CYP1B1 (4326C>G) have been shown to encode enzymes with increased catalytic activity compared to the common alleles. Furthermore, these polymorphisms have also been associated with increased risk of cancer in various extra-hepatic tissues. These findings form the basis of our interest in their potential role in the development of OSCC as a result of BaP exposure from tobacco smoke. We hypothesize that the high activity alleles of CYP1A1 and CYP1B1 would metabolically activate BaP to BPDE at a faster rate during Phase I metabolism, and that the resulting high levels of BPDE would enhance the risk of developing cancer.

While the CYP1A1 4889A>G polymorphic variant was only present in KYSE 150, the genotypes for the CYP1B1 4326C>G polymorphism were shown to vary among the WHCO, KYSE and EPC-2 cell lines. It was not unexpected that all four WHCO cell lines possessed the CYP1A1 A/A genotype, given that the frequency of this polymorphism is high in African populations (http://www.ncbi.nlm.nih.gov/SNP), thereby suggesting that metabolic activation by CYP1A1 may not be important in WHCO cell lines. Similarly, the CYP1B1 C/G genotype occurred in four of seven KYSE cell lines, which agrees with the evidence that the frequency of this genotype is

highest in Asian populations (http://www.ncbi.nlm.nih.gov/SNP). The varied distribution of the CYP1B1 4326C>G polymorphism in these twelve cell lines suggests that the role of CYP1B1 in the metabolic activation of BaP may be more important than CYP1A1. Although other studies have linked these polymorphic sites to increased catalytic activity, CYP1A1 and CYP1B1 enzyme activity was not directly measured. One should consider methods of measuring CYP1A1 and CYP1B1 enzyme activity, such as the 7-ethoxyresorufin O-deethylase (EROD) assay, either in intact cells (Donato *et al*., 1993) or in microsomal extracts (Burke and Mayer, 1974). Enzyme activity may also be influenced by other polymorphic sites in the CYP1A1 gene, either alone or in combination, for example, the 3801T>C *Msp*I polymorphism, which is also linked with increased enzyme inducibility and risk for lung and breast cancer (Zhou *et al*., 2009).

Since CYP1B1 genotypes varied greatly between cell lines, it is possible that CYP1B1 may be playing a more important role in BaP bioactivation than CYP1A1, especially in the two high activity cell lines, EPC-2 and KYSE 180. The high CYP1B1 activity in EPC-2 cells suggests that normal cells may metabolically activate BaP more rapidly than cancer cells; however a generalization cannot be made since this study is limited by the use of only one normal cell line. CYP1B1 enzyme activity can also be assessed using the EROD assay, however not in our intact cell model since the assay cannot distinguish between the relative contributions made by CYP1A1 and CYP1B1, except for the observation that CYP1B1 is inhibited by lower concentrations of the CYP1 inhibitor, αNF (McFadyen *et al*., 2004).

Our hypothesis is based on the concept that increased Phase I enzyme activity would result in an imbalance between metabolic activation and detoxification and an accumulation of BPDE that eventually results in carcinogenesis. However, researchers in the field argue that *in vitro* experiments such as this one do not accurately reflect the coupling between Phase I and II metabolism that occurs within intact animals (Nebert *et al*., 2004; Nebert and Dalton, 2006). Indeed, in our experiments, the focus is on Phase I metabolism by the CYP1 family only. The total detoxification of a xenobiotic such as BaP depends on the rate of both oxidation and conjugation reactions. If metabolic activation by CYP1 occurs rapidly and is coupled to rapid conjugation, then there should be efficient detoxification and removal of the harmful products. However, if rapid metabolic activation by CYP1 is coupled to slow conjugation, then there is an accumulation of the reactive intermediate (BPDE) which then binds to DNA and forms mutagenic adducts that can initiate cancer. Therefore, high activity CYP1 enzymes coupled with low activity Phase II enzymes or null allele Phase II genes should infer increased risk to OSCC development from gene-environment interactions.

Although it is possible to genotype the polymorphic alleles in candidate Phase II genes and infer the balance between metabolic activation and detoxification within our cell line model, more precise conclusions can be made about BaP detoxification and coupling between Phase I and II metabolism through population-based case-control studies. Previous research in our laboratory has investigated the role of polymorphisms within several Phase I and Phase II detoxification genes and risk of OSCC associated with cigarette smoking and alcohol consumption (Table 1.1). Polymorphic phase I genes investigated include CYP2E1 (7632T>A) and CYP3A5 (6986A>G), while phase II genes analyzed include SULT1A1 (638G>A), GSTM1 (*0), GSTT1 (*0) and GSTP1 (341 C>T).

Results from our laboratory have shown that in South African populations, the CYP1A1 4889A>G and CYP1B1 4326C>G polymorphisms may play a role in the development of smoking-associated OSCC (Li *et al*, unpublished results). The CYP1A1 polymorphism together with smoking status was marginally associated with increased risk of OSCC in the South African Mixed Ancestry population. This is consistent with studies carried out in French, Japanese and North American populations, but not in Chinese (Bartsch *et al*., 2000; Abbas *et al*., 2004; Suzuki *et al*., 2004; Wideroff *et al*., 2007). In contrast, the CYP1B1 polymorphism was associated with reduced risk of OSCC in the Mixed Ancestry population. This finding has not been reported in any other studies, although no significant association was found between the CYP1B1 Val432Leu polymorphism and OSCC risk in a Chinese population (Wang *et al*., 2006). Since the CYP1B1 4326C>G polymorphism is associated with increased risk in other cancers, these results may reflect differences in sample size and ethnic genetic variation.

2.3.2 Induction of CYP1A1 and CYP1B1 mRNA and protein by BaP

The tissue-specific expression patterns of CYP1A1 and CYP1B1 are thought to directly affect the balance between detoxification and metabolic activation of procarcinogens such as BaP and therefore influence BaP toxicity and carcinogenicity (reviewed by Nebert and Dalton, 2006, Shimada and Fujii-Kuriyama, 2004). From extensive research using cyp1a1(-/-), cyp1b1(-/-), cyp1a2(-/-) single knockout mice, cyp1a1/1a2(-/-), cyp1a2/1b1(-/-), cyp1a1/1b1(-/-) double knockout mice and cyp1a1/1a2/1b1(-/-) triple knockout mice, it has been demonstrated that CYP1A1 plays a more protective role in detoxification of BaP, whereas CYP1B1 plays a more important role in metabolic activation in the intact animal (Uno *et al*., 2004, 2006, Dragin *et al*., 2008).

Other studies using animal or cell line models have shown that expression of CYP1A1 and CYP1B1 mRNA and protein is induced by BaP in various normal and cancer tissue types, but that CYP induction varies greatly.

mRNA quantification showed that BaP-induced CYP1A1 levels ranged from 1.5-fold in ACHN (renal carcinoma), A549 (lung adenocarinoma) and NEC14 cells (testis embryonal carcinoma, Iwanari *et al*., 2002) to 110-fold in BEP2D cells (human immortalized bronchial epithelium, Uppstad *et al*., 2010). In WHCO1 cells, CYP1A1 was induced 10-fold by BaP at 24h, which is similar to CYP1A1 induction in HepG2 (hepatocarcinoma, 11-fold, Iwanari *et al*., 2002) and rat liver cells (11.3-fold, Harrigan *et al*., 2006). In EPC-2 cells, CYP1A1 was induced 6-fold by BaP at 48h, which is most similar to CYP1A1 induction in HepG2 cells (7.5-fold, Wen *et al*., 2005). Different induction of CYP1A1 in HepG2 cells can be explained by different BaP concentrations, despite having the same duration of treatment: HepG2 cells were treated for 24h with 5μM BaP (Iwanari *et al*., 2002), or with 1μM BaP (Wen *et al*., 2005), correlating with higher CYP1A1 mRNA induction and lower induction, respectively.

BaP-induced CYP1B1 mRNA levels ranged from 1.5-fold in NEC14 cells (Iwanari *et al*., 2002) and 1.7-fold at 24h in EPC-2 cells, to 40-fold in NHMECs (normal human mammary epithelial cells, Keshava *et al*., 2009). In WHCO1 cells, CYP1B1 induction at 24h by BaP was 7-fold, which is similar to CYP1B1 induction in MCF-10A (human mammary epithelium, 6-fold, Chang *et al*., 2010) and NHMECs (8.7-fold, Keshava *et al*., 2005). In EPC-2 cells, CYP1B1 induction was 20-fold at 48h by BaP, which is similar to CYP1B1 induction in LS-180 (colon carcinoma, 20-fold, Iwanari *et al*., 2002) and BEP2D cells (19-fold, Uppstad *et al*., 2010). Different fold induction of CYP1B1 in NHMECs resulted from different BaP treatment periods, despite treatment with the same BaP concentration: NHMECs were treated with 4μM BaP for 12h (Keshava *et al*., 2005) or 24h (Keshava *et al*., 2009), which relates to lower CYP1B1 mRNA induction and higher induction, respectively.

CYP1A1 and/or CYP1B1 mRNA induction is increased by BaP treatment in MSK-Leuk1 (oral leukoplakia) and KYSE 450 cells (OSCC, Hughes *et al*., 2008), RL95-2 (human endometrial epithelium, Bao *et al*., 2002), SCC449 cells (OSCC, Port *et al*., 2004) and OVCA (ovarian carcinoma, Leung *et al.*, 2006). Since the fold induction was not quantified, no comparisons can be made to our data in WHCO1 and EPC-2 cells.

CYP1A1 protein levels are elevated by BaP treatment of MSK-Leuk1, KYSE 450 (Hughes *et al*., 2008), HOSE (human ovarian surface epithelium, Leung *et al*., 2006), HepG2, SCC-9 (human oral epithelial squamous cell carcinoma, Wen and Walle, 2005, Wen *et al*., 2005) and rat liver cells (Umannova *et al*., 2008), although no quantification was done. Similarly, quantification of increased CYP1B1 protein levels in SCC449 (Port *et al*., 2004), MSK-Leuk1, KYSE 450 (Hughes *et al*., 2008) and SCC-9 cells (Wen and Walle, 2005) was not carried out. Interestingly, CYP1B1 protein was not detected in mouse liver and lung (Galvan *et al*., 2005) or HepG2 cells (Wen *et al*., 2005). These observations are difficult to compare to our findings of increased CYP1A1 and CYP1B1 protein levels by BaP treatment in WHCO1 and EPC-2 cells.

Collectively, these results suggest that CYP1A1 and CYP1B1 mRNA and/or protein induction are cell-, tissue- and species-specific. Our data is consistent with the observations in other cell lines and animal models which show that BaP-induced CYP1 mRNA levels and protein levels are linked with each other. In addition, our data agrees with the generalization that CYP1 induction by BaP appears to be greater in cancer cell lines than in normal or immortalized cell lines. Higher levels of CYP1 mRNA and protein in cancer cells should make these cells more capable of metabolically activating BaP to DNA-damaging metabolites than normal cells.

When comparing CYP1A1 and CYP1B1 inducibility in OSCC cell lines from different ethnic origins, our results showed that CYP1 induction by BaP was on average higher in South African OSCC cell lines than Japanese OSCC cell lines. The differential CYP1 mRNA and protein induction patterns could contribute to inter-population differences in BaP metabolism and detoxification, and therefore susceptibility to tobacco smoking-associated OSCC.

mRNA and protein levels did not clearly associate with the genotypes for the CYP1A1 4889A>G and CYP1B1 4326C>G polymorphic sites. The absence of a simple relationship suggests that the link between CYP1 inducibility and genotype – inferring enzyme activity – is more complex than can be demonstrated here.

A possible explanation for the diverse inducibility patterns of CYP1A1 and CYP1B1 is their regulation through epigenetic mechanisms, particularly gene or promoter methylation (Nakajima *et al*., 2003). Aberrant DNA methylation occurs frequently in cancer and while hypermethylation is associated with gene silencing, hypomethylation is linked to gene over-expression (Esteller, 2007). Interestingly, CYP1B1 is hypomethylated and overexpressed in prostate cancer (Tokizane *et al*., 2005) but is downregulated by promoter methylation in colorectal cancers (Habano *et al*.,

2009, Kang *et al*., 2008). CYP1B1 is also down-regulated by methylation in HepG2 cells (Beedanagari *et al*., 2010), while CYP1A1 is possibly down-regulated by methylation in HeLa cells (Nakajima *et al*., 2003). Therefore the epigenetic regulation of CYP1B1 may contribute to the metabolic activation and carcinogenicity of BaP.

CYP1A2, primarily a hepatic enzyme, has been shown to be expressed to a limited degree in extra-hepatic tissues including the oesophagus (Lechevral *et al*., 1999). However, metabolism of BaP by CYP1A2 is thought to be negligible (Shimada *et al*., 1996; Shimada and Fujii-Kuriyama, 2004) and instead CYP1A2 plays a more important role in the metabolic activation of other procarcinogens. CYP1A2 mRNA and protein were shown to be mildly inducible in WHCO1 cells, and while CYP1A2 mRNA was not detectable in EPC-2 cells, CYP1A2 protein was maintained at low constitutive levels. The inability to detect CYP1A2 mRNA in EPC-2 cells is consistent with undetectable CYP1A2 mRNA in ACHN, A549, NEC14 and HeLa cells (Iwanari *et al*., 2002). CYP1A2 protein was not detected in SCC-9 cells (Wen and Walle, 2005), but was constitutively expressed in HepG2 cells (Wen *et al*., 2005). These results, together with our data, show that CYP1A2 expression may not play an important role in the metabolic activation of BaP in the oesophagus.

2.3.3 Nuclear translocation of AhR and ARNT in response to BaP

A role for the AhR has clearly been demonstrated in carcinogenesis and BaP-associated carcinogenesis (Dietrich and Kaina, 2010, Nebert *et al*., 2004, Beischlag *et al*., 2008, Kawajiri and Fujii-Kuriyama, 2007, Marlowe and Puga, 2005). The effects of BaP treatment on AhR and ARNT mRNA and protein levels and nuclear translocation rate may provide insight into why EPC-2 and WHCO1 cells have different CYP1 induction capacities when exposed to BaP. This work is the first to describe the effect of BaP treatment and withdrawal on the rate of AhR and ARNT nuclear translocation in oesophageal normal and tumour cells.

Since the ligand-activated AhR, together with the ARNT, functions as a transcription factor, it was not surprising to see an increase in their nuclear translocation after treatment with BaP. Our results are consistent with the nuclear translocation of the AhR in Hepa1c1c7 cells after exposure to TCDD or BaP quinone (BPQ, Burczynski and Penning, 2000). After 90min treatment, nuclear translocation of the AhR was evident in TCDD- or BPQ-treated cells, but not in BPDE-treated cells (Burczynski and Penning, 2000). Since our work only assessed translocation after 24h, future work could investigate nuclear translocation at earlier time points (between 90min and

24h), and use other methods of monitoring translocation, such as tagging the AhR and ARNT with the green fluorescent protein (GFP) reporter.

From our results, we hypothesize that the prolonged duration of the AhR in the nuclei of WHCO1 cells may lead to sustained AhR signaling – and therefore CYP1 induction – in WHCO1 cells, whereas in EPC-2 cells, the rapid nuclear exit of the AhR and ARNT may lead to shorter AhR signaling – and therefore reduced CYP1 induction. The AhR also cross-talks with other signaling pathways involved in cell proliferation and apoptosis, including MAPK cascades (Puga *et al*., 2009, Beischlag *et al*., 2008). The AhR has been shown to interact, either directly or indirectly, with NFκB, ERα, GR, Rb and E2F. Differences in AhR signaling may help explain why EPC-2 and WHCO1 cells showed differences in CYP1 induction, AhR-ARNT nuclear translocation and cellular proliferation in response to BaP.

The complete metabolism of BaP generates many other BaP metabolites (Fig. 1.7) which may serve as AhR ligands that sustain AhR activation (Spink *et al*., 2008). BaP ultimately initiates cancer through the action of its carcinogenic metabolite, BPDE, however the other metabolites generated may play an important role in CYP1 induction, AhR activation and nuclear translocation, and cell proliferation. BaP metabolites could also have different specificity for the AhR. There is already evidence that structurally diverse PAHs and inducers have varied effects on CYP1 induction potency. For example, in a range of cell lines, CYP1A1 and CYP1B1 are induced at higher levels by TCDD and 3-MC than by BaP, which itself has a higher induction potency than 6-nitroBaP (Iwanari *et al*., 2002). The complete effects of BaP treatment in EPC-2 and WHCO1 cells are therefore also mediated by the formation of AhR-activating BaP metabolites. Although CYP1 induction is dependent on the AhR and ARNT, BaP biotransformation and the formation of BPDE-DNA adducts still occur in AhR(-/-) knockout mice (Sagredo *et al*., 2006). These mice still had significant basal CYP1B1 levels that were not affected by BaP treatment, so BaP activation was most probably attributable to basal CYP1B1 activity (Sagredo *et al*., 2006).

AhR and ARNT mRNA and protein levels were much higher in WHCO1 compared to EPC-2 cells. Decreased AhR and ARNT mRNA and protein levels in EPC-2 cells appear to relate to lower CYP1 induction capacity, a shorter duration in the nucleus and therefore less AhR signaling in EPC-2 cells compared to WHCO1 cells. These results are consistent with increased AhR mRNA levels demonstrated in response to BaP treatment in Caco-2 colon carcinoma cells (Niestroy *et al*., 2011) but disagree with the decrease in AhR mRNA levels due to BaP treatment

in mouse embryo fibroblasts (Kann *et al*., 2005) and the decrease in AhR mRNA and protein after BaP exposure in mouse aortic endothelial cells (Wang *et al*., 2009). In addition, previous research has shown that AhR mRNA levels are up-regulated 1.4-fold after exposure to 10nM TCDD in T24 transitional cancer cells (Ishida *et al*., 2010) but are down-regulated by 30% after exposure to 5nM TCDD and by 25% after exposure to 10μM β-NF in HepG2 cells (Dvorak *et al*., 2008, Iwano *et al*., 2010). AhR mRNA levels were up-regulated 4-fold and 6-fold in MCF10AT1 and MCF-7 breast cancer cells, respectively, after exposure to 1nM 17-β-estradiol (Wong *et al*., 2009). These results collectively suggest that AhR mRNA and protein levels vary in a cell-type and compound-specific manner.

Our results showed that nuclear ARNT protein levels were induced to a greater degree in response to BaP treatment than AhR levels in WHCO1 cells and that ARNT mRNA levels were up-regulated in response to BaP treatment in both EPC-2 and WHCO1 cells. This disagrees with the observed down-regulation of ARNT mRNA levels by BaP treatment in Caco-2 cells (Niestroy *et al*., 2011), and there is no evidence for increased ARNT mRNA levels in response to BaP. However, since the ARNT has been shown to be essential for BaP-induced tumour initiation (Shi *et al*., 2009), it must still play an important role in CYP1 induction in EPC-2 and WHCO1 cells.

The observed increase in nuclear AhR and ARNT levels appeared to associate with decreased cytoplasmic AhR and ARNT levels, although the cytoplasmic proteins appear to disappear completely. This does not seem to be because all the protein has entered the nucleus, since their nuclear levels also decline after BaP withdrawal. The decrease in protein levels is therefore probably attributable to cytoplasmic AhR and ARNT protein degradation by the proteasome, which occurs in response to ligand binding (Davarinos and Pollenz, 1999, Ma and Baldwin, 2000) and is mediated by ROS signaling (Choi *et al*., 2008).

The nuclear protein western blot results suggest that Lamin B1 is a poor loading control in EPC-2 cells. In untreated cells, Lamin B1 levels are extremely low and appear to be inducible upon BaP treatment. However, levels are maintained even after BaP withdrawal. Lamin B1 levels appear to be constant in nuclear extracts from WHCO1 cells, and although not presented here, all SDS gels were routinely stained with Coomassie to confirm equal loading of protein extracts. These findings suggest that nuclear expression of Lamin B1 is affected by BaP treatment in EPC-2 cells, and that another loading control should be used, such as histone H3. Interestingly, Lamin B1 mRNA is down-regulated by BPDE treatment in FL normal human amnion epithelial cells (Lu *et al*., 2009) and WI38 foetal lung fibroblasts (Dreij *et al*., 2010). Alternatively, the low level of

Lamin B1 detected in untreated EPC-2 cells could reflect loss of the Lamin B1-containing nuclear membrane during the nuclear protein extraction process.

2.3.4 BaP-induced changes in cellular proliferation and cell morphology

The cytotoxicity of BaP suggests that BaP treatment may have a negative effect on cellular proliferation in our cell line model. Our results show that BaP-treated EPC-2 cells had lower proliferation than untreated cells, whereas WHCO1 cells were more resistant to BaP-associated growth reduction. The decreased cell growth in both EPC-2 and WHCO1 cells may be explained by BaP-induced apoptosis or cell cycle arrest. BaP treatment has indeed been shown to induce apoptosis through various mechanisms in several cell line models, including HepG2 (human hepatocarcinoma, Chen *et al*., 2003), Hepa1c1c7 (mouse hepatoma, Solhaug *et al*., 2004a), H460 (human lung cancer, Xiao *et al*., 2007) and F258 cells (rat liver epithelial cells, Tekpli *et al*., 2010). BaP-induced apoptosis is thought to be a result of oxidative stress signaling (Nebert *et al*., 2000). The complete effects of BaP on cellular proliferation are probably more complex: BaP induces both pro- and anti-apoptotic signaling events in mouse hepatoma Hepa1c1c7 cells (Solhaug *et al*., 2004). The effects may therefore depend on various parameters such as cell type, species and BaP concentration.

The analysis of cellular proliferation using three different methods – cell viability (MTT metabolism), DNA synthesis (BrdU incorporation) and cell number – showed a general trend that while BaP-treated EPC-2 cells displayed reduced growth, BaP treatment showed no effect on WHCO1 cell growth. This concordance between different methods was however not consistent with the MTT assay, which showed higher cell viability in BaP-treated WHCO1 cells after 48h. Increased MTT levels after 48h may simply reflect increased mitochondrial reductase enzyme activity, since treatment with BaP increases the activity of many metabolic enzymes. Alternatively, increased MTT activity may also represent increased BaP metabolism by mitochondrial CYP1A1, since both mitochondrial and microsomal CYP1A1 metabolize BaP (Dong *et al*., 2009). Despite the difference shown using the MTT assay, the two other methods confirmed the trend of decreased cellular proliferation in BaP-treated EPC-2 cells compared to WHCO1 cells. It should be noted that there is no evidence to suggest that BaP interacts with any components of the different growth media used to culture WHCO1 and EPC-2 cells (DMEM and KSFM, respectively) and therefore the observed differences in cellular proliferation do not reflect an effect of BaP on the different culture media.

The oxidative metabolism of BaP by Phase I XMEs contributes to the production of oxidative stress as a result of increased ROS, for example, hydrogen peroxide and superoxide (Burdick *et al*., 2003, Miller and Ramos, 2001). Oxidative stress signaling during BaP metabolism may trigger apoptosis (Nebert *et al*., 2000, Tekpli *et al*., 2010), which would be reflected as decreased cellular proliferation in BaP-treated cells, as observed in BaP-treated EPC-2 and WHCO1 cells.

The results show that prolonged treatment with BaP resulted in altered morphology in EPC-2 cells. The most obvious effects were the formation of elongated cells and membrane blebbing. This observation is consistent with evidence that membrane remodeling is a primary step in BaP-induced apoptosis in F258 rat liver epithelial cells (Tekpli *et al*., 2010). The small, rounded cells observed in Figure 2.9 are similar to the apoptotic cells identified after BaP exposure in Hepa1c1c7 cells (Solhaug *et al*., 2004a). Therefore our results suggest that prolonged BaP treatment causes apoptosis in most EPC-2 cells.

Prolonged exposure to low concentrations of BaP or BPDE has been shown to lead to transformation and deregulated growth kinetics in MRC-5 SV2 human lung fibroblasts and MCF-7 breast cancer cells (Pliskova *et al*., 2005, Zhu and Gooderham, 2002, Jiao *et al*., 2007, Jeffy *et al*., 2000). Our results show that BaP has a profound negative effect on EPC-2 cell morphology and membrane integrity, although the ability of BaP to transform EPC-2 cells has yet to be determined.

BaP- or BPDE-induced transformation has recently been shown to involve other key players. For example, the ERK/cyclin D1 pathway and JNK and p38 MAPK activation are required for BaP-induced transformation in human lung fibroblasts (Du *et al*., 2006), while NFAT3 and TNF are critical in BPDE-induced transformation in mouse epidermal CI41 cells (Ouyang *et al*., 2007). There is evidence that CDC25B phosphatase levels are important for BPDE-induced transformation (Srivastava *et al*., 2007) and transformation through Cyclin D1 also depends on the PI3K/Akt/MAPK pathway (Ding *et al*., 2009). Transformation of EPC-2 cells in particular, also requires various factors, such as the EGFR (epidermal growth factor receptor, Andl *et al*., 2002), ILGFBP3 (insulin-like growth factor binding protein 3), TGFB1 (transforming growth factor beta, Natsuizaka *et al*., 2010), TLR3 (toll-like receptor 3), NFκB (nuclear factor kappa B, Lim *et al*., 2009), or various combinations of expressed oncogenes (Kim *et al*., 2006). This evidence highlights that cellular transformation from BaP exposure is a complex and multi-factorial process.

2.3.5 Summary

BaP, a PAH procarcinogen present in tobacco smoke, binds to and activates the AhR, which dissociates from its cytoplasmic chaperone complex and enters the nucleus together with the ARNT. Here the AhR-ARNT transcription factor binds to xenobiotic response elements (XREs) in the promoter regions of its target genes, such as CYP1A1, CYP1A2, CYP1B1 and some phase II detoxification genes, thereby activating their transcription (Nebert and Dalton, 2006, Androutsopolous *et al*., 2009, Whitlock, 1999, Barouki *et al*., 2007). CYP1A1 and CYP1B1 enzymes are primarily responsible for the Phase I metabolism of BaP to its activated metabolites including BPDE. BaP therefore stimulates its own metabolism in a feedback loop.

Figure 2.10 represents the response to BaP in WHCO1 and EPC-2 cells based on the findings presented in this chapter. In normal (EPC-2) cells, there are lower levels of AhR and ARNT proteins which transcribe fewer CYP1A1 and CYP1B1 mRNA transcripts, resulting in lower amounts of enzyme to metabolize BaP. Rapid nuclear exit of AhR and ARNT reduces the duration of AhR signaling. BaP and its metabolites accumulate and cells reduce growth in response to BaP toxicity and possibly enhanced ROS production and apoptosis (Fig. 2.10A). In cancer (WHCO1) cells, however, there are higher levels of AhR and ARNT which transcribe more CYP1A1 and CYP1B1 transcripts, and therefore increased enzyme levels enhance BaP metabolic activation to BPDE. Increased levels of BaP metabolites may also serve as AhR ligands that can sustain AhR activation (Spink *et al*., 2008). The higher levels of AhR and ARNT and their prolonged duration in the nucleus may result in a constitutively active or sustained AhR signaling cascade which may predispose WHCO1 cells to AhR-mediated abnormal cell proliferation in the presence and even after the removal of BaP, which may contribute to cancer progression (Fig. 2.10B).

Our proposed model of the molecular events occurring in response to BaP in EPC-2 and WHCO1 cells, however, does not take into consideration the expression of all possible genes involved in this response. In order to further our understanding of the effects of BaP on gene expression patterns in normal and transformed oesophageal cells, a DNA microarray is an obvious next step in our investigation.

(A)

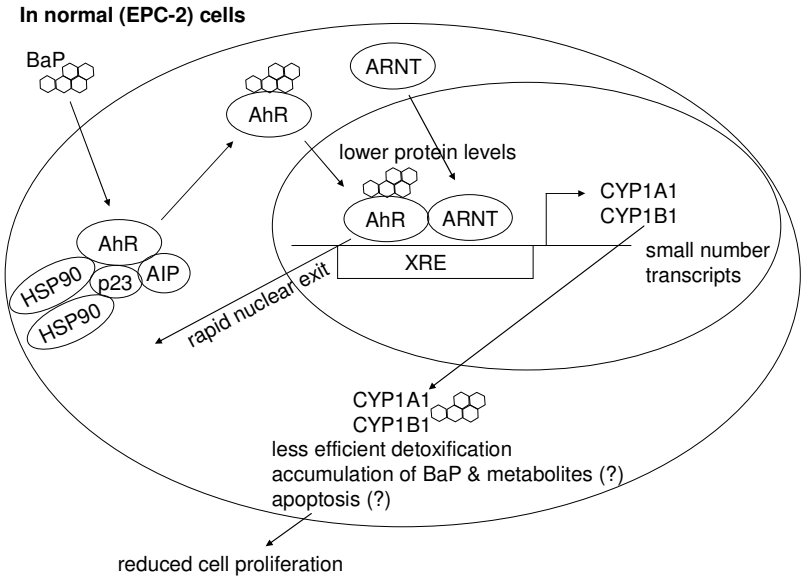

(B)

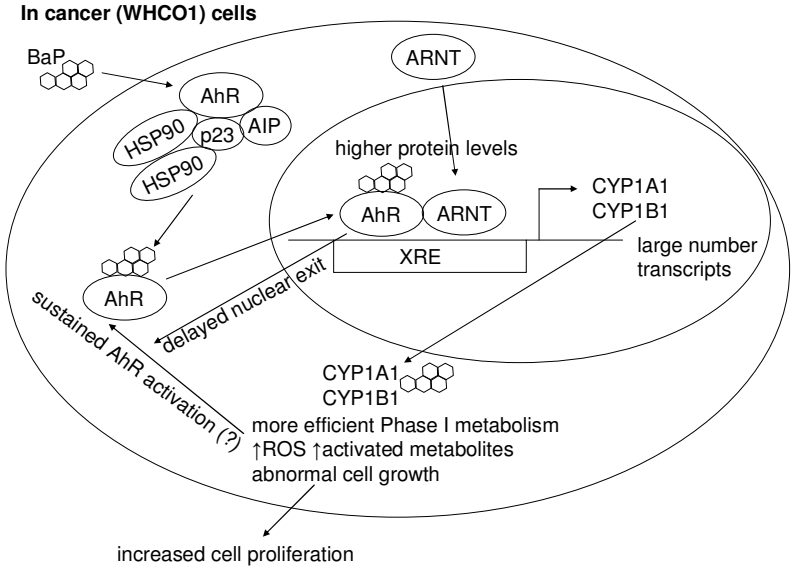

Figure 2.10 Summary of the molecular response to BaP treatment in normal and transformed oesophageal epithelial cells. **(A)** In normal (EPC-2) cells, there are lower levels of AhR and ARNT, which, in response to BaP treatment, translocate more rapidly into and out of the nucleus, resulting in the transcription of lower amounts of CYP1A1 and CYP1B1 mRNA and protein, which metabolize BaP less efficiently and cellular proliferation is reduced due to the accumulation of toxic BaP metabolites and possibly from increased apoptosis. **(B)** In transformed (WHCO1) cells, there are higher levels of AhR and ARNT, which, in response to BaP treatment, transcribe greater amounts of CYP1A1 and CYP1B1 mRNA and protein, which metabolically activate BaP more efficiently, resulting in a higher production of ROS. Prolonged duration of AhR-ARNT in the nucleus may lead to sustained AhR activation and AhR signaling, which may contribute to deregulated cellular proliferation.

Chapter 3
Transcriptional profiling of normal and tumour oesophageal epithelial cells in response to treatment with benzo[a]pyrene

3.1 Introduction

Transcriptional profiling by microarray analysis is frequently used to analyze the toxic, therapeutic or carcinogenic effects of various compounds on whole-genome expression in cell lines and tissues. BaP has been recognized for its carcinogenic potential for many years (IARC, 2004) but the detailed molecular mechanisms are still unsolved. Microarray studies have shown the effects of BaP treatment on global gene expression in various cell lines, including MCF-7 (breast carcinoma), HepG2 (hepatocarcinoma), A549 (lung adenocarcinoma), WI38 (foetal lung fibroblasts) and NHMEC (normal human mammary epithelial cells). This chapter investigates the effect of BaP on global gene expression in a normal oesophageal epithelial cell line (EPC-2) and an oesophageal cancer cell line (WHCO1), since no prior studies have focused on oesophageal cell lines.

3.2 Results

RNA from WHCO1 and EPC-2 cells treated with 0.1% DMSO or 10μM BaP were amplified, labeled and hybridized to the Illumina WG6 v3 Expression BeadChip. Gene expression data was analyzed using Illumina's BeadStudio/GenomeStudio software and with the assistance of Dr Otu from the Department of Bioengineering, Istanbul Bilgi University, Istanbul, Turkey and Department of Medicine, BIDMC Genomics Centre, Harvard Medical School, Boston, USA, and Dr Nicki Tiffin from the South African National Bioinformatics Institute (SANBI) at the University of the Western Cape. Lists of differentially expressed genes were analyzed using Ingenuity Pathways Analysis (IPA) and GOstat.

3.2.1 Microarray sample selection and clustering analysis

Data were analyzed and the gene expression fold change was calculated. In order to determine the concordance between biological replicates, untreated and BaP-treated samples from both WHCO1 and EPC-2 microarrays were clustered according to the similarity of genes expressed (Fig. 3.1A-B). From the dendrograms it was clear that sample "BaP1" from the WHCO1 groupset was an outlier (Fig. 3.1B) and that samples "Un1" and "BaP3" from the EPC-2 groupset clustered

in the incorrect groups (Fig. 3.1A). These samples were subsequently removed as outliers before further analysis, generating a final combined cluster (Fig. 3.1C).

Differentially expressed genes were clustered together, generating heat maps (Fig. 3.2) that indicate the variation of gene expression fold change between 0.6 and 3-fold up- (red) or down- (green) regulation across the samples in each groupset. Despite the low fold change within one sample, overall fold change for Un or BaP groups were greater than 2-fold in all genes. In the WHCO1 heat map, there were a larger number of up-regulated than down-regulated genes (Fig. 3.2B), whereas in the EPC-2 heat map, there were a larger number of down-regulated genes (Fig. 3.2A).

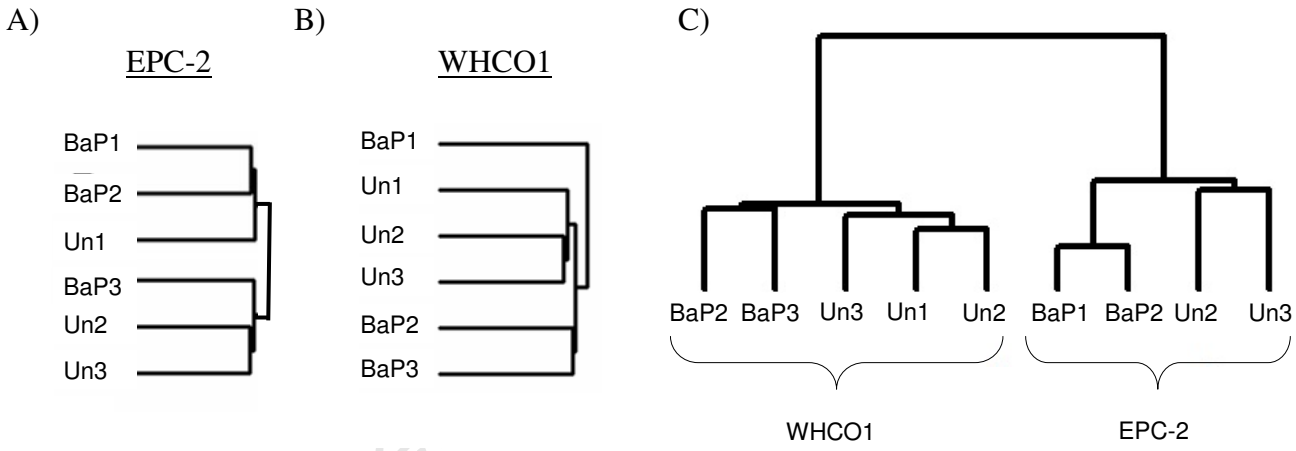

Figure 3.1 Sample clustering dendrograms. Triplicate samples of 0.1% DMSO- or 10μM BaP-treated cRNAs from WHCO1 and EPC-2 cells were clustered by similarity of expressed genes as described in *Methods*. Original clustering of EPC-2 **(A)** and WHCO1 **(B)** samples shows that triplicates do not all cluster together. Outlier samples were removed to generate a final combined dendrogram **(C)** showing the replicates used for subsequent analysis. Un denotes cells treated with 0.1% DMSO; BaP denotes cells treated with 10μM BaP.

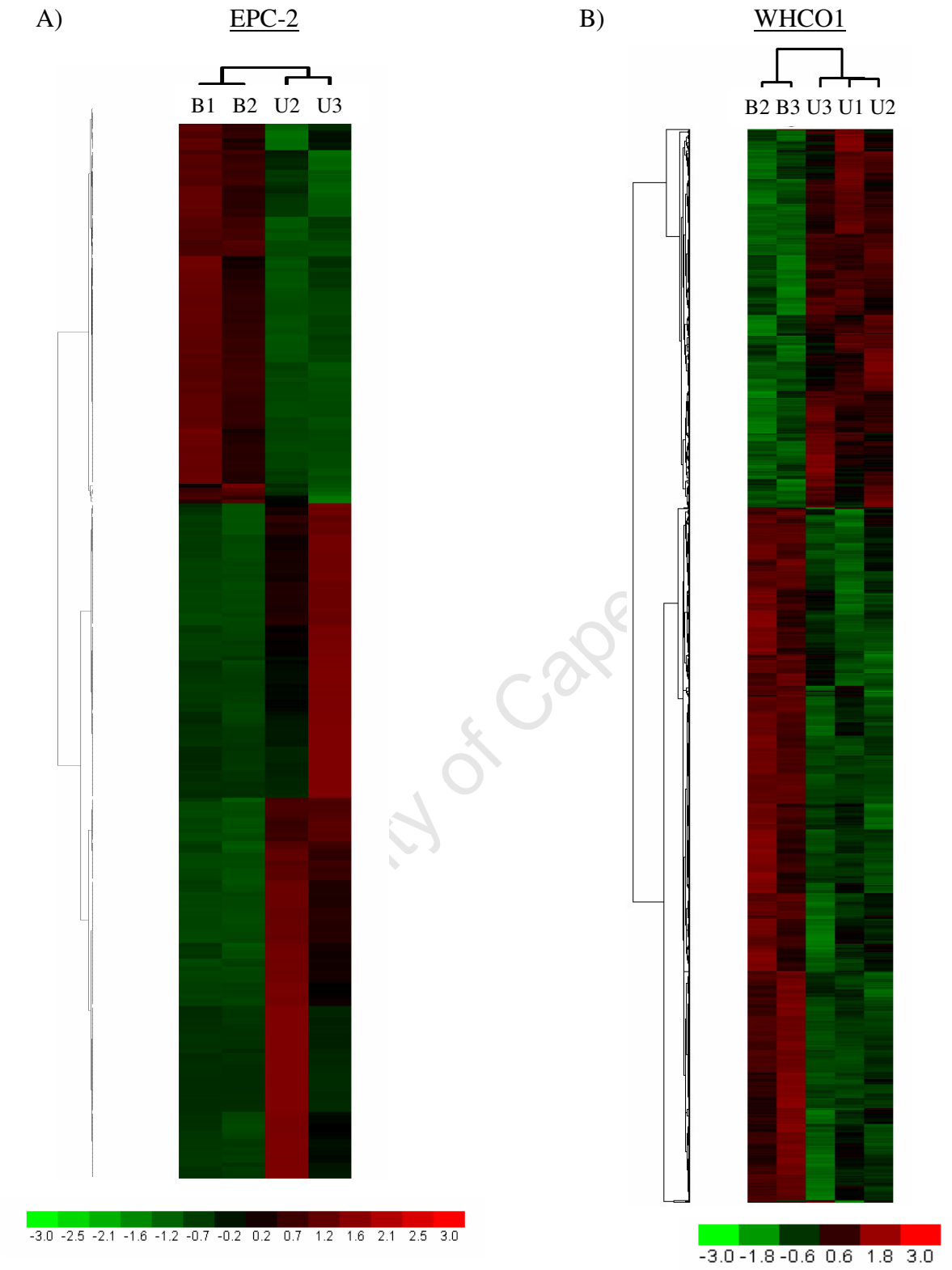

Figure 3.2 Differential gene expression heat maps. Heat maps depict signal intensity and clustering of differentially expressed genes in **(A)** EPC-2 and **(B)** WHCO1 cells. Green indicates down-regulated genes; red indicates up-regulated genes. Colour intensity indicates fold change as shown in the legend below the heat maps. B denotes BaP-treated samples; U denotes 0.1% DMSO-treated samples.

3.2.2 Differentially expressed genes in response to BaP treatment

BaP treatment resulted in differential expression of several hundred genes in both EPC-2 and WHCO1 cells (Fig. 3.3). Gene expression fold change was calculated for each gene by dividing "BaP" average signal values by "Un" average signal values. In addition, each treatment group was compared to every other treatment group, generating a total of 6 comparisons: EPC-2 BaP vs EPC-2 Un, WHCO1 BaP vs WHCO1 Un, WHCO1 BaP vs EPC-2 Un, WHCO1 Un vs EPC-2 BaP, WHCO1 Un vs EPC-2 Un and WHCO1 BaP vs EPC-2 BaP. The number of differentially expressed genes varied widely between comparisons (Fig. 3.3), from 183 genes up-regulated in BaP-treated WHCO1 cells compared to untreated cells, to 2900 genes up-regulated in BaP-treated EPC-2 cells compared to untreated WHCO1 cells. The top 50 genes up- or down-regulated in each comparison (except for WHCO1 BaP vs EPC-2 Un, which is not relevant in this study) are listed in Appendix A.

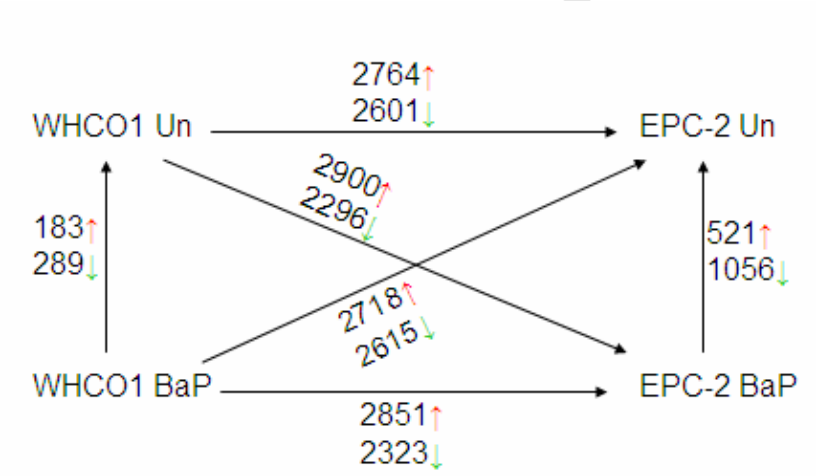

Figure 3.3 Number of up- and down-regulated genes in each dataset comparison. All possible comparisons made between EPC-2 and WHCO1 treatment groups generate twelve lists of up-regulated (↑) and down-regulated (↓) genes differentially expressed by at least two-fold in each comparison. Un indicates 0.1% DMSO-treated samples; BaP indicates 10μM BaP-treated samples.

3.2.3 Validation of Microarray Data by qRT-PCR

Genes were selected from the lists of differentially expressed genes to confirm the validity of microarray gene expression fold changes by qRT-PCR. Genes were selected from the EPC-2 and WHCO1 gene lists, respectively, and fold change comparisons were made between qRT-PCR and microarray gene expression (Fig. 3.4).

In general, microarray fold change and qRT-PCR fold change followed the same trend. Gene expression was often exaggerated by the microarray data, for example, for MMP9, GPX3, P53AIP1 and ITGB7 (Fig 3.4A). The only gene whose expression was not consistent between microarray and qRT-PCR is UGT2B7 (Fig 3.4B). The common gene, ITGB7, was up-regulated in WHCO1 cells (Fig. 3.4B) but down-regulated in EPC-2 cells (Fig 3.4A). The general concordance between gene expression fold changes suggests that the microarray gene expression data are reproducible by qRT-PCR.

3.2.4 Genes and biological pathways affected by BaP treatment

The first objective was to determine which genes are differentially expressed in response to BaP treatment in normal and tumour oesophageal cell lines. BaP induced the up-regulation of 521 and 183 genes and the down-regulation of 1056 and 289 genes in EPC-2 and WHCO1 cells respectively. The functional relevance of differentially expressed genes was analyzed by determining the biological functions, canonical pathways and gene ontology (GO) terms (molecular function, biological process or cellular component) that were affected during the response to BaP treatment. Gene ontology was investigated using IPA and GOstat. The top genes up- and down-regulated in response to BaP treatment in EPC-2 and WHCO1 cells are indicated in Appendix A.

A) **EPC-2**

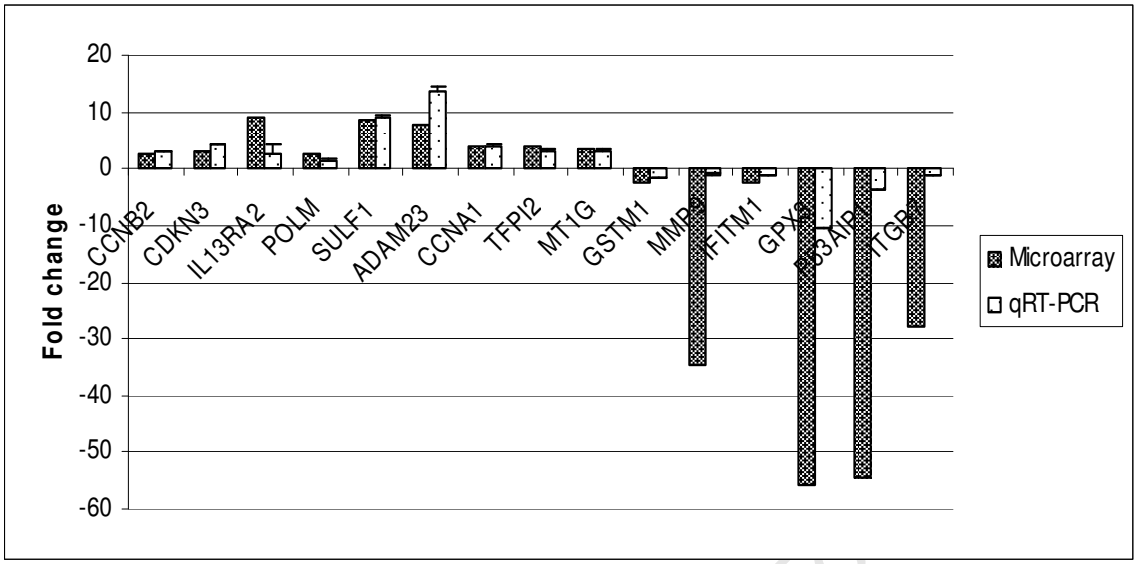

B) **WHCO1**

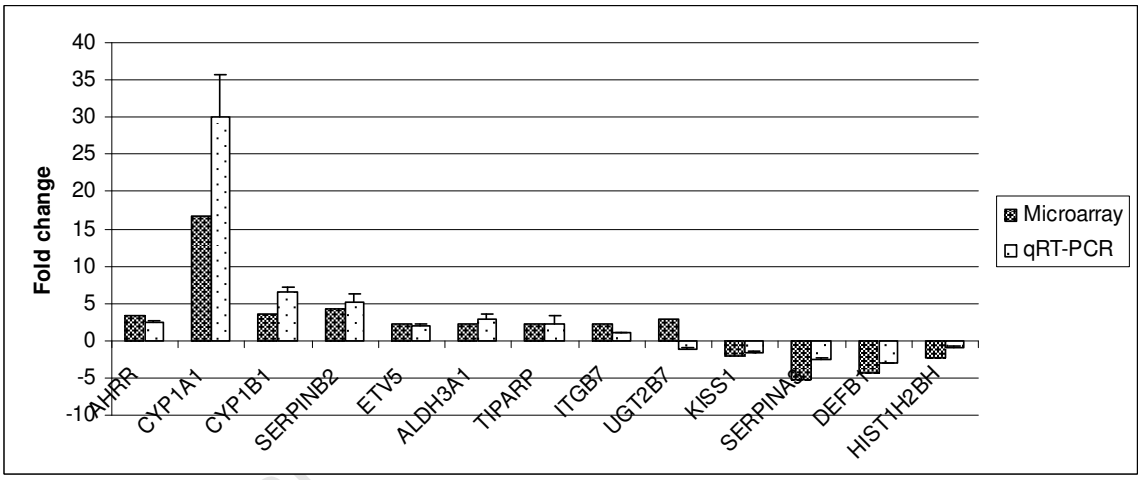

Figure 3.4 Validation of microarray fold change by qRT-PCR on selected genes. Selected genes with altered expression in response to BaP exposure in EPC-2 **(A)** and WHCO1 **(B)** cells were analyzed by qRT-PCR as described in *Methods*. Fold change shown was normalized to GAPDH mRNA levels and relative to 0.1% DMSO-treated replicates. Results shown are mean + standard deviation from triplicate samples per biological replicate. CCNB2: cyclin B2; CDKN3: cyclin-dependent kinase inhibitor 3; IL13RA2: interleukin 13 receptor alpha 2; POLM: DNA polymerase mu; SULF1: sulfatase 1; ADAM23: ADAM metallopeptidase domain 23; CCNA1: cyclin A1; TFPI2: tissue factor pathway inhibitor 2; MT1G: metallothionein 1G; GSTM1: glutathione S-transferase M1; MMP9: matrix metallopeptidase 9; IFITM1: interferon induced transmembrane protein 1; GPX3: glutathione peroxidase 3; P53AIP1: p53-regulated apoptosis-inducing protein 1; ITGB7: integrin beta 7; AHRR: aryl hydrocarbon receptor repressor; CYP1A1: cytochrome P450 1A1; CYP1B1: cytochrome P450 1B1; SERPINB2: serpin peptidase inhibitor B2; ETV5: ets variant gene 5; ALDH3A1: aldehyde dehydrogenase 3A1; TIPARP: TCDD-inducible poly(ADP-ribose) polymerase; UGT2B7: UDP glucuronosyltransferase 2B7; KISS1: KiSS-1 metastasis suppressor; SERPINA3: serpin peptidase inhibitor A3; DEFB1: defensin beta 1; HIST1H2BH: histone cluster 1 H2bh.

In EPC-2 cells, the most important biological functions as determined by IPA altered in response to BaP treatment were Cancer, Cellular Growth and Proliferation, and Cellular Movement (Fig. 3.5A). The most significant IPA canonical pathways affected include Acute Phase Response Signaling and Graft-vs-Host Disease Signaling, but most pathways showed more down-regulated than up-regulated genes (Fig. 3.5B). This agrees with the larger number of down-regulated genes than up-regulated genes in the heat map (Fig 3.2A).

In WHCO1 cells, the important IPA biological functions were Cell-to-Cell Signaling and Interaction, Cell Death, Inflammatory Response and Cellular Growth and Proliferation (Fig. 3.6A). Most canonical pathways contained more up-regulated than down-regulated genes, and the most important pathways include Xenobiotic Metabolism Signaling and Aryl Hydrocarbon Receptor Signaling (Fig. 3.6B). The higher number of up-regulated than down-regulated genes in these canonical pathways also agrees with the WHCO1 heat map (Fig. 3.2B).

In both cell lines, BaP frequently altered diverse metabolic pathways, such as Arachidonic Acid Metabolism, Taurine and Hypotaurine Metabolism (Fig 3.5B), Retinol Metabolism, Xenobiotic Metabolism (Fig 3.6B) and LXR/RXR Activation, which is involved in the regulation of lipid metabolism (Fig 3.5B, 3.6B). These findings suggest that metabolic pathways were altered in response to BaP in both cell lines, but that detoxification pathways were affected more significantly in WHCO1 cells. A large number of xenobiotic metabolism genes were differentially expressed in WHCO1 cells in response to BaP exposure. These include the up-regulation of CYP1A1, CYP1B1, UGT1A6, UGT1A10, UGT2B7 and ALDH3A1 and the down-regulation of GSTA4 and SULT1C3. The altered xenobiotic metabolism agrees with GOrilla (Gene Ontology enRIchment anaLysis and visuaLizAtion tool) analysis indicating the most significant biological process was “Response to toxin”.

EPC-2

A)

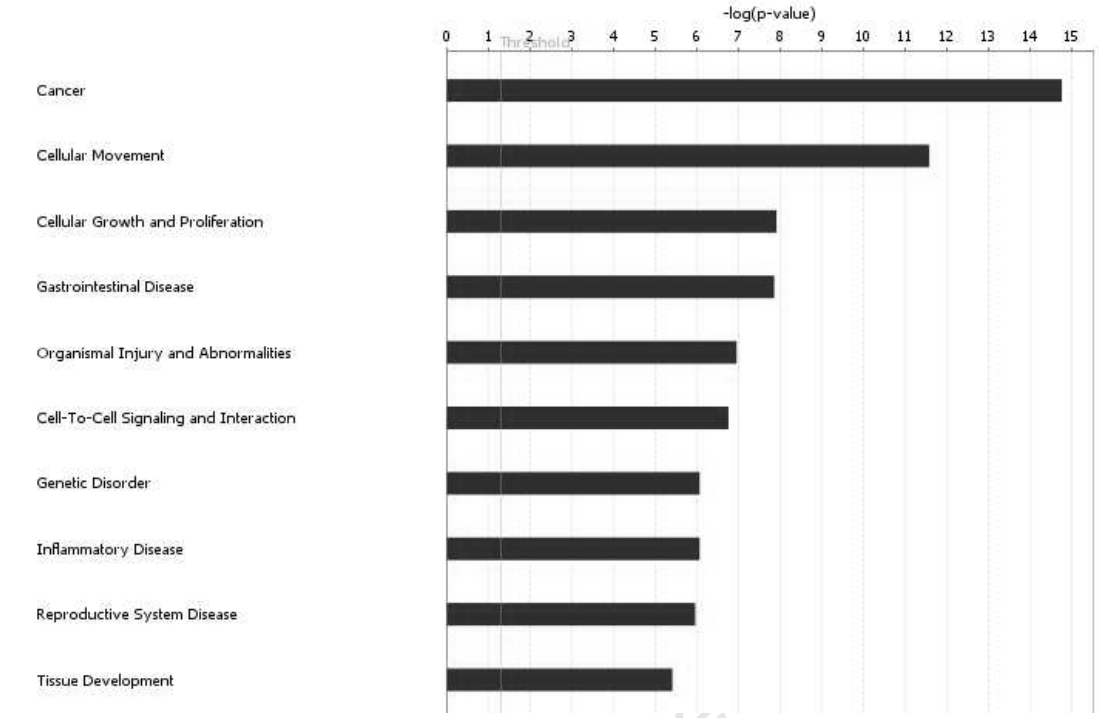

B)

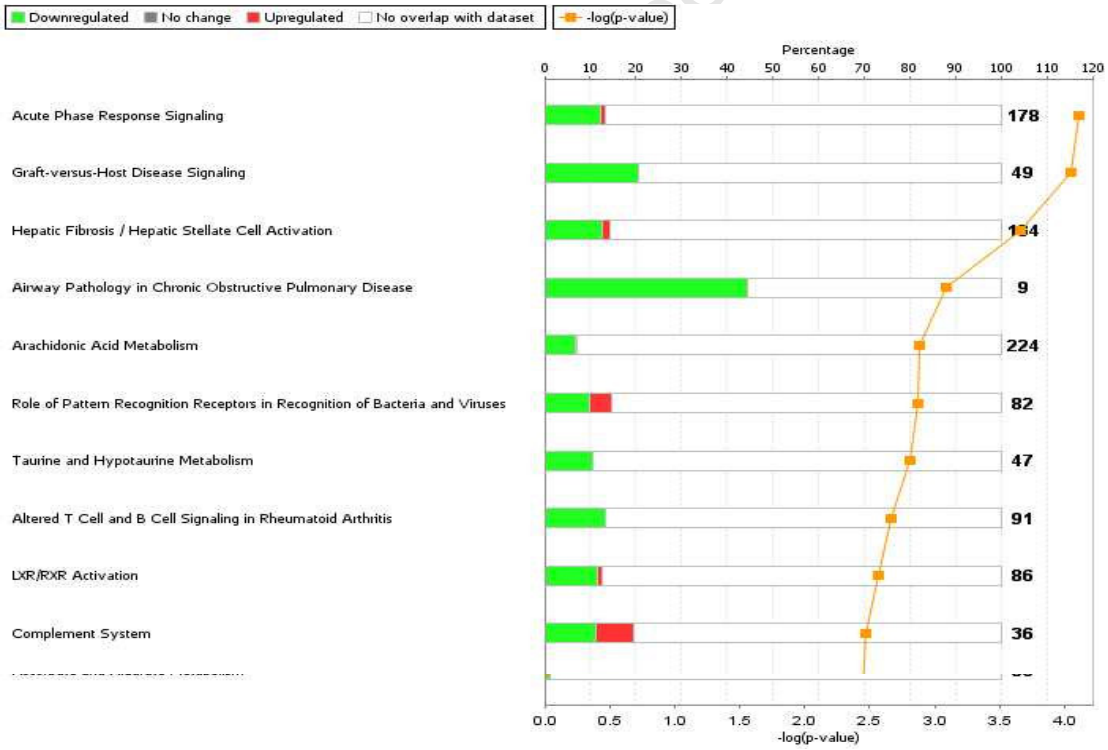

Figure 3.5 Functions and Pathways affected by BaP treatment in EPC-2 cells. Biological functions **(A)** and canonical pathways **(B)** were generated from the list of differentially expressed genes in EPC-2 cells by IPA. In **(A)** –log(p-value) indicates significance of biological function. In **(B)** green indicates down-regulated; red indicates up-regulated. Number above bar indicates number of genes within the pathway. Bar represents percentage of genes within pathway that are up- or down-regulated. Orange line graph indicates significance of canonical pathway [-log(p-value)] according to secondary scale.

WHCO1

A)

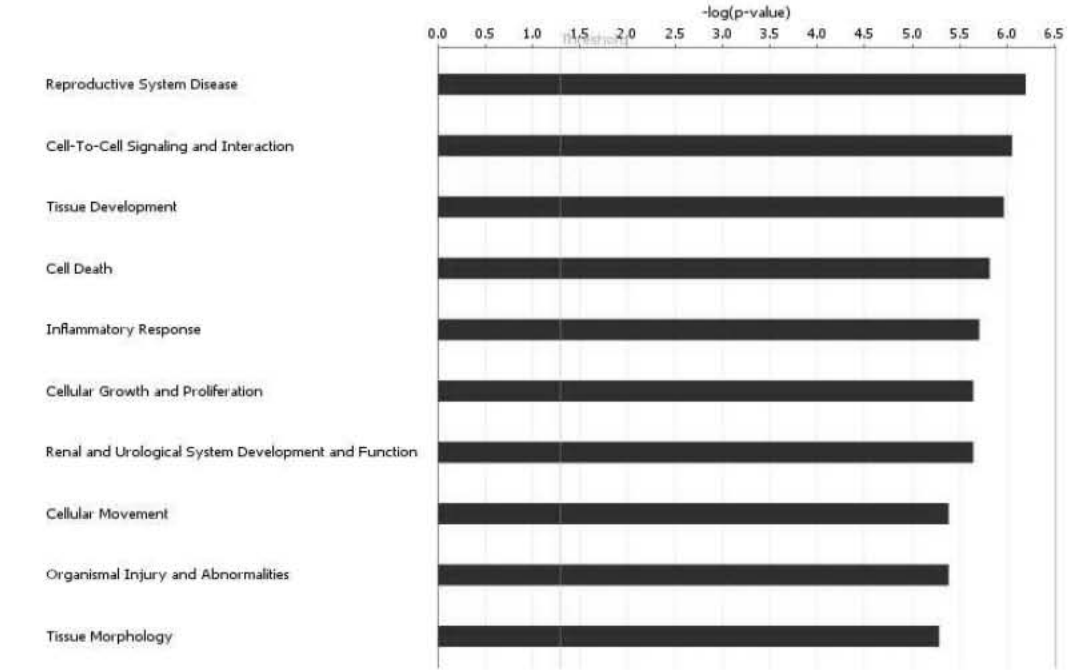

B)

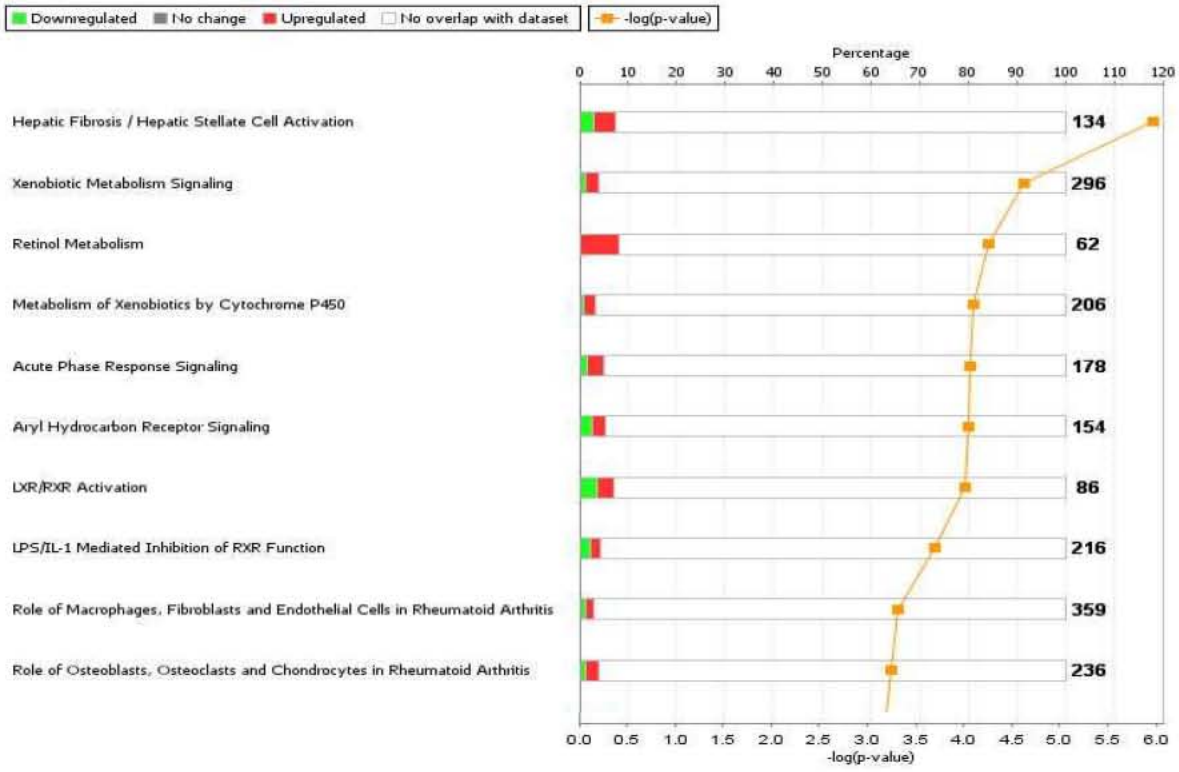

Figure 3.6 Functions and Pathways affected by BaP treatment in WHCO1 cells. Biological functions **(A)** and canonical pathways **(B)** were generated from the list of differentially expressed genes in WHCO1 cells by IPA. In **(A)** –log(p-value) indicates significance of biological function. In **(B)** green indicates down-regulated; red indicates up-regulated. Number above bar indicates number of genes within the pathway. Bar represents percentage of genes within pathway that are up- or down-regulated. Orange line graph indicates significance of canonical pathway [-log(p-value)] according to secondary scale.

In WHCO1 cells, the Inflammatory Response function was significantly altered by BaP treatment (Fig. 3.6A). BaP induced the expression of several pro-inflammatory cytokines in these cells, such as IL6, IL1B, IL11, IL1F9 and other molecules involved in pro-inflammation such as CXCL1, PTGS2, LIF and CXCL10, and anti-inflammatory molecules such as IL10RA. The up-regulation of genes involved in inflammation in WHCO1 cells, such as the IL6 gene interaction network (Fig. 3.7B) occurred in contrast to the down-regulation of inflammatory genes in EPC-2 cells, for example the TNF gene interaction network (Fig. 3.7A). These findings highlight the difference in inflammatory response between normal and cancer cells. This is important since both tobacco smoking and BaP metabolism are associated with increased inflammation which is linked to cancer risk.

In EPC-2 cells, a large number of cell cycle-related genes were differentially expressed. These include the up-regulation of CCNB1, CCNB2, CCNA1, CDC25C, CDC20, CDC2, CDCA2, CDCA3 and CDKN3, and the down-regulation of CDKN1A and CDKN2A. Interestingly, the most significantly over-represented GO terms in BaP-treated EPC-2 cells were Cell Cycle, M Phase, Mitosis and Cell Division (Fig. 3.8). Significantly over-represented GO terms are shown in Figure 3.8A. The most significant biological processes, shown in red in Figure 3.8B, include Cell Division and M Phase of Mitotic Cell Cycle. However, the up-regulation of cell cycle genes and cell cycle processes did not result in increased cellular proliferation when EPC-2 cells were treated with BaP (Fig. 2.8). This suggests that increased cellular proliferation was suppressed or overridden by another mechanism. Indeed, when examining further canonical pathways below the top ten (Fig. 3.5B) IPA analysis showed that pathways involved in DNA damage checkpoints and cell cycle checkpoint regulation were up-regulated (Fig. 3.9). These results suggest that DNA damage from BaP metabolism caused cell cycle checkpoints that inhibit proliferation, despite an increase in expression of cell cycle-related genes.

A) EPC-2 B) WHCO1

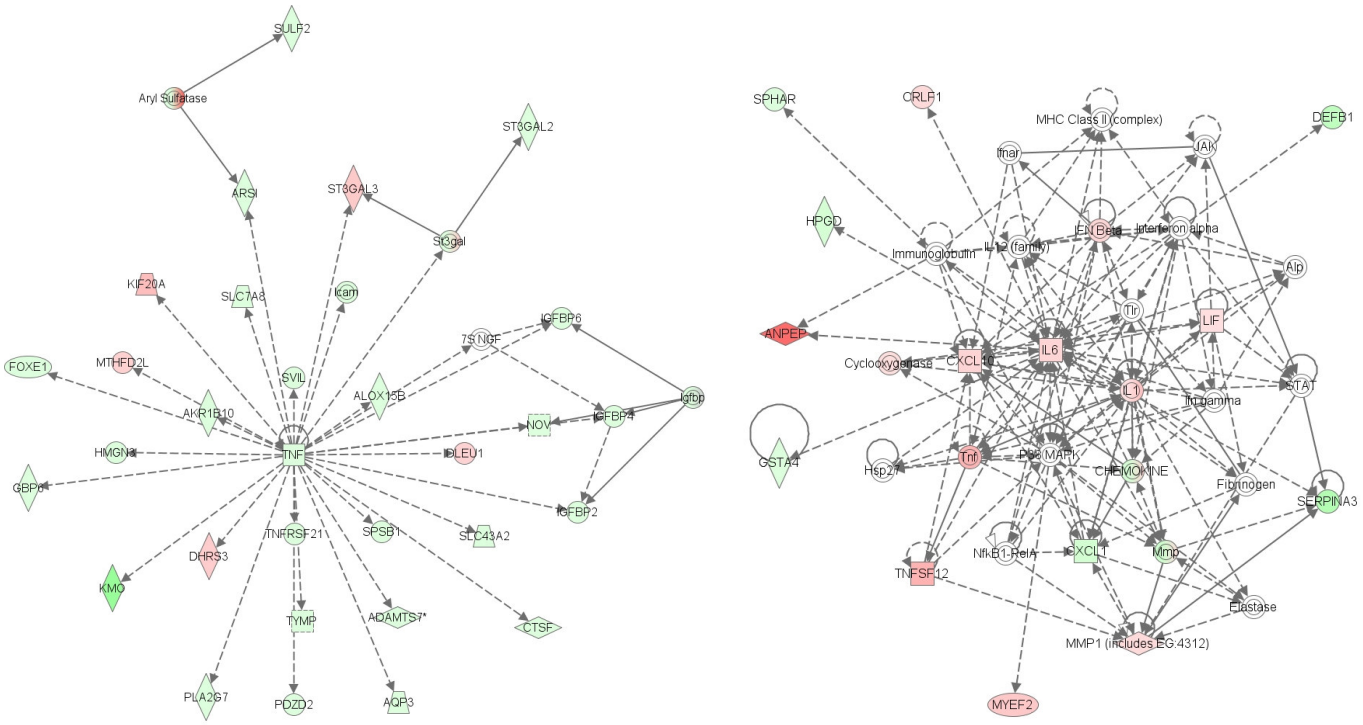

Figure 3.7 Differential response of inflammatory genes in BaP-treated EPC-2 and WHCO1 cells. Significant gene interaction networks were generated by IPA from lists of differentially expressed genes in BaP-treated EPC-2 **(A)** and WHCO1 **(B)** cells. TNF and interacting genes are mostly down-regulated in EPC-2 cells **(A)**, while IL6 and its interacting genes are mostly up-regulated in WHCO1 cells **(B)**. Solid lines indicate direct interactions; dotted lines indicate indirect interactions. In EPC-2: TNF: tumour necrosis factor, AKR1B10: aldo-keto reductase 1B10, HMGN: high mobility group nucleosomal binding domain, KMO: kynurenine 3-monooxygenase, DHRS3: dehydrogenase/reductase SDR family, TNFRSF21: tumour necrosis factor receptor superfamily 21, SPSB1: splA/ryanodine receptor domain and SOCS box containing 1, TYMP: TIMP metallopeptidase inhibitor, PDZD2: PDZ domain-containing 2, PLA2G7: phospholipase A2 group 7, AQP3: aquaporin 3, CTSF: cathepsin F, SLC43A2: solute carrier 43A2, ADAMTS7: ADAM metallopeptidase with thrombospondin motif 7, TGFBP2: transforming growth factor binding protein 2, DLEU1: deleted in lymphocytic leukemia 1, NOV: nephroblastoma overexpressed, IGFBP4: insulin-like growth factor binding protein 4, ALOX15B: arachidonate 15-lipoxygenase type B, SVIL: supervillin, FOXE1: forkhead box E1, MTHFD2L: methylenetetrahydrofolate dehydrogenase 2-like, KIF20A: kinesin family member 20A, SLC7A6: solute carrier 7A6, IGFBP6: insulin-like growth factor binding protein 6, ICAM: intercellular adhesion molecule, SULF2: sulfatase 2, ST3GAL2: ST3 beta-galactoside alpha-2,3-sialyltransferase 2, ST3GAL3: ST3 beta-galactoside alpha-2,3-sialyltransferase 3, ARS: aryl sulfatase. In WHCO1: MYEF2: myelin expression factor 2, TNFSF12: tumour necrosis factor superfamily 12, CXCL1: chemokine (C-X-C motif) ligand 1, MMP1: matrix metallopeptidase 1, SERPINA3: serpin peptidase inhibitor A3, GSTA4: glutathione S-transferase A4, IL1: interleukin 1, IL6: interleukin 6, LIF: leukaemia inhibitory factor, CXCL10: chemokine (C-X-C motif) ligand 10, ANPEP: alanyl aminopeptidase, HPGD: hydroxyprostaglandin dehydrogenase 15-(NAD), SPHAR: S-phase response, CRLF1: cytokine receptor-like factor 1, IFNB: interferon beta, DEFB1: defensin beta 1.

A)

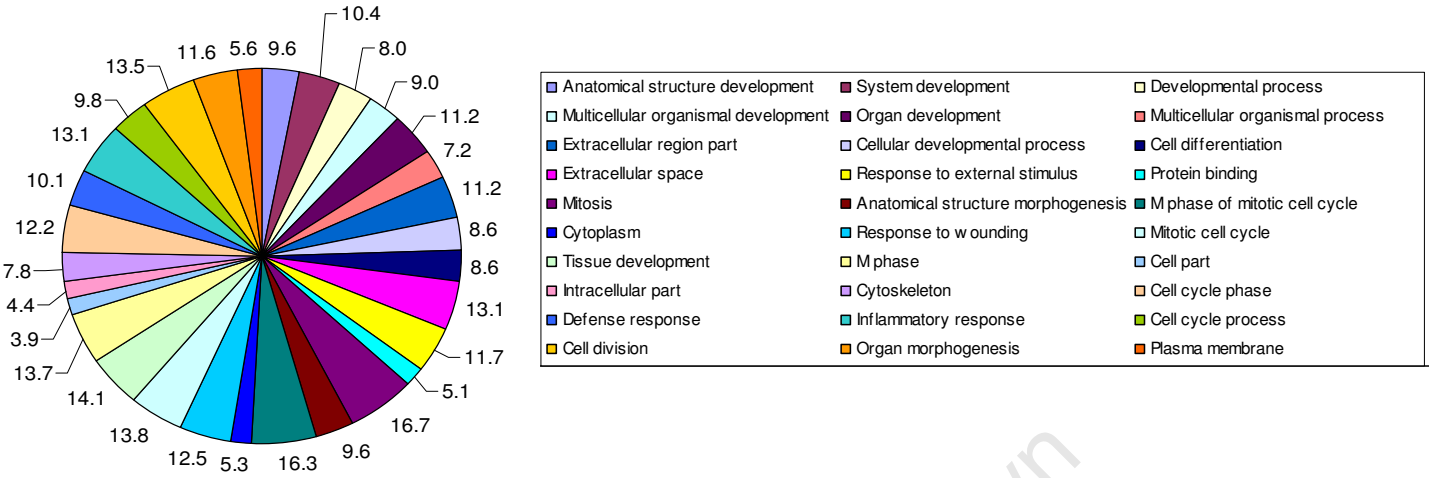

B)

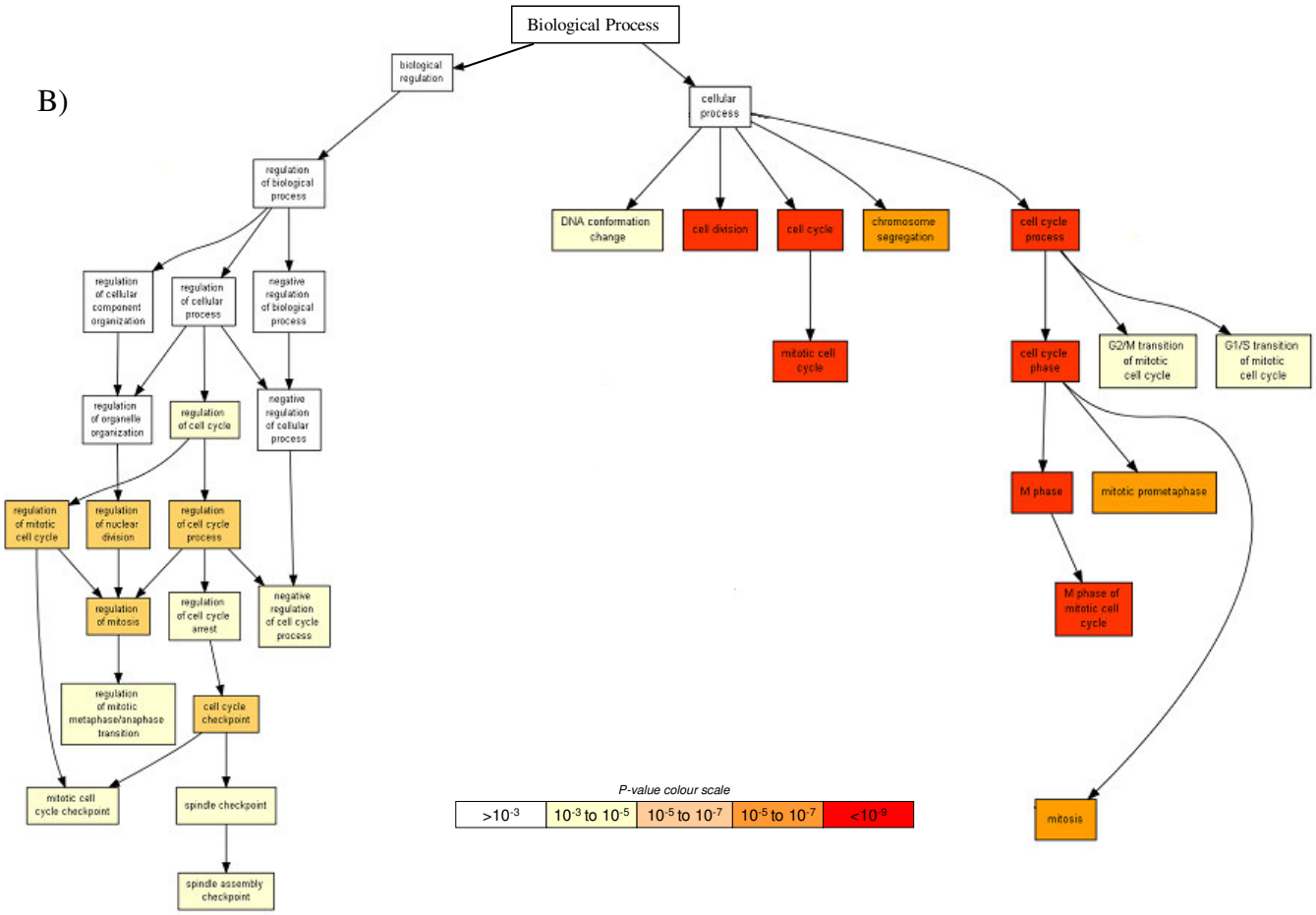

Figure 3.8 Significant over-representation of Cell Cycle gene ontology in response to BaP treatment in EPC-2 cells. Lists of differentially expressed genes in BaP-treated EPC-2 cells were entered into GOstat **(A)** and GOrilla **(B)**. GOstat results show percentage of genes that are significantly over-represented in a GO term out of the entire list of genes in the same GO term. GOrilla results graphically show the most significant biological process GO terms from GOstat. Legend shows p-value significance of GO term. Adapted from GOrilla results.

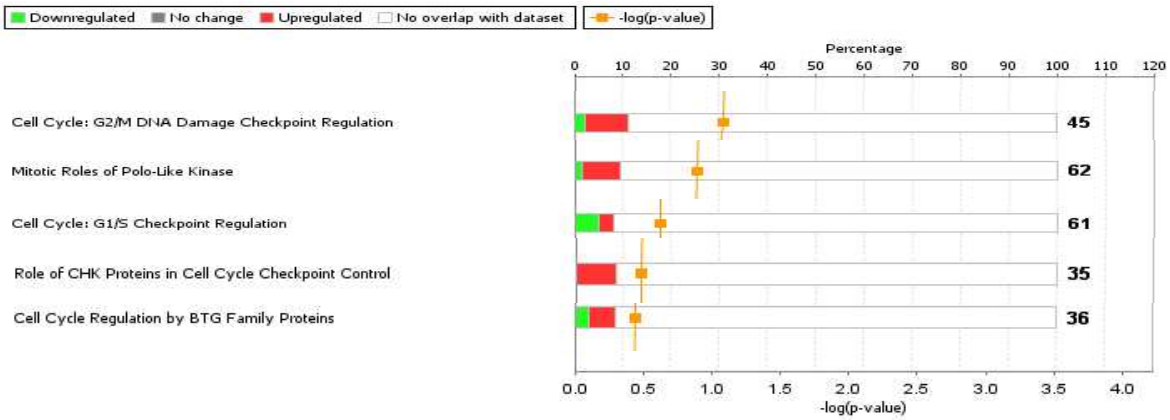

Figure 3.9 Up-regulation of cell cycle checkpoint pathways in EPC-2 cells in response to BaP. Differentially expressed genes in BaP-treated compared to untreated EPC-2 cells were entered into IPA to determine significant canonical pathways. Most pathways show down-regulated genes, but the genes involved in cell cycle checkpoint pathways were mostly up-regulated. Green indicates down-regulated; red indicates up-regulated. Number above bar indicates number of genes within the pathway. Bar represents percentage of genes within pathway that are up- or down-regulated. Orange dots indicate significance of canonical pathway [-log(p-value)] according to secondary scale. Adapted from IPA results.

3.2.5 Fundamental differences in gene expression between EPC-2 and WHCO1 cells

The differentially expressed genes between WHCO1 and EPC-2 cells in the absence of BaP treatment were determined in order to assess the baseline transcriptional differences between normal and cancer cells (WHCO1 Un vs EPC-2 Un). The genes with the highest and lowest fold changes were not known to be directly involved in cancer or cancer-related pathways. Further analysis therefore shifted to which canonical pathways and biological processes were altered in untreated WHCO1 cells compared to untreated EPC-2 cells (reference cell line).

Interestingly, biological functions (Fig. 3.10A) and biological processes (Fig. 3.11) both showed significant representation of the Cell Cycle, Cellular Growth and Proliferation, DNA Replication, Recombination and Repair and Mitotic Phase of the Cell Cycle. The top canonical pathways in WHCO1 compared to EPC-2 cells were p53 Signaling, Molecular Mechanisms of Cancer, VEGF Signaling and Role of BRCA1 in DNA Damage Response (Fig. 3.10B). In Figure 3.11, the significant GO biological processes were grouped together into four representative groups, since the figure is too large to visualize all the biological processes.

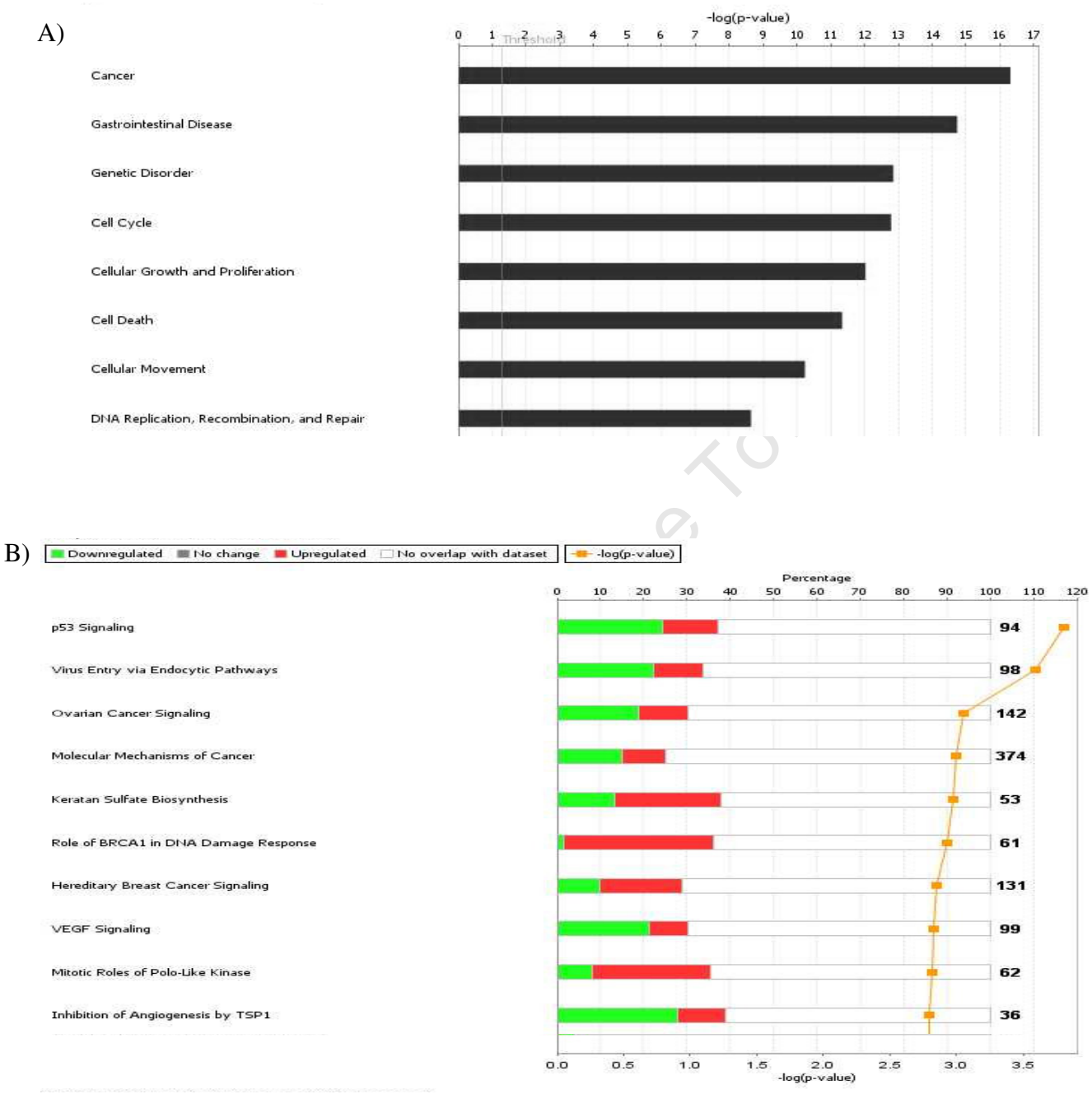

Figure 3.10 Baseline transcriptional differences in untreated WHCO1 cells compared to untreated EPC-2 cells. Differentially expressed genes in the WHCO1 Un vs EPC-2 Un comparison were analyzed using IPA and GOstat. Significant biological functions **(A)** and canonical pathways **(B)** shown are described as in Fig. 3.5 above.

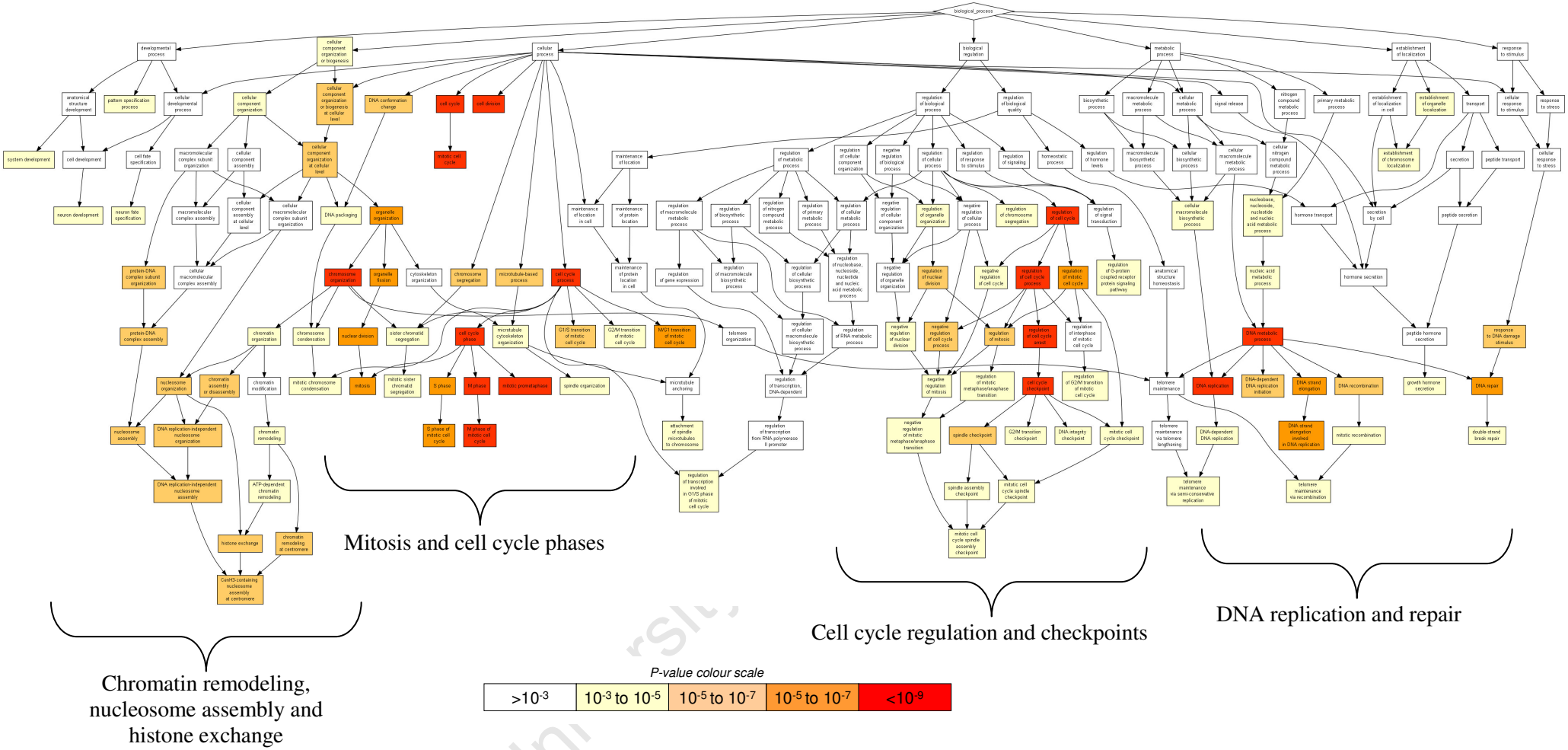

Figure 3.11 Biological processes significantly over-represented in untreated WHCO1 cells compared to untreated EPC-2 cells. Differentially expressed genes in the WHCO1 Un vs EPC-2 Un comparison were entered into GOrilla to visualize significant GO terms involved in biological processes. The most significant biological processes were grouped together into four representative groups to aid visualization. Legend indicates p-value significance of GO term. Taken from GOrilla results.

3.2.6 The role of BaP exposure in transformation: do BaP-treated EPC-2 cells have similar gene expression profiling to untreated WHCO1 cells?

Previous publications have shown that normal cells treated with either BaP or BPDE can undergo transformation into cancer cells. Phase contrast photographs in Figure 2.9 showed that prolonged treatment of EPC-2 cells with BaP resulted in morphological changes associated with apoptosis. BaP-treated EPC-2 cells were compared with untreated WHCO1 cells to determine whether BaP treatment causes EPC-2 cells to become like cancer cells.

The top biological functions analyzed by IPA were Cancer, Genetic Disorder, Cell Death, Cell Cycle, Cellular Growth and Proliferation, and DNA Replication, Recombination and Repair (Fig. 3.12A). GOstat analysis showed an over-representation of cell cycle GO terms, including Mitotic Cell Cycle (39% of all mitotic cell cycle genes over-represented), M phase (39.9%), Cell Proliferation (29.7%) and Cell Cycle (31.3%). Cell cycle genes such as cell division cycle genes (CDC2 [CDK1], CDC66, CDC7, CDC20, CDC25C) cell division cycle-associated or –like genes (CDCA1, CDCA3, CDCA5, CDCA7, CDCA8, CDC45L, CDCA7L), cyclins (CCNB1, CCNB2, CCNA1, CCNA2, CCNE2, CCNF), cyclin-dependent kinases (CDK1, CDK2, CDK3, CDK4, CDKL1) and their inhibitors (CDKN2A, CDKN2D, CDKN3), were down-regulated in BaP-treated EPC-2 cells compared to untreated WHCO1 cells.

Canonical pathway analysis showed aberrant expression of pathways known to be involved in cancer, including p53 signaling, ERK/MAPK signaling, Wnt/β-catenin signaling, Breast and Ovarian Cancer signaling and AhR signaling (Fig. 3.12B). Genes involved in the DNA damage response were up-regulated (Fig. 3.12B, Fig. 3.13). The down-regulated expression of genes involved in the cell cycle and up-regulation of genes involved in the repair of DNA damage suggests that BaP-treated EPC-2 cells do not become like WHCO1 cells because EPC-2 cells decrease cell proliferation through cell cycle arrests to repair BaP-induced DNA damage.

Figure 3.12 Biological functions and canonical pathways altered in BaP-treated EPC-2 cells compared to untreated WHCO1 cells. Differential expression gene lists of WHCO1 Un vs EPC-2 BaP were entered into IPA to determine significant biological functions **(A)** and canonical pathways **(B)** in this comparison. Significance is indicated by –log(p-value). Green indicates down-regulated; red indicates up-regulated. Number above bar indicates number of genes within the pathway. Bar represents percentage of genes within pathway that are up- or down-regulated. The top canonical pathway is represented graphically in Figure 3.13.

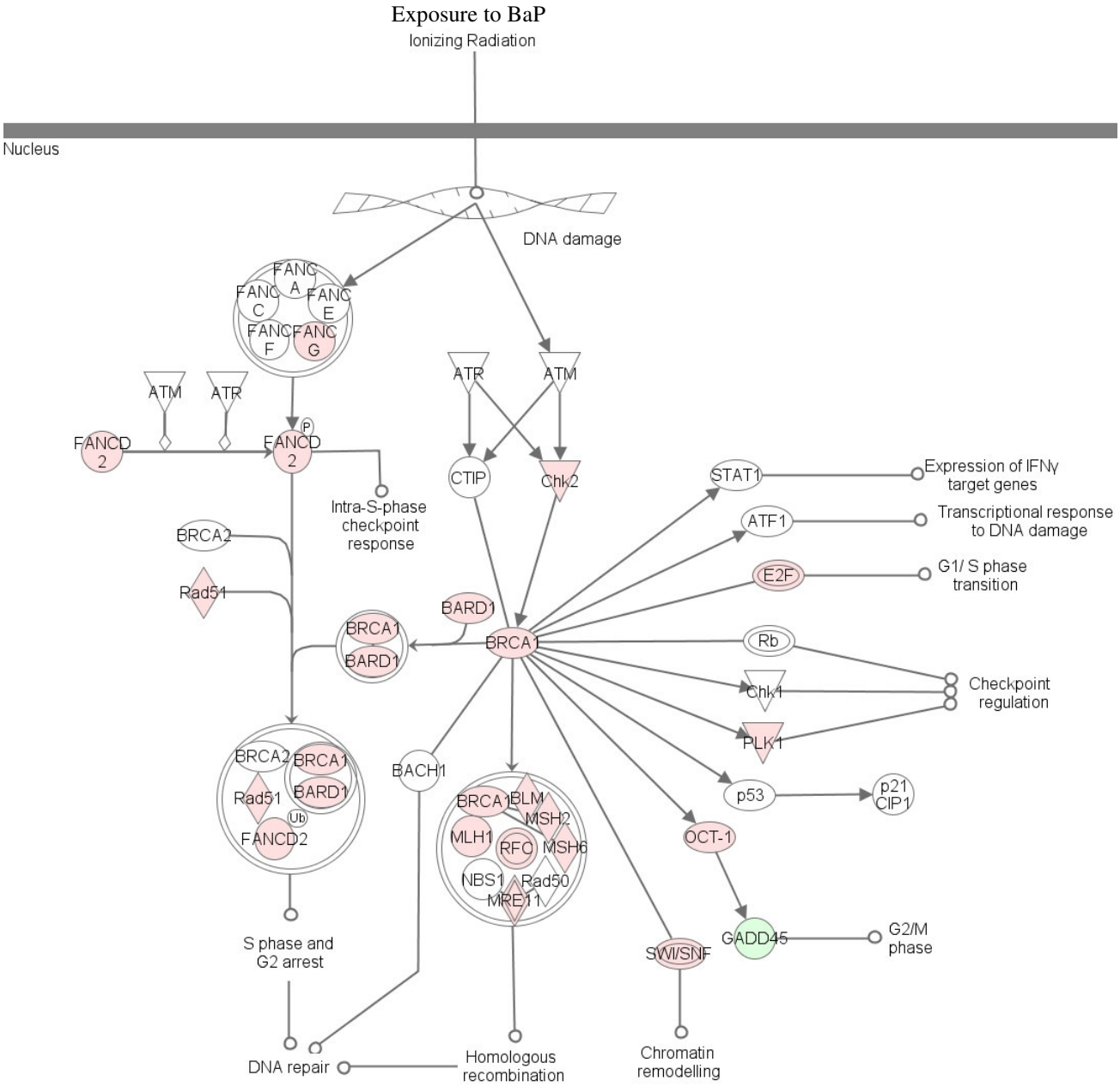

Figure 3.13 Up-regulation of the DNA Damage Response pathway in BaP-treated EPC-2 cells. The most significant canonical pathway was the role of BRCA1 in the DNA damage response. In response to DNA damage, such as exposure to BaP or ionizing radiation, nuclear BRCA1 (breast cancer 1) associates with several other molecules to allow for DNA repair (with repair genes MLH1, MSH2, MSH6, BLM, MRE11, CHK2, Rad51 and RFC), cell cycle arrest at cell cycle checkpoints (involving FANCD2, PLK1, OCT1, GADD45) and progression through the cell cycle (E2F). Red shaded genes are up-regulated; green shaded genes are down-regulated. Arrow indicates direction of pathway; circle indicates biological result.

3.2.7 Similarities and differences between the transcriptional responses of EPC-2 and WHCO1 cells to treatment with BaP

BaP-treated EPC-2 and WHCO1 datasets were compared to determine which genes were commonly and uniquely expressed after BaP exposure, and therefore whether EPC-2 and WHCO1 cells respond in the same way to BaP treatment (Fig. 3.14). There were more commonly down-regulated genes between WHCO1 and EPC-2 cells (45, Fig. 3.14B) than commonly up-regulated genes (19, Fig. 3.14A). The lists of commonly up- and down-regulated genes are indicated in Appendix A.

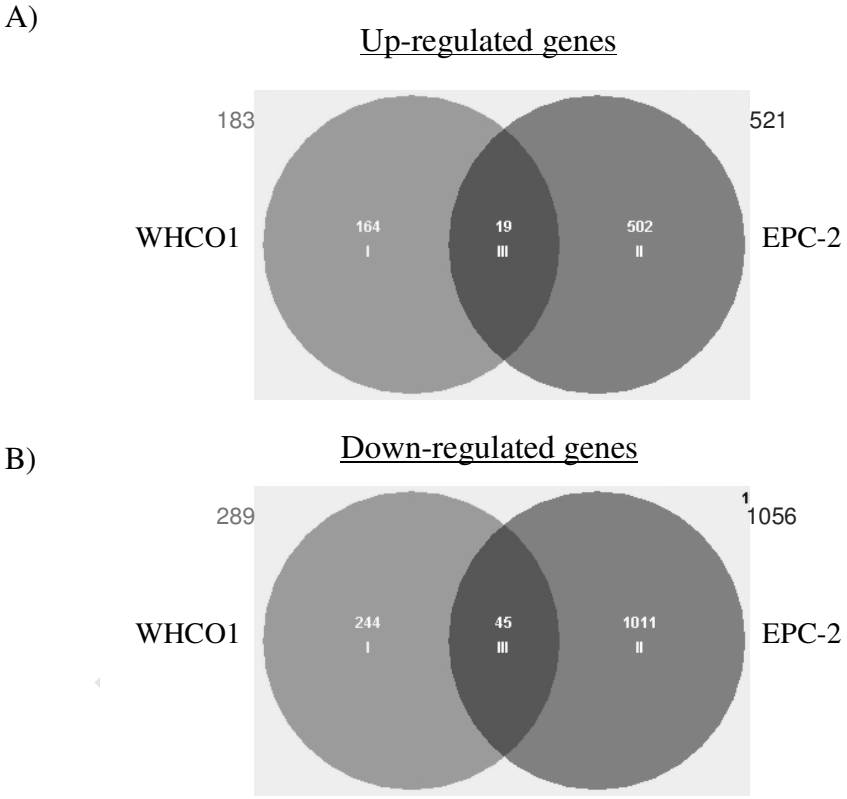

Figure 3.14 Common genes up- or down-regulated in response to BaP exposure. Venn diagrams show number of genes commonly and uniquely up-regulated **(A)** or down-regulated **(B)** by BaP exposure in WHCO1 (left) and EPC-2 (right) cells. I: Genes uniquely expressed by BaP exposure in WHCO1 cells; II: Genes uniquely expressed by BaP exposure in EPC-2 cells; III: Genes commonly expressed by BaP exposure in both WHCO1 and EPC-2 cells. Total numbers of up- or down-regulated genes are indicated at top left and right corners for WHCO1 and EPC-2, respectively.

Commonly up-regulated genes of interest include EREG (epiregulin), FOSL1 (FOS-like antigen 1) and IL10RA (interleukin 10 receptor alpha), although many of the genes up-regulated were hypothetical protein loci, open reading frames and cloned sequences (Appendix A). The most up-regulated genes were ANPEP (alanyl membrane aminopeptidase, 10.05-fold) for WHCO1 and HS.389988 (cDNA clone, 9.02-fold) for EPC-2.

Commonly down-regulated genes of interest include TGFB2 (transforming growth factor beta 2), SULT1C3 (sulfotransferase 1C3) and ITGB8 (integrin beta 8), while, similar to the commonly up-regulated genes, many of the genes were hypothetical protein loci and cDNA clones (Appendix A). The most down-regulated genes were HS.537735 (cDNA clone, -8.99-fold) and DHRS2 (-8.28-fold) for WHCO1 and KRT4 (keratin 4, -61.76-fold) and H19 (non-coding maternally expressed transcript, -45.94-fold) for EPC-2. Although genes in common between BaP-treated WHCO1 and EPC-2 cells varied widely in function, many are involved in metabolic pathways.

IPA analysis showed that important biological functions in the transcriptional response to BaP in WHCO1 and EPC-2 cells were Cancer, Cell Cycle, Cell Death, Cellular Growth and Proliferation, and DNA Replication Recombination and Repair (Fig. 3.15A). Important canonical pathways were Role of BRCA1 in DNA Damage Response, Role of CHK Proteins in Cell Cycle Checkpoint Control, and p53 Signaling (Fig. 3.15B). The up-regulation of 40-50% of genes in DNA damage pathways (Role of BRCA1 in DNA damage response and Role of CHK proteins in cell cycle checkpoint control) suggests an important common response to BaP exposure.

A)

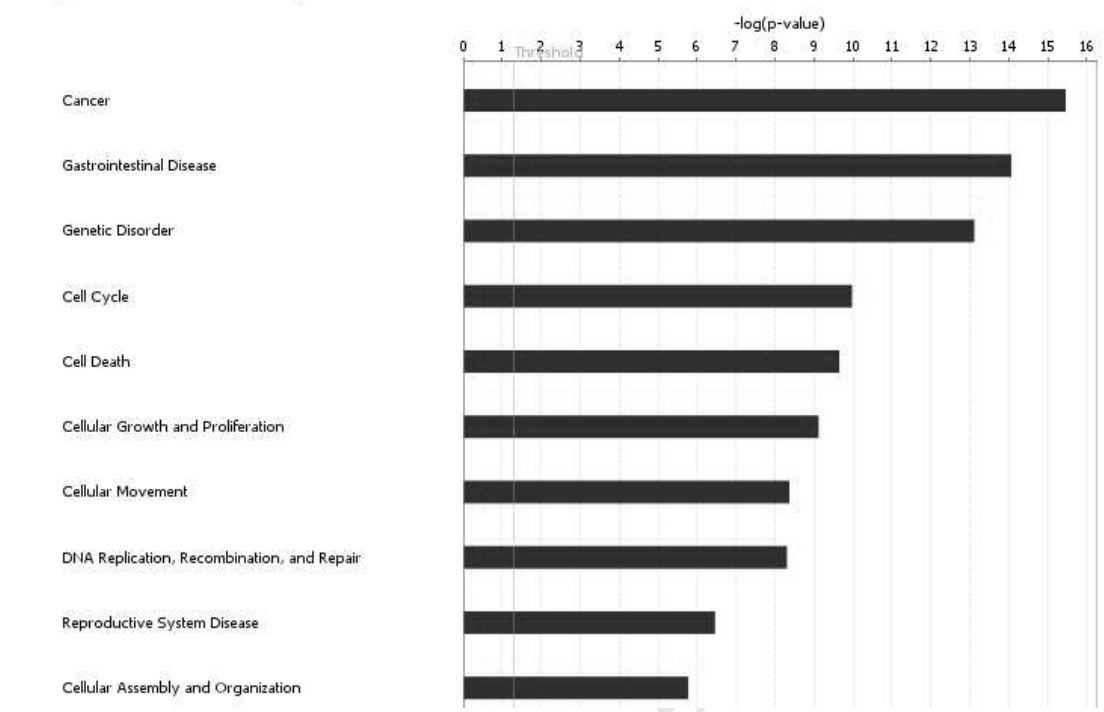

B)

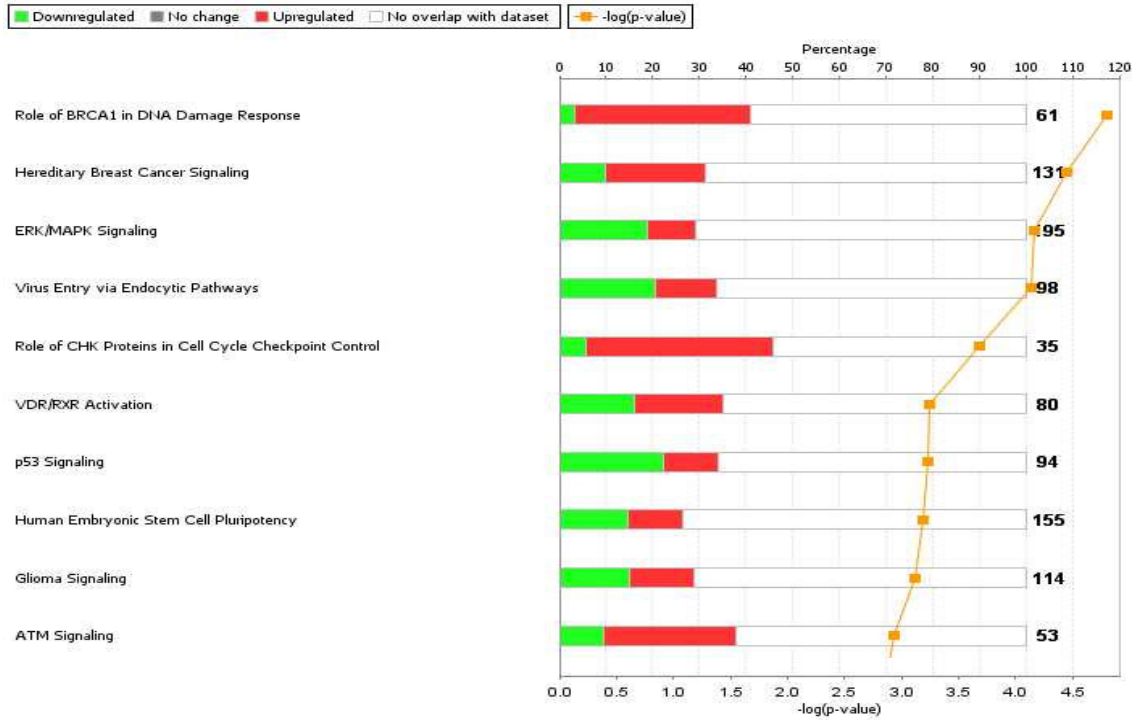

Figure 3.15 Functions and Pathways affected in the common transcriptional response to BaP treatment in EPC-2 and WHCO1 cells. Biological functions **(A)** and canonical pathways **(B)** were generated in IPA from the list of differentially expressed genes in BaP-treated WHCO1 cells compared to BaP-treated EPC-2 cells. In **(A)** –log(p-value) indicates significance of biological function. In **(B)** green indicates down-regulated; red indicates up-regulated. Number above bar indicates number of genes within the pathway. Bar represents percentage of genes within pathway that are up- or down-regulated. Orange line graph indicates significance of canonical pathway [-log(p-value)] according to secondary scale.

3.2.8 Meta-analysis: common differentially expressed genes affected by BaP treatment in normal and transformed cell lines

The final objective was to determine whether normal and cancer cells from the oesophagus respond to BaP treatment in the same way as cells from other tissues. Genes differentially expressed in response to BaP in WHCO1 and EPC-2 cells were compared to gene lists from published microarray data from other BaP-treated cell lines (Table 1.2) in a meta-analysis as described in *Methods*.

The genes most commonly affected in response to BaP were CYP1A1 (shared by 5 cell lines), CYP1B1, NQO1, TIPARP, MMP1, AKR1C2 and CTGF (Table 3.1). The expression of several metabolism genes suggests common mechanisms of BaP metabolism by the cells from the breast, oesophagus and liver. BaP-treated EPC-2 cells had more genes in common with mammary epithelial cells (NHMECs, 5 genes in common) than with normal cell lines derived from lung fibroblasts (WI38), skin keratinocytes (NHEK) or oral epithelial cells (HIOEC, Table 3.1). BaP-treated WHCO1 cells had more genes in common with liver carcinoma cells (HepG2, 5 genes in common) than breast carcinoma (MCF-7), colorectal carcinoma (HCT116; Caco-2) or lung adenocarcinoma cells (A549, Table 3.1).

The cell lines sharing the most common genes were NHMEC and WHCO1 cells, commonly expressing 7 genes (MMP1, CYP1A1, CYP1B1, SERPINB2, IL1B, CA9 and TIPARP, Table 3.1). Six genes were shared by NHMEC and MCF-7 (CYP1A1, CYP1B1, AKR1C2, PPARG, NQO1 and TIPARP), NHMEC and HepG2 (CYP1A1, CYP1B1, SERPINB2, AKR1C2, CTGF and NQO1) and MCF-7 and HepG2 (CYP1A1, CYP1B1, AKR1C2, AKR1C3, OKL38 and NQO1, Table 3.1). These findings suggest a small common transcriptional response to BaP exposure between cell lines derived from the breast, oesophagus and liver. However, since gene expression was more divergent than common between the normal and transformed cell lines, the transcriptional responses to BaP exposure appear to be cell type-specific.

Table 3.1 Meta-analysis: Common genes with altered expression in response to BaP exposure

↑: up-regulation; ↓: down-regulation; MMP1: matrix metalloprotease 1; CYP1A1: cytochrome P450 1A1; CYP1B1: cytochrome P450 1B1; ID1: inhibitor of DNA binding 1; SERPINB2: serine peptidase inhibitor B2; AKR1C2: aldo-keto reductase C2; IL1B: interleukin 1 beta; FN1: fibronectin 1; RRAD: Ras-related associated with diabetes; PPARG: peroxisome proliferators-activated receptor gamma; OKL38: pregnancy-induced growth inhibitor; CTGF: connective tissue growth factor; AKR1C3: aldo-keto reductase 1C3; S100A8: S100 calcium binding protein A8; CXCL10: chemokine (C-X-C motif) ligand 10; CA9: carbonic anhydrase 9; SPP1: secreted phosphoprotein 1; NQO1: NADPH quinone oxidoreductase; TIPARP: TCDD-inducible poly(ADP)-ribose polymerase

	Normal					Cancer					
Genes	**Cell Line and Tissue Origin**										
	EPC-2	**WI38**	**NHMEC**	**NHEK**	**HIOEC**	**WHCO1**	**HepG2**	**MCF-7**	**HCT116**	**Caco-2**	**A549**
	Oesophagus	**Lung**	**Breast**	**Skin**	**Mouth**	**Oesophagus**	**Liver**	**Breast**	**Colon**	**Colon**	**Lung**
MMP1	↓		↑			↑				↑	
CYP1A1			↑			↑	↑	↑		↑	
CYP1B1			↑			↑	↑	↑		↑	
ID1	↑				↑		↑				
SERPINB2			↑			↑	↑				
AKR1C2			↑		↓		↑	↑			
IL1B			↑	↑		↑					
FN1	↓	↓									↑
RRAD	↓		↓	↑							
PPARG			↓	↑				↑			
OKL38						↑	↑	↑			
CTGF	↓		↓				↓				↑
AKR1C3	↓						↑	↑			
S100A8	↓		↑		↓						
CXCL10	↓				↓	↑					
CA9	↓		↓			↓					
SPP1	↓					↑	↑				
NQO1			↑				↑	↑	↑		
TIPARP			↑			↑		↑	↑		

3.3 Discussion

Characterizing the complex transcriptional responses of normal and transformed oesophageal epithelial cells to BaP provides insight into the mechanisms of action of BaP and its role in carcinogenesis.

3.3.1 Microarray data analysis

The method used for data analysis may influence the final differential gene expression pattern and interpretation of the results. Methods of data pre-processing such as filtering, background subtraction, truncating signal values and trimmed mean scaling lead to the exclusion of some signal values, and therefore some gene expression information may be lost. We omitted background subtraction in our analysis as it should not greatly affect the outcome (de Waard *et al*., 2008, C. Waterfall, Illumina UK, personal communication). Gene expression fold change was frequently exaggerated by the microarray differential expression analysis, generating more than 2000-fold regulation of many genes (Appendix A). Since fold change was reproducible by qRT-PCR but shown to be overestimated in some genes, fold change by microarray analysis should be considered an indication but not a direct measurement of gene expression.

3.3.2 Differential gene expression in response to BaP exposure

Transcriptional profiling of BaP-treated EPC-2 and WHCO1 cells showed differential expression of many interesting genes (objective i). The expression of many xenobiotic metabolism genes in WHCO1 cells in response to BaP was not unexpected. The up-regulation of several UDP-glucuronosyltransferases (UGT1A1, UGT1A6, UGT1A10, UGT2B7) suggests that glucuronidation is an important BaP Phase II detoxification mechanism, which agrees with previous studies (Zheng *et al*., 2002, Miller and Ramos, 2001). In contrast, GSTA4 (WHCO1), GSTM1, GSTM2 (EPC-2) and SULT1C3 (WHCO1 and EPC-2) were down-regulated; suggesting that formation of sulfate and glutathione conjugates are not the preferred methods of BaP phase II detoxification.

CYP1A1 and CYP1B1 were greatly up-regulated in WHCO1 cells in response to BaP but were not differentially changed in EPC-2 cells. These findings agree with the known role of CYP1A1 and CYP1B1 in Phase I metabolism of BaP, and in our results, the up-regulation of these genes during BaP treatment in WHCO1 cells (Fig. 2.2). CYP1A1 and CYP1B1 expression was

frequently induced in BaP microarray analyses in other cell lines (NHMEC, Gwinn *et al*., 2005, Keshava *et al*., 2005, John *et al*., 2008, HepG2, Staal *et al*., 2006, van Delft *et al*., 2004, Hockley *et al*., 2006, 2007, 2009, MCF-7, Mahadevan *et al*., 2005, Hockley *et al*., 2006, 2007, Kemp *et al*., 2006, Caco-2, de Waard *et al*., 2008). The absence of CYP1A1 and CYP1B1 induction in EPC-2 microarray data agrees with the results in Figure 2.3 (CYP1 induction in twelve cell lines). The absence of xenobiotic metabolism pathways in the EPC-2 microarray data suggests that metabolic activation and detoxification of BaP are not the major response in BaP-treated EPC-2 cells. CYP1A2 was not differentially expressed in either WHCO1 or EPC-2 cells, thereby confirming its insignificant role in BaP metabolism.

In EPC-2 cells, the major response to BaP treatment was the expression of genes involved in cell cycle regulation and up-regulation of the DNA damage response (Fig. 3.8-9). Negative regulation of the cell cycle was evident as BaP-treated EPC-2 cells had decreased cellular proliferation compared to untreated cells (Fig. 2.8). Reduced cellular proliferation is believed to be a result of cell cycle arrest to allow repair of BPDE-damaged DNA. One of the consequences of the DNA damage response is the induction of programmed cell death or apoptosis in cells where damaged DNA cannot be repaired. This would protect cells against transformation from genotoxicity and mutations. In BaP-treated EPC-2 cells, however, no increase in pro-apoptotic pathways or up-regulated expression of apoptotic genes was observed. In contrast, caspase 14 (apoptosis-related cysteine peptidase) was down-regulated 16-fold in BaP-treated EPC-2 cells. However, changes in EPC-2 cell morphology during prolonged BaP treatment showed an increase in the number of apoptotic cells (Fig. 2.9), suggesting that while apoptosis was not induced after 48h BaP treatment in the microarray, apoptosis was induced in some cells only after successive treatments with BaP.

The inflammatory response was significantly altered in response to BaP treatment in WHCO1 cells. Both pro-inflammatory genes and xenobiotic metabolism genes were up-regulated. The increase in the inflammatory response is probably due to the increased production of ROS during phase I metabolism of BaP, which increases oxidative stress signaling. Oxidative stress and chronic inflammation are known to be associated with cancer, and oxidative stress signaling in response to BaP has been reported in MCF-7 and HepG2 cells (Hockley *et al*., 2006). Our microarray results agree with the model that increased BaP metabolism in WHCO1 cells results in increased production of oxygenated metabolites and subsequently ROS (Fig. 2.10).

Some alcohol metabolizing genes (ADH7, ALDH3A1, ALDH1L2, ALDH3B2) were expressed in response to BaP treatment in WHCO1 and EPC-2 cells. The observed induction of ALDH3A1 is consistent with the fact that it is a target gene for the ligand-activated AhR (Androutsopoulos *et al*., 2009). The regulation of alcohol metabolizing genes by BaP may be important in mediating the synergistic effects of tobacco smoking and alcohol consumption on the risk of developing OSCC. In other words, BaP exposure during tobacco smoking may regulate expression of alcohol metabolizing genes that activate ethanol to the carcinogenic acetaldehyde, thereby enhancing DNA damage and OSCC risk.

Interestingly, the AHRR is up-regulated 3.27-fold in BaP-treated WHCO1 cells, suggesting that AhR signaling should be negatively regulated in this response. However, AhR signaling was not entirely down-regulated (Fig. 3.6B), which suggests that the AHRR is not fully repressing AhR activity in WHCO1 cells. Future work should therefore further investigate the role of the AHRR protein and its function.

Lamin B1 (LMNB1) was up-regulated 2.68-fold in BaP-treated EPC-2 cells but was not affected in WHCO1 cells. This result is consistent with the increase in Lamin B1 nuclear protein levels in BaP-treated EPC-2 cells compared to untreated cells (Fig. 2.6) and the evidence that BPDE induces Lamin B1 mRNA in normal human amnion epithelial cells and foetal lung fibroblasts (Lu *et al*., 2009, Dreij *et al*., 2010). These findings further support the need for alternative nuclear protein loading controls.

Integrin beta 7 (ITGB7), a target gene for the ligand-activated AhR (Monteiro *et al*., 2008), was up-regulated in WHCO1 cells but down-regulated in EPC-2 cells in response to BaP treatment (Fig. 3.4). Integrins are cellular adhesion molecules that are involved in cell fate control between growth, differentiation and apoptosis. Up-regulation of ITGB7 in response to BaP was observed in macrophages (Sparfel *et al*., 2010). However, down-regulation of other integrins (ITGB6, ITGB8, ITGAV) was observed in BaP-treated WHCO1 and/or EPC-2 cells. In epidermal keratinocytes, down-regulation of integrins is associated with differentiation (Tennenbaum *et al*., 1996), suggesting that differentiation may be part of the cellular response to BaP in EPC-2 cells.

Several histone genes (HIST1H2BH, HIST1H2BC, HIST1H2BF, HIST1H2AM, HIST1H3G) were differentially regulated in BaP-treated WHCO1 and EPC-2 cells. Down-regulation of other histone genes (HIST1H2BG, HIST1H4B, HIST1H2BJ, HIST1H3D, HIST1H4C) and

nucleosome and chromatin assembly by BaP was observed in MCF-7 and HepG2 cells (Hockley *et al*., 2006). Histone gene suppression is believed to be important for cell cycle arrest following DNA damage to allow for DNA repair (Hockley *et al*., 2007). Consistent with this, the DNA damage response and DNA repair pathways were significantly altered in response to BaP in WHCO1 and EPC-2 cells.

The role of BaP in carcinogenesis is not limited to changes in gene expression profiles and cellular responses to AhR activation. BaP has also been shown to disrupt DNA methylation (Sadikovic and Rodenhiser, 2006) and recruit DNA methyltransferases to silence target genes, such as RARβ2 (Ye and Xu, 2010). In addition, natural DNA methylation inhibitors like tea polyphenols and soy isoflavones are able to reverse BaP-associated gene methylation (Manna *et al*., 2009, Fang *et al*., 2003) and DNA damage (Baumeister *et al*., 2009). Genes known to be silenced by methylation in OSCC (Ishii *et al*., 2007, Roth *et al*., 2006) were also down-regulated in BaP-treated WHCO1 and EPC-2 cells, including MGMT (O-6 methylguanine methyltransferase), SFRP1 (secreted frizzled-related protein), DAPK3 (death-associated protein kinase 3) and p16INK4a/p14ARF, although COX2 (cyclooxygenase 2), CLDN3 (claudin 3) and MT1G (metallothionein 1G) were up-regulated. These findings implicate a role for BaP in gene silencing by methylation in WHCO1 and EPC-2 cells, which opens up a new avenue for future work.

IPA analysis showed that p53 signaling was significantly affected with around 35% of total p53 signaling genes affected in three of the comparisons: BaP-treated normal cells compared to cancer cells, the common transcriptional response to BaP and the baseline differences in gene expression between normal and cancer cells (WHCO1 Un vs EPC-2 BaP, WHCO1 BaP vs EPC-2 BaP and WHCO1 Un vs EPC-2 Un). Since cell cycle regulatory and DNA repair pathways were frequently altered in response to BaP and in untreated cancer cells, the role and function of p53 in the cellular response to BaP should be explored further.

Transcriptional profiling of untreated WHCO1 compared to untreated EPC-2 cells allowed for the examination of fundamental differences in gene expression in the absence of the BaP response (objective ii). Cell cycle regulatory genes and cell cycle processes were up-regulated in untreated WHCO1 compared to EPC-2 cells (Fig. 3.10-11), suggesting increased proliferation occurs in the absence of BaP. This agrees with our results showing increased cellular proliferation in WHCO1 compared to EPC-2 cells (Fig. 2.8). Significant expression of mitosis, proliferation and cell cycle

processes in untreated WHCO1 compared to untreated EPC-2 cells is also in agreement with the established fact that enhanced proliferative potential is a hallmark of cancer (Hanahan and Weinberg, 2000).

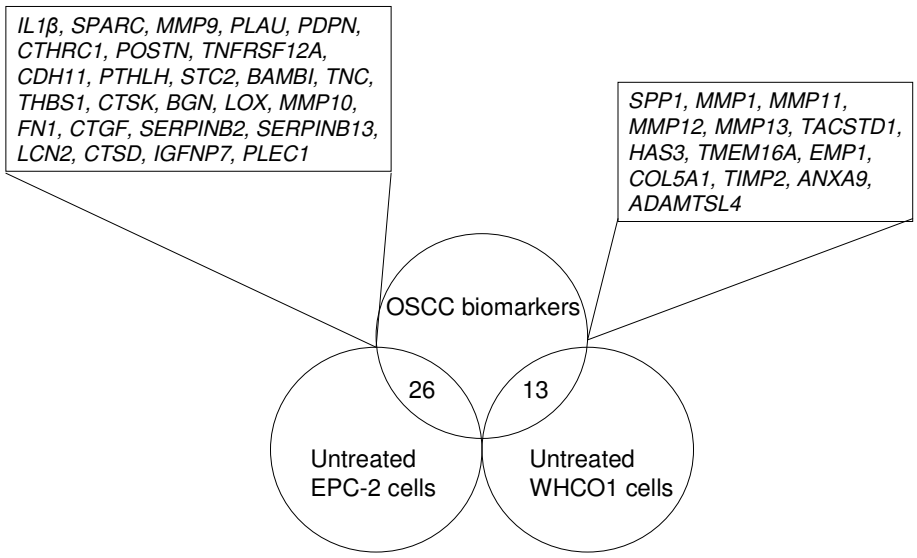

Figure 3.16 Common genes shared between untreated EPC-2 and WHCO1 cells and known OSCC biomarkers. Genes known to be over-expressed or down-regulated in OSCC (Kashyap *et al*., 2009, 2010) were found to be expressed in WHCO1 and EPC-2 cells in the absence of BaP. Over-expressed genes: SPP1: secreted phosphoprotein 1, MMP11: matrix metalloproteinase 11 (stromelysin 3), TACSTD1: tumour associated calcium signal inducer 1, HAS3: hyaluronic acid synthase 3, EMP1: epithelial membrane protein 1, MMP13: matrix metalloproteinase 13 (collagenase), MMP1: matrix metalloproteinase 1, COL5A1: collagen type 5 alpha 1, MMP12: matrix metalloproteinase 12, TIMP2: TIMP metallopeptidase inhibitor 2, ANXA9: annexin A9, ADAMTSL4: ADAMTS-like 4. Down-regulated genes: PLAU: urokinase plasminogen activator, SPARC: secreted protein acidic cysteine rich osteonectin, IL1β: interleukin 1 beta, PDPN: podoplanin, MMP9: matrix metalloproteinase 9 (gelatinase B), CTHRC1: collagen triple helix repeat containing 1, POSTN: periostin, TNFRSF12A: tumour necrosis factor receptor superfamily 12A, CDH11: cadherin 11, PTHLH: parathyroid hormone-like hormone, STC2: stanniocalcin 2, BAMBI: BMP and activin membrane-bound inhibitor homolog, TNC: tenascin C, THBS1: thrombospondin 1, CTSK: cathepsin K, BGN: biglycan, LOX: lysyl oxidase, MMP10: matrix metalloproteinase 10 (stromelysin 2), FN1: fibronectin 1, CTGF: connective tissue growth factor, SERPINB2: serpin peptidase inhibitor B2, SERPINB13: serpin peptidase inhibitor B13, LCN2: lipocalin 2, CTSD: cathepsin D, IGFBP7: insulin-like growth factor binding protein 7, PLEC1: plectin 1 intermediate filament binding protein.

Kashyap and colleagues have recently shown that several genes are over-expressed or down-regulated in patients with OSCC (Kashyap *et al*., 2009, 2010). These OSCC genes or biomarkers were compared to the genes expressed in untreated EPC-2 and WHCO1 cells. In the absence of BaP, untreated EPC-2 and WHCO1 cells share the expression of 26 and 13 genes, respectively, with known OSCC biomarkers (Fig. 3.16). The most featured genes associated with OSCC are

the matrix metalloproteinases (MMP). MMPs play an important role in the breakdown of extracellular matrix (ECM) proteins during primary steps in the invasion, migration and tissue remodeling associated with cancer progression. EPC-2 and WHCO1 cells express MMP1, 9, 10, 11, 12 and 13 (Fig. 3.16), suggesting that these cells are more active in ECM degradation.

When examining the role of BaP in carcinogenesis in normal cells, we hypothesized that BaP treatment causes normal cells to become like cancer cells (objective iii). There was significant aberrant regulation of known cancer-related pathways (AhR, p53, ERK/MAPK and Wnt/β-catenin) in BaP-treated EPC-2 cells compared to untreated WHCO1 cells (Fig. 3.12). ERK/MAPK and Wnt/β-catenin pathways are signal transduction cascades that are important in cell growth, differentiation and proliferation, and therefore deregulated gene expression in these pathways may play a role in carcinogenesis. Together with the dynamic expression of genes known to be over-expressed in OSCC, these results suggest that BaP treatment has the potential to lead to cancer initiation in EPC-2 cells. However, EPC-2 cells protect against genotoxicity and possible oncogenic mutations by regulating the DNA damage response and conducting cell cycle checkpoints (Fig. 3.12). The balance between BaP-induced transformation and prevention of carcinogenesis is therefore mediated by the interplay between pro-cancer pathways and anti-cancer cell cycle regulation and DNA repair. However, no studies to date have shown that a single treatment with BaP can induce cellular transformation. Therefore our results suggest that while events preceding cancer initiation occur in BaP-treated EPC-2 cells, complete carcinogenesis does not occur. It is likely that consecutive BaP treatments, which more closely mimic chronic tobacco smoking although do not take into account the presence of other tobacco smoke carcinogens, will be more effective at initiating cancer.

3.3.3 Comparison to other BaP microarrays

Published BaP microarray data have shown that the transcriptional responses to BaP are complex and dependent on various factors such as length of BaP treatment, BaP concentration and cell type (Hockley *et al*., 2006, 2007, objective v). The treatment conditions used in our experiment were 10μM BaP treatment for 48h, but conditions in other BaP microarrays varied from 6h-72h and even 6 months treatment with BaP of concentrations varying from 0.25μM to 9mM. However, while specific gene expression profiles may vary in a time- and concentration-dependent and cell-specific manner, common transcriptional and cellular responses were found.

Most published microarray studies have shown that the transcriptional response to BaP involved xenobiotic metabolism, cell cycle regulation, DNA damage repair, apoptosis, cell proliferation, oxidative stress signaling and nucleosome assembly (Hockley *et al*., 2006, 2007, 2008, 2009, de Waard *et al*., 2008, Perez *et al*., 2008, Keshava *et al*., 2005, van Delft *et al*., 2004, Mahadevan *et al*., 2005, Sohn *et al*., 2008, Gwinn *et al*., 2005, John *et al*., 2008). Our results are consistent with these findings, except there is no obvious effect on apoptotic signaling processes in our cell lines. The down-regulation of apoptosis-related genes and the absence of apoptosis in response to BaP has been reported in HepG2 and WI38 cells (Staal *et al*., 2006, Sohn *et al*., 2008), and apoptotic signaling genes were not up-regulated in the absence of p53 in HCT116 cells (Hockley *et al*., 2008). Collectively, these results suggest that the regulation of apoptosis is complex and depends on other factors such as p53 status and cell type.

Common genes were found to be differentially expressed by BaP in multiple cell types by meta-analysis of our results and other BaP microarrays. Xenobiotic metabolism genes (CYP1A1, CYP1B1, NQO1, AKR1C2, AKR1C3) were the most commonly shared, followed by genes involved in cell cycle or growth regulation (IL1β, RRAD, PPARG, OKL38, CTGF), adhesion and invasion (FN1, SPP1, MMP1, CA9), inflammation (FN1, S100A8, CXCL10), DNA damage-induced repair (TIPARP) and apoptosis (S100A8, SERPINB2). Aldo-keto reductases (AKRs) represent another mechanism of BaP metabolic activation and a source of oxidative stress. BaP-diols are converted by AKRs to BPQ ortho-quinones which greatly amplify ROS while participating in useless redox cycles (Burczynski and Penning, 2000). BPQs also form DNA adducts and cause oxidative DNA damage (Burczynski and Penning, 2000). The elevated expression of AKRs suggests that an increase in the metabolic activation of BaP to BPQ and generation of ROS is a common pathway activated during BaP exposure. S100A8 (S100 calcium binding protein A8) is a pro-inflammatory gene that together with its dimerization partner, S100A9, is down-regulated in OSCC (Zhang *et al*., 2004). S100A9 is a p53 target and S100A8 and 9 have been shown to play a role in inhibition of cell growth and induction of apoptosis (Li *et al*., 2009). TIPARP (TCDD-inducible poly(ADP-ribose) polymerase) is a member of the PARP family of enzymes that are induced in response to DNA strand breakage and participate in DNA repair pathways (Ma *et al*., 2001). The expression of TIPARP is therefore a cellular defense mechanism against DNA damage. The common expression of these genes (Table 3.1) suggests that, despite different treatment conditions and cell types, there are universal transcriptional responses to BaP.

Consistent with one of the major responses to BaP in multiple cell types, the common transcriptional response to BaP in WHCO1 and EPC-2 cells was an increase in the DNA damage response and DNA repair pathways (objective iv). This suggests that, regardless of cell type or CYP1 induction capacity, exposure to BaP results in increased levels of BPDE and BPQ that effectively bind and damage DNA.

The transcriptional response to BaP has both similar and distinguishable gene expression patterns to other PAHs. This may reflect their different properties and mechanisms of action. BaP is readily metabolized and exhibits genotoxic effects due to DNA binding (de Waard *et al*., 2008). Benzo[e]pyrene (BeP), the non-carcinogenic isomer of BaP, allows for determination of toxic compared to genotoxic effects (Hockley *et al*., 2006). TCDD, which is not readily biodegradable, activates the AhR but does not bind DNA (de Waard *et al*., 2008, Hockley *et al*., 2007). BPDE, the carcinogenic metabolite of BaP, causes DNA damage but does not activate the AhR (Hockley *et al*., 2007). Despite mediating different gene expression profiles, these PAHs also share overlapping gene expression patterns that will be important when considering the combined role of all tobacco smoke components in carcinogenesis.

3.3.4 Summary

Transcriptional profiling of BaP-treated EPC-2 and WHCO1 cells has shown that the response to BaP exposure is complex and, despite a small common response, is generally divergent between normal and transformed oesophageal epithelial cells.

Normal cells (EPC-2) differentially express cell cycle regulation genes and up-regulate DNA damage response pathways in response to BaP (Fig. 3.17). Cell proliferation is slowed, most likely to allow for repair of BPDE-damaged DNA. EPC-2 cells therefore try to protect themselves against BaP-induced genomic instability and transformation. While expression of apoptotic genes and pathways was not evident after 48h BaP treatment, apoptotic cells were prevalent after prolonged exposure to BaP, suggesting that a single treatment is not sufficient to induce apoptosis in these cells.

EPC-2 cells treated with BaP become somewhat like cancer cells due to their aberrant regulation of cancer-related signaling pathways and expression of genes known to be over-expressed in OSCC. However, EPC-2 cells protect against BaP-induced transformation by regulating cell

cycle checkpoints and DNA damage repair. This suggests that BaP has the potential to initiate transformation of EPC-2 cells, but since BPDE-damaged DNA is repaired, a single treatment does not initiate transformation.

Cancer cells (WHCO1) increase expression of genes involved in xenobiotic metabolism and the oxidative stress response (Fig. 3.17). The increased expression of xenobiotic metabolism genes allows for the increased production of ROS and other DNA damaging metabolites during BaP metabolism, which enhance oxidative stress signaling. Sustained AhR signaling may lead to cancer maintenance or progression.

The common transcriptional response of WHCO1 and EPC-2 cells to BaP treatment involves the DNA damage response and DNA repair pathways. This suggests that the DNA damage caused by the carcinogenic metabolite of BaP, BPDE, is significant.

Genes involved in xenobiotic metabolism, cell cycle regulation, adhesion, invasion, inflammation, DNA repair and apoptosis are commonly expressed in response to BaP in multiple cell lines, from normal breast and breast carcinoma, hepatocarcinoma, normal and transformed oesophageal epithelium, colon carcinoma, oral epithelium, normal lung and lung adenocarcinoma, and epidermal keratinocytes.

Our results agree with the major conclusions drawn from microarrays in other cell lines treated with BaP. However, transcriptional profiling does not take into account the role of gene products in the cellular response to BaP. It is therefore important to look at the proteomic response to BaP for a more complete understanding of the cellular response to BaP (Heijne *et al*., 2003).

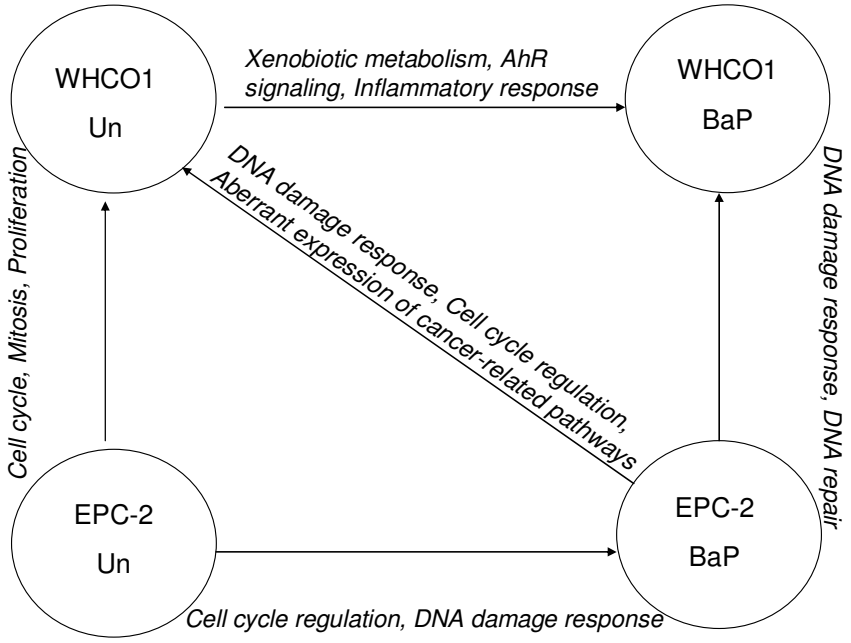

Figure 3.17 Summary of the transcriptional response to BaP in WHCO1 and EPC-2 cells. BaP treatment results in increased expression of genes involved in xenobiotic metabolism, AhR signaling and the inflammatory/oxidative stress response in WHCO1 cells and cell cycle regulation and the DNA damage response in EPC-2 cells. In the absence of BaP, WHCO1 cells have enhanced cell proliferation and mitosis compared to EPC-2 cells. The common transcriptional response to BaP treatment in WHCO1 and EPC-2 cells is the DNA damage response and DNA repair pathways. Treatment with BaP causes EPC-2 cells to differentially express genes involved in the DNA damage response, cell cycle regulation and cancer-related pathways (AhR, p53, Wnt/β-catenin, ERK/MAPK) compared to untreated WHCO1 cells.

Chapter 4
Conclusion

This study investigated the cellular and transcriptional responses to BaP in a normal oesophageal epithelial cell line (EPC-2) and an OSCC cell line (WHCO1) in order to characterize and gain insight into the mechanisms of carcinogenesis of BaP and its role in tobacco smoking-associated OSCC.

BaP is metabolically activated to its carcinogenic metabolite, BPDE, by the Phase I XMEs, CYP1A1 and CYP1B1. CYP1 transcription is activated by the AhR-ARNT transcription factor dimer when BaP binds the AhR. The project's first objective was to determine the effect of BaP on the expression of XMEs and the AhR in WHCO1 and EPC-2 cells. The results showed that WHCO1 cells were more efficient at CYP1 induction and subsequent BaP bioactivation than EPC-2 cells. CYP1A1 and CYP1B1 activities were sustained at higher levels after the removal of BaP in WHCO1 than EPC-2 cells. AhR and ARNT entered and exited the nucleus more rapidly after BaP treatment and withdrawal, respectively, in EPC-2 than WHCO1 cells. CYP1A1 and CYP1B1 induction in the panel of South African WHCO cell lines were more efficient at BaP activation than the Japanese KYSE cell lines.

The project's second objective was to investigate the effects of BaP on cellular proliferation and morphology in WHCO1 and EPC-2 cells. Treatment with BaP had no effect on WHCO1 cell proliferation but severely reduced EPC-2 cell growth. WHCO1 cells were therefore more resistant to BaP-induced reduction in cell growth than EPC-2 cells. Reduction in EPC-2 growth was linked to an increase in apoptotic cells following prolonged BaP treatment.

The project's third objective was to explore global gene expression profiles in response to BaP in WHCO1 and EPC-2 cells. Within this investigation, the five sub-objectives were to determine (i) which genes and pathways were affected by BaP in WHCO1 and EPC-2 cells, (ii) differences in gene expression profiles in the absence of BaP, (iii) whether BaP-treated EPC-2 cells have a similar gene expression profile to untreated WHCO1 cells, (iv) whether there was a common transcriptional response to BaP in both cell lines, and (v) which genes were expressed in common with other BaP-treated cell lines from published microarrays. Transcriptional profiling showed differential gene expression responses to BaP. WHCO1 cells showed increased expression of xenobiotic metabolism and inflammatory genes, while EPC-2 cells showed increased expression of cell cycle regulation and DNA damage response genes (sub-objective i). In the absence of BaP,

fundamental differences in gene expression included cell cycle and proliferation genes (sub-objective ii). BaP-treated EPC-2 cells have the potential to become like WHCO1 cells owing to their expression of genes known to be over-expressed in OSCC, but cells are protected against transformation by up-regulation of DNA damage repair pathways (sub-objective iii). The common transcriptional response to BaP in WHCO1 and EPC-2 cells was DNA damage repair (sub-objective iv), while common gene expression induced by BaP but independent of cell type, length of treatment or BaP concentration included genes involved in xenobiotic metabolism, cell cycle regulation, inflammation, adhesion, invasion and apoptosis (sub-objective v).

From these results we hypothesize that sustained CYP1 induction in WHCO1 cells increases BaP metabolic activation and subsequent production of ROS, resulting in oxidative stress signaling and the expression of inflammatory genes. Sustained nuclear AhR signaling may contribute to cancer maintenance or progression in WHCO1 cells. The differences in CYP1 induction capacity between the Japanese and South African cell lines may contribute to inter-population differences in susceptibility to BaP-associated OSCC. In EPC-2 cells, lower CYP1 and Phase II XME induction capacity may result in less efficient BaP detoxification and subsequent accumulation of DNA-damaging metabolites, such as BPDE and BPQ, which cause reduced cell proliferation to allow for DNA damage repair.

This work examined the transcriptional response to BaP in oesophageal cells and compared global gene expression in normal and transformed oesophageal epithelial cells to other cell lines from published microarray data. This work also demonstrates how AhR/ARNT nuclear translocation and prolonged duration in the nucleus (shown by immunofluorescence) corresponds to increased AhR signaling (shown by microarray analysis) in WHCO1 cells compared to EPC-2 cells. Sustained AhR signaling may play an important role in BaP-associated OSCC. Gene expression profiling demonstrated that a major response to BaP exposure was up-regulation of DNA repair genes, indicating that BaP is metabolically activated to its DNA-damaging carcinogenic metabolites more rapidly than it is detoxified.

This research provides an indication of the role of BaP-associated gene expression profiles in the initiation and maintenance of OSCC, and can contribute to further research characterizing the role of whole tobacco smoke in oesophageal carcinogenesis. Transcriptional profiling also aids the identification of new molecular targets (such as AhR signaling and the oxidative stress response) that can be further studied for the prevention and treatment of BaP-associated OSCC.

Chapter 5
Materials and Methods

5.1 Reagents

All chemicals were analytical grade, purchased from Merck (Darmstadt, Germany) while all other reagents were purchased from the specified manufacturers. BaP powder and DMSO were purchased from Sigma-Aldrich (Steinholm, Germany). Primary antibodies against CYP1A1, CYP1A2, CYP1B1, AhR, ARNT, Lamin B1 and β-tubulin, were obtained from Santa Cruz Biotechnology (La Jolla, CA, USA), secondary antibodies (goat anti-rabbit IgG-HRP conjugate and goat anti-mouse IgG-HRP conjugate) from Bio-Rad (Hercules, CA, USA) and fluorescent secondary antibodies (goat anti-mouse IgG fluorescein conjugate and goat anti-rabbit IgG Texas Red conjugate) from Calbiochem (San Diego, CA, USA). Other reagents used are described in Appendix C.

5.2 Cell Culture and Benzo[a]pyrene Treatment

The oesophageal squamous cell carcinoma cell lines, WHCO1, WHCO3, WHCO5 and WHCO6, derived from surgical biopsies from South African OSCC patients were obtained from Prof. Thornley, University of the Witwatersrand, South Africa (Veale and Thornley, 1984); while the KYSE series of cell lines, KYSE 30, KYSE 70, KYSE 150, KYSE 180, KYSE 410, KYSE 450 and KYSE 520, were obtained from Prof. Yutaka Shimada, Kyoto University, Japan (Shimada *et al*., 1992). The WHCO and KYSE series of cell lines were grown in Dulbecco's Modified Eagle Medium (DMEM) containing 10% foetal calf serum (FCS), 100U/ml penicillin and 100µg/ml streptomycin, in a humidified atmosphere of 5% CO_2 at 37°C. The telomerase-immortalized normal oesophageal epithelial cell line, EPC-2, was obtained from Harada *et al*., (2003) and cultured in Keratinocyte Serum Free Medium (KSFM, Gibco, Invitrogen, Carlsbad, CA, USA) containing 100U/ml penicillin and 100µg/ml streptomycin and supplemented with 50µg/ml bovine pituitary extract (BPE, Invitrogen, Carlsbad, CA, USA) and 1ng/ml epidermal growth factor (EGF, Invitrogen, Carlsbad, CA, USA).

Cells were trypsinized using Trypsin-EDTA, neutralized (using DMEM for WHCO and KYSE cell lines and Sodium Trypsin Inhibitor for the EPC-2 cell line) and pelleted by centrifugation at 1000 x g for 5 min at 4°C. Cells were seeded at 3 x 10^5 cells per 100mm dish. Twenty-four hours after plating, the cells were treated with 10µM BaP (Sigma, Steinholm, Germany) by the addition

of BaP dissolved in DMSO (of final concentration 0.1%) to the medium, while untreated cells were treated with 0.1% DMSO and grown for a further 24 hours. The time points investigated are indicated in the relevant figure legends.

For cell growth assays, cells were seeded at 1-2 x 10^4 cells/well in 12-well plates and incubated for 24h. Cells were treated with either 0.1% DMSO (Un) or 10µM BaP (BaP) in medium in triplicate wells and incubated for 5 days. At days 1, 3, 4 and 5, cells were trypsinized, neutralized, stained with 0.4% trypan blue and counted using the Countess Automated Cell Counter (Invitrogen, Carlsbad, CA, USA).

The effects of long-term BaP exposure on cell morphology were examined by phase contrast microscopy at 100x and 40x magnification were taken before and after each BaP treatment using an Olympus SC30 camera calibrated for our Olympus CKX41 microscope (Center Valley, PA, USA), and were compared to phase contrast images of untreated EPC-2 cells and untreated WHCO1 cells.

5.3 Genomic DNA Isolation and Quantification

Genomic DNA was extracted from cultured cells using the method of Strauss (1998). Cells were harvested by trypsinisation and pelleted by centrifugation at 1000 x g for 5 min at 4°C. Cells were washed twice with 5ml ice-cold PBS pH 7.4 and centrifuged for 5 min at 500 x g. The cells were resuspended in 5ml digestion buffer (100mM NaCl, 10mM Tris-HCl pH 8, 25mM EDTA, 0.5% SDS, 0.1mg/ml proteinase K) and incubated overnight at 50°C. An equal volume of phenol:chloroform:isoamylalcohol (25:24:1) was added. The sample was mixed by vortexing, centrifuged for 10 min at 1700 x g and the top aqueous layer transferred to a new tube. This process was repeated until no precipitate accumulated at the interphase. The aqueous phase was transferred to a clean microfuge tube and the DNA precipitated by the addition of one half volume of 7.5M ammonium acetate and two volumes of cold 100% ethanol. DNA was pelleted by centrifugation at 1700 x g for 2 min. The supernatant was discarded, the DNA pellet was washed twice with 70% ethanol, air-dried and resuspended in 100µl TE buffer (10mM Tris-HCl, 1mM EDTA pH 7.5).

DNA was quantified by absorbance at 260 and 280nm using a Nanodrop 2000 spectrophotometer (Thermo Scientific, Waltham, MA, USA). DNA purity was determined by samples having a

260/280 ratio of between 1.8 and 2. DNA integrity was determined by agarose gel electrophoresis.

5.4 Polymerase Chain Reaction-Restriction Fragment Length Polymorphism (PCR-RFLP) Analysis

Primers used to genotype the CYP1 genes in the twelve cell lines were adapted from Landi *et al*. (2005) and Dandara *et al*. (2004). Each PCR reaction contained 100ng genomic DNA, 1 x PCR buffer (Green GoTaq Flexi Buffer, Promega, Madison, WI, USA), 2mM $MgCl_2$ (for CYP1A1) or 1.2mM $MgCl_2$ (for CYP1B1), 0.2mM dNTP mix (Promega, Madison, WI, USA), 1pmol forward primer, 1pmol reverse primer and 1U Kapa *Taq* DNA polymerase (Kapa Biosystems, Woburn, MA, USA) in a final reaction volume of 50µl. PCR reactions were carried out according to the conditions described in Table 5.1. The primer pairs used are described in Table 5.2. Reactions were carried out using an Applied Biosystems Veriti 96 well thermal cycler (Carlsbad, CA, USA).

Table 5.1 PCR cycling conditions for amplification of CYP1 genes

Gene	Initial denaturation		35 cycles						Final extension	
			Denaturation		Annealing		Extension			
CYP1A1	95°C	5 min	95°C	30 sec	63°C	30 sec	72°C	30 sec	72°C	7 min
CYP1B1				30 sec	60°C	30 sec		30 sec		

Table 5.2 Primer pairs used for PCR amplification of CYP1 genes

Gene	Forward Primer	Reverse Primer
CYP1A1	5'-CTG TCT CCC TCT GGT TAC AGG AAG C-3'	5'-TTC CAC CCG TTG CAG CAG GAT AGC C-3'
CYP1B1	5'-TAT GAA GCC ATG CGC TTC TC-3'	5'AAG TTC TTC GCC AAT GCA CC-3'

To check for the specificity of the PCR products, 10µl of each PCR product were electrophoresed on a 1% agarose gel containing 0.5µg/µl ethidium bromide in 1 x TBE buffer at 60V for 40 min. Bands were visualised using a UV transilluminator (UVP BioSpectrum^{TM} 500 Imaging System, Upland, CA, USA) and VisionWorks LS Image Acquisition and Analysis Software (Version 6.8).

After PCR amplification of the desired product, 10µl of PCR product was digested overnight at 37°C with the appropriate restriction endonuclease: 5 units of *BsrD* I (Fermentas, Hanover, MD, USA) for CYP1A1 and 5 units of *Eco57* I (Fermentas, Hanover, MD, USA) for CYP1B1, in 1 x

Buffer (specific for each restriction enzyme, Fermentas, Hanover, MD, USA) in a final reaction volume of 20µl. 10µl of undigested PCR product and 10µl of digested PCR product were loaded onto 2% agarose gels containing 0.5µg/µl ethidium bromide and electrophoresed at 60V for 80 min. The bands were visualised under UV light and CYP1 genotypes for each cell line were determined by restriction enzyme fragments generated according to Table 5.3 below.

Table 5.3 CYP1 polymorphic sites, alleles and restriction fragments used for PCR-RFLP genotyping of cell lines

Gene	Position*	Wild-type allele	Variant allele	PCR product size (bp)	Non-restricted allele	Restriction site allele	Restriction fragment sizes (bp)
CYP1A1	4889	A	G	204	G	A	149, 55
CYP1B1	4326	C	G	270	C	G	165, 105

* relative to transcription start site

5.5 RNA Isolation and Quantification

Cells were washed twice with ice cold 1 x PBS, after which 1ml of the TRIzol lysis reagent (Invitrogen, Carlsbad, CA, USA) was added to each dish. Cells were aspirated and transferred to an eppendorf tube. After 5 min at room temperature, 200µl chloroform was added and each sample was mixed vigorously. After 3 min at room temperature, samples were centrifuged at 12000 x g for 15 min at 4°C. The top aqueous layer was transferred to a new tube and an equal volume of isopropanol was added. After 10 min at room temperature, samples were centrifuged at 12000 x g for 10 min at 4°C and the supernatant was discarded. Pellets were washed twice by the addition of 500µl 75% ethanol, vortexing and centrifugation at 7500 x g for 5 min at 4°C. Samples were left to dry at room temperature, dissolved in 25µl DEPC-treated water and stored at -80°C. The absorbance of the samples was measured at 260nm and 280nm using a Nanodrop 2000 Spectrophotometer (Thermo Scientific, Waltham, MA, USA). RNA purity was determined by a 260/280 ratio of greater than 2 and the RNA integrity was determined by running RNA samples on a 1.5% agarose gel containing 2% formaldehyde in MOPS buffer (0.2M MOPS, 0.05M Na Acetate, 0.01M EDTA). Intact RNA was monitored by a 28S:18S ratio of 2:1.

5.6 Quantitative Real-Time PCR (qRT-PCR)

qRT-PCR was used to determine mRNA transcript levels.

5.6.1 Reverse Transcription of mRNA

Five micrograms of RNA was mixed with 1µl oligo dT 20 (Promega, Madison, WI, USA), 10mM dNTP mix (Promega, Madison, WI, USA) and DEPC-treated water to a final volume of 13µl. Samples were briefly centrifuged, heated at 65°C for 5 min, left on ice for 2 min and then briefly centrifuged again. To each was added 4µl of 5 x First Strand Buffer (Invitrogen, Carlsbad, CA, USA), 1µl 0.1M DTT, 1µl RNasin RNase inhibitor (Promega, Madison, WI, USA) and 1µl Superscript III reverse transcriptase (Invitrogen, Carlsbad, CA, USA). Samples were mixed, incubated at 50°C for 60 min, followed by enzyme inactivation by heating at 70°C for 15 min. 30µl DEPC-treated water was mixed into each sample and stored at -20°C.

5.6.2 qRT-PCR

qRT-PCR for CYP1A1, CYP1B1, AhR, ARNT and the house-keeping gene GAPDH (glyceraldehyde-3-phosphate dehydrogenase) was performed using 200ng cDNA, 1µl forward primer, 1µl reverse primer, 12.5µl KAPA SYBR FAST qPCR master mix (Kapa Biosystems, Woburn, MA, USA) and DEPC-treated water to a final volume of 25µl. For CYP1A2, qRT-PCR was carried out using 300ng cDNA was mixed with 1µl forward primer, 1µl reverse primer (both primers final concentration 10µM), 12.5µl KAPA SYBR FAST qPCR master mix, 2.5µl DMSO and DEPC-treated water to a final volume of 25µl.

qRT-PCR was carried out according to the PCR cycling conditions described in Table 5.4 below, using a Roche LightCycler 480 II (Roche, Mannheim, Germany), with 45 cycles of denaturation, annealing and extension for CYP1A1, CYP1A2, CYP1B1 and GAPDH, and 40 cycles for AhR and ARNT. Both C(t) values and melting curve analysis were calculated using the LightCycler 480 software (Version 1.5.0.39). Duplicate samples were analysed at each time point. The primers used for qRT-PCR are listed in Table 5.5. The data were analysed using the comparative critical threshold [C(t)] method where fold change was calculated as $2^{-\Delta\Delta C(t)}$. The level of gene expressed was normalised to GAPDH, the internal control, and was expressed as fold induction relative to the mean of the control (Un) samples.

Table 5.4 qRT-PCR cycling conditions for mRNA amplification of CYP1, AhR and ARNT genes

Gene	Pre-incubation		Denaturation		Annealing		Extension	
CYP1A1	95°C	5 min	95°C	10 sec	60°C	10 sec	72°C	10 sec
CYP1B1					55°C			
GAPDH					60°C			
CYP1A2				20 sec	59°C	15 sec		20 sec
AhR				30 sec	65°C	30 sec		30 sec
ARNT								

Table 5.5 Primers used for qRT-PCR analysis of gene expression

Gene	Forward primer	Reverse primer	Product size (bp)
CYP1A1	5'-GAG CTG GGT TTG ACA CAG TCA-3'	5'- CCC ATA GCT TCT GGT CAT GGT -3'	317
CYP1A2	5`-CTT TGA CAA GAA CAG TGT CCG -3'	5'-AGT GTC CAG CTC CTT CTG GAT-3'	226
CYP1B1	5`-GAT TTG GAC AAC GTA CCG GCC -3'	5'-ACC CAT ACA AGG CAG ACG G -3'	174
GAPDH	5`-GCC TGC TTC ACC ACC TTC -3'	5'-GGC TCT CCA GAA CAT CC -3'	192
AhR	5'-GTC GTC TAA GGT GTC TGC TGGA-3'	5'-CGC AAA CAA AGC CAA CTG AGG TG-3'	137
ARNT	5'-CTG TCA TCC TGA AGA CCA GCAG-3'	5'-CTG GTT CTC ATC CAG AGC CAT TC-3'	129

5.7 Cytoplasmic, Nuclear and Total Protein Isolation and Quantification

Nuclear and cytoplasmic protein fractions were isolated from from WHCO1 and EPC-2 cells using the ProteoJET Cytoplasmic and Nuclear Protein Extraction Kit (Fermentas, Hanover, MD, USA). Briefly, after the removal of growth medium, cell layers were rinsed with PBS and collected in PBS using a cell scraper. Cells were pelleted by centrifugation at 250 x g for 5 min and the supernatant was discarded. Ten volumes of Cell Lysis Buffer containing protease inhibitors and 0.1M DTT was added to one volume of packed cells. Cells were lysed by vortexing for 10 min, left on ice for 10 min and vortexed again. The cytoplasmic fraction was separated from nuclei by centrifugation at 500 x g for 7 min at 4°C. The supernatant containing the cytoplasmic fraction was cleared by centrifugation at 20 000 x g for 15 min at 4°C, transferred to a new tube and stored at -70°C. The nuclear pellet was washed twice by the addition of 500µl Nuclei Washing Buffer containing protease inhibitors and 0.1M DTT, vortexing, incubation on ice for 2 min and centrifugation at 500 x g for 7 min at 4°C. Ice-cold Nuclei Storage Buffer

(150µl) containing protease inhibitors and 0.1M DTT was added to the nuclei pellet and clumps were broken up by pipetting. One tenth the volume of Nuclei Lysis Reagent was added to the nuclear suspension. Samples were briefly vortexed and then shaken for 15 min at 4°C at 900rpm. Samples were cleared by centrifugation at 20 000 x g for 5 min at 4°C, and the supernatant containing the nuclear protein extract was transferred to a new tube and stored at -70°C.

For the isolation of total protein, cells were washed three times with ice-cold PBS and harvested in 150µl RIPA buffer (150mM NaCl, 1% Triton X-100, 1% Na deoxycholate, 0.1% SDS, 10mM Tris pH 7.4), containing 5µl PMSF (Roche, Mannheim, Germany) and 100µl 10 x PI (Proteinase Inhibitor) using a cell scraper. The sample was transferred to an eppendorf tube, and sonicated (Model CML-4, Misonix XL-2000 Series, Newtown, CT, USA) for 20 sec to fragment the DNA to reduce viscosity. After incubation on ice for 30 min, samples were centrifuged at 13000 x g for 20 min at 4°C, the supernatant containing total protein, transferred to a clean tube and stored at -80°C.

Protein concentrations were determined using the bicinchoninic acid (BCA) protein assay kit, according to the manufacturer's instructions (Thermo Scientific, Pierce, Rockford, IL, USA). Briefly, samples were diluted 1:10 in dH_20 in a 96-well plate followed by the addition of 200µl of mixed A and B solutions in a ratio of 50:1 followed by incubation at 37°C for 1 hour. Absorbance was measured at 595nm using a Multiskan FC plate reader (Thermo Scientific) and sample concentrations were determined from absorbance values using BSA to construct a standard curve.

5.8 Western Blotting

Twenty to sixty micrograms of protein were mixed with 0.1M DTT, 5 x loading buffer (250mM Tris-HCl pH 6.8, 40% v/v glycerol, 5% p/v SDS, 0.005% p/v bromophenol blue, 10% β-mercaptoethanol) and RIPA buffer (150mM NaCl, 1% Triton X-100, 1% Na-deoxycholate, 0.1% SDS, 10mM Tris pH 7.4) in a final volume of 30µl. In order to solubilise the proteins, samples were heated at 99°C for 5-10 min, cooled on ice and centrifuged briefly.

SDS-polyacrylamide gels were prepared (4% acrylamide/bisacrylamide, 0.125M Tris pH 6.8 containing 1% SDS, 0.5 % APS and 0.1% TEMED for stacking gels; and 0.375M Tris pH 8.8 containing 1% SDS, 0.5% APS and 0.05% TEMED for separating gels). 10% polyacrylamide gels were prepared for cytoplasmic and total protein samples, while 7% polyacrylamide gels were prepared for nuclear protein samples. Samples and molecular weight marker (PageRuler Plus

Prestained Protein Ladder, Fermentas, Hanover, MD, USA) were loaded and electrophoresed in running buffer (0.25M Tris, 0.250mM glycine, 0.1% SDS) at 100V for approximately 1 hour or until marker bands were adequately separated. Proteins were transferred onto nitrocellulose membranes (Amersham Hybond-ECL, GE Healthcare, Buckinghamshire, UK) in transfer buffer (25mM Tris, 192mM glycine, 20% methanol) at 100V for 1.5 hours. Gels were stained using coomassie blue staining solution (50% methanol, 10% glacial acetic acid, 0.25% coomassie blue). Nitrocellulose membranes were rinsed three times in TBS (50mM Tris pH7.5, 150mM NaCl) containing 0.1% Tween-20 (TBST) and blocked in 7% non-fat milk in TBST for 1 hour with shaking at room temperature to reduce non-specific binding. Primary antibodies against CYP1A1, CYP1A2, CYP1B1, AhR, ARNT, β-tubulin and Lamin B1 were diluted 1:1000 in blocking solution. Membranes were incubated with the indicated primary antibody at 4°C overnight with shaking. Membranes were washed twice for 10 min in TBST and then twice for 10 min in 5% non-fat milk blocking solution. Horseradish peroxidase-conjugated secondary antibodies were diluted 1:1000 in 5% blocking solution. Membranes were incubated with secondary antibody for 1 hour at room temperature with shaking.

Protein bands were detected using the Lumiglo Reserve chemiluminescent substrate system detection kit (KPL, Gaithersburg, MD, USA) and the UVP BioSpectrum chemiluminescent detection system (BioSpectrum^{TM} 500 Imaging System, Upland, CA, USA) with VisionWorks LS Image Acquisition and Analysis Software (Version 6.8). Membranes were stripped of primary and secondary antibodies by washing with 1M glycine pH 2.5 for 10 min with shaking, after which 1ml Tris pH 7.5 was added and membranes were washed three times for 10 min in TBST. Membranes were incubated with blocking solution for 1 hour before being re-probed with a different primary antibody.

5.9 Immunofluorescence

0.5 x 10^5 cells were seeded onto sterilized coverslips in 2ml medium and grown for 24h in 6-well plates. Cells were then grown in fresh medium or BaP as described in the figure legend. After each time point, cells were washed with ice-cold PBS, fixed with methanol at -20°C for 5 min, washed with ice-cold PBS and then fixed with 4% paraformaldehyde at room temperature for 5 min. Cells were again washed with ice-cold PBS then incubated for 1h in blocking solution (1% BSA in PBS) at room temperature. Cells were incubated with 1:100 dilution of primary antibody against AhR or ARNT (Santa Cruz Biotechnology, La Jolla, CA, USA) in blocking buffer overnight. After washing with ice-cold PBS, cells were incubated with 1:100 dilution of Texas

Red- or fluorescein-conjugated secondary antibody (Calbiochem) in blocking buffer for 45 min followed by incubation with 1:200 dilution of DAPI nuclear stain (4', 6-diamidino-2-phenylinole dihydrochloride, Merck) for 15 min at room temperature. Coverslips were mounted onto slides using Mowiol reagent (Calbiochem) and analysed using a fluorescent microscope (Zeiss, Germany).

5.10 MTT Assay

Cell viability was determined using the MTT (3-(4,5-dimethylthiazol-2-yl)-2,5-diphenyl tetrazolium bromide) assay (MTT, Sigma-Aldrich, Steinholm, Germany). Cells were seeded at 2000 cells per well in 90µl complete medium with or without BaP. Cells were grown for 1, 2, 3, 4 or 5 days. At each time point, 10µl MTT solution (5mg/ml in PBS) was added to give a final concentration of 0.5mg/ml. Cells were incubated a further 4 hours, after which 200µl of the solubilisation reagent (10% SDS in 0.01M HCl) was added. Cells were incubated at 37°C overnight and a Multiskan FC plate reader (Thermo Scientific) microtiter plate reader was used to measure the absorbance at 595nm. Average background absorbance from the medium-only controls was subtracted from Untreated and BaP values.

5.11 Bromodeoxyuridine Incorporation Colorimetric ELISA

The Cell Proliferation ELISA kit, BrdU (colorimetric) (Roche, Mannheim, Germany) was used according to the manufacturer's instructions. Cells were seeded at 2000 cells per well in 96-well plates and grown in their respective media overnight and treated with BaP as described in the figure legend. For the last 6h of DMSO or BaP treatment, 10µl BrdU labelling solution (final concentration 10µM in growth medium) was added to each well and plates were re-incubated at 37°C. Labelling media were removed and 200µl FixDenat solution was added to each well, followed by 30 min incubation at room temperature. FixDenat solution was removed and 100µl anti-BrdU-horseradish peroxidase (POD) working solution (1:100 dilution in antibody dilution solution) was added to each well, followed by 90 min incubation at room temperature. Antibody solution was removed and wells were washed three times with PBS (washing solution). Finally, 100µl/well substrate solution (TMB, tetramethyl-benzidine) was added and plates were incubated at room temperature for 20 min until colour development occured. The ELISA was stopped by the addition of 25µl/well 1M H_2SO_4 and 1 min shaking. Plates were read at 450nm with a reference wavelength of 650nm, using the Multiskan FC plate reader (Thermo Scientific, Waltham, MA, USA). In addition to the DMSO control, a Blank (without cells) and a Background Control (without BrdU) were used to account for non-specific binding of BrdU to the

plate and anti-BrdU to cells, respectively. Blank values were subtracted from Untreated and BaP values for each time point.

5.12 Statistical Analyses of Molecular Data

The statistical analyses of the molecular data were done using the student's t-test. A difference was considered significant if $p \leq 0.05$ and highly significant if $p \leq 0.001$.

5.13 cDNA Microarray Analysis

5.13.1 Microarray RNA Quality Control: Agilent 2100 Bioanalyzer

RNA samples were quantified as described in 5.2.5 and taken on dry ice to the Department of Medical and Molecular Genetics at King's College London where RNA integrity was determined using the Agilent 2100 BioAnalyzer (Agilent Technologies, Waldbronn, Germany) and the RNA 6000 Nano Kit according to the manufacturer's protocol. Briefly, 1µl RNA 6000 Nano dye concentrate was added to 65µl filtered gel matrix. The solution was vortexed, centrifuged at 13 000 x g for 10 min at room temperature and 9µl gel-dye was pipetted into three wells of the RNA 6000 Nano chip. Gel was spread through action of the syringe plunger for 30 sec. RNA 6000 Nano marker (5µl) was added to twelve sample wells and one ladder well. Samples were heat denatured at 70°C for 2 min, briefly centrifuged and 1µl of each sample was added to the sample wells, while 1µl prepared ladder was added to the ladder well. The chip was vortexed for 1 min at 2400 rpm, after which it was run in the Agilent 2100 bioanalyzer. Electrodes were decontaminated before set-up with 350µl RNase ZAP for 1 min and 350µl RNase-free water for 10 sec. The bioanalyzer electrophoretically separates RNA fragments based on their size and generates an accurate RNA concentration and an image of 28S, 18S and 5S RNA bands. The bioanalyzer also generates the RNA integrity number (RIN), which indicates the quality of the RNA. An RIN $\geq$ 7.8 qualifies the RNA for use in a microarray, although RIN between 8.4-9.0 is ideal. All WHCO1 and EPC-2 RNA samples were deemed high-enough quality to continue with the microarray experiment.

5.13.2 RNA Amplification & Biotin Labelling

RNA samples were amplified and labeled with biotin using the Illumina TotalPrep RNA Amplification Kit (Ambion, Austin, TX, USA). Briefly, RNA was reverse transcribed to synthesize first strand cDNA, after which second strand cDNA was synthesized with the simultaneous removal of RNA. cDNA was purified and used to transcribe cRNA, which was

purified and yield analyzed spectrophotometrically. The protocol is as follows: RNA (500ng) from each sample was prepared with nuclease-free water to 11µl total volume. Reverse transcriptase master mix (1µl T7 oligo(dT) primer, 2µl 10x first strand buffer, 4µl dNTP mix, 1µl RNase inhibitor and 1µl ArrayScript reverse transcriptase per reaction) was added to each sample to bring the volume to 20µl. Samples were incubated at 42°C for 2h and then briefly centrifuged and placed on ice. Second strand master mix (63µl nuclease-free water, 10µl second strand buffer, 4µl dNTP mix, 2µl DNA polymerase and 1µl RNase H per reaction) was added to each sample to bring the volume to 100µl. Samples were incubated at 16°C for 2h then placed on ice. cDNA binding buffer (250µl) was added to each sample and the mixture was passed through a cDNA filter cartridge (Ambion, Austin, TX, USA) by centrifugation at 10 000 x g for 1 min. The flow-through was discarded and 500µl wash buffer containing 100% ethanol was added to each cartridge. Samples were centrifuged at 10 000 x g for 1 min and flow-through was discarded. Filter cartridges were transferred to cDNA elution tubes. Preheated nuclease-free water (50-55°C, 10µl) was added to the filter cartridges; samples were incubated at room temperature for 2 min then centrifuged for 1.5 min at 10 000 x g. A second aliquot of 9µl nuclease-free water was added and samples were centrifuged again, leaving eluted double-stranded cDNA in the tube. An in vitro transcription (IVT) master mix was prepared at room temperature (2.5µl T7 10x reaction buffer, 2.5µl T7 enzyme mix and 2.5µl biotin-NTP mix) and 7.5µl was mixed with each cDNA sample. Tubes were incubated at 37°C for 14h in a hybridization oven to maintain constant temperature. Reactions were stopped by the addition of 75µl nuclease-free water, bringing the final volume to 100µl. cRNA binding buffer (350µl) was added to each sample, followed by 250µl 100% ethanol and mixing by pipetting. Samples were immediately placed onto cRNA filter cartridges (Ambion, Austin, TX, USA) and centrifuged at 10 000 x g for 1 min. Flow-through was discarded and 650µl wash buffer was added to each cartridge. Samples were centrifuged at 10 000 x g for 1 min and flow-through was discarded. cRNA was eluted by the addition of 100µl preheated nuclease-free water (50-60°C) and centrifugation for 1.5 min at 10 000 x g. Purified cRNA was concentrated by precipitation by the addition of one tenth volume of 5M NH_4OAc and 2.5 volumes of 100% ethanol and left at -20°C for 30 min. Samples were microcentrifuged at top speed at room temperature for 15 min. Supernatants were discarded and pellets were washed with 500µl 70% cold ethanol by centrifugation. Pellets were air-dried and resuspended in 50µl RNase-free water. cRNA yield was assessed using the Nanodrop 1000A spectrophotometer at 260nm.

5.13.3 Illumina Whole-Genome Gene Expression Direct Hybridization Assay

cRNA samples (1.5µg) were resuspended in RNase-free water to a final volume of 10µl, after which 20µl of Hybridization Buffer (HYB) was added to each cRNA sample. The Hyb chamber gaskets were inserted into the BeadChip Hyb chamber and 200µl Humidity Control Buffer (HCB) was loaded into each of the humidifying buffer reservoirs. BeadChips (Illumina WG6-v3 Gene Expression BeadChips, Illumina, San Diego, CA, USA) were placed into the chamber inserts. Samples were heated at 65°C for 5 min and then loaded onto the BeadChips. The sealed Hyb chamber containing the BeadChips was then incubated overnight at 58°C on a rocking platform. BeadChips were submerged in E1BC Wash Solution and their coverseals were removed, after which both chips were inserted into a submerged slide rack. The slide rack was then transferred into a Hybex waterbath containing preheated High-Temp Wash Buffer (55°C) and chips were incubated at 55°C for 10 min. The slide rack was transferred into 250ml E1BC Wash buffer, agitated and shaken on an orbital shaker for 5 min at the highest possible speed at room temperature. The slide rack was transferred into 250ml 100% ethanol, agitated and shaken on an orbital shaker for 10 min at room temperature. The rack was transferred into 250ml fresh Wash E1BC solution, agitated and shaken on an orbital shaker for 2 min at room temperature. Block E1 buffer (8ml) was added to two wash trays; BeadChips were placed into the trays and blocked for 10 min at medium speed on a rocker. For detection, 4ml Block E1 buffer containing 4µl streptavidin-Cy3 (from 1mg/ml in RNase-free water stock solution) was added to two fresh wash trays. BeadChips were placed face-up into the wash trays, which were covered and rocked at medium speed for 10 min. BeadChips were transferred back to the slide rack submerged in 250ml Wash E1BC solution, agitated then shaken on an orbital shaker for 5 min at room temperature. The rack of BeadChips was centrifuged at 25°C for 4 min. Dry BeadChips were stored in a dark box until scanned with the Illumina BeadArray Reader. Signal intensities were recorded as iDAT files (image data) for each chip.

5.13.4 Microarray Data Analysis

iDAT files were converted into data tables by Illumina BeadStudio version 3 Gene Expression Module software (www.illumina.com). The upgraded version of BeadStudio, GenomeStudio, which has an equivalent Gene Expression Analysis tool, was used towards the end of the project. BeadStudio analysis was carried out with the assistance of Dr Peter Green from the Genomics Laboratory at the Department of Medical and Molecular Genetics at King's College London. Data pre-processing and clean-up was conducted in collaboration with Dr Hasan Otu from the

Istanbul Bilgi University, Istanbul, Turkey and Department of Medicine, BIDMC Genomics Centre, Harvard Medical School, Boston, USA. Further analysis was conducted in collaboration with Dr Nicki Tiffin at the South African Bioinformatics Institute (SANBI) at the University of the Western Cape.

Samples were classified into two groupsets (WHCO1 and EPC-2) and two groups within those groupsets (BaP and Un, the reference group). This allowed the generation of data manifest tables containing probe and gene lists and their associated signal intensities. For each gene, there are up to 30 probe replicates, which enhance the sensitivity of measuring mRNA abundance and therefore differential gene expression. Clusters (dendrograms) were generated in BeadStudio using the Correlation method to determine which samples are most similar based on the expression levels of genes within them. Absolute correlation, Manhattan and Euclidian methods were also used for comparison. Outliers were determined from the clusters and were removed before further analysis.

A differential expression analysis was run with the following parameters: average normalization, no background subtraction, Benjamini and Hochberg false discovery rate calculation and the Mann-Whitney method of calculating false discovery rate. Normalization is a method of minimizing the effects of variation from non-biological factors by adjusting signal values. The Control Summary Report (hybridization control, negative control, low stringency control, gene intensity control of housekeeping vs all genes, biotin and high stringency control, background and labeling control) indicated that the performance of the built-in controls was satisfactory for both WHCO1 and EPC-2 microarrays.

Information within gene lists includes an average signal value for each gene and its probes, and a detection p-value which describes whether the signal is detected significantly above background. Detection p-value is calculated from negative probes in the chip that measure non-specific hybridization. In addition, BeadStudio generated a Diff Score for each gene, which is a transformation of the significance p-value based on the difference in average signal in Un (the reference group) vs BaP. The p-value is calculated from the Diff Score by the equation: $p = 10'(DiffScore*sgn(\mu_{cond}-\mu_{ref})/10)$. A p-value of 0.05 corresponds to a Diff Score of ± 13. However, since outliers were removed from both groupsets, no statistical analysis could be conducted on the EPC-2 groupset, and therefore nor on the combined analysis of WHCO1 and EPC-2.

For the combined analysis of both groupsets, data were filtered for detection p-value <0.05, which corresponds to a 5% false positive rate. Following advice from Dr Christy Waterfall at Illumina UK, no background subtraction was carried out, since this resulted in negative signal values for some genes. Any remaining negative signal values were truncated to 1. Average signal values were then filtered using 2% trimmed mean scaling in order to set the target average intensity of both chips to 500. This method removes highest and lowest 2% expressed genes. Genes with expression level below 40 in all 9 samples were then eliminated and all 6 possible comparisons were carried out (Un vs BaP and WHCO1 vs EPC-2). Fold change was calculated by averaging BaP and Un values within each cell line and dividing average BaP by average Un. Using the Illumina BeadChip, the minimum statistically significant detectable fold-change is 1.35-fold for single replicates. We chose 2-fold as a cut-off since this is widely used. Lastly, genes were again eliminated if signal was not detected in all samples where the gene was supposedly up- or down-regulated. Comparative analysis using Venn diagrams was used to show genes that are up- or down-regulated by BaP both commonly and uniquely in WHCO1 and EPC-2 cells.

5.13.5 Quantitative Real-Time PCR (qRT-PCR) on Selected Genes for Validation of Microarray Results

In order to confirm that the fold change of differentially expressed genes observed in the WHCO1 and EPC-2 microarrays were reproducible results, qRT-PCR was carried out on selected genes. These genes are listed in Tables 5.7 and 5.8. The primers for CYP1A1, CYP1B1 and GAPDH and their cycling conditions are described in Table 5.6 and 5.4, respectively. The primers for AHRR, UGT2B7, KISS1, ETV5, SERPINB2, SERPINA3, DEFB1, HIST1H2BH, ALDH3A1 and TIPARP were purchased from SA Biosciences (Frederick, MD, USA). Primers were designed using proprietary algorithms and therefore sequences are not available. The primer sequences for GSTM1, MMP9, IFITM1, CCNB2, CDKN3, POLM, IL13RA2, SULF1, ADAM23, CCNA1, TFPI2, MT1G, GPX3, P53AIP1 and ITGB7 were obtained from Origene (www.origene.com) and primers were synthesized at the Department of Molecular and Cell Biology at the University of Cape Town. qRT-PCR was carried out using 2µl cDNA, 12,5µl of either KAPA Biosystems Universal qPCR Master Mix (Kapa Biosystems, Woburn, MA, USA) or SA Biosciences RT^2 Master Mix (for the primers bought from SA Biosciences), 1µl forward primer, 1µl reverse primer (both primers final concentration of 10µM) or 1µl primer mix (for SA Biosciences primers) and dH_2O to a final volume of 25µl. qRT-PCR cycling conditions for either SA Biosciences or Origene primers are described in Table 5.6. Available primer sequences,

melting temperatures and amplified product sizes are listed in Table 5.7, while Table 5.8 lists available information for the SA Biosciences primers.

Table 5.6 qRT-PCR cycling conditions for amplification of selected genes for microarray validation

Group	Cycling conditions		
	Temperature (°C)	Time (min)	Cycles
SA Biosciences	95	10:00	1
	95 55 72	00:15 00:40 00:30	40
Origene	95	05:00	1
	95 65 72	00:30 00:30 00:30	40

Fold change was determined using the $2^{-\Delta\Delta Ct}$ method described in the SA Biosciences RT^2 qPCR Primer Assay protocol. Threshold cycle (Ct) values were determined for each gene of interest (GOI) and the housekeeping gene GAPDH using the Bio-Rad MiniOpticon software (Hercules, CA, USA). The difference between Ct values (ΔCt) was calculated for control (Un) and experimental (BaP) conditions by subtracting Ct (GAPDH) from Ct (GOI). The difference in ΔCt values for the GOI (ΔΔCt) was calculated by subtracting ΔCt (Un) from ΔCt (BaP). Fold change in gene expression was calculated as $2^{-\Delta\Delta Ct}$ and compared to microarray fold change.

Table 5.7 Primers used for qRT-PCR analysis of gene expression for validation of microarray fold change

Gene/ RefSeq Accession no.	**Forward primer**	**Reverse primer**	**Melt temp (°C)**	**Product size (bp)**
GAPDH NM_002046.3	5`-GCC TGC TTC ACC ACC TTC-3’	5'-GGC TCT CCA GAA CAT CC-3’	83	192
CYP1A1 NM_000499	5’-GAG CTG GGT TTG ACA CAG TCA-3’	5'- CCC ATA GCT TCT GGT CAT GGT -3'	84	317
CYP1B1 NM_000104	5`-GAT TTG GAC AAC GTA CCG GCC -3'	5'-ACC CAT ACA AGG CAG ACG G -3'	85	174
MMP9 NM_004994	5’-GAG ACA GCA TGG CCA A-3’	5’-CTC TAG AAA CTG CTG AGG-3’	87	14
GSTM1 NM_000561	5’-GAA CTC CCT GAA AAG CTA AAG C-3’	5’-GTT GGG CTC AAA TAT ACG GTG G-3’	80	219

IFITM1 NM_003641	5'-GGC TTC ATA GCA TTC GCC TAC TC-3'	5'-AGA TGT TCA GGC ACT TGG CGG T-3'	84	106
CCNB2 NM_004701	5'-CAA CCA GAG CAG CAC AAG TAG C-3'	5'-GGA GCC AAC TTT TCC ATC TGT AC-3'	80	136
CDKN3 NM_005192	5'-ATG GAG GGA CTC CTG ACA TAG C-3'	5'-TCT CCC AAG TCC TCC ATA GCA G-3'	79	110
IL13RA2 NM_000640	5'-GTG GAG TGA TAA ACA ATG CTG GG-3'	5'-TGG GTA GGT GTT TGG CTT ACG C-3'	78	139
POLM NM_013284	5'-TGT GAG GAG GTG GAG AGA GTT C-3'	5'-TCG GAG GTC ATC TAA GGT TCG C-3'	83	135
SULF1 NM_015170	5'-GGT CCA AGT GTA GAA CCA GGA TC-3'	5'-GAC AGA CTT GCC GTC CAC ATC A-3'	82	120
ADAM23 NM_003812	5'-CTT TGG AGG TGT CTG TTC TCG C-3'	5'-GGA TTC CAA GGT TTT GAG CCA GG-3'	80	110
CCNA1 NM_003914	5'-GCA CAC TCA AGT CAG ACC TGC A-3'	5'-ATC ACA TCT GTG CCA AGA CTG GA-3'	80	118
TFPI2 NM_006528	5'-TAC TGG CTG TGG AGG GAA TGA C-3'	5'-CGG ATT CTA CTG GCA AAG CGA AG-3'	79	120
MT1G NM_005950	5'-AGA GTG CAA ATG CAC CTC CTG C-3'	5'-TTG TAC TTG GGA GCA GGG CTG T-3'	86	150
GPX3 NM_002084	5'-TAC GGA GCC CTC ACC ATT GAT G-3'	5'-CAG ACC GAA TGG TGC AAG CTC T-3'	83	156
P53AIP1 NM_022112	5'-AGA CCA GAA CCT CTC GGT GAT G-3'	5'-ACC ACG GTG AGA GCA GAG TCT G-3'	84	86
ITGB7 NM_000889	5'-ATC GAG GAC AGT GCA ACC ACG T-3'	5'-TCA GCT CCT CTG AGA AGC CAA G-3'	84	129

Table 5.8 SA Biosciences primers information for qRT-PCR analysis of gene expression for validation of microarray fold change

Gene	RefSeq Accession no.	Reference position*	Melt temp (°C)	Product size (bp)
SERPINA3	NM_001085.4	1396	85	140
KISS1	NM_002256.3	210	79	71
DEFB1	NM_005218.3	162	83	171
ETV5	NM_004454.2	1640	85	157
HIST1H2BH	NM_003524.2	87	83	113
SERPINB2	NM_002575.2	1375	77	106
UGT2B7	NM_001074.2	1543	83	121
AHRR	NM_020731.3	4956	84	109
ALDH3A1	NM_000691	705	85	166
TIPARP	NM_015508	1827	80	159

* The reference position is contained within the sequence of the amplicon relative to the start of the RefSeq sequence

5.13.6 Ontology and Functional Analysis using Ingenuity Pathways Analysis Software

Since many gene ontology (GO) programs are routinely used with Affymetrix microarrays, our Illumina-specific iDAT files were not recognized by the software and therefore could not be

uploaded for functional analysis. Following primary analysis in BeadStudio and pre-processing, lists of differentially expressed genes from the WHCO1 and EPC-2 chips were uploaded into Ingenuity Pathways Analysis (Ingenuity® Systems, www.ingenuity.com). The software generated several graphical outputs used to represent gene interactions and biological functions and pathways affected by BaP treatment in the gene lists. These outputs, described below, are: gene interaction networks, biological functions, canonical pathways and cellular flow diagrams. IPA also generated its own significance p-value associated with each network, function or pathway which further highlighted the notable results.

In addition to IPA, gene ontology was analyzed using GOstat (Beissbarth and Speed, 2004, http://gostat.wehi.edu.au/) and GOrilla (Gene Ontology enRIchment anaLysis and visuaLizAtion tool, Eden *et al*., 2009, http://cbl-gorilla.cs.technion.ac.il/) which determine which Gene Ontology terms (cellular location, molecular function or biological process) are significantly over-represented in each gene list compared to the entire genome.

5.13.7 Meta-Analysis of Microarray Data

Data generated from the WHCO1 and EPC-2 microarrays were compared to previously published results from other BaP-treated cell lines, as shown in Table 1.2. Cell line origins and full names are also indicated in Table 1.2. Gene lists were entered into an Excel spreadsheet and manually compared for selection of common genes. Where a specific cell line had more than one microarray publication, data were pooled together.

References

Abbas A, Delvinquière K, Lechevrel M, Lebailly P, Gauduchon P, Launoy G, Sichel F. GSTM1, GSTT1, GSTP1 and CYP1A1 genetic polymorphisms and susceptibility to esophageal cancer in a French population. World J Gastroenterol 2004;10:3389-3393.

Abdelrahim M, Smith R III, Safe S. Aryl hydrocarbon receptor gene silencing with small inhibitory RNA differentially modulates Ah-responsiveness in MCF-7 and HepG2 cancer cells. Mol Pharmacol 2003;63:1373-1381.

Agudo A, Peluso M, Sala N, Capellá G, Munnia A, Piro S, Marín F, Ibáñez R, Amiano P, Tormo MJ, Ardanaz E, Barricarte A, Chirlaque MD, Dorronsoro M, Larrañaga N, Martínez C, Navarro C, Quirós JR, Sánchez MJ, González CA. Aromatic DNA adducts and polymorphisms in metabolic genes in healthy adults: findings from the EPIC-Spain cohort. Carcinogenesis 2009;30:968–976.

Akerman GS, Rosenzweig BA, Domon OE, McGarrity LJ, Blankenship LR, Tsai CA, Culp SJ, MacGregor JT, Sistaire FD, Chen JJ, Morris SM. Gene expression profiles and genetic damage in benzo[a]pyrene diol epoxide-exposed TK6 cells. Mutat Res 2004;549:43-64.

Andersson P, McGuire J, Rubio C, Gradin K, Whitelaw ML, Pettersson S, Hanberg A, Poellinger L. A constitutively active dioxin/aryl hydrocarbon receptor induces stomach tumors. Proc Natl Acad Sci USA 2002;99:9990–9995.

Andl CD, Mizushima T, Nakagawa H, Oyama K, Harada H, Chruma K, Herlyn M, Rustgi AK. Epidermal growth factor receptor mediates increased cell proliferation, migration, and aggregation in esophageal keratinocytes in vitro and in vivo. J Biol Chem 2002;278:1824-1830.

Androutsopoulos VP, Tsatsakis AM, Spandidos DA. Cytochrome P450 CYP1A1: wider roles in cancer progression and prevention. BMC Cancer 2009: 9:187.

Baird WM, Hooven LA, Mahadevan B. Carcinogenic polycyclic aromatic hydrocarbon-DNA adducts and mechanism of action. Environ Mol Mutagen 2005;45:106-114.

Bandiera S, Weidlich S, Harth V, Broede P, Ko Y, Friedberg T. Proteasomal degradation of human CYP1B1: Effect of the Asn453Ser polymorphism on the post-translational regulation of CYP1B1 expression. Mol Pharmacol 2005;67:435–443.

Bao H, Vepakomma M, Sarkar MA. Benzo(a)pyrene exposure induces CYP1A1 activity and expression in human endometrial cells. J Steroid Biochem Mol Biol 2002;81:37–45.

Barouki R, Coumoul X, Fernandez-Salguero PM. The aryl hydrocarbon receptor, more than a xenobiotic interacting protein. FEBS Letters 2007;581:3608-3615.

Bartsch H, Nair U, Risch A, Rojas M, Wikman H, Alexandrov K. Genetic polymorphisms of CYP genes, alone or in combination, as a risk modifier of tobacco-related cancers. Cancer Epidemiol Biomarkers Prev 2000;9:3-28.

Baumeister P, Reiter M, Kleinsasser N, Matthias C, Harréus U. Epigallocatechin-3-gallate reduces DNA damage induced by benzo[a]pyrene diol epoxide and cigarette smoke condensate in human mucosa tissue cultures. Eur J Cancer Prev 2009;18:230-235.

Beedanagari SR, Taylor RT, Bui P, Wang F, Nickerson DW, Hankinson O. Role of epigenetic mechanisms in differential regulation of the dioxin-inducible human CYP1A1 and CYP1B1 genes. Mol Pharmacol 2010;78:608-616.

Beischlag TV, Morales JL, Hollingshead BD, Perdew GH: The aryl hydrocarbon receptor complex and the control of gene expression. Crit Rev Eukaryot Gene Expr 2008;18:207-250.

Beissbarth T, Speed TP. GOstat: Find statistically overrepresented Gene Ontologies within a group of genes. Bioinformatics 2004;20:1464-1465.

Belitskaya-Levy I, Hajjou M, Su WC, Yie TA, Tchou-Wong KM, Tang MS, Goldberg JD, Rom WN. Gene profiling of normal human bronchial epithelial cells in response to asbestos and benzo[a]pyrene diol epoxide (BPDE). J Environ Pathol Toxicol Oncol 2007;26:281-294.

Bernhardt R. Cytochromes P450 as versatile biocatalysts. J Biotechnology 2006;124:128–145.

Boström CE, Gerde P, Hanberg A, Jernström B, Johansson C, Kyrklund T, Rannug A, Törnqvist M, Victorin K, Westerholm R. Cancer risk assessment, indicators, and guidelines for polycyclic aromatic hydrocarbons in the ambient air. Environ. Health Perspect 2002;110:451–488.

Bozina N, Bradamante V, Lovric M. Genetic polymorphism of metabolic enzymes P450 (CYP) as a susceptibility factor for drug response, toxicity and cancer risk. Arh Hig Rada Toksikol 2009;60:217-242.

Burbach KM, Poland A, Bradfield CA. Cloning of the Ah-receptor cDNA reveals a distinctive ligand-activated transcription factor. Proc Natl Acad Sci USA 1992;89:8185–8189.

Burczynski ME, Penning TM. Genotoxic polycyclic aromatic hydrocarbon ortho-quinones generated by aldo-keto reductases induce CYP1A1 via nuclear translocation of the aryl hydrocarbon receptor. Cancer Res 2000;60:908–915.

Burdick AD, Davis JW, Liu KJ, Hudson LG, Shi H, Monske ML, Burchiel SW. Benzo[a]pyrene quinones increase cell proliferation, generate reactive oxygen species, and transactivate the epidermal growth factor receptor in breast epithelial cells. Cancer Res 2003;63:7825-7833.

Burke MD, Mayer RT. Ethoxyresorufin: direct fluorimetric assay of a microsomal O-deethylation which is preferentially inducible by 3-methylcholanthrene. Drug Metab Dispos 1974;2:583-588.

Buters JT, Sakai S, Richter T, Pineau T, Alexander DL, Savas U, Doehmer J, Ward JM, Jefcoate CR, Gonzalez FJ. Cytochrome P450 CYP1B1 determines susceptibility to 7,12-dimethylbenz[a]anthracene-induced lymphomas. Proc Natl Acad Sci USA 1999;96:1977-1982.

Chang TKH, Chen J, Yang G, Yeung EYH. Inhibition of procarcinogen-bioactivating human CYP1A1, CYP1A2 and CYP1B1 enzymes by melatonin. J. Pineal Res 2010;48:55–64.

Chen D, Tian T, Wang H, Liu H, Hu Z, Wang Y, Liu Y, Ma H, Fan W, Miao R, Sun W, Wang Y, Qian J, Jin L, Wei Q, Shen H, Huang W, Lu D. Association of human aryl hydrocarbon receptor gene polymorphisms with risk of lung cancer among cigarette smokers in a Chinese population. Pharmacogenet Genomics 2009;19:25-34.

Chen JX, Zheng Y, West M, Tang M. Carcinogens preferentially bind at methylated CpG in the p53 mutational hotspots. Cancer Res 2001;58:2070-2075.

Chen S, Nguyen N, Tamura K, Karin M, Tukey RH: The role of the Ah receptor and p38 in benzo[a]pyrene-7,8-dihydrodiol and benzo[a]pyrene-7,8-dihydrodiol-9,10-epoxide-induced apoptosis. J Biol Chem 2003;278:19526-19533.

Cheng SC, Hilton BD, Roman JM, Dipple A. DNA adducts from carcinogenic and noncarcinogenic enantiomers of benzo[a]pyrene dihydrodiol epoxide. Chem Res Toxicol 1989;2:334.

Chiapperino D, Kroth H, Kramarczuk IH, Sayer JM, Masutani C, Hanaoka F, Jerina DM, Cheh AM. Preferential misincorporation of purine nucleotides by human DNA polymerase eta opposite benzo[a]pyrene 7,8-diol 9,10-epoxide deoxyguanosine adducts. J Biol Chem 2002;277:11765-71.

Choi H, Chun YS, Shin YJ, Ye SK, Kim MS, Park JW. Curcumin attenuates cytochrome P450 induction in response to 2,3,7,8-tetrachlorodibenzo-p-dioxin by ROS-dependently degrading AhR and ARNT. Cancer Sci 2008; 99:2518–2524.

Chun YJ, Kim S. Discovery of cytochrome P450 1B1 inhibitors as new promising anti-cancer agents. Med Res Rev 2003;23:657-668.

Cook JW, Hewett CL, Hieger I. The isolation of a cancer-producing hydrocarbon from coal tar. J Chem Soc 1933;395:1-3.

Coussens LM, Werb Z. Inflammation and cancer. Nature 2002;420:860-867.

Cox MB, Miller CA. Cooperation of heat shock protein 90 and p23 in aryl hydrocarbon receptor signaling. Cell Stress Chaperones 2004;9:4–20.

Dalton TP, Dieter MZ, Matlib RS, Childs NL, Shertzer HG, Genter MB, Nebert DW. Targeted knockout of Cyp1a1 gene does not alter hepatic constitutive expression of other genes in the mouse [Ah] battery. Biochem Biophys Res Comm 2000;267:184-189.

Dandara C, Ballo R, Parker MI. CYP3A5 genotypes and risk of oesophageal cancer in two South African populations. Cancer Lett 2005;225:275-282.

Dandara C, Basvi PT, Bapiro TE, Sayi J, Hasler JA. Frequency of -163C>A and 63C>G single nucleotide polymorphism of cytochrome P450 1A2 in two African populations. Clin Chem Lab Med 2004;42:939-941.

Dandara C, Li DP, Walther G, Parker MI. Gene-environment interaction: the role of SULT1A1 and CYP3A5 polymorphisms as risk modifiers for squamous cell carcinoma of the oesophagus. Carcinogenesis 2006;27:791-97.

Davarinos NA, Pollenz RS. Aryl hydrocarbon receptor imported into the nucleus following ligand binding is rapidly degraded via the cytoplasmic proteasome following nuclear export. J Biol Chem 1999;274:28708–28715.

Denissenko MF, Pao A, Tang M, Pfeifer GP. Preferential formation of benzo[a]pyrene adducts at lung cancer mutational hotspots in p53. Science 1996;274:430-432.

de Waard WJ, Aarts JMMJG, Peijnenburg AACM, Baykus H, Talsma E, Punt A, de Kok TMCM, van Schooten FJ, Hoogenboom LAP. Gene expression profiling in Caco-2 human colon cells exposed to TCDD, benzo[a]pyrene, and natural Ah receptor agonists from cruciferous vegetables and citrus fruits. Toxicol in Vitro 2008;22:396-410.

Dietrich C, Kaina B. The aryl hydrocarbon receptor (AhR) in the regulation of cell-cell contact and tumour growth. Carcinogenesis 2010;31:1319-1328.

Ding J, Ning B, Gong W, Wen W, Wu K, Liang J, He G, Huang S, Sun W, Han T, Huang L, Cao G, Wu M, Xie W, Wang H. Cyclin D1 induction by benzo[a]pyrene-7,8-diol-9,10-epoxide via the phosphatidylinositol 3-kinase/Akt/MAPK- and p70s6k-dependent pathway promotes cell transformation and tumorigenesis. J Biol Chem 2009;284:33311-33319.

Ding YS, Ashley DL, Watson CH. Determination of 10 carcinogenic polycyclic aromatic hydrocarbons in mainstream cigarette smoke. J Agric Food Chem 2007;55:5966-5973.

Donato MT, Gomez-Lechon MJ, Castell JV. A microassay for measuring cytochrome P450IA1 and P450IIB1 activities in intact human and rat hepatocytes cultures on 96-well plates. Anal Biochem 1993;213:29-33.

Dong H, Dalton TP, Miller ML, Chen Y, Uno S, Shi Z, Shertzer HG, Bansal S, Avadhani NG, Nebert DW. Knock-in mouse lines expressing either mitochondrial or microsomal CYP1A1: Differing responses to dietary benzo[*a*]pyrene as proof of principle. Mol Pharmacol 2009;75:555–567.

Dragin N, Shi Z, Madan R, Karp CL, Sartor MA, Chen C, Gonzalez FJ, Nebert DW. Phenotype of the Cyp1a1/1a2/1b1(-/-) triple-knockout mouse. Mol Pharmacol 2008;73:1844–1856.

Dreij K, Rhrissorrakrai K, Gunsalus KC, Geacintov NE, Scicchitano DA. Benzo[a]pyrene diol epoxide stimulates an inflammatory response in normal human lung fibroblasts through a p53 and JNK mediated pathway. Carcinogenesis 2010;31:1149–1157.

Du HJ, Tang N, Liu BC, You BR, Shen FH, Ye M, Gao A, Huang CS. Benzo[a]pyrene-induced cell cycle progression is through ERKs/cyclin D1 pathway and requires the activation of JNKs and p38 mapk in human diploid lung fibroblasts. Mol Cell Biochem 2006;287:79-89.

Dvořák Z, Vrzal R, Pávek P, Ulrichová J. An evidence for regulatory cross-talk between aryl hydrocarbon receptor and glucocorticoid receptor in HepG2 cells. Physiol Res 2008;57:427-435.

Eden E, Navon R, Steinfeld I, Lipson D, Yakhini Z. GOrilla: A tool For discovery and visualization of enriched GO terms in ranked gene lists. BMC Bioinformatics 2009;10:48.

Esteller M. Cancer epigenomics: DNA methylomes and histone-modification maps. Nat Rev Genetics 2007;8:286-298.

Evans BR, Karchner SI, Allan LL, Pollenz RS, Tanguay RL, Jenny MJ, Sherr DH, Hahn ME. Repression of aryl hydrocarbon receptor (AHR) signaling by AHR repressor: role of DNA binding and competition for AHR nuclear translocator. Mol Pharmacol 2008;73:387-398.

Fang MZ, Wang Y, Ai N, Hou Z, Sun Y, Lu H, Welsh W, Yang CS. Tea polyphenol epigallocatechin 3-gallate inhibits DNA methyltransferase and reactivates methylation-silenced genes in cancer cell lines. Cancer Res 2003;63:7563-7570.

Ferlay J, Shin HR, Bray F, Forman D, Mathers C, Parkin DM. Estimates of worldwide burden of cancer in 2008: GLOBOCAN 2008. Int J. Cancer 2010;127:2893-2917.

Fertmann R, Tesseraux I, Schümann M, Neus H. Evaluation of ambient air concentrations of polycyclic aromatic hydrocarbons in Germany from 1990 to 1998. J Expo Anal Environ Epidemiol 2002;12:115–23.

Franceschi S, Bidoli E, Negri E, Zambon P, Talamini R, Ruol A, Parpinel M, Levi F, Simonato L, La Vecchia C. Role of macronutrients, vitamins and minerals in the aetiology of squamous-cell carcinoma of the oesophagus. Int J Cancer 2000;86:626–631.

Fritsche E, Brüning T, Jonkmanns C, Ko Y, Bolt HM, Abel J. Detection of cytochrome P450 1B1 Bfr I polymorphism: genotype distribution in healthy German individuals and in patients with colorectal carcinoma. Pharmacogenetics 1999;9:405-408.

Galván N, Teske DE, Zhou G, Moorthy B, MacWilliams PS, Czuprynski CJ, Jefcoate CR. Induction of CYP1A1 and CYP1B1 in liver and lung by benzo(a)pyrene and 7,12-dimethylbenz(a)anthracene do not affect distribution of polycyclic hydrocarbons to target tissue: role of AhR and CYP1B1 in bone marrow cytotoxicity. Toxicol Appl Pharmacol 2005;202:244-257.

Gao H, Wang LD, Zhou Q, Hong JY, Huang TY, Yang CS. p53 tumour suppressor gene mutation in early esophageal precancerous lesions and carcinoma among high-risk populations in Henan, China. Cancer Res 1994;54:4342-4346.

Gibson P, Gill JH, Khan PA, Seargent JM, Martin SW, Batman PA, Griffith J, Bradley C, Double JA, Bibby MC, Loadmanet PM. Cytochrome P450 1B1 (CYP1B1) is overexpressed in human colon adenocarcinomas relative to normal colon: Implications for drug development. Mol Cancer Ther 2003;2:527-534.

Glick J, Xiong W, Lin Y, Noronha AM, Wilds CJ, Vouros P, The influence of cytosine methylation on the chemoselectivity of benzo[a]pyrene diol epoxide-oligonucleotide adducts determined using nanoLC/MS/MS. J Mass Spectrom 2009;44:1241–1248.

Goodman MT, McDuffie K, Kolonel LN, Terada K, Donlon TA, Wilkens LR, Guo C, Le Marchand L. Case-control study of ovarian cancer and polymorphisms in genes involved in catecholestrogen formation and metabolism. Cancer Epidemiol Biomarkers Prev 2001;10:209-216.

Green CR, Rodgman A. The tobacco chemists' research conference: a half century forum for advances in analytical methodology of tobacco and its products. Recent Adv Tob Sci 1996;22:131–304.

Gsur A, Zidek T, Schnattinger K, Feik E, Haidinger G, Hollaus P, Mohn-Staudner A, Armbruster C, Madersbacher S, Schatzi G, Trieb K, Vutuc C, Micksche M. Association of microsomal epoxide hydrolase polymorphisms and lung cancer risk. Br J Cancer 2003;89:702-706.

Gu J, Horikawa Y, Chen M, Dinney CP, Wu X. Benzo(a)pyrene diol epoxide-induced chromosome 9p21 aberrations are associated with increased risk of bladder cancer. Cancer Epidemiol Biomarkers Prev 2008;17:2445–50.

Guengerich FP, Chun YJ, Kim D, Gillam EMJ, Shimada T. Cytochrome P450 1B1: a target for inhibition in anticarcinogenesis strategies. Mutat Res 2003;523–524:173–182.

Guengerich FP, Shimada T. Activation of procarcinogens by human cytochrome P450 enzymes. Mutat Res 1998;400:201-213.

Gwinn MR, Keshava C, Olivero OA, Humsi JA, Poirier MC, Weston A. Transcriptional signatures of normal human mammary epithelial cells in response to benzo[a]pyrene exposure: a comparison of three microarray platforms. OMICS 2005;9:334-350.

Habano W, Gamo T, Sugai T, Otsuka K, Wakabayashi G, Ozawa S. CYP1B1, but not CYP1A1, is downregulated by promoter methylation in colorectal cancers. Int J Oncol 2009;34:1085-1091.

Hahn WC, Weinberg RA. Rules for making human tumor cells. N Engl J Med 2002;347:1593-1603.

Hainaut P, Pfeifer GP. Patterns of p53 G>T transversions in lung cancers reflect the primary mutagenic signature of DNA-damage by tobacco smoke. Carcinogenesis 2001;22:367-374.

Hanahan D, Weinberg RA. The hallmarks of cancer. Cell 2000;100:57–70.

Hanna IH, Dawling S, Roodi N, Guengerich FP, Parl FF. Cytochrome P450 1B1 (CYP1B1) pharmacogenetics: Association of polymorphisms with functional differences in estrogen hydroxylation activity. Cancer Res 2000;60:3440–3444.

Harada H, Nakagawa H, Oyama K, Takaoka M, Andl CD, Jacobmeier B, von Werder A, Enders GH, Opitz OG, Rustgi AK. Telomerase induces immortalization of human esophageal keratinocytes without p16INK4a inactivation. Mol Cancer Res 2003;1:729-738.

Harrigan JA, McGarrigle BP, Sutter TR, Olson JR. Tissue specific induction of cytochrome P450 (CYP) 1A1 and 1B1 in rat liver and lung following in vitro (tissue slice) and in vivo exposure to benzo(a)pyrene. Toxicology in Vitro 2006;20:426–438.

Harris CC, Autrup H, Stoner GD, Trump BF, Hillman E, Schafer PW, Jeffrey AM. Metabolism of benzo(a)pyrene, JV-nitrosodimethylamine, and A/-nitrosopyrrolidine and identification of the major carcinogen-DNA adducts formed in cultured human esophagus. Cancer Res 1979;39:4401-4406.

Hazra A, Grossman HB, ZhuY, Luo S, Spitz MR, Wu X. Benzo(a)pyrene diol epoxide-induced 9p21 aberrations associated with genetic predisposition to bladder cancer. Genes Chromosomes Cancer 2004;41:330–338.

Hecht SS. Cigarette smoking: cancer risks, carcinogens, and mechanisms. Langenbecks Arch Surg 2006;391:603-613.

Heijne WHM, Stierum RH, Slijper M, van Bladeren PJ, van Ommen B. Toxicogenomics of bromobenzene hepatotoxicity: a combined transcriptomics and proteomics approach. Biochem Pharmacol 2003;65:857-875.

Hendricks D, Parker MI. Oesophageal cancer in Africa. IUBMB Life 2002;53:263-268.

Hiyama T, Yoshihara M, Tanaka S, Chayama K. Genetic polymorphisms and oesophageal cancer risk. Int. J. Cancer 2007;121:1643-1658.

Hockley SL, Arlt VM, Brewer D, Giddings I, Philips DH. Time- and concentration-dependent changes in gene expression induced by benzo[a]pyrene in two human cell lines, MCF-7 and HepG2. BMC Genomics 2006;7:260.

Hockley SL, Arlt VM, Brewer D, te Poele R, Workman P, Giddings I, Philips DH. AHR- and DNA-damage-mediated gene expression responses induced by benzo[a]pyrene in human cell lines. Chem Res Toxicol 2007;20:1797-1810.

Hockley SL, Arlt VM, Jahnke G, Hartwig A, Giddings I, Philips DH. Identification through microarray gene expression analysis of cellular responses to benzo(a)pyrene and its diol-epoxide that are dependent or independent of p53. Carcinogenesis 2008;29:202-210.

Hockley SL, Mathijs K, Staal YCM, Brewer D, Giddings I, van Delft JHM, Philips DH. Interlaboratory and interplatform comparison of microarray gene expression analysis of HepG2 cells exposed to benzo[a]pyrene. OMICS 2009;13:115-125.

Houlston RS. CYP1A1 polymorphisms and lung cancer risk: a meta-analysis. Pharmacogenetics 2000;10:105–114.

Hughes D, Guttenplan JB, Marcus CB, Subbaramaiah K, Dannenberg AJ. HSP90 inhibitors suppress aryl hydrocarbon receptor-mediated activation of CYP1A1 and CYP1B1 transcription and DNA adduct formation. Cancer Prev Res (Phila Pa) 2008;6:485–493.

Ihsan R, Chattopadhyay I, Phukan R, Mishra AK, Purkayastha J, Sharma J, Zomawia E, Verma Y, Mahanta J, Saxena S, Kapur S. Role of epoxide hydrolase 1 gene polymorphisms in esophageal cancer in a high-risk area in India. J Gastroenterol Hepatol 2010;25:1456-1462.

Ikeya K, Jaiswal AK, Owens RA, Jones JE, Nebert DW, Kimura S. Human CYP1A2: sequence, gene structure, comparison with the mouse and rat orthologous gene, and differences in liver 1A2 mRNA expression. Mol Endocrinol 1989;3:1399-1408.

Ingelman-Sundberg M. Genetic susceptibility to adverse effects of drugs and environmental toxicants: The role of the CYP family of enzymes. Mutat Res 2001;482:11-19

Ingelman-Sundberg M. Human drug metabolising cytochrome P450 enzymes: properties and polymorphisms. Naunyn-Schmiedeberg's Arch Pharmacol 2004;369:89-104.

Ingelman-Sundberg M, Daly AK, Nebert DW. Home Page of the Human Cytochrome P450 (*CYP*) Allele Nomenclature Committee. http://www.cypalleles.ki.se/

The International Agency for Research on Cancer. Tobacco smoke and involuntary smoking. IARC Monogr Eval Carcinog Risks Hum 2004;83.

Ishida M, Mikami S, Kikuchi E, Kosaka T, Miyajima A, Nakagawa K, Mukai M, Okada Y, Oya M. Activation of the aryl hydrocarbon receptor pathway enhances cancer cell invasion by upregulating the MMP expression and is associated with poor prognosis in upper urinary tract urothelial cancer. Carcinogenesis 2010;31:287–295.

Ishii T, Murakami J, Notohara K, Cullings HM, Sasamoto H, Kambara T, Shirakawa Y, Naomoto Y, Ouchida M, Shimizu K, Tanaka N, Jass JR, Matsubara N. Oesophageal squamous cell carcinoma may develop within a background of accumulating DNA methylation in normal and dysplastic mucosa. Gut 2007;56:13-19.

Islami F, Boffetta P, Ren JS, Pedoeim L, Khatib D, Kamangar F. High-temperature beverages and foods and esophageal cancer risk – A systematic review. Int. J. Cancer 2009;125:491–524.

Iwanari M, Nakajima M, Kizu R, Hayakawa K, Yokoi T. Induction of CYP1A1, CYP1A2, and CYP1B1 mRNAs by nitropolycyclic aromatic hydrocarbons in various human tissue-derived cells: chemical-, cytochrome P450 isoform-, and cell-specific differences. Arch Toxicol 2002;76:287–298.

Iwano S, Ichikawa M, Takizawa S, Hashimoto H, Miyamoto Y. Identification of AhR-regulated genes involved in PAH-induced immunotoxicity using a highly-sensitive DNA chip, 3D-GeneTM Human Immunity and Metabolic Syndrome 9k. Toxicol in Vitro 2010;24:85-91.

Jain M, Tilak AR, Upadhyay R, Kumar A, Mittal B. Microsomal epoxide hydrolase (EPHX1), slow (exon 3, 113His) and fast (exon 4, 139Arg) alleles confer susceptibility to squamous cell esophageal cancer. Toxicol Appl Pharmacol 2008;230:247-251.

Jaiswal AK, Gonzalez FJ, Nebert DW. Human dioxin-inducible cytochrome P1 450: complementary DNA and amino acid sequence. Science 1985;228:80-83.

Jeffy BD, Chen EJ, Gudas JM, Romagnolo DF. Disruption of cell cycle kinetics by benzo[a]pyrene: inverse expression patterns of BRCA-1 and p53 in MCF-7 cells arrested in S and G_2. Neoplasia 2000;2:460-470.

Jia L, Geacintov NE, Broyde S. The N-clasp of human DNA polymerase kappa promotes blockage or error-free bypass of adenine- or guanine-benzo[a]pyrenyl lesions. Nucleic Acids Res 2008;36:6571–6584.

Jiao H, Allinson SL, Walsh MJ, Hewitt R, Cole KJ, Phillips DH, Martin FL. Growth kinetics in MCF-7 cells modulate benzo[*a*]pyrene-induced CYP1A1 up-regulation. Mutagenesis 2007;22:111-116.

John K, Keshava C, Richardson DL, Weston A, Nath J. Transcriptional profiles of benzo[a]pyrene exposure in normal human mammary epithelial cells in the absence of presence of chlorophyllin. Mutat Res 2008;640:145-152.

Kang GH, Lee S, Cho NY, Gandamihardja T, Long TI, Weisenberger DJ, Campan M, Laird PW. DNA methylation profiles of gastric carcinoma characterized by quantitative DNA methylation analysis. Lab Invest 2008;88:161–170.

Kann S, Huang MY, Estes C, Reichard JF, Sartor MA, Xia Y, Puga A. Arsenite induced aryl hydrocarbon receptor nuclear translocation results in additive induction of phase I and synergistic induction of phase II genes. Mol Pharmacol 2005;68:336–346.

Kao SY, Wu CH, Lin SC, Yap SK, Chang CS, Wong YK, Chi LY, Liu TY. Genetic polymorphism of cytochrome P4501A1 and susceptibility to oral squamous cell carcinoma and oral precancer lesions associated with smoking/betel use. J Oral Pathol Med 2002;31:505–511.

Kashyap MJ, Marimuthu A, Kishore CJH, Peri S, Keerthikumar S, Prasad TSK, Mahmood R, Rao S, Ranganathan P, Sanjeeviah RC, Vijayakumar M, Kumar KVV, Montgomery E, Kumar RV, Pandey A. Genomewide mRNA profiling of esophageal squamous cell carcinoma for identification of biomarkers. Cancer Biol Ther 2009;8:1-11.

Kashyap MJ, Marimuthu A, Peri S, Kumar GSS, Jacob HKC, Prasad TSK, Mahmood R, Kumar KVV, Kumar MV, Meltzer SJ, Montgomery EA, Kumar RV, Pandey A. Overexpression of periostin and lumican in esophageal squamous cell carcinoma. Cancers 2010;2:133-142.

Kawajiri K, Fujii-Kuriyama Y. Cytochrome P450 gene regulation and physiological functions mediated by the aryl hydrocarbon receptor. Arch Biochem Biophys 2007;464:207-212.

Kazlauskas A, Poellinger L, Pongratz I. Evidence that the co-chaperone p23 regulates ligand responsiveness of the dioxin (Aryl hydrocarbon) receptor. J Biol Chem 1999;274:13519–13524.

Kemp MQ, Liu W, Thorne PA, Kane MD, Selmin O, Romagnolo DF. Induction of the transferring receptor gene by benzo[a]pyrene in breast cancer MCF-7 cells: potential as a biomarker of PAH exposure. Environ Mol Mutagen 2006;47:518-526.

Keshava C, Divi RL, Einem TL, Richardson DL, Leonard SL, Keshava N, Poirier MC, Weston A. Chlorophyllin significantly reduces benzo[*a*]pyrene [BP]-DNA adduct formation and alters Cytochrome P450 1A1 and 1B1 expression and EROD activity in normal human mammary epithelial cells (NHMECs). Environ Mol Mutagen 2009;50:134–144.

Keshava C, Divi RL, Whipkey DL, Frye BL, McCanlies E, Kuo M, Poirier MC, Weston A. Induction of CYP1A1 and CYP1B1 and formation of carcinogen–DNA adducts in normal human mammary epithelial cells treated with benzo[a]pyrene. Cancer Lett 2005;221:213–224.

Keshava C, Whipkey D, Weston A. Transcriptional signatures of environmentally relevant exposures in normal human mammary epithelial cells: benzo[a]pyrene. Cancer Lett 2005;221:201-211.

Kim DW, Gazourian L, Quadri SA, Romieu-Mourez R, Sherr DH, Sonenshein GE. The RelA NFκB subunit and the aryl hydrocarbon receptor (AhR) cooperate to transactivate the c-myc promoter in mammary cells. Oncogene 2000;19:5498-5506.

Kim JH, Kim H, Lee KY, Kang JW, Lee KH, Park SY, Yoon HI, Jheon SH, Sung SW, Hong YC: Aryl hydrocarbon receptor gene polymorphisms affect lung cancer risk. Lung Cancer 2007;56:9-15.

Kim SH, Nakagawa H, Navaraj A, Naomoto Y, Klein-Szanto AJ, Rustgi AK, El-Deir WS. Tumorigenic conversion of primary human esophageal epithelial cells using oncogene combinations in the absence of exogenous Ras. Cancer Res 2006;66:10415-10424.

Ko Y, Abel J, Harth V, Bröde P, Antony C, Donat S, Fischer HP, Ortiz-Pallardo ME, Their R, Sachinidis A, Vetter H, Bolt HM, Herberhold C, Brüning T. Association of CYP1B1 codon 432 mutant allele in head and neck squamous cell cancer is reflected by somatic mutations of p53 in tumor tissue. Cancer Res 2001;61:4398-4404.

Koliopanos A, Kleeff J, Xiao Y, Safe S, Zimmermann A, Buchler MW, Friess H: Increased arylhydrocarbon receptor expression offers a potential therapeutic target for pancreatic cancer. Oncogene 2002;21:6059-6070.

Kometani T, Yoshino I, Miura N, Okazaki H, Ohba T, Takenaka T, Shoji F, Yano T, Maehara Y. Benzo[a]pyrene promotes proliferation of human lung cancer cells by accelerating the epidermal growth factor receptor signaling pathway. Cancer Lett 2009;278:27-33.

Kozack R, Seo KY, Jelinsky SA, Loechler EL. Toward an understanding of the role of DNA adduct conformation in defining mutagenic mechanism based on studies of the major adduct (formed at N(2)-dG) of the potent environmental carcinogen, benzo[a]pyrene. Mutat Res 2000;450:41–59.

Kropachev K, Kolbanovskii M, Cai Y, Rodríguez F, Kolbanovskii A, Liu Y, Zhang L, Amin S, Patel D, Broyde S, Geacintov NE. The sequence dependence of human nucleotide excision repair efficiencies of benzo[a]pyrene-derived DNA lesions: Insights into the structural factors that favor dual incisions. J Mol Biol 2009;386:1193–1203.

Landi MT, Bergen AW, Baccarelli A, Patterson DG Jr, Grassman J, Ter-Minassian M, Mocarelli P, Caporaso N, Masten A, Pesatori AC, Pittman GS, Bell DA. CYP1A1 and CYP1B1 genotypes, haplotypes, and TCDD-induced gene expression in subjects from Seveso, Italy. Toxicology 2005;207:191–202.

Lechevrel M, Casson AG, Wolf CR, Hardie LJ, Flinterman MB, Montesano R, Wild CP. Characterization of cytochrome P450 expression in human oesophageal mucosa. Carcinogenesis 1999;20: 243-248.

Lee CM, Chen SY, Lee YCG, Huang CYF, Chen YMA. Benzo[a]pyrene and glycine N-methyltransferase interactions: gene expression profiles of the liver detoxification pathway. Toxicol Appl Pharmaol 2006;214:126-135.

Le Marchand L, Guo C, Benhamou S, Bouchardy C, Cascorbi I, Clapper ML, Garte S, HaugenA, Ingelman-Sundberg M, Kihara M, Rannug A, Ryberg D, Stücker I, Sugimura H, Taioli E. Pooled analysis of the CYP1A1 exon 7 polymorphism and lung cancer (United States). Cancer Causes Control 2003;14:339–346.

Leung YK, Lau KM, Mobley J, Jiang Z, Ho SM. Overexpression of cytochrome P450 1A1 and its novel spliced variant in ovarian cancer cells: Alternative subcellular enzyme compartmentation may contribute to carcinogenesis. Cancer Res 2005;65:3726-3734.

Levine AJ. p53, the cellular gatekeeper for growth and division. Cell 1997;88:323-331.

Li C, Chen H, Ding F, Zhang Y, Luo A, Wang M, Liu Z. A novel p53 target gene, S100A9, induces p53-dependent cellular apoptosis and mediates the p53 apoptosis pathway. Biochem J 2009;422:363-372.

Li DN, Seidel A, Pritchard MP, Wolf CR, Friedberg T. Polymorphisms in P450 CYP1B1 affect the conversion of estradiol to the potentially carcinogenic metabolite 4-hydroxyestradiol. Pharmacogenetics 2000;10:343-353.

Li DP, Dandara C, Walther G, Parker MI. Genetic polymorphisms of alcohol metabolizing enzymes: their role in susceptibility to oesophageal cancer. Clin Chem Lab Med 2008;46:323-28.

Li DP, Dandara C, Parker MI. Association of cytochrome P450 2E1 genetic polymorphisms with squamous cell carcinoma of the oesophagus. Clin Chem Lab Med 2005;43:370-375.

Li DP, Dandara C, Parker MI. The 341C/T polymorphism in the GSTP1 gene is associated with increased risk of oesophageal cancer. BMC Genetics 2010;11:47.

Li JZ, Pan HY, Zheng JW, Zhou XJ, Zhang P, Chen WT, Zhang ZY. Benzo[a]pyrene induced tumorigenesity of human immortalized oral epithelial cells: transcriptional profiling. Chin Med J 2008;121:1882-1890.

Liang HC, Li H, McKinnon RA, Duffy JJ, Potter SS, Puga A, Nebert DW. Cyp1a2(-/-) null mutant mice develop normally but show deficient drug metabolism. PNAS 1996;93:1671-1676.

Liang HC, McKinnon RA, Nebert DW. Sensitivity of CYP1A1 mRNA inducibility by dioxin is the same in Cyp1a2(+/+) wild-type and Cyp1a2(-/-) null mutant mice. Biochem Pharmacol 1997;54:1127-1131.

Lin P, Chang H, Tsai WT, Wu MH, Liao YS, Chen JT, Su JM. Overexpression of aryl hydrocarbon receptor in human lung carcinomas. Toxicol Pathol 2003;31:22-30.

Lim DM, Narasimhan S, Michaylira CZ, Wang ML. TLR3-mediated NFKB signaling in human esophageal epithelial cells. Am J Physiol Gastrointest Liver Physiol 2009;297:G1172-G1180.

Lipworth L, Rossi M, McLaughlin JK, Negri E, Talamini R, Levi F, Franceschi S, La Vecchia C. Dietary vitamin D and cancers of the oral cavity and esophagus. Ann Oncol 2009;20:1576–1581.

London SJ, Yuan JM, Coetzee GA, Gao YT, Ross RK, Yu MC. CYP1A1 I462V genetic polymorphism and lung cancer risk in a cohort of men in Shanghai, China. Cancer Epidemiol Biomarkers Prev 2000;9:987-991.

Long JR, Egan KM, Dunning L, Shu XO, Cai Q, Cai H, Dai Q, Holtzman J, Gao YT, Zheng W. Population-based case-control study of AhR (aryl hydrocarbon receptor) and CYP1A2 polymorphisms and breast cancer risk. Pharmacogenet Genomics 2006;16:237-243.

Lu X, Shao J, Li H, Yu Y. Early whole-genome transcriptional response induced by benzo[a]pyrene diol epoxide in a normal human cell line. Genomics 2009;93:332-342.

Luch A. Nature and nurture - lessons from chemical carcinogenesis. Nat Rev Cancer 2005;5:113–125.

Luo W, Fan W, Xie H, Jing L, Ricicki E, Vouros P, Zhao LP, Zarbl H. Phenotypic anchoring of global gene expression profiles induced by N-hydroxy-4-acetylaminobiphenyl and benzo[a]pyrene diol epoxide reveals correlations between expression profiles and mechanism of toxicity. Chem Res Toxicol 2005;18:619-629.

Ma Q, Baldwin KT. 2,3,7,8-Tetrachlorodibenzo-p-dioxin-induced degradation of aryl hydrocarbon receptor (AhR) by the ubiquitin–proteasome pathway: role of the transcription activation and DNA binding of AhR. J Biol Chem 2000;275:8432–8438.

Ma Q, Baldwin KT, Renzelli AJ, McDaniel A, Dong L. TCDD-inducible poly(ADP-ribose) polymerase: a novel response to 2,3,7,8-tetrachlorodibenzo-p-dioxin. Biochem Biophys Res Comm 2001;289:499-506.

Ma Q, Lu AYH. CYP1A induction and human risk assessment: An evolving tale of in vitro and in vivo studies. Drug Metab Dispos 2007;35:1009-1016.

MacLeod SL, Tang YM, Yoko I. The role of recently discovered genetic polymorphisms in the regulation of the human CYP1A2 gene. Proc Am Assoc Cancer Res 1998;39:396.

Mahadevan B, Keshava C, Musafia-Jeknic T, Pecaj A, Weston A, Baird WM. Altered gene expression patterns in MCF-7 cells induced by the urban dust particulate complex mixture standard reference material 1649a. Cancer Res 2005;65:1251-1258.

Manna S, Mukherjee S, Roy A, Das S, PandaCK. Tea polyphenols can restrict benzo[a]pyrene-induced lung carcinogenesis by altered expression of p53-associated genes and H-ras, c-myc and cyclin D1. J Nutr Biochem 2009;20:337-349.

Marasas WFO. Discovery and occurrence of the fumonisins: A historical perspective. Environ Health Perspect 2001;109:239-243.

Marlowe JL, Puga A. Aryl hydrocarbon receptor, cell cycle regulation, toxicity, and tumorigenesis. J Cell Biochem 2005;96:1174-1184.

Matsha T, Brink L, van Rensburg S, Hon D, Lombard C, Erasmus R. Traditional home-brewed beer consumption and iron status in patients with esophageal cancer and healthy control subjects from Transkei, South Africa. Nutr Cancer 2006;56:67-73.

Matsha T, Erasmus R, Kafuko AB, Mugwanya D, Stepien A, Parker MI, CANSA/MRC Oesophageal Cancer Research Group. Human papillomavirus associated with oesophageal cancer. J Clin Path 2002;55:587-590.

Matsha T, Stepien A, Blanco-Blanco E, Brink LT, Lombard CJ, van Rensburg S, Erasmus RT. Self-induced vomiting – risk for oesophageal cancer? S Afr Med J 2006;96:209-212.

Matthews J, Gustafsson J. Estrogen receptor and aryl hydrocarbon receptor signaling pathways. Nuclear Receptor Signaling 2006;4:e016.

McFadyen MCE, Melvin WT, Murray GI. Cytochrome P450 1B1 activity in renal cell carcinoma. Br J Cancer 2004;91:966-971.

Meyer BK, Pray-Grant MG, Vanden Heuvel JP, Perdew GH. Hepatitis B virus X-associated protein 2 is a subunit of the unliganded aryl hydrocarbon receptor core complex and exhibits transcriptional enhancer activity. Mol Cell Biol 1988;18:978–988.

Miller KP, Ramos KS. Impact of cellular metabolism on the biological effects of benzo[a]pyrene and related hydrocarbons. Drug Metab Rev 2001;33:1-35.

Mimura J, Ema M, Sogaza K, Fujii-Kuriyama Y. Identification of a novel mechanism of regulation of Ah (dioxin) receptor function. Genes Dev 1999;13:20-25.

Miyoshi Y, Takahashi Y, Egawa C, Noguchi S. Breast cancer risk associated with CYP1A1 genetic polymorphisms in Japanese women. Breast J 2002;8:209-215.

Moennikes O, Loeppen S, Buchmann A, Andersson P, Ittrich C, Poellinger L, Schwarz M. A constitutively active dioxin/aryl hydrocarbon receptor promotes hepatocarcinogenesis in mice. Cancer Res 2004;64:4707–4710.

Monteiro P, Gilot D, Langouet S, Fardel O. Activation of the aryl hydrocarbon receptor by the calcium/calmodulin-dependent protein kinase kinase inhibitor 7-oxo-7H-benzimidazo[2,1-a]benz[de]isoquinoline-3-carboxylic acid (STO-609). Drug Metab Dispos 2008;2556-2563.

Mqoqi N, Kellet P, Sitas F, Jula M. National Cancer Registry of South Africa. Incidence of histologically diagnosed cancer in South Africa, 1998-1999. Johannesburg: National Cancer Registry, South African Institute for Medical Research 2004.

Nakajima M, Iwanari M, Yokoi T. Effects of histone deacetylation and DNA methylation on the constitutive and TCDD-inducible expressions of the human CYP1 family in MCF-7 and HeLa cells. Toxicol Lett 2003;144:247-256.

Nakajima M, Yokoi T, Mizutani M, Kinoshita M, Funayama M, Kamataki T. Genetic polymorphisms in the 5'-flnking region of the human CYP1A2 gene: effect on the CYP1A2 inducibility in humans. J Biochem 1999;125:803-806.

Nakajima T, Wang RS, Yoshinori N, Pin YM, He M, Vainio H, Murayama N, Aoyama T, Iida F. Expression of cytochrome P450s and glutathione S-transferases in human esophagus with squamous-cell carcinomas. Carcinogenesis 1996;17:1477–1481.

Natsuizaka M, Ohashi S, Wong GS, Ahmadi A, Kalman RA, Budo D, Klein-Szanto AJ, Herlyn M, Diehl A, Nakagawa H. Insulin-like growth factor-binding protein-3 promotes transforming growth factor-b1-mediated epithelial-to-mesenchymal transition and motility in transformed human esophageal cells. Carcinogenesis 2010;31:1344-1353.

Nebert DW, Dalton TP. The role of cytochrome P450 enzymes in endogenous signaling pathways and environmental carcinogenesis. Nat Rev Cancer 2006;6:947-960.

Nebert DW, Dalton TP, Okey AB, Gonzalez FJ. Role of aryl hydrocarbon receptor-mediated induction of the CYP1 enzymes in environmental toxicity and cancer. J Biol Chem 2004;279:23847–23850.

Nebert DW, Roe AL, Dieter MZ, Solis WA, Yang Y, Dalton TP. Role of the aromatic hydrocarbon receptor and [*Ah*] gene battery in the oxidative stress response, cell cycle control, and apoptosis. Biochem Pharmacol 2000;59:65–85.

Nebert DW, Russell DW. Clinical importance of the cytochromes P450. Lancet 2002;360:1155-1162.

Niestroy J, Barbara A, Herbst K, Rode S, van Liempt M, Roos PH. Single and concerted effects of benzo[a]pyrene and flavonoids on the AhR and Nrf2-pathway in the human colon carcinoma cell line Caco-2. Toxicol in Vitro 2011;25:671–683.

Nimura Y, Yokoyama S, Fujimori M, Aoki T, Adachi W, Nasu T, He M, Ping YM, Iida F. Genotyping of the CYP1A1 and GSTM1 genes in esophageal carcinoma patients with special reference to smoking. Cancer 1997;80:852-857.

Ohtake F, Takeyama K, Matsumoto T, Kitagawa H, Yamamoto Y, Nohara K, Tohyama C, Krust A, Mimura J, Chambon P, Yanagisawa J, Fujii-Kuriyama Y, Kato S. Modulation of oestrogen receptor signalling by association with the activated dioxin receptor. Nature 2003;423:545-550.

Ouyang W, Hu Y, Li J, Ding M, Lu Y, Zhang D, Yan Y, Song L, Qu Q, Desai D, Amin S, Huang C. Direct evidence for the critical role of NFAT3 in benzo[a]pyrene diol-epoxide-induced cell transformation through mediation of inflammatory cytokine TNF induction in mouse epidermal CI41 cells. Carcinogenesis 2007;28:2218-2226.

Pacella-Norman R, Urban MI, Sitas F, Carrara H, Sur R, Hale M, Ruff P, Patel M, Newton R, Bull D, Beral V. Risk factors for oesophageal, lung, oral and laryngeal cancers in black South Africans. Br J Cancer 2002;86:1751-1756.

Pande M, Amos CI, Eng C, Frazier ML. Interactions between cigarette smoking and selected polymorphisms in xenobiotic metabolizing enzymes in risk for colorectal cancer: A case-only analysis. Mol Carcinogenesis 2010;49:974-980.

Paracchini V, Raimondi S, Gram IT, Kang D, Kocabas NA, Kristensen VN, Li D, Parl FF, Rylander-Rudqvist T, Soucek P, Zheng W, Wedren S, Taioli E. Meta- and pooled analyses of the cytochrome P-450 1B1 Val432Leu polymorphism and breast cancer: A HuGE–GSEC Review. Am J Epidemiol 2007;165:115–125.

Perdew GH. Association of the Ah receptor with the 90-kDa heat shock protein. J Biol Chem 1988;263:13802–13805.

Perez DS, Handa RJ, Yang RSH, Campain JA. Gene expression changes associated with altered growth and differentiation in benzo[a]pyrene or arsenic exposed normal human epidermal keratinocytes. J Appl Toxicol 2008;28:491-508.

Phillips DH. Polycyclic aromatic hydrocarbons in the diet. Mutat Res 1999;443:139-147.

Pickens A, Orringer MB. Geographical distribution and racial disparity in esophageal cancer. Ann Thorac Surg 2003;76:S1367-S1369.

Pisani P, Parkin DM, Bray F, Ferlay J. Estimates of the worldwide mortality from 25 cancers in 1990. Int J Cancer 1999;83:18-29.

Plíšková M, Vondráček J, Vojtěšek B, Kozubík A, Machala M: Deregulation of cell proliferation by polycyclic aromatic hydrocarbons in human breast carcinoma MCF-7 cells reflects both genotoxic and nongenotoxic events. Toxicol Sci 2005;83:246-256.

Pollenz RS, Barbour ER. Analysis of the complex relationship between nuclear export and aryl hydrocarbon receptor-mediated gene regulation. Mol Cell Biol 2000;20:6095–6104.

Port JL, Yamaguchi K, Du B, De Lorenzo M, Chang M, Heerdt PM, Kopelovich L, Marcus CB, Altorki NK, Subbaramaiah K, Dannenberg AJ. Tobacco smoke induces CYP1B1 in the aerodigestive tract. Carcinogenesis 2004;25:2275-2281.

Probst MR, Reisz-Porszasz S, Agbunag RV, Ong MS, Hankinson O. Role of the aryl hydrocarbon receptor nuclear translocator protein in aryl hydrocarbon (dioxin) receptor action. Mol Pharmacol 1993;44:511–518.

Puga A, Barnes SJ, Dalton TP, Chang C, Knudsen ES, Maier MA. Aromatic hydrocarbon receptor interaction with the retinoblastoma protein potentiates repression of E2F-dependent transcription and cell cycle arrest. J Biol Chem 2000;275:2943-2950.

Puga A, Ma C, Marlowe JL. The aryl hydrocarbon receptor cross-talks with multiple signal transduction pathways. Biochem Pharmacol 2009;77:713-722.

Ramos KS, Steffen MC, Falahatpisheh MH, Nanez A. From genomics to mechanistic insight: A global perspective on molecular deficits induced by environmental agents. Environ Mol Mutagen 2007;48:395-399.

Rechkoblit O, Zhang Y, Guo D, Wang Z, Amin S, Krzeminsky J, Louneva N, Geacintov NE. Trans-Lesion synthesis past bulky benzo[a]pyrene diol epoxide N2-dG and N6-dA lesions catalyzed by DNA bypass polymerases. J Biol Chem 2002;277:30488-30494.

Reisz-Porszasz S, Probst MR, Fukunaga BN, Hankinson O. Identification of functional domains of the aryl hydrocarbon receptor nuclear translocator protein. Mol Cell Biol 1994;14:6075-6086.

Roth MJ, Abnet CC, Hu N, Wang QH, Wei WQ, Green L, D'Alelio M, Qiao YL, Dawsey SM, Taylor PR, Woodson K. p16, MGMT, RARB2, CLDN3, CRBP and MT1G gene methylation in esophageal squamous cell carcinoma and its precursor lesions. Oncol Rep 2006;15:1591-1597.

H Rubin. Synergistic mechanisms in carcinogenesis by polycyclic aromatic hydrocarbons and by tobacco smoke: A biohistorical perspective with updates. Carcinogenesis 2001;22:1903-1930.

Sadikovic B, Rodenhiser DI. Benzopyrene exposure disrupts DNA methylation and growth dynamics in breast cancer cells. Toxicol Appl Pharmacol 2006;216:458-468.

Sagredo C, Øvrebø S, Haugen A, Fujii-Kuriyama Y, Bæra R, Botnen IV, Mollerup S. Quantitative analysis of benzo[a]pyrene biotransformation and adduct formation in AhR knockout mice. Toxicol Lett 2006;167:173-182.

Sasaki M, Tanaka Y, Kaneuchi M, Sakuragi N, Dahiya R. CYP1B1 gene polymorphisms have higher risk for endometrial cancer, and positive correlations with estrogen receptor α and estrogen receptor β expressions. Cancer Res 2003;63:3913–3918.

Scherer G, Frank S, Riedel K, Meger-Kossien I, Renner T. Biomonitoring of exposure to polycyclic aromatic hydrocarbons of nonoccupationally exposed persons. Cancer Epidemiol Biomarkers Prev 2000;9:373–380.

Schlezinger JJ, Liu D, Farago M, Seldin DC, Belguise K, Sonenshein GE, Sherr DH. A role for the aryl hydrocarbon receptor in mammary gland tumorigenesis. Biol Chem 2006;387:1175-1187.

Schmeltz I, Hoffmann D, Wynder EL. Toxic and tumorigenic agents in tobacco smoke. Analytical Methods and Modes of Origin. Trace Subst Environ Health 8, Symp 1974:281–295.

Seitz HK, Stickel F. Molecular mechanisms of alcohol-mediated carcinogenesis. Nat Rev Cancer 2007;7:599-612.

Shamma A, Yamamoto H, Doki Y, Okami J, Kondo M, Fujiwara Y, Yano M, Inoue M, Matsuura N, Shiozaki H, Monden M. Up-regulation of cyclooxygenase-2 in squamous carcinogenesis of the esophagus. Clin Cancer Res 2000;6:1229–1238.

Shi S, Yoon DY, Hodge-Bell KC, Bebenek IG, Whitekus MJ, Zhang R, Cochran AJ, Huerta-Yepez S, Yim SH, Gonzalez FJ, Jaiswal AK, Hankinson O. The aryl hydrocarbon receptor nuclear translocator (Arnt) is required for tumor initiation by benzo[a]pyrene. Carcinogenesis 2009;30:1957-1961.

Shi S, Yoon DY, Hodge-Bell KC, Huerta-Yepez S, Hankinson O. Aryl hydrocarbon receptor nuclear translocator (hypoxia inducible factor 1β) activity is required more during early than late tumor growth. Mol Carcinogenesis 2010;49:157-165.

Shibagaki I, Tanaka H, Shimada Y, Wagata T, Ikenaga M, Imamura M, Ishizaki K. p53 mutation, murine double minute 2 amplification, and human papillomavirus infection are frequently involved but not associated with each other in esophageal squamous cell carcinoma. Clin Cancer Res 1995;1:769-773.

Shimada T. Xenobiotic-metabolizing enzymes involved in activation and detoxification of carcinogenic polycyclic aromatic hydrocarbons. Drug Metab Pharmacokinet 2006;21:257-276.

Shimada T, Fujii-Kuriyama Y. Metabolic activation of polycyclic aromatic hydrocarbons to carcinogens by cytochromes P450 1A1 and 1B1. Cancer Sci 2004;95:1–6.

Shimada T, Hayes CL, Yamazaki H, Amin S, Hecht SS, Guengerich FP, Sutler TR. Activation of chemically diverse procarcinogens by human cytochrome P-450 IBI. Cancer Res 1996;56:2979-2984.

Shimada T, Watanabe J, Kawajiri K, Sutter TR, Guengerich FP, Gillam EMJ, Inoue K. Catalytic properties of polymorphic human cytochrome P450 1B1 variants. Carcinogenesis 1999;20:1607-1613.

Shimada Y, Imamura M, Wagata T, Yamaguchi N, Tobe T. Characterization of 21 newly established esophageal cancer cell lines. Cancer 1992;69:277-284.

Shimba S, Komiyama K, Moro I, Tezuka M. Overexpression of the aryl hydrocarbon receptor (AhR) accelerates the cell proliferation of A549 cells. J Biochem 2002;132:795-802.

Shimizu Y, Nakatsuru Y, Ichinose M, Takahashi Y, Kume H, Mimura J, Fujii-Kuriyama Y, Ishikawa T. Benzo[a]pyrene carcinogenicity is lost in mice lacking the aryl hydrocarbon receptor. Proc Natl Acad Sci 2000;97:779-782.

Shinmura K, Iwaizumi M, Igarashi H, Nagura K, Yamada H, Suzuki M, Fukasawa K, Sugimura H. Induction of centrosome amplification and chromosome instability in p53-deficient lung cancer cells exposed to benzo[a]pyrene diol epoxide (B[a]PDE). J Pathol 2008;216:365-374.

Sohn SH, Kim KN, Kim IK, Lee EI, Ryu JJ, Kim MK. Effects of tobacco compounds on gene expression in fetal lung fibroblasts. Environ Toxicol 2008;23:423-434.

Solhaug A, Refsnes M, Holme JA. Role of cell signalling involved in induction of apoptosis by benzo[a]pyrene and cyclopenta[c,d]pyrene in Hepa1c1c7 cells. J Cell Biochem 2004;93:1143–1154.

Solhaug A, Refsnes M, Låg M, Schwarze PE, Husøy T, Holme JA. Polycyclic aromatic hydrocarbons induce both apoptotic and anti-apoptotic signals in Hepa1c1c7 cells. Carcinogenesis 2004;25:809-819.

Somdyala NI, Bradshaw D, Gelderblom WC, Parkin DM. Cancer incidence in a rural population of South Africa, 1998-2002. Int J Cancer 2010;127:2420-2429.

Song S, Lippman SM, Zou Y, Ye X, Ajani JA, Xu XC. Induction of cyclooxygenase-2 by benzo[a]pyrene diol epoxide through inhibition of retinoic acid receptor-β2 expression**.** Oncogene 2005;24:8268-8276.

Sparfel L, Pinel-Marie ML, Boize M, Koscielny S, Desmots S, Pery A, Fardel O. Transcriptional signatures of human macrophages exposed to the environmental contaminant benzo[a]pyrene. Toxicol Sci 2010;114:247-259.

Spink DC, Wu SJ, Spink BC, Hussain MM, Vakharia DD, Pentecost BT, Kaminsky LS. Induction of CYP1A1 and CYP1B1 by benzo(*k*)fluoranthene and benzo(*a*)pyrene in T-47D human breast cancer cells: Roles of PAH interactions and PAH metabolites. Toxicol Appl Pharmacol 2008;226:213-224.

Srivastava SK, Bansal P, Oguri T, Lazo JS, Singh SV. Cell division cycle 25B phosphatase is essential for benzo[a]pyrene-7,8-diol-9,10-epoxide-induced neoplastic transformation. Cancer Res 2007;67:9150-9157.

Staal YCM, van Herwijnen MHM, van Schooten FJ, van Delft JHM. Modulation of gene expression and DNA adduct formation in HepG2 cells by polycyclic aromatic hydrocarbons with different carcinogenic potencies. Carcinogenesis 2005;27:646-655.

Strauss WM. Preparation and analysis of DNA. In Current Protocols in Molecular Biology 1998 (Ausubel FM, Brent R, Kingston RE, Moore DD, Seidman JG, Smith JA and Struhl K, ed.), unit 2.2.2-2.2.3, John Wiley & Sons Inc., New York .

Sutter TR, Tang YM, Hayes CL, Wo YYP, Jabs EW, Li X, Yin H, Cody CW, Greenlee WF. Complete cDNA sequence of a human dioxin inducible mRNA identifies a new gene subfamily of cytochrome P450 that maps to chromosome 2. J Biol Chem 1994;269:13092-13099.

Suzuki S, Muroishi Y, Nakanishi I, Oda Y. Relationship between genetic polymorphisms of drug-metabolizing enzymes (CYP1A1, CYP2E1, GSTM1 and NAT2) drinking habits, histological subtypes and p53 gene mutations in Japanese patients with gastric cancer. J Gastroenterol 2004;39:220-230.

Taioli E, Gaspari L, Benhamou S, Boffetta P, Brockmoller J, Butkiewicz D, Cascorbi I, Clapper ML, Dolzan V, Haugen A, Hirvonen A, Husgafvel-Pursiainen K, Kalina I, Kremers P, Le Marchand L, London S, Rannug A, Romkes M, Schoket B, Seidegard J, Strange RC, Stucker I, To-Figueras J, Garte S. Polymorphisms in CYP1A1, GSTM1, GSTT1 and lung cancer below the age of 45 years. Int J Epidemiol 2003;32:60–63.

Tan Z, Chang X, Puga A, Xia Y. Activation of mitogen-activated protein kinases (MAPKs) by aromatic hydrocarbons: role in the regulation of aryl hydrocarbon receptor (AHR) function. Biochem Pharmacol 2002;64:771-780.

Tanaka Y, Sasaki M, Kaneuchi M, Shiina H, Igawa M, Dahiya R. Polymorphisms of the CYP1B1 gene have higher risk for prostate cancer. Biochem Biophys Res Comm 2002;296:820–826.

Tannheimer SL, Ethier SP, Caldwell KK, Burchiel SW. Benzo[a]pyrene- and TCDD-induced alterations in tyrosine phosphorylation and insulin-like growth factor signaling pathways in the MCF-10A human mammary epithelial cell line. Carcinogenesis 1998;19:1291-1297.

Tekpli X, Rissel M, Huc L, Catheline D, Sergent O, Rioux V, Legrand P, Holme JA, Dimanche-Boitrel M, Lagadic-Gossmann D. Membrane remodeling, an early event in benzo[a]pyrene-induced apoptosis. Toxicol Appl Pharmacol 2010;243:68-76.

Tennenbaum T, Li L, Belanger AJ, De Luca LM, Yuspa SH. Selective changes in laminin adhesion and alpha 6 beta 4 integrin regulation are associated with the initial steps in keratinocyte maturation. Cell Growth Differ 1996;**7**: 615–628.

Tian Y. Ah receptor and NF-κB interplay on the stage of epigenome. Biochem Pharmacol 2009;77:670-680.

Toh Y, Oki E, Ohgaki K, Sakamoto Y, Ito S, Egasira A, Saeki H, Kakeji Y, Morita M, Sakaguchi Y, Okamura T, Maehara Y. Alcohol drinking, cigarette smoking, and the development of squamous cell carcinoma of the esophagus: molecular mechanisms of carcinogenesis. Int J Clin Oncol 2010;15:135-144.

Tokizane T, Shiina H, Igawa M, Enokida H, Urakami S, Kawakami T, Ogishima T, Okino ST, Li LC, Tanaka Y, Nonomura N, Okuyama A, Dahiya R. Cytochrome P450 1B1 is overexpressed and regulated by hypomethylation in prostate cancer. Clin Cancer Res 2005;11:5793-5801.

Tsuchiya Y, Nakajima M, Itoh S, Iwanari M, Yokoi T. Expression of aryl hydrocarbon receptor repressor in normal human tissues and inducibility by PAHs in tumour-derived cell lines. Toxicol Sci 2003;72:253-259.

Umannová L, Machala M, Topinka J, Nováková Z, Milcová A, Kozubík A, Vondráček J. Tumor necrosis factor-α potentiates genotoxic effects of benzo[*a*]pyrene in rat liver epithelial cells through upregulation of cytochrome P450 1B1 expression. Mutat Res 2008;640:162–169.

Uno S, Dalton TP, Shertzer HG, Genter MB, Warshawsky D, Talaska G, Nebert DW. Benzo[a]pyrene-induced toxicity: paradoxical protection in Cyp1a1(-/-) knockout mice having increased hepatic benzo[a]pyrene-DNA adduct levels. Biochem Biophys Res Commun 2001;289:1049-1056.

Uno S, Dalton TP, Derkenne S, Curran CP, Miller ML, Shertzer HG, Nebert DW. Oral exposure to benzo[*a*]pyrene in the mouse: Detoxication by inducible cytochrome P450 Is more important than metabolic activation. Mol Pharmacol 2004;65:1225–1237.

Uno S, Dalton TP, Dragin N, Curran CP, Derkenne S, Miller ML, Shertzer HG, Gonzalez FJ, Nebert DW. Oral benzo[a]pyrene in Cyp1 knockout mice lines: CYP1A1 important in detoxication, CYP1B1 metabolism required for immune damage independent of total-body burden and clearance rate. Mol Pharmacol 2006;69:1103-1114.

Uppstad H, Øvrebø S, Haugen A, Mollerup S. Importance of CYP1A1 and CYP1B1 in bioactivation of benzo[a]pyrene in human lung cell lines. Toxicol Lett 2010;192:221–228.

Valko M, Rhodes CJ, Moncol J, Izakovic M, Mazur M. Free radicals, metals and antioxidants in oxidative stress-induced cancer. Chemico-Biol Interactions 2006;160:1-40.

van Delft JHM, van Agen E, van Breda SGJ, Herwijnen MH, Staal YCM, Kleinjans JCS. Discrimination of genotoxic from non-genotoxic carcinogens by gene expression profiling. Carcinogenesis 2004;25:1265-1276.

Veale RB, Thornley AL. Atypical cytokeratins synthesized by human oesophageal carcinoma cells in culture. S Afr J Sci 1984;80:260-267.

Vos M, Adams CH, Victor TC, van Helden PD. Polymorphisms and mutations found in the regions flanking exons 5 to 8 of the TP53 gene in a population at high risk for esophageal cancer. Cancer Genet Cytogenet 2003;140:23-30.

Wang A, Gu J, Judson-Kremer K, Powell KL, Mistry H, Simhambhatla P, Aldaz CM, Gaddis S, MacLeod MC. Response of human mammary epithelial cells to DNA damage induced by BPDE: involvement of novel regulatory pathways. Carcinogenesis 2003;24:225-234.

Wang Z, Tang L, Sun G, Tang Y, Xie Y, Wang S, Hu X, Gao W, Cox SB, Wang JS. Etiological study of esophageal squamous cell carcinoma in an endemic region: a population-based case control study in Huaian, China. BMC Cancer 2006;6:287.

Wang Z, Yang H, Ramesh A, Roberts LJ II, Zhou LC, Lin X, Zhao Y, Guo ZM. Overexpression of Cu/Zn-superoxide dismutase and/or catalase accelerates benzo(*α*) pyrene detoxification by upregulation of the aryl hydrocarbon receptor in mouse endothelial cells. Free Radic Biol Med 2009;47:1221–1229.

Watabe Y, Nazuka N, Tezuka M, Shimba S. Aryl hydrocarbon receptor functions as a potent coactivator of E2F1-dependent trascription activity. Biol Pharm Bull 2010;33:389-397.

Watanabe J, Shimada T, Gillam EMJ, Ikuta T, Suemasu K, Higashi Y, Gotoh O, Kawajiri K. Association of CYP1B1 genetic polymorphism with incidence to breast and lung cancer. Pharmacogenetics 2000;10:25-33.

Watanabe T, Imoto I, Kosugi Y, Fukuda Y, Mimura J, Fujii Y, Isaka K, Takayama M, Sato A, Inazawa J. Human arylhydrocaron receptor repressor (AhRR) gene: Genomic structure and analysis of polymorphism in endometriosis. J Hum Genet 2001;46:342–346.

Wen X, Walle T. Preferential induction of CYP1B1 by benzo[a]pyrene in human oral epithelial cells: impact on DNA adduct formation and prevention by polyphenols. Carcinogenesis 2005;26:1774–1781.

Wen X, Walle UK, Walle T. 5,7-Dimethoxyflavone downregulates CYP1A1 expression and benzo[a]pyrene-induced DNA binding in Hep G2 cells. Carcinogenesis 2005;26:803-809.

Wen X, Walle T. Cytochrome P450 1B1, a novel chemopreventive target for benzo[a]pyrene-initiated human esophageal cancer. Cancer Lett 2007;246:109–114.

Whitelaw M, Pongratz I, Wilhelmsson A, Gustafsson JA, Poellinger L. Ligand-dependent recruitment of the Arnt coregulator determines DNA recognition by the dioxin receptor. Mol Cell Biol 1993;13:2504–2514.

Whitlock JP Jr. Induction of cytochrome P450 1A1. Annu Rev Pharmacol Toxicol 1999;39:103–125.

Wideroff L, Vaughan TL, Farin FM, Gammon MD, Risch H, Stanford JL, Chow WH. GST, NAT1, CYP1A1 polymorphisms and risk of esophageal and gastric adenocarcinomas. Cancer Detect Prev 2007;31:233-236.

Wild CP, Gong YY. Mycotoxins and human disease: a largely ignored global health issue. Carcinogenesis 2010:31:71-82.

Wong PS, Li W, Vogel CF, Matsumura F. Characterization of MCF mammary epithelial cells overexpressing the arylhydrocarbon receptor (AhR). BMC Cancer 2009;9:234.

Wormke M, Castro-Rivera E, Chen I, Safe S. Estrogen and aryl hydrocarbon receptor expression and crosstalk in human Ishikawa endometrial cancer cells. J Steroid Biochem Mol Biol 2000;72:197-207.

Wu X, Zhao Y, Honn SE, Tomlinson GE, Minnua JD, Hong WK. Benzo(a)pyrene diol epoxide-induced 3p21.3 aberrations and genetic predisposition to lung cancer. Cancer Res 1998;58:1605-1608.

Xiao H, Rawal M, Hahm E, Singh SV. Benzo[a]pyrene-7,8-diol-9,10-epoxide causes caspase-mediated apoptosis in H460 human lung cancer cell line. Cell Cycle 2007;6:2826-2834.

Yamagiwa K, Ichikawa K. Experimental study of the pathogenesis of carcinoma. CA Cancer J Clin 1977;27:174-181.

Yan C, Wu W, Li H, Zhang G, Duerksen-Hughes PJ, Zhu X, Yang J. Benzo[a]pyrene treatment leads to changes in nuclear protein expression and alternative splicing. Mutat Res 2010;686:47–56.

Yan Z Subbaramaiah K, Camilli T, Zhang F, Tanabe T, McCaffrey TA, Dannenberg AJ, Weksler BB. Benzo(a)pyrene induces the transcription of cyclooxygenase-2 in vascular smooth muscle cells. Evidence for the involvement of extracellular signal-regulated kinase and NF-kappaB. J Biol Chem 2000;275:4949–4955.

Yang H, Mazur-Melnyk M, de Boer JG, Glickman BW. A comparison of mutational specificity of mutations induced by S9-activated B[a]P and Benzo[a]pyrene-7,8-diol-9,10-epoxide at the endogenous aprt gene in CHO cells. Mutat Res 1999;423:23-32.

Ye F, Xu XC. Benzo[a]pyrene diol epoxide suppresses retinoic acid receptor-β2 expression by recruiting DNA (cytosine-5) methyltransferase 3A. Mol Cancer 2010;9:93.

Yokoyama T, Yokoyama A, Kato H, Tsujinaka T, Muto M, Omori T, Haneda T, Kumagai Y, Igaki H, Yokoyama M, Watanabe H, Yoshimizu H. Alcohol flushing, alcohol and aldehyde dehydrogenase genotypes, and risk for esophageal squamous cell carcinoma in Japanese men. Cancer Epidemiol Biomarkers Prev 2003;12:1227-1233.

Yoon JH, Smith LE, Feng Y, Tang MS, Lee CS, Pfeifer GP. Methylated CpG dinucleotides are the preferential targets for G-to-T transversion mutations induced by benzo[a]pyrene diol epoxide in mammalian cells: similarities with the p53 mutation spectrum in smoking-associated lung cancers. Cancer Res 2001;61:7110-7117.

Yoshino I, Kometani T, Shoji F, Osoegawa A, Ohba T, Kouso H, Takenaka T, Yohena T, Maehara Y. Induction of epithelial-mesenchymal transition-related genes by benzo[a]pyrene in lung cancer cells. Cancer 2007;110:369-374.

Yu Z, Ford BN, Glickman BW. Identification of genes responsive to BPDE treatment in HeLa cells using cDNA expression assays. Environ Mol Mutagen 2000;36:201-205.

Zhang J, Gao FL, Zhi HY, Luo AP, Ding F, Wu M, Liu ZH. Expression patterns of esophageal cancer deregulated genes in C57BL/6J mouse embryogenesis. World J Gastroenterol 2004;10:1088-1092.

Zheng Z, Fang JL, Lazarus P. Glucuronidation: an important mechanism for detoxification of benzo[a]pyrene metabolites in aerodigestive tract tissues. Drug Metab Dispos 2002;30:397-403.

Zhou S, Liu J, Chowbay B. Polymorphisms of human cytochrome P450 enzymes and its clinical impact. Drug Metab Rev 2009;41:89-295.

Zhu H, Gooderham N. Neoplastic transformation of human lung fibroblast MRC-5 SV2 cells induced by benzo[*a*]pyrene and confluence culture. Cancer Res 2002;62:4605-4609.

Zudaire E, Cuesta N, Murty V, Woodson K, Adams L, Gonzalez N, Martínez A, Narayan G, Kirsch I, Franklin W, Hirsch F, Birrer M, Cuttitta F. The aryl hydrocarbon receptor repressor is a putative tumor suppressor gene in multiple human cancers. J Clin Invest 2008;118:640–650.

Appendix A: Microarray Gene Lists

Table A1: Genes up-regulated by treatment with BaP in EPC-2 cells (top 50)
* indicates selection for investigation of fold change by qRT-PCR

Gene Symbol	Gene Name	Fold Change
SAMD5	Sterile alpha motif domain containing 5	23.85
C7ORF57	Chromosome 7 open reading frame 57	23.65
ZIC2	Zic family member 2 (odd-paired homolog, Drosophila)	18.91
ADRA1B	Adrenergic, alpha-1B-, receptor	18.09
HS.581429	DB225675 TRACH3 cDNA clone TRACH3017643 5	16.68
MEOX2	Mesenchyme homeobox 2	15.67
HS.8038	UI-E-EJ0-ahj-d-03-0-UI.r2 UI-E-EJ0 cDNA clone UI-E-EJ0-ahj-d-03-0-UI 5	14.3
OBSCN	Obscurin, cytoskeletal calmodulin and titin-interacting RhoGEF	13.84
PLD5	Phospholipase D family, member 5	12.72
HS.463420	UI-E-CK1-aga-k-24-0-UI.s1 UI-E-CK1 cDNA clone UI-E-CK1-aga-k-24-0-UI 3	11.71
EML1	Echinoderm microtubule associated protein like 1	11.05
SUSD3	Sushi domain containing 3	10.04
RHOF	Ras homolog gene family, member F (in filopodia)	9.84
LRRC38	Predicted: Leucine rich repeat containing 38	9.59
PDLIM3	PDZ and LIM domain 3	9.16
ESM1	Endothelial cell-specific molecule 1	9.05
HS.389988	K-EST0184252 L9SNU354 cDNA clone L9SNU354-11-G07 5	9.02
IL13RA2*	Interleukin 13 receptor, alpha 2	8.98
SULF1*	Sulfatase 1	8.74
LOC730456	Predicted: Hypothetical protein LOC730456	8.05
ANPEP	Alanyl (membrane) aminopeptidase (aminopeptidase N, aminopeptidase M, microsomal aminopeptidase, CD13, p150)	7.94
ACBD7	Predicted: Acyl-Coenzyme A binding domain containing 7	7.86
LOC649396	Predicted: Hypothetical LOC649396	7.67
MESP1	Mesoderm posterior 1 homolog (mouse)	7.65
CLDN3	Claudin 3	7.55
ADAM23*	ADAM metallopeptidase domain 23	7.54
GOLT1A	Golgi transport 1 homolog A (S. cerevisiae)	7.15
KIAA1244	KIAA1244	6.86
XK	X-linked Kx blood group (McLeod syndrome) (XK)	6.49
C14ORF72	Predicted: Chromosome 14 open reading frame 72	6.49
SRPX2	Sushi-repeat-containing protein, X-linked 2	6.46
SLC47A1	Solute carrier family 47, member 1	6.45
LOC284757	Hypothetical protein LOC284757	6.24
LOC402377	Predicted: Similar to UDP-Gal:betaGlcNAc beta 1,3-galactosyltransferase, polypeptide 4	6.13
SNORD25	Small nucleolar RNA, C/D box 25, non-coding RNA.	6.09
CD160	CD160 molecule	6
FOXL1	Forkhead box L1	5.92
LOC652697	Predicted: Hypothetical protein LOC652697	5.88
SLCO1B3	Solute carrier organic anion transporter family, member 1B3	5.8
GLDN	Gliomedin	5.74
HS.579631	AGENCOURT_10229596 NIH_MGC_141 cDNA clone IMAGE:6563923	5.73

	5	
LOC728070	Predicted: Similar to chromosome 16 open reading frame 54	5.64
GLRB	Glycine receptor, beta	5.59
HS.493947	cDNA FLJ41455 fis, clone BRSTN2012284	5.51
HS.314414	Clone IMAGE:5743779	5.47
APOLD1	Apolipoprotein L domain containing 1	5.36
FLJ40288	Hypothetical protein FLJ40288	5.35
ZDHHC23	Zinc finger, DHHC-type containing 23	5.33
LOC653981	Predicted: Similar to olfactory receptor, family 2, subfamily T, member 34	5.28
ULBP1	UL16 binding protein 1	5.19

Table A2: Genes down-regulated by treatment with BaP in EPC-2 cells (top 50)
* indicates selection for investigation of fold change by qRT-PCR

Gene Symbol	Gene Name	Fold Change
A2ML1	Alpha-2-macroglobulin-like 1	-201.21
FAM131A	Family with sequence similarity 131, member A	-122.95
S100A8	S100 calcium binding protein A8	-114.96
KRT13	Keratin 13	-109.5
LOC653506	Predicted: Similar to meteorin, glial cell differentiation regulator-like	-100.38
PTPN20A	Protein tyrosine phosphatase, non-receptor type 20A	-90.86
SLURP1	Secreted LY6/PLAUR domain containing 1	-86.2
SPRR1A	Small proline-rich protein 1A	-83.5
SPRR3	Small proline-rich protein 3	-81.98
CTHRC1	Collagen triple helix repeat containing 1	-80.77
SPRR2D	Small proline-rich protein 2D	-75.65
HS.311428	cDNA FLJ14199 fis, clone NT2RP3002713	-74.21
ESPN	Espin	-73.75
C1ORF51	Chromosome 1 open reading frame 51	-69.9
MMP7	Matrix metallopeptidase 7 (matrilysin, uterine)	-69.27
CRABP2	Cellular retinoic acid binding protein 2	-69.16
SPRR2A	Small proline-rich protein 2A	-65.29
KRT4	Keratin 4	-61.76
CALML3	Calmodulin-like 3	-60.02
SPRR2E	Small proline-rich protein 2E	-57.27
SBSN	Suprabasin	-57.22
S100A12	S100 calcium binding protein A12	-56.72
GPX3*	Glutathione peroxidase 3 (plasma)	-55.88
P53AIP1*	p53-regulated apoptosis-inducing protein 1	-54.54
C10ORF99	Chromosome 10 open reading frame 99	-53.41
SPRR2C	Small proline-rich protein 2C (pseudogene)	-53.22
C4ORF26	Chromosome 4 open reading frame 26	-50.89
NMU	Neuromedin U	-48.56
MFAP5	Microfibrillar associated protein 5	-47.18
H19	H19, imprinted maternally expressed transcript (non-protein coding)	-45.94
ACTG2	Actin, gamma 2, smooth muscle, enteric	-45.88

APOE	Apolipoprotein E	-44.56
PRODH	Proline dehydrogenase (oxidase) 1, nuclear gene encoding mitochondrial protein	-42.7
KMO	Kynurenine 3-monooxygenase (kynurenine 3-hydroxylase)	-40.93
LOC648585	Predicted: Similar to p53-regulated apoptosis-inducing protein 1	-40.23
ESPNL	Espin-like	-39.53
S100A9	S100 calcium binding protein A9 (calgranulin B)	-38.52
SPRR2F	Small proline-rich protein 2F	-38.35
FLJ10916	Hypothetical protein FLJ10916	-38
GGTLC2	Gamma-glutamyltransferase light chain 2	-36.9
SPRR1B	Small proline-rich protein 1B (cornifin)	-36.86
GBP2	Guanylate binding protein 2, interferon-inducible	-35.59
CFB	Complement factor B	-35.5
UBA7	Ubiquitin-like modifier activating enzyme 7	-34.58
MMP9*	Matrix metallopeptidase 9 (gelatinase B, 92kDa gelatinase, 92kDa type IV collagenase)	-34.47
MYL9	Myosin, light chain 9, regulatory	-33.38
RRAD	Ras-related associated with diabetes	-33.34
RPTN	Predicted: Repetin	-33.04
IGFL2	IGF-like family member 2	-32.57
PI3	Peptidase inhibitor 3, skin-derived (SKALP)	-31.56

Table A3: Genes up-regulated by treatment with BaP in WHCO1 cells (top 50)
* indicates selection for investigation of fold change by qRT-PCR

Gene Symbol	Gene Name	Fold Change
TLR4	Toll-like receptor 4	29.02
HIST1H2BI	Histone cluster 1, H2bi	19
CYP1A1*	Cytochrome P450, family 1, subfamily A, polypeptide 1	16.63
HS.150022	Human lacrimal gland, unamplified: oj cDNA clone oj52h05 5	15.62
HS.144129	EST386809 MAGE resequences, MAGN Homo sapiens cDNA	15.05
C20ORF160	Chromosome 20 open reading frame 160	13.95
CTTNBP2	Cortactin binding protein 2	10.53
HS.545554	xd52h03.x1 NCI_CGAP_Ov23 cDNA clone IMAGE:2597429 3	10.23
ANPEP	Alanyl (membrane) aminopeptidase (aminopeptidase N, aminopeptidase M, microsomal aminopeptidase, CD13, p150)	10.05
HR	Hairless homolog (mouse)	9.78
LOC653276	Predicted: Hypothetical LOC653276	8.56
C14ORF162	Chromosome 14 open reading frame 162	8.05
STRA6	Stimulated by retinoic acid gene 6 homolog (mouse)	7.57
NRCAM	Neuronal cell adhesion molecule	7.4
LOC554223	Predicted: Hypothetical LOC554223, transcript variant 4, misc RNA.	7.32
TREM2	Triggering receptor expressed on myeloid cells 2	6.63
HS.539591	wa38a03.x1 NCI_CGAP_Kid11 cDNA clone IMAGE:2300332 3	6.52
HS.568832	603078567F1 NIH_MGC_119 cDNA clone IMAGE:5170193 5	6.32
POSTN	Periostin, osteoblast specific factor	6.31
C2ORF27	Chromosome 2 open reading frame 27	6.16
APLP1	Amyloid beta (A4) precursor-like protein 1	5.9

KRT34	Keratin 34	5.67
HS.23681	BX111083 Soares_fetal_heart_NbHH19W cDNA clone IMAGp998G09825	5.59
TNFSF12	Tumor necrosis factor (ligand) superfamily, member 12	5.16
FABP6	Fatty acid binding protein 6, ileal	5.13
HS.543172	ym03e05.s1 Soares infant brain 1NIB cDNA clone IMAGE:46630 3	5.04
IL24	Interleukin 24	4.97
HS.563175	UI-H-BI3-ako-c-02-0-UI.s1 NCI_CGAP_Sub5 cDNA clone IMAGE:2734850 3	4.88
IL1F9	Interleukin 1 family, member 9	4.63
HS.541726	UI-CF-DU1-adj-b-02-0-UI.s1 UI-CF-DU1 cDNA clone UI-CF-DU1-adj-b-02-0-UI 3	4.6
TMEM200B	Transmembrane protein 200B	4.46
LOC652656	Predicted: Similar to ATP-binding cassette, sub-family G (WHITE), member 1	4.26
SERPINB2*	Serpin peptidase inhibitor, clade B (ovalbumin), member 2	4.2
LHB	Luteinizing hormone beta polypeptide	3.97
HS.582788	RST44785 Athersys RAGE Library cDNA	3.92
HS.560163	qp49h09.x1 NCI_CGAP_Co8 cDNA clone IMAGE:1926401 3	3.85
PPP1R9B	Protein phosphatase 1, regulatory (inhibitor) subunit 9B	3.8
MB	Myoglobin	3.75
MYEF2	Myelin expression factor 2	3.65
HS.145250	BX095239 Soares_testis_NHT Homo sapiens cDNA clone IMAGp998E214456	3.59
LOC441632	Predicted: Similar to ribosomal protein L13a	3.52
MCOLN2	Mucolipin 2	3.5
HS.535592	UI-H-BI2-aie-e-08-0-UI.s1 NCI_CGAP_Sub4 Homo sapiens cDNA clone IMAGE:2729174 3	3.5
CYP1B1*	Cytochrome P450, family 1, subfamily B, polypeptide 1	3.5
HS.578068	DB337475 TESTI2 Homo sapiens cDNA clone TESTI2022141 3	3.44
PDGFRB	Platelet-derived growth factor receptor, beta polypeptide	3.43
HS.437037	UI-H-BI3-ajx-g-10-0-UI.s1 NCI_CGAP_Sub5 Homo sapiens cDNA clone IMAGE:2733499 3	3.43
LOC728811	Predicted: Similar to UDP glycosyltransferase 2 family, polypeptide B17	3.4
GREM1	Gremlin 1, cysteine knot superfamily, homolog (Xenopus laevis)	3.36
CD74	Homo sapiens CD74 molecule, major histocompatibility complex, class II invariant chain	3.33

Table A4: Genes down-regulated by treatment with BaP in WHCO1 cells (top 50)
* indicates selection for investigation of fold change by qRT-PCR

Gene Symbol	Gene Name	Fold Change
LOC645434	Predicted: hCG1786283	-26.22
USP31	Ubiquitin specific peptidase 31	-19.36
HS.563928	UI-CF-DU1-aah-j-04-18-UI.s18 UI-CF-DU1 cDNA clone UI-CF-DU1-aah-j-04-18-UI 3	-16.24
C1ORF167	Predicted: Chromosome 1 open reading frame 167	-15.9
HS.338140	AGENCOURT_10185031 NIH_MGC_107 cDNA clone IMAGE:6569320 5	-15.76
VAX2	Ventral anterior homeobox 2	-15.63
HS.584369	DB310535 BRSTN2 cDNA clone BRSTN2003973 3	-12.64

HS.542481	UI-H-BI1-adl-g-11-0-UI.s1 NCI_CGAP_Sub3 cDNA clone IMAGE:2717373 3	-9.62
HS.537735	xk13b01.x1 NCI_CGAP_Co20 cDNA clone IMAGE:2666569 3	-8.99
DHRS2	Dehydrogenase/reductase (SDR family) member 2	-8.28
HS.46693	BX096334 Soares_multiple_sclerosis_2NbHMSP cDNA clone IMAGp998J15617	-8.09
LOXHD1	Lipoxygenase homology domains 1	-8.01
HS.553145	RST11549 Athersys RAGE Library cDNA	-7.94
LOC124220	Similar to common salivary protein 1	-7.92
ZFP57	Predicted: Zinc finger protein 57 homolog (mouse)	-7.6
ZNF717	Predicted: Zinc finger protein 717	-7.32
HS.580929	DB259922 UTERU2 cDNA clone UTERU2017075 5	-7.31
HS.209882	wh39c03.x1 NCI_CGAP_Kid11 cDNA clone IMAGE:2383108 3	-7.26
HS.582641	DB336782 TESTI2 cDNA clone TESTI2010942 3	-7.14
LOC643403	Predicted: Hypothetical protein LOC643403	-7.1
SPRR2G	Small proline-rich protein 2G	-7.04
CA9	Carbonic anhydrase IX	-6.92
LOC284757	Hypothetical protein LOC284757	-6.9
HS.306690	BX090584 Soares fetal liver spleen 1NFLS cDNA clone IMAGp998G06117 ; IMAGE:122909	-6.38
HS.382845	602387320F1 NIH_MGC_93 cDNA clone IMAGE:4516253 5	-6.26
HS.490243	Full length insert cDNA clone YB64E03	-6.04
HS.151207	BX094762 Soares_testis_NHT cDNA clone IMAGp998B084412	-5.97
TMEM121	Transmembrane protein 121	-5.63
ATP13A4	ATPase type 13A4	-5.6
CRCT1	Cysteine-rich C-terminal 1	-5.58
LOC286076	Hypothetical protein LOC286076	-5.49
OR7G2	Olfactory receptor, family 7, subfamily G, member 2	-5.29
SERPINA3*	Serpin peptidase inhibitor, clade A (alpha-1 antiproteinase, antitrypsin), member 3	-5.21
LOC732157	Predicted: Hypothetical protein LOC732157	-5.13
ZNF516	Predicted: Zinc finger protein 516	-5.06
HS.563390	K-EST0153644 L7N800102 cDNA clone L7N800102-2-A04 5	-5.04
CIT	Citron (rho-interacting, serine/threonine kinase 21)	-5.01
HS.277205	602506953F1 NIH_MGC_79 cDNA clone IMAGE:4604245 5	-5
TGFB2	Transforming growth factor, beta 2	-4.99
PLCXD2	Phosphatidylinositol-specific phospholipase C, X domain containing 2	-4.94
HS.570118	UI-CF-EC1-abz-d-17-0-UI.s1 UI-CF-EC1 cDNA clone UI-CF-EC1-abz-d-17-0-UI 3	-4.89
HS.546710	cDNA FLJ26122 fis, clone SYN00634	-4.88
ALDH1L2	Predited: Aldehyde dehydrogenase 1 family, member L2	-4.86
HS.128328	AGENCOURT_7590873 NIH_MGC_72 cDNA clone IMAGE:6065319 5	-4.81
HS.441813	UI-H-CO0-asl-e-02-0-UI.s1 NCI_CGAP_Sub9 cDNA clone IMAGE:5859147 3	-4.75
KRT4	Keratin 4	-4.47
C6ORF91	Chromosome 6 open reading frame 91	-4.46
DEFB1*	Defensin, beta 1	-4.45
TMOD2	Tropomodulin 2 (neuronal)	-4.44
TAS2R5	Taste receptor, type 2, member 5	-4.4

Table A5: Genes up-regulated by treatment with BaP in EPC-2 cells compared to untreated WHCO1 cells (top 50)

Gene Symbol	Gene Name	Fold Change
EEF1A2	Eukaryotic translation elongation factor 1 alpha 2	3447.3
KRT13	Keratin 13	2588.09
LOC653506	Predicted: Similar to meteorin, glial cell differentiation regulator-like	1905.7
KRT81	Keratin 81	1708.89
GAL	Galanin prepropeptide	1280.9
SOX2	SRY (sex determining region Y)-box 2	1148.56
FGD3	FYVE, RhoGEF and PH domain containing 3	792.49
MOSC1	MOCO sulphurase C-terminal domain containing 1	772.53
THY1	Thy-1 cell surface antigen	766.09
PRSS3	Protease, serine, 3 (mesotrypsin)	726.12
ECHDC3	Enoyl Coenzyme A hydratase domain containing 3	678.04
CRISPLD2	Cysteine-rich secretory protein LCCL domain containing 2	638.97
MUC20	Mucin 20, cell surface associated	572.98
PPARG	Peroxisome proliferator-activated receptor gamma	542.79
HSPB8	Heat shock 22kDa protein 8	466.64
GSTT1	Glutathione S-transferase theta 1	464.4
CLDN11	Claudin 11 (oligodendrocyte transmembrane protein)	442.21
GPX3	Glutathione peroxidase 3 (plasma)	428.71
RBP1	Retinol binding protein 1, cellular	427.15
MYO5C	Myosin VC	423.65
NKD2	Naked cuticle homolog 2 (Drosophila)	401.62
RASEF	RAS and EF-hand domain containing	395.79
DNAJA4	DnaJ (Hsp40) homolog, subfamily A, member 4	387.43
NDN	Necdin homolog (mouse)	349.18
ELF3	E74-like factor 3 (ets domain transcription factor, epithelial-specific)	338.5
ANXA9	Annexin A9	333.93
MSLN	Mesothelin	319.81
LOC200810	Similar to beta-1,4-mannosyltransferase; beta-1,4 mannosyltransferase	287.18
C9ORF58	Chromosome 9 open reading frame 58	245.82
NMU	Neuromedin U	237.81
SUSD2	Sushi domain containing 2	224.9
LIMCH1	LIM and calponin homology domains 1	222.01
TNFAIP2	Tumor necrosis factor, alpha-induced protein 2	221.56
HRASLS3	HRAS-like suppressor 3	219.14
MOSC2	MOCO sulphurase C-terminal domain containing 2	217.06
KLHDC9	Kelch domain containing 9	211.36
FAM71E1	Family with sequence similarity 71, member E1	211.3
ZNF695	Zinc finger protein 695	209.52
SEMA4D	Sema domain, immunoglobulin domain (Ig), transmembrane domain (TM) and short cytoplasmic domain, (semaphorin) 4D	204.82
S100P	S100 calcium binding protein P	201.14
SOX21	SRY (sex determining region Y)-box 21	193.24
HOXD10	Homeobox D10	182.04
KRT7	Keratin 7	176.84
UCHL1	Ubiquitin carboxyl-terminal esterase L1 (ubiquitin thiolesterase)	174.93

FAM131A	Family with sequence similarity 131, member A	173.29
S100A4	S100 calcium binding protein A4	173.13
ATP2C2	ATPase, Ca++ transporting, type 2C, member 2	172.57
LOC652644	Predicted: Similar to tumor protein p53 inducible protein 5	171.58
FER1L4	fer-1-like 4 (C. elegans)	167.01
CEACAM6	Carcinoembryonic antigen-related cell adhesion molecule 6 (non-specific cross reacting antigen)	164.92

Table A6: Genes down-regulated by treatment with BaP in EPC-2 cells compared to untreated WHCO1 cells (top 50)

Gene Symbol	Gene Name	Fold Change
KRT14	Keratin 14 (epidermolysis bullosa simplex, Dowling-Meara, Koebner)	-23507.8
CNTNAP2	Contactin associated protein-like 2	-1426.75
HSD17B2	Hydroxysteroid (17-beta) dehydrogenase 2	-1011.76
C5ORF13	Chromosome 5 open reading frame 13	-592.2
C3ORF14	Chromosome 3 open reading frame 14	-435.17
HS.254632	RST7893 Athersys RAGE Library cDNA	-426.84
NRCAM	Neuronal cell adhesion molecule	-371.78
SCG5	Secretogranin V (7B2 protein)	-349.91
GPR68	G protein-coupled receptor 68	-341.9
WNT5A	Wingless-type MMTV integration site family, member 5A	-337.92
TSPAN7	Tetraspanin 7	-291.87
TMEM16D	Transmembrane protein 16D	-284.11
TFCP2	Transcription factor CP2	-272.59
MSC	Musculin (activated B-cell factor-1)	-266.36
VIM	Vimentin	-265.54
G0S2	G0/G1switch 2	-250.59
ANPEP	Alanyl (membrane) aminopeptidase (aminopeptidase N, aminopeptidase M, microsomal aminopeptidase, CD13, p150)	-240.27
TSHZ2	Teashirt zinc finger homeobox 2	-203.62
HNT	Neurotrimin	-201.97
HLA-A29.1	Major histocompatibility complex class I HLA-A29.1	-187.44
TNF	Tumor necrosis factor (TNF superfamily, member 2)	-179.16
HS3ST2	Heparan sulfate (glucosamine) 3-O-sulfotransferase 2	-173.89
PLD5	Phospholipase D family, member 5	-163.54
MEX3B	Mex-3 homolog B (C. elegans)	-154.93
XG	Xg blood group	-151.15
FCRLA	Fc receptor-like A	-150.79
SFRP1	Secreted frizzled-related protein 1	-138.89
D4S234E	DNA segment on chromosome 4 (unique) 234 expressed sequence	-134.62
HS.100261	cDNA FLJ26539 fis, clone KDN09310	-134.37
GSTM2	Glutathione S-transferase M2 (muscle)	-121.97
CLCA2	Chloride channel, calcium activated, family member 2	-115.32
TAGLN3	Transgelin 3	-114.96
AOX1	Aldehyde oxidase 1	-112.11
ACP5	Acid phosphatase 5, tartrate resistant	-109.1
CHSY3	Chondroitin sulfate synthase 3	-106.98

ANO4	Anoctamin 4	-99.04
HR	Hairless homolog (mouse)	-95.39
GLT8D2	Glycosyltransferase 8 domain containing 2	-92.99
HS.144479	AGENCOURT_13979145 NIH_MGC_179 cDNA clone IMAGE:30367627 5	-88.09
HS.128708	602505656F1 NIH_MGC_77 cDNA clone IMAGE:4619364 5	-82.49
ERV3	Endogenous retroviral sequence 3 (includes zinc finger protein H-plk/HPF9)	-79.38
ZNF215	Zinc finger protein 215	-78.57
C7ORF10	Chromosome 7 open reading frame 10	-77.69
SPOCK1	Sparc/osteonectin, cwcv and kazal-like domains proteoglycan (testican) 1	-77.28
ANKRD29	Ankyrin repeat domain 29	-75.57
LRRC38	Predicted: Leucine rich repeat containing 38	-71.77
PLCL4	Predicted: Phospholipase C-like 4	-71.21
PDCD1LG2	Programmed cell death 1 ligand 2	-70.76
FN1	Fibronectin 1	-70.18
DNER	Delta/notch-like EGF repeat containing	-69.78

Table A7: Genes up-regulated in untreated WHCO1 cells compared to untreated EPC-2 cells (top 50)

Gene Symbol	Gene Name	Fold Change
GAL	Galanin prepropeptide	1298.76
NDN	Necdin homolog (mouse)	1097.85
FGD3	FYVE, RhoGEF and PH domain containing 3	729.7
HOXA9	Homeobox A9	708.05
ECHDC3	Enoyl Coenzyme A hydratase domain containing 3	687.49
LIM	LIM and calponin homology domains 1	551.38
SEMA4D	Sema domain, immunoglobulin domain (Ig), transmembrane domain (TM) and short cytoplasmic domain, (semaphorin) 4D	521.72
GSTT1	Glutathione S-transferase theta 1	470.87
RBP1	Retinol binding protein 1, cellular	433.1
NKD2	Naked cuticle homolog 2 (Drosophila)	407.22
RASEF	RAS and EF-hand domain containing	401.31
KRT81	Keratin 81	373.75
NLRP2	NLR family, pyrin domain containing 2	295.71
SOX21	SRY (sex determining region Y)-box 21	284.13
EEE1A2	Eukaryotic translation elongation factor 1 alpha 2	272.86
MUC20	Mucin 20, cell surface associated	262.39
ELF3	E74-like factor 3 (ets domain transcription factor, epithelial-specific)	253.23
CRISPLD2	Cysteine-rich secretory protein LCCL domain containing 2	233.84
GOLT1A	Golgi transport 1 homolog A (S. cerevisiae)	229.74
HS.579631	AGENCOURT_10229596 NIH_MGC_141 cDNA clone IMAGE:6563923 5	221.92
ZNF695	Zinc finger protein 695	212.44
GLB1L2	Galactosidase, beta 1-like 2	211.06
PRSS3	Protease, serine, 3 (mesotrypsin)	207.63
SUSD3	Sushi domain containing 3	189.98
HOXD10	Homeobox D10	184.58
MSLN	Mesothelin	177.95
HSPB8	Heat shock 22kDa protein 8	170.64
CEACAM6	Carcinoembryonic antigen-related cell adhesion molecule 6 (non-specific cross reacting antigen)	167.22
HRASLS3	HRAS-like suppressor 3	162.9
PPARG	Peroxisome proliferator-activated receptor gamma	148.04
THY1	Thy-1 cell surface antigen	138.83

DNAH2	Dynein, axonemal, heavy chain 2.	136.29
MPP2	Membrane protein, palmitoylated 2 (MAGUK p55 subfamily member 2)	134.42
HS.545589	Small nuclear RNA U6atac, partial sequence	132.82
HS.384594	Full length insert cDNA clone ZD67H01	127.83
NUF2	NUF2, NDC80 kinetochore complex component, homolog (S. cerevisiae)	125.89
KRT7	Keratin 7	125.14
TSPYL5	TSPY-like 5	123.68
B3GNTL1	UDP-GlcNAc:betaGal beta-1,3-N-acetylglucosaminyltransferase-like 1	122.29
NES	Nestin	115.64
ACBD7	Predicted: Acyl-Coenzyme A binding domain containing 7	112.18
C17ORF60	Chromosome 17 open reading frame 60	112.04
MMP13	Matrix metallopeptidase 13 (collagenase 3)	111.8
SLITRK5	SLIT and NTRK-like family, member 5	111.7
XK	X-linked Kx blood group (McLeod syndrome)	110.36
HS.436189	17000532640995 GRN_ES cDNA 5	107.78
PCDH20	Protocadherin 20	101.78
DDN	Dendrin	101.28
SLC27A2	Solute carrier family 27 (fatty acid transporter), member 2	101.11
SUSD2	Sushi domain containing 2	100.81

Table A8: Genes down-regulated in untreated WHCO1 cells compared to untreated EPC-2 cells (top 50)

Gene Symbol	Gene Name	Fold Change
KRT14	Keratin 14 (epidermolysis bullosa simplex, Dowling-Meara, Koebner)	-22199.5
CNTNAP2	Contactin associated protein-like 2	-1740.76
CALML3	Calmodulin-like 3	-1549.04
HSD17B2	Hydroxysteroid (17-beta) dehydrogenase 2	-1085.18
WNT5A	Wingless-type MMTV integration site family, member 5A	-857.03
C5ORF13	Chromosome 5 open reading frame 13	-810.4
TNF	Tumor necrosis factor (TNF superfamily, member 2)	-657.34
G0S2	G0/G1switch 2	-489.8
SPRR2D	Small proline-rich protein 2D	-441.4
HLA-A29.1	Homo sapiens major histocompatibility complex class I HLA-A29.1	-438.7
LOC729252	Predicted: Similar to Keratin, type I cytoskeletal 14 (Cytokeratin-14) (CK-14) (Keratin-14) (K14)	-413.82
HS3ST2	Heparan sulfate (glucosamine) 3-O-sulfotransferase 2	-388.83
SCG5	Secretogranin V (7B2 protein)	-382.54
GPR68	G protein-coupled receptor 68	-369.63
C30RF14	Chromosome 3 open reading frame 14	-369.11
MSC	Musculin (activated B-cell factor-1)	-357.97
ACP5	Acid phosphatase 5, tartrate resistant	-354.79
TMEM16D	Transmembrane protein 16D	-351.81
GSTM2	Glutathione S-transferase M2 (muscle)	-341.54
HNT	Neurotrimin	-316.99
TFCP2	Transcription factor CP2	-307.84
GLT8D2	Glycosyltransferase 8 domain containing 2	-298.1
LOC400578	Predicted: Similar to Keratin, type I cytoskeletal 14 (Cytokeratin-14) (CK-14) (Keratin-14) (K14)	-282.09
S100A8	S100 calcium binding protein A8	-279.96
D4S234E	DNA segment on chromosome 4 (unique) 234 expressed sequence	-272.89
IGFL1	IGF-like family member 1	-272.27
XG	Xg blood group	-243.12
MEX3B	Mex-3 homolog B (C. elegans)	-239.81
HS.100261	cDNA FLJ26539 fis, clone KDN09310	-238.94
DAPL1	Death associated protein-like 1	-232.07
FN1	Fibronectin 1	-223.25

HS.311428	cDNA FLJ14199 fis, clone NT2RP3002713	-221.78
KRT6B	Keratin 6B	-202.08
VIM	Vimentin	-194.1
SFRP1	Secreted frizzled-related protein 1	-189.69
STON2	Stonin 2	-186.22
C10ORF99	Chromosome 10 open reading frame 99	-180.63
TSPAN7	Tetraspanin 7	-164.58
HS.254632	RST7893 Athersys RAGE Library cDNA	-162.05
C7ORF10	Chromosome 7 open reading frame 10	-161.4
CRYAB	Crystallin, alpha B	-152.37
SERPINB3	Serpin peptidase inhibitor, clade B (ovalbumin), member 3	-150.41
TSHZ2	Teashirt zinc finger homeobox 2	-148.72
CHSY3	Chondroitin sulfate synthase 3	-148.21
SAA1	Serum amyloid A1	-136.57
KCTD14	Potassium channel tetramerisation domain containing 14	-135.1
PTPN20A	Protein tyrosine phosphatase, non-receptor type 20A	-132.42
FCRLA	Fc receptor-like A	-130.79
CLCA2	Chloride channel, calcium activated, family member 2	-129.28
COL22A1	Collagen, type XXII, alpha 1	-126.43

Table A9: Genes up-regulated by BaP in BaP-treated WHCO1 cells compared to BaP-treated EPC-2 cells (top 50)

Gene Symbol	Gene Name	Fold Change
EEF1A2	Eukaryotic translation elongation factor 1 alpha 2	4010.87
KRT13	Keratin 13	2396.84
LOC653506	Predicted: Similar to meteorin, glial cell differentiation regulator-like	1714.88
KRT81	Keratin 81	1447.09
GAL	Galanin prepropeptide	1134
CRISPLD2	Cysteine-rich secretory protein LCCL domain containing 2	914.69
PRSS3	Protease, serine, 3 (mesotrypsin)	852.64
THY1	Thy-1 cell surface antigen	814.88
MOSC1	MOCO sulphurase C-terminal domain containing 1	795.36
NKD2	Naked cuticle homolog 2 (Drosophila)	736.53
SOX2	SRY (sex determining region Y)-box 2	686.86
PPARG	Peroxisome proliferator-activated receptor gamma	630.76
GPX3	Glutathione peroxidase 3 (plasma)	599.03
FGD3	FYVE, RhoGEF and PH domain containing 3	580.23
MUC20	Mucin 20, cell surface associated	544.56
ECHDC3	Enoyl Coenzyme A hydratase domain containing 3	527.3
GSTT1	Glutathione S-transferase theta 1	523.37
DNAJA4	DnaJ (Hsp40) homolog, subfamily A, member 4	473.79
HSPB8	Heat shock 22kDa protein 8	465.95
MYO5C	Myosin VC	429.24
RASEF	RAS and EF-hand domain containing	409.54
NDN	Necdin homolog (mouse)	368.3
MSLN	Mesothelin	312.49
ANXA9	Annexin A9	301.01
ELF3	E74-like factor 3 (ets domain transcription factor, epithelial-specific)	296.68
RBP1	Retinol binding protein 1, cellular	291.33
CLDN11	Claudin 11 (oligodendrocyte transmembrane protein)	289.66
METTL7B	Methyltransferase like 7B	284.96
LOC200810	Similar to beta-1,4-mannosyltransferase; beta-1,4 mannosyltransferase	272.36
KLHDC9	Kelch domain containing 9	270.76
FAM71E1	Family with sequence similarity 71, member E1	265.56
C9ORF58	Chromosome 9 open reading frame 58	265.54
MOSC2	MOCO sulphurase C-terminal domain containing 2	250.1
TNFAIP2	Tumor necrosis factor, alpha-induced protein 2	246.99
UCHL1	Ubiquitin carboxyl-terminal esterase L1 (ubiquitin thiolesterase)	246.33
HRASLS3	HRAS-like suppressor 3	246.04
HOXD10	Homeobox D10	235.17
NMU	Neuromedin U	213.44
FER1L4	Fer-1-like 4 (C. elegans)	199.37
FAM131A	Family with sequence similarity 131, member A	194.82
LIMCH1	LIM and calponin homology domains 1	190.96
ZNF695	Zinc finger protein 695	185.34
EMILIN2	Elastin microfibril interfacer 2	185.05
SEMA4D	Sema domain, immunoglobulin domain (Ig), transmembrane domain (TM) and short	183.34

	cytoplasmic domain, (semaphorin) 4D	
HOXA9	Homeobox A9	179.32
C17ORF60	Chromosome 17 open reading frame 60	178.52
CEACAM6	Carcinoembryonic antigen-related cell adhesion molecule 6 (non-specific cross reacting antigen)	170.24
DGKG	Diacylglycerol kinase, gamma 90kDa	169.97
ATP2C2	ATPase, Ca++ transporting, type 2C, member 2	167.26
SUSD2	Sushi domain containing 2	166.99

Table A10: Genes down-regulated by BaP in BaP-treated WHCO1 cells compared to BaP-treated EPC-2 cells (top 50)

Gene Symbol	Gene Name	Fold Change
KRT14	Keratin 14 (epidermolysis bullosa simplex, Dowling-Meara, Koebner)	-6101.44
CNTNAP2	Contactin associated protein-like 2	-1248.32
GPR68	G protein-coupled receptor 68	-852.93
C5ORF13	Chromosome 5 open reading frame 13	-596.74
HSD17B2	Hydroxysteroid (17-beta) dehydrogenase 2	-585.43
CHES1	Checkpoint suppressor 1	-496.43
SFRP1	Secreted frizzled-related protein 1	-484.11
G0S2	G0/G1switch 2	-389.61
WNT5A	Wingless-type MMTV integration site family, member 5A	-340.51
TMEM16D	Transmembrane protein 16D	-335.02
SCG5	Secretogranin V (7B2 protein)	-301.39
TSPAN7	Tetraspanin 7	-294.11
VIM	Vimentin	-293.6
CAMP	Cathelicidin antimicrobial peptide	-286.54
HNT	Neurotrimin	-255.62
C3ORF14	Chromosome 3 open reading frame 14	-253.83
TAGLN3	Transgelin 3	-242.31
TSHZ2	Teashirt zinc finger homeobox 2	-205.18
HS.553145	RST11549 Athersys RAGE Library cDNA	-200.24
HLA-A29.1	Homo sapiens major histocompatibility complex class I HLA-A29.1	-197.84
TFCP2	Transcription factor CP2	-183.55
CLCA2	Chloride channel, calcium activated, family member 2	-181.87
HS.100261	cDNA FLJ26539 fis, clone KDN09310	-172.28
HS.254632	RST7893 Athersys RAGE Library cDNA	-167.51
PLD5	Phospholipase D family, member 5	-164.79
PGCP	Plasma glutamate carboxypeptidase	-157.86
MEX3B	Mex-3 homolog B (C. elegans)	-156.12
C21ORF63	Chromosome 21 open reading frame 63	-155.46
XG	Xg blood group	-152.31
ZNF717	Predicted: Zinc finger protein 717	-152.23
SLIT3	Slit homolog 3 (Drosophila)	-150.98
AOX1	Aldehyde oxidase 1	-149.39
ERV3	Endogenous retroviral sequence 3 (includes zinc finger protein H-plk/HPF9)	-142.61
CPS1	Carbamoyl-phosphate synthetase 1, mitochondrial	-142.5

C7ORF10	Chromosome 7 open reading frame 10	-125.04
MRGPRX3	MAS-related GPR, member X3	-124.96
IGFL1	IGF-like family member 1	-119.62
MYBPHL	Myosin binding protein H-like	-118.96
HS3ST2	Heparan sulfate (glucosamine) 3-O-sulfotransferase 2	-118.28
PNLIPRP3	Pancreatic lipase-related protein 3	-108.83
CHSY3	Chondroitin sulfate synthase 3	-107.8
COL22A1	Collagen, type XXII, alpha 1	-107.37
KCTD14	Potassium channel tetramerisation domain containing 14	-103.84
LRRC38	Predicted: Leucine rich repeat containing 38	-95.22
FN1	Fibronectin 1	-90.32
FLJ14213	Protor-2	-89.22
ALDH1L2	Predicted: Aldehyde dehydrogenase 1 family, member L2	-84.98
STON2	Stonin 2	-84.37
HS.128708	602505656F1 NIH_MGC_77 cDNA clone IMAGE:4619364 5	-83.13
PRICKLE2	Prickle homolog 2 (Drosophila)	-82.96

Table A.11 Genes commonly up-regulated by BaP exposure in WHCO1 and EPC-2 cells from Fig. 3.14A

Symbol	**Gene**	**WHCO1 Fold Change**	**EPC-2 Fold Change**
HS.568832	603078567F1 NIH_MGC_119 Homo sapiens cDNA clone IMAGE:5170193 5	6.32	2.11
GLT1D1	Glycosyltransferase 1 domain containing 1	2.43	3.76
LOC730456	Predicted: Hypothetical protein LOC730456	2.74	8.05
HS.517692	UI-E-EJ1-ajw-b-16-0-UI.r1 UI-E-EJ1 Homo sapiens cDNA clone UI-E-EJ1-ajw-b-16-0-UI 5	2.06	2.41
HS.389988	K-EST0184252 L9SNU354 Homo sapiens cDNA clone L9SNU354-11-G07 5	2.78	9.02
TMEM200B	Transmembrane protein 200B	4.46	3.78
ANPEP	Alanyl (membrane) aminopeptidase (aminopeptidase N, aminopeptidase M, microsomal aminopeptidase, CD13, p150)	10.05	7.94
NIPSNAP3B	Nipsnap homolog 3B (C. elegans)	2.26	3.08
HS.127934	UI-H-BI1-afm-f-03-0-UI.s1 NCI_CGAP_Sub3 Homo sapiens cDNA clone IMAGE:2722324 3	2.35	2.95
C8ORF13	Chromosome 8 open reading frame 13	2.12	2.01
SPRY4	Sprouty homolog 4 (Drosophila)	2.22	2.56
C14ORF162	Chromosome 14 open reading frame 162	8.05	3.31
NRCAM	Neuronal cell adhesion molecule	7.4	3.41
C1QTNF8	C1q and tumor necrosis factor related protein 8	2.14	4.13
EREG	Epiregulin	2.36	3.2
IL10RA	Interleukin 10 receptor, alpha	3.2	2.15
LOC647488	Predicted: Hypothetical protein LOC647488	3.16	2.59
HS.552160	xd91c02.x1 Soares_NFL_T_GBC_S1 Homo sapiens cDNA clone IMAGE:2604962 3	2.57	2.23
FOSL1	FOS-like antigen 1	2.39	2.19

Table A.12 Genes commonly down-regulated from Fig. 3.14B by BaP exposure in WHCO1 and EPC-2 cells

Symbol	Gene	WHCO1 Fold Change	EPC-2 Fold Change
CXCL1	Chemokine (C-X-C motif) ligand 1 (melanoma growth stimulating activity, alpha)	-3.08	-7.69
RNF39	Ring finger protein 39	-2.2	-2.35
SPRR2G	Small proline-rich protein 2G	-7.04	-13.24
SPINK4	Serine peptidase inhibitor, Kazal type 4	-3.34	-13.91
GRIN3B	Glutamate receptor, ionotropic, N-methyl-D-aspartate 3B	-3.39	-4.57
HS.582641	DB336782 TESTI2 Homo sapiens cDNA clone TESTI2010942 3	-7.14	-2.15
H19	H19, imprinted maternally expressed transcript (non-protein coding)	-2.23	-45.94
TGFB2	Transforming growth factor, beta 2	-4.99	-4.7
HS.537735	xk13b01.x1 NCI_CGAP_Co20 Homo sapiens cDNA clone IMAGE:2666569 3	-8.99	-2.94
HS.441213	UI-E-CK0-aao-f-09-0-UI.r1 UI-E-CK0 Homo sapiens cDNA clone UI-E-CK0-aao-f-09-0-UI 5	-2.29	-2.59
HS.542990	UI-H-BI1-afq-a-03-0-UI.s1 NCI_CGAP_Sub3 Homo sapiens cDNA clone IMAGE:2722468 3	-4.28	-19.87
ITGB8	Integrin, beta 8	-3	-2.67
HS.46693	BX096334 Soares_multiple_sclerosis_2NbHMSP Homo sapiens cDNA clone IMAGp998J15617	-8.09	-2.02
HS.544253	Clone HED10 Cri-du-chat region mRNA	-3.24	-2.92
SERPINA3	Serpin peptidase inhibitor, clade A (alpha-1 antiproteinase, antitrypsin), member 3	-5.21	-14.21
LOC124220	Similar to common salivary protein 1	-7.92	-2.1
KRT3	Keratin 3	-2.34	-4.22
KRT4	Keratin 4	-4.47	-61.76
SULT1C3	Sulfotransferase family, cytosolic, 1C, member 3	-2.1	-9.92
LOC440438	Predicted: Similar to spergen-3	-2.41	-2.88
CIB2	Calcium and integrin binding family member 2	-3.13	-2.39
S100A1	S100 calcium binding protein A1	-3.47	-2.19
HS.209882	wh39c03.x1 NCI_CGAP_Kid11 Homo sapiens cDNA clone IMAGE:2383108 3	-7.26	-2.33
HS.382845	602387320F1 NIH_MGC_93 Homo sapiens cDNA clone IMAGE:4516253 5	-6.26	-3.09
CAPNS2	Calpain, small subunit 2	-2.32	-8.08
LOC643841	Predicted: Hypothetical protein LOC643841	-2.85	-4.9
LOC653855	Predicted: Similar to rho guanine nucleotide exchange factor 5 isoform 1, transcript variant 2	-2.43	-2.47
PLXNB3	Plexin B3	-3.01	-2.09
CHST2	Carbohydrate (N-acetylglucosamine-6-O) sulfotransferase 2	-4.32	-2.15
FRMPD3	Predicted: FERM and PDZ domain containing 3	-3.66	-4.39
HS.537109	cDNA FLJ42489 fis, clone BRACE2032538	-2.76	-2.13
HS.93739	BX098660 Soares placenta Nb2HP Homo sapiens cDNA clone IMAGp998L03214	-2.08	-7.22
COL5A2	Collagen, type V, alpha 2	-2.14	-7.57
LOC644347	Predicted: Hypothetical protein LOC644347	-2.65	-2.85
FLJ37078	Hypothetical protein FLJ37078	-2.19	-4.39
HS.570118	UI-CF-EC1-abz-d-17-0-UI.s1 UI-CF-EC1 Homo sapiens cDNA clone UI-CF-EC1-abz-d-17-0-UI 3	-4.89	-15.71
SH2D3C	SH2 domain containing 3C	-2.47	-4.04
DHRS2	Dehydrogenase/reductase (SDR family) member 2	-8.28	-2.54
CRCT1	Cysteine-rich C-terminal 1	-5.58	-19.48

CPE	Carboxypeptidase E	-3.57	-4.29
CA9	Carbonic anhydrase IX	-6.92	-14.87
LOC648149	Predicted: Hypothetical protein LOC648149	-2.21	-3.04
LOC402573	Hypothetical LOC402573	-2.37	-2.2
FBXL7	F-box and leucine-rich repeat protein 7	-2.37	-3.01
HS.541304	xu70h11.x1 NCI_CGAP_Kid8 Homo sapiens cDNA clone IMAGE:2807109 3	-2.95	-2.79

Appendix B: Solutions

B.1 Genomic DNA Isolation

Digestion buffer

5M NaCl 2ml

0.5M Tris-HCl pH 8 2ml

0.5M EDTA 5ml

10% SDS 5ml

0.1mg/ml proteinase K

Add distilled water to 100ml, store at room temperature. The proteinase K is labile and therefore must be added fresh with each use.

0.5M EDTA, pH 8.0

Dissolve 37.22g $Na_2EDTA{\cdot}2H_2O$ in 140ml distilled water, adjust pH to 8.0 with concentrated NaOH (~ 10ml), adjust volume up to 200ml with distilled water and autoclave.

Phenol:Chloroform:Isoamyl alcohol (25:24:1)

Mix one part of phenol and one part of chloroform:isoamyl alcohol (24:1).

7.5M Ammonium acetate, pH 7.6

Dissolve 57.81g ammonium acetate in 50ml of distilled water, adjust pH to 7.6 with ammonia solution, adjust volume up to 100ml with distilled water and sterilize by filtration through a 0.45µm filter.

70% Ethanol

140ml absolute ethanol

Make up volume to 200ml with distilled water.

TE buffer, pH 7.5

200µl 1M Tris-HCl, pH 7.5

40µl 0.5M EDTA, pH 8.0

19.76ml distilled water

Autoclave.

B.2 PCR-RFLP

10 × TBE

108g Tris

55g Boric acid

40ml 0.5M EDTA, pH 8.0

Make up volume to 1 litre with distilled water and autoclave.

B.3 Cell Culture

DMEM

450ml DMEM media

50ml FCS

5ml penicillin/ streptamicin

KSFM

500ml KSFM

50ug/ml BPE

1ng/ul EGF

pen/strep

10 × PBS (phosphate-buffered saline)

2.0g KCl

80g NaCl

2.0g KH_2PO_4

11.5g Na_2HPO_4

Adjust pH to 7.4 using 1N HCl or 1N NaOH if necessary, adjust volume up to 1 litre with distilled water and autoclave.

1 × Trypsin-EDTA solution

0.05% (w/v) trypsin

0.53mM EDTA

Prepare in a calcium- and magnesium-free salt solution such as 1×PBS.

Cell freezing down solution (WHCO and KYSE series)

70% foetal calf serum

20% DMEM

10% Dimethylsulphoxide (DMSO)

Cell freezing down solution (EPC-2)

90% foetal calf serum

10% DMSO

50mM Benzo[a]pyrene

Weigh out 0.012g benzo[a]pyrene and add to 1ml pure DMSO. Heat to dissolve at 100°C, store at 4°C. Make 10mM working solution by mixing 20µl 50mM stock solution with 80µl pure DMSO. Treat cells with 10µM BaP by diluting 10mM BaP stock 1:1000 with cell culture medium.

B.4 MTT Assay

MTT Solution

Weigh 100mg MTT (dimethylthiazol diphenyltetrazolium bromide) in a 50ml tube; dissolve in 20ml 1 x PBS pH 7.4. Mix, vortex and incubate in a water bath at 37°C for 15min. In tissue culture, filter through a 0.2µm filter. Store at 4°C.

Solubilisation Reagent

Dissolve 2.5g SDS in 25ml distilled water. Add 7.66ml HCl (32.64M) and mix.

B.5 BrdU ELISA

BrdU Labeling Solution

Dilute BrdU labeling reagent (1000x BrdU, 10mM 5-bromo-2'-deoxyuridine in PBS, pH 7.4, filtered through 0.2µm pore size membrane) 1:100 in sterile culture medium (working concentration 100µM). Add 10µl labeling solution to each well. Final concentration: 10µM BrdU.

Anti-BrdU-POD

Add 1.1ml ddH_2O to lyophilized monoclonal antibody and dissolve for 10min. Store 20µl aliquots of antibody at -20°C. Dilute antibody 1:100 in antibody dilution solution directly before use.

B.6 RNA Work

DEPC-treated water

Add DEPC (diethylpyrocarbonate) to 0.01% (v/v) to distilled water, stir, let stand overnight and autoclave.

10 × MOPS running buffer

0.4M MOPS, pH 7.0

0.1M Sodium acetate

0.01M EDTA, pH 8.0

Dissolve 20.6g MOPS in 400ml 50mM sodium acetate (DEPC-treated), adjust pH to 7.0 with 10N NaOH, add 10ml 0.5M EDTA (pH 8.0, DEPC-treated), adjust volume up to 500ml with autoclaved DEPC-treated water.

RNA loading buffer (25ml)

	Final concentration
50µl 0.5M EDTA, pH 8.0	1mM
62.5mg Bromophenol blue	0.25% (w/v)
62.5mg Xylene cyanol	0.25% (w/v)
12.4ml Water	
12.5ml Glycerol	50%
50µl DEPC	

Stir overnight, then autoclave.

75% Ethanol

75ml absolute ethanol

Make up volume to 100ml with autoclaved DEPC-treated water.

B.7 Protein Work

RIPA buffer

150mM NaCl

1% Triton X100

0.1% SDS

25mM Tris, pH 7.5

1% Sodium deoxycholate

1M DTT

Dissolve 3.09g DTT (Dithiothreitol) in 20ml of 10mM sodium acetate (pH 5.2), filter sterilize and freeze aliquots at −20ºC.

Proteinase K (10mg/ml)

Dissolve proteinase K in autoclaved water to a final concentration of 10mg/ml, and freeze aliquots at −20ºC.

100mM PMSF

Dissolve PMSF (phenylmethylsulphonyl fluoride) in absolute ethanol to a final concentration of 100mM, and freeze aliquots at -20ºC.

Buffer A

10mM HEPES, pH 8.0

1.5mM $MgCl_2$

10mM KCl

1mM DTT

1µg/ml Pepstatin

1µg/ml Leupeptin

B.8 Western Blotting

30% Acrylamide/0.8% Bisacrylamide solution

30g acrylamide

0.8g bisacrylamide

0.1g SDS

Make up to 100ml with distilled water and store at 4ºC.

10% SDS

Dissolve 10g SDS (sodium dodecyl sulfate) in 80ml distilled water; heat to 68ºC, adjust volume up to 100ml with distilled water.

1M Tris pH 6.8

Dissolve 60.5g Tris base in 300ml distilled water, pH with concentrated HCl to 6.8, adjust volume up to 500ml with distilled water, autoclave.

1M Tris pH 8.8

Dissolve 60.5g Tris base in 300ml distilled water, pH with concentrated HCl to 8.8, adjust volume up to 500ml with distilled water, autoclave.

5 × Protein loading buffer

Dissolve 1.75g Tris in 10 ml distilled water, add 30ml of glycerine, adjust pH to 6.8 with concentrate HCl, add 5g SDS, adjust volume to 50ml with distilled water.

5 × Protein loading dye

200µl 5 × protein loading buffer

50µl β-mercaptoethanol

10µl bromophenol blue

10 × Running buffer

Take 29g Tris, 144g Glycine and 10g SDS, adjust volume to 1 litre with distilled water.

10 × Transfer buffer

144g glycine

38g Tris

Make up volume to 1 litre with distilled water.

1 × Transfer buffer

100ml 10 × transfer buffer

200ml methanol

700ml distilled water

TBST

Mix 50ml 1M Tris, 30ml 5M NaCl and 500µl Tween20. Adjust volume to 1 litre with distilled water.

5% Non-fat milk blocking solution

Dissolve 2.5g powder non-fat milk in 30ml TBST, make up volume to 50ml with TBST.

27% Non-fat milk blocking solution

Dissolve 3.5g powder non-fat milk in 30ml TBST, make up volume to 50ml with TBST.

Coomassie blue staining solution

500ml methanol

0.5g Coomassie brilliant blue

100ml acetic acid

400ml distilled water

Destaining solution

50ml methanol

70ml acetic acid

880ml distilled water

1M Glycine pH 2.0

Dissolve 37.535g glycine in 300ml distilled water, pH with concentrated HCl to 2.0 and adjust volume to 500ml with distilled water.

1M Tris-HCl, pH 7.5

Dissolve 24.22g Tris in 160ml of distilled water, adjust pH to 7.5 with HCl (~ 15ml), adjust volume up to 200ml with distilled water and autoclave.

Stacking gel (4%)

Solution	**Volume**
ddH_2O	3.65ml
1M Tris pH 6.8	0.625ml
30% acrylamide/bisacrylamide	0.650ml
10% SDS	50µl
10% APS	25µl
TEMED	5µl
Total volume	**5ml**

Separating gel

Solution	**7% gel (nuclear protein)**	**10% gel (total protein)**
ddH_2O	3.76ml	2.75ml
1M Tris pH 8.8	3.75ml	3.75ml
10% SDS	100µl	100µl
30% acrylamide/bisacrylamide	2.33ml	3.35ml
10% APS	50µl	50µl
TEMED	5µl	5µl
Total volume	**10ml**	**10ml**

B.9 Immunofluorescence

16% paraformaldehyde

Add 80ml dH_2O to 16g paraformaldehyde. Cover with foil, stir for 1h on heated stirrer. Do not let temperature exceed 60°C. Add a few drops of 10M NaOH, just until solution turns clear. Filter through 0.45µm filter. Adjust to pH 7 with concentrated HCl. Make up to 100ml with dH_2O. Store in 2.5ml aliquots at -20°C.

Blocking solution

1% BSA dissolved in 1 x PBS

DAPI nuclear stain

Add 50µg DAPI (4', 6-diamidino-2-phenylinole dihydrochloride) to 1ml dH_2O. Store covered in foil at -20°C. Dilute 1:200 in PBS before mounting.

Mowiol

Add 2g mowiol to 2ml glycerol. While stirring, add 4ml ddH_2O. Leave at room temperature for about 4h, the longer the better.

B.10 Microarray Hybridization

Streptavidin-Cy3

Prepare 1mg/ml stock solution by adding 1ml RNase-free water to 1mg streptavidin-Cy3 powder. Mix. Dilute 1:1000 with Block E1 buffer before incubating BeadChips for detection.

Appendix C: Molecular Weight Markers

Fermentas O'GeneRuler™ 100 bp DNA Ladder, ready-to-use

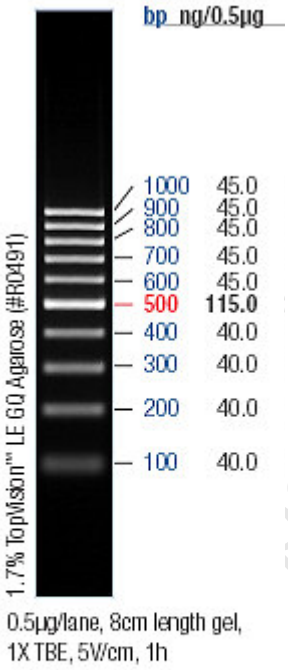

Fermentas PageRuler Plus Prestained Protein Marker

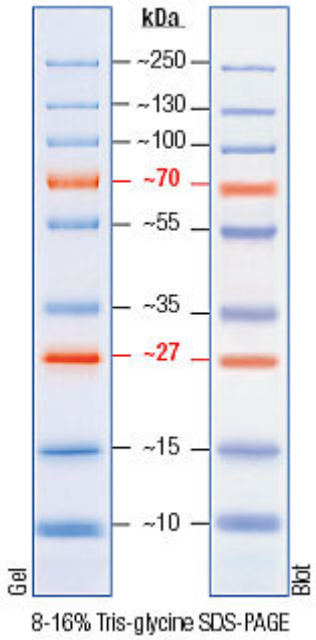

Appendix D: Cell Line Nomenclature

Cell Line	***Origin***
A549	Lung adenocarcinoma cells
ACHN	Renal carcinoma cells
BEP2D	Immortalized bronchial epithelial cells
Caco-2	Colon carcinoma cells
CI41	Mouse normal epidermal cells
EPC-2	Immortalized normal oesophageal epithelial cells
F258	Normal rat liver epithelial cells
FL	Normal amnion epithelial cells
H460	Lung cancer
HeLa	Cervical carcinoma cells
Hepa1c1c7	Mouse hepatoma cells
HepG2	Hepatocarcinoma cells
HCT116	Colorectal carcinoma cells
HIOEC	Human immortalized oral epithelial cells
HME87	Normal mammary epithelial cells
HOSE	Ovarian epithelial cells
KYSE	Oesophageal squamous cell carcinoma cells
LS-180	Colon carcinoma cells
MCF-7	Breast carcinoma cells
MCF-10A	Mammary epithelial cells
MCF-10AT1	Breast carcinoma cells
MSK-LEUK1	Oral leukoplakia cells
MRC-5	SV2-immortalized lung fibroblasts
NEC14	Testis embryonal carcinoma cells
NHBE	Normal human bronchial epithelial cells
NHEK	Normal human epidermal keratinocytes
NHMEC	Normal human mammary epithelial cells
OVCA	Ovarian carcinoma
RL95-2	Endometrial epithelial cells
SCC-9	Oral epithelial squamous cell carcinoma
SCC-449	Oesophageal squamous cell carcinoma cells
T24	Transitional cancer cells
TK6	Lymphoblastoid cells
WHCO1	Oesophageal squamous cell carcinoma cells
WI38	Normal foetal lung fibroblasts